AD-A056 983 NORTHROP CORP HAWTHORNE CA AIRCRAFT GROUP F/G 5/8
PREDICTION, EVALUATION, AND SPECIFICATION OF CLOSED LOOP AND MU--ETC(U)
FEB 78 E D ONSTOTT, W H FAULKNER F33615-77-C-3008
UNCLASSIFIED NOR-77-162 AFFDL-TR-78-3 NL

1 OF 3
AD
A056983

AFFDL-TR-78-3

PREDICTION, EVALUATION, AND SPECIFICATION OF CLOSED LOOP AND MULTIAXIS FLYING QUALITIES

E. D. ONSTOTT
W. H. FAULKNER

NORTHROP CORPORATION
AIRCRAFT GROUP
HAWTHORNE, CALIFORNIA

FEBRUARY 1978

TECHNICAL REPORT AFFDL-TR-78-3

Approved for public release; distribution unlimited.

AIR FORCE FLIGHT DYNAMICS LABORATORY
AIR FORCE WRIGHT AERONAUTICAL LABORATORIES
AIR FORCE SYSTEMS COMMAND
WRIGHT-PATTERSON AIR FORCE BASE, OHIO 45433

NOTICE

When Government drawings, specifications, or other data are used for any purpose other than in connection with a definitely related Government procurement operation, the United States Government thereby incurs no responsibility nor any obligation whatsoever; and the fact that the Government may have formulated, furnished, or in any way supplied the said drawings, specifications, or other data, is not to be regarded by implication or otherwise as in any manner licensing the holder or any other person or corporation, or conveying any rights or permission to manufacture, use, or sell any patented invention that may in any way be related thereto.

This report has been reviewed by the Information Office (OI) and is releasable to the National Technical Information Service (NTIS). At NTIS, it will be available to the general public, including foreign nations.

This technical report has been reviewed and is approved for publication.

Frank L. George
Frank L. George
Project Engineer
Control Dynamics Branch

R. O. Anderson
R. O. Anderson, Chief
Control Dynamics Branch
Flight Control Division

FOR THE COMMANDER

Robert F. Lopina
R. F. Lopina, Col., USAF
Chief, Flight Control Division
Air Force Flight Dynamics Laboratory

"If your address has changed, if you wish to be removed from our mailing list, or if the addressee is no longer employed by your organization please notify AFFDL/STINFO, W-PAFB, OH 45433 to help us maintain a current mailing list."

Copies of this report should not be returned unless return is required by security considerations, contractual obligations, or notice on a specific document.

AIR FORCE/56780/10 July 1978 — 500

UNCLASSIFIED

SECURITY CLASSIFICATION OF THIS PAGE (When Data Entered)

19 REPORT DOCUMENTATION PAGE

READ INSTRUCTIONS BEFORE COMPLETING FORM

1. REPORT NUMBER 18 AFFDL TR-78-3

2. GOVT ACCESSION NO.

3. RECIPIENT'S CATALOG NUMBER 9

4. TITLE (and Subtitle) 6 Prediction, Evaluation, and Specification of Closed Loop and Multiaxis Flying Qualities.

5. TYPE OF REPORT & PERIOD COVERED Final Report, Mar[redacted]-Dece[redacted] 1977,

6. PERFORMING ORG. REPORT NUMBER 14 NOR-77-162

7. AUTHOR(s) 10 E.D./Onstott, W.H./Faulkner

8. CONTRACT OR GRANT NUMBER(s) 15 F33615-77-C-3008 new

9. PERFORMING ORGANIZATION NAME AND ADDRESS
Northrop Corporation, Aircraft Group,
3901 West Broadway
Hawthorne, California 90250

10. PROGRAM ELEMENT, PROJECT, TASK AREA & WORK UNIT NUMBERS
61102F
16 2307/O3 03 17 03

11. CONTROLLING OFFICE NAME AND ADDRESS
Air Force Flight Dynamics Laboratory (FGC)
Wright-Patterson Air Force Base, Ohio 45433

12. REPORT DATE 11 Febr[redacted] 1978

13. NUMBER OF PAGES 263

14. MONITORING AGENCY NAME & ADDRESS (if different from Controlling Office)
12 278p.

15. SECURITY CLASS. (of this report) Unclassified

15a. DECLASSIFICATION/DOWNGRADING SCHEDULE

16. DISTRIBUTION STATEMENT (of this Report)

Approved for public release; distribution unlimited

17. DISTRIBUTION STATEMENT (of the abstract entered in Block 20, if different from Report)

18. SUPPLEMENTARY NOTES

19. KEY WORDS (Continue on reverse side if necessary and identify by block number)

Flying Qualities
Performance Prediction Methods
Specification Criteria
Pilot-Vehicle Analysis Methods
Pilot Model Theory
Manual Control

20. ABSTRACT (Continue on reverse side if necessary and identify by block number)

A general technology for the prediction, evaluation, and specification of closed loop and multiaxis flying qualities is documented. A comprehensive scheme for the classification of precision piloted tasks is presented, and a nonlinear multiaxis pilot model is described. Demonstrations of the aircraft/pilot/task analysis method are given for a number of precision piloted tasks and aircraft configurations. The analysis method is also applied to a comparison of Gaussian and non-Gaussian (Reeves) turbulence models, and to a study of the effects of control system lags on tracking — over

DD FORM 1 JAN 73 1473 EDITION OF 1 NOV 65 IS OBSOLETE

UNCLASSIFIED

SECURITY CLASSIFICATION OF THIS PAGE (When Data Entered)

410 275 LB

performance. Piloted flight simulations were performed to validate all pilot model analyses; complete simulation and pilot model data is presented. Specification methods suitable for MIL-F-8785B are suggested in the areas of step target tracking and pilot reserve attention capacity. A computer program embodying the analysis method is available from AFFDL/FGC; a user guide, listing, and sample data set are included in the report.

FOREWORD

This report was prepared by the Northrop Corporation, Aircraft Group, Hawthorne, California, under United States Air Force Contract F33615-77-C-3008. The program was administered by the Control Dynamics Branch, Air Force Flight Dynamics Laboratory, Air Force Systems Command, Wright-Patterson Air Force Base, Ohio. The project engineer was Frank L. George (AFFDL/FGC). The effort was funded under Program Element 61102F, and performed as part of Project 2307, Task O3, Flight Control Research.

The contract work was performed during the period March 1977 to December 1977. The draft of this report was submitted in December 1977.

The authors acknowledge their gratitude to L. B. Hartsook of Northrop Corporation for his guidance and assistance in the development of the technology documented in this report, and to E. P. Salmon, also of Northrop Corporation, for urging the development of a true multiaxis pilot model.

CONTENTS

Section		Page
I	INTRODUCTION	1
	A. Scope and Purpose of Report	1
	B. Precision Piloted Flying Qualities	2
	C. Urgency Decision Pilot Model	2
	D. Prediction and Evaluation of Flying Qualities	3
	E. Specification of Flying Qualities	4
	F. A Reader's Guide to the Report	4
II	PRECISION PILOTED FLYING QUALITIES	5
	A. Precision Piloted Tasks in Flying Qualities Evaluation	5
	B. Classification of Precision Piloted Flight Tasks	6
III	THE URGENCY DECISION PILOT MODEL	11
	A. Definition of Statistical and Dynamical Pilot Models	11
	B. Principles of Human Optimality and Human Dynamic Limitations	14
	C. Single-Axis Pilot Models	17
	D. Multiaxis Pilot Models	22
IV	PREDICTION OF PILOTED AIRCRAFT PERFORMANCE	31
	A. Attitude Stabilization in Turbulence	31
	B. Validation of the Model for Two-Axis Attitude Stabilization	57
	C. A Self-Generated VTOL Hover Task	66
	D. Error Rate Information in Attention Allocation Pilot Models	74
	E. Comparison of the Multiaxis Pilot Model With Wanamaker-Sower Data	85
	F. Target Tracking With Visual Delays and Side Task	91
V	COMPARISON OF TURBULENCE MODELS AND CONTROL SYSTEM LAG EFFECTS	101
	A. Aircraft Descriptions and Equations of Motion	101
	B. Comparison of Gaussian and Reeves Non-Gaussian Turbulence	106
	C. The Influence of Control System Lags on Two-Axis Attitude Stabilization	124

CONTENTS (continued)

Section		Page
VI	STEP TARGET TRACKING ANALYSIS AND PERFORMANCE SPECIFICATION	137
	A. Coordination of Flying Qualities Analysis with Flight Test and Simulation	137
	B. Pilot — Aircraft Analysis of Longitudinal Step Target Tracking	139
	C. Correlation of Pilot Ratings with Step Target Data	163
	D. Multiaxis Step Target Tracking	166
	E. Validation of the Step Target Prediction Method by F-5E Aircraft	168
	F. Specification of Air-to-Air Tracking Performance	178
VII	PREDICTION OF PILOT RESERVE ATTENTION CAPACITY	181
	A. Side Tasks and Pilot Reserve Attention	181
	B. Prediction of Pilot Reserve Attention Capacity for Constant Urgency Side Tasks	182
	C. Reserve Attention Capacity During Attitude Stabilization in Turbulence	185
	D. Selection of Candidate Side Tasks for Reserve Attention Prediction	194
	E. Interpretations of Pilot Workload	197
	F. Correlation of Pilot Workload and Pilot Ratings with Performance	199
	G. Specification of Pilot Reserve Attention	199
VIII	SUMMARY AND RECOMMENDATIONS	201
	REFERENCES	205
Appendix		
A	INFLUENCE OF MOTION CUES ON PILOT RATINGS IN TURBULENCE	209
B	PREDICTION OF CRITICAL TASK PERFORMANCE	215
C	COMPUTER PROGRAM USER GUIDE	223

ILLUSTRATIONS

Figure		Page
1	Characteristics of Precision Flight Tasks	6
2	Generic Classification of Precision Task Components	8
3	Classifications of Applications in This Report	9
4	Urgency Decision Pilot Model Advantages	13
5	Remnant Model Calibration Method	19
6	Single-Loop Pilot Model	20
7	Heading Command Task	21
8	Demonstration of Pilot Attention Allocation by Cross Plot of Lateral and Longitudinal Stick Commands During Hover Task	24
9	Urgency Decision Pilot Model Structure	27
10	Equations of Motion	32
11	Matrix of Aircraft Configurations	32
12	Two-Axis Flight Simulation Display	34
13	Display Ratios Tested	34
14	Control Configuration for Turbulence Task	36
15	Lateral and Longitudinal Pilot Compensation for Attitude Stabilization in Turbulence	37
16	Comparison of Pilot Model with Flight Simulation Tracking Error Data for Single-Axis Turbulence Stabilization	40
17	Rules for Data Acquisition	40
18	Comparison of Standard Deviations of Pilot Model and Flight Simulation Tracking Error Data for Single-Axis Turbulence Stabilization Task	41
19	Comparison of Two-Axis Bank Angle Tracking Error	45
20	Comparison of Two-Axis Pitch Angle Tracking Error	45
21	Comparison of Radial Errors for Turbulence Stabilization	46
22	Attention Shifting Episodes From Flight Simulation	46
23	Longitudinal Task Interference	47
24	Lateral Task Interference	47
25	Example Task Interference Graph	48
26	Task Interference Graph for Configuration 1A	50

ILLUSTRATIONS (continued)

Figure		Page
27	Task Interference Graph for Configuration 1B	50
28	Task Interference Graph for Configuration 2A	51
29	Task Interference Graph for Configuration 2B	51
30	Task Interference Graph for Configuration 3A	52
31	Task Interference Graph for Configuration 3B	52
32	Pilot Model and Flight Simulation Data Dispersion for 30-Second Flights of Configuration 1B at μ/α = 16	53
33	Pilot Model and Flight Simulation Data Dispersion for 30-Second Flights of Configuration 3B at μ/α = 16	53
34	Lateral Time Histories for Single- and Two-Axis Turbulence Stabilization of Configuration B Lateral Dynamics	55
35	YF-17 Flight Conditions Surveyed	57
36	Lateral Stabilization of the YF-17 Single-Axis	58
37	Longitudinal Stabilization of the YF-17 Single-Axis	59
38	Lateral Stabilization of the YF-17 Two-Axis	60
39	Longitudinal Stabilization of the YF-17 Two-Axis	61
40	Two-Axis YF-17 Task Interference Graph for 5000 Ft at Mach 0.4	61
41	Two-Axis YF-17 Task Interference Graph for 30,000 Ft at Mach 0.4	62
42	Two-Axis YF-17 Task Interference Graph for 5000 Ft at Mach 0.8	62
43	Two-Axis YF-17 Task Interference Graph for 40,000 Ft at Mach 0.8	63
44	Two-Axis YF-17 Task Interference Graph for 60,000 Ft at Mach 0.9	63
45	Two-Axis YF-17 Task Interference Graph for 10,000 Ft at Mach 1.1	64
46	VTOL Aircraft System Dynamics	66
47	VTOL Pilot Model Compensation for Lateral Control	67
48	Urgency Functions for the VTOL Hover Task	67
49	Interpretation of VTOL Urgency Functions	67
50	X-Y Plot of Lateral Versus Longitudinal Stick for VTOL Hover	68
51	Definition of Crossfeed, Bias, and Skewness	69
52	Complete System Model for VTOL Hover	70

ILLUSTRATIONS (continued)

Figure		Page
53	VTOL Flight Simulation Display	71
54	Model and Flight Simulation Ground Paths for VTOL Hover	71
55	Theta Time Histories from Model and Simulation	72
56	Histograms of Pilot Switching	72
57	Comparison of Model and Simulation Statistics	73
58	Optimum VTOL Pilot Model Parameters	73
59	Command Tracking Signal Generation	74
60	Configurations Simulated for Command Tracking Task	75
61	Control Configuration for Command Tracking Task	76
62	Flight Simulation Display	77
63	Agreement of Model and Flight Simulation Tracking Scores	82
64	Sample Tracking Command Time Histories	82
65	Example Time Histories Generated by the Pilot Model	85
66	Comparison Data, Case 1	86
67	Comparison Data, Case 2	86
68	Comparison Data, Case 3	87
69	Comparison Data, Case 4	87
70	Comparison Data, Case 5	88
71	Comparison Data, Case 6	88
72	Comparison of Tracking Errors	89
73	Comparison of Mean Control Periods	89
74	Control Configuration for Target Tracking Task	92
75	Pre-assigned Pilot Model Parameters for Target Tracking Task	93
76	Case 5 Vertical Tracking Data	96
77	Case 5 Horizontal Tracking Data	96
78	Comparison of Flight Simulation and Pilot Model Target Tracking Errors	97
79	Time History of Pilot Model Control Episodes	98
80	F-5E Primary Operating Envelope	102
81	Aircraft Equations of Motion	106
82	Agreement of Pilot Model and Flight Simulation Data for F-5E Lateral Tracking Errors, Gaussian Turbulence	110

ILLUSTRATIONS (continued)

Figure		Page
83	Agreement of Pilot Model and Flight Simulation Data for F-5E Longitudinal Tracking Errors, Gaussian Turbulence	110
84	Agreement of Pilot Model and Flight Simulation Data for F-5E Radial Tracking Errors, Gaussian Turbulence	111
85	Agreement of Pilot Model and Flight Simulation Standard Deviation Data for F-5E Lateral Tracking, Gaussian Turbulence	111
86	Agreement of Pilot Model and Flight Simulation Standard Deviation Data for F-5E Longitudinal Tracking, Gaussian Turbulence	112
87	Reeves Non-Gaussian Turbulence Simulation	113
88	Agreement of Pilot Model and Flight Simulation Data For F-5E Lateral Tracking Errors, Reeves Turbulence	117
89	Agreement of Pilot Model and Flight Simulation Data for F-5E Longitudinal Tracking Errors, Reeves Turbulence	117
90	Agreement of Pilot Model and Flight Simulation Data for F-5E Radial Tracking Errors, Reeves Turbulence	118
91	Agreement of Pilot Model and Flight Simulation Standard Deviation Data for F-5E Lateral Tracking, Reeves Turbulence	118
92	Agreement of Pilot Model and Flight Simulation Standard Deviation Data for F-5E Longitudinal Tracking, Reeves Turbulence	119
93	Comparison of Gaussian and Reeves F-5E Open Loop Lateral Attitude Errors	120
94	Comparison of Gaussian and Reeves F-5E Open Loop Longitudinal Attitude Errors	121
95	Comparison of Gaussian and Reeves F-5E Lateral Tracking Errors, Pilot Model and Flight Simulation Data	121
96	Comparison of Gaussian and Reeves F-5E Longitudinal Tracking Errors, Pilot Model and Flight Simulation Data	122
97	Comparison of Gaussian and Reeves F-5E Radial Tracking Errors, Pilot Model and Flight Simulation Data	122
98	Comparison of Gaussian and Reeves F-5E Lateral Tracking Error Standard Deviations, Pilot Model and Flight Simulation Data	123
99	Comparison of Gaussian and Reeves F-5E Longitudinal Tracking Error Standard Deviations, Pilot Model and Flight Simulation Data	123

ILLUSTRATIONS (continued)

Figure		Page
100	Agreement of Pilot Model and Flight Simulation Data for F-5E Lateral Tracking Errors, Gaussian Turbulence With Control System Lags	128
101	Agreement of Pilot Model and Flight Simulation Data for F-5E Longitudinal Tracking Errors, Gaussian Turbulence With Control System Lags	129
102	Effect of Control System Lags on F-5E Case 1 With Augmenter, Gaussian Turbulence	130
103	Effect of Control System Lags on F-5E Case 1 Without Augmenter, Gaussian Turbulence	130
104	Effect of Control System Lags on F-5E Case 2 With Augmenter, Gaussian Turbulence	131
105	Effect of Control System Lags on F-5E Case 2 Without Augmenter, Gaussian Turbulence	131
106	Effect of Control System Lags on F-5E Case 3 With Augmenter, Gaussian Turbulence	132
107	Effect of Control System Lags on F-5E Case 4 With Augmenter, Gaussian Turbulence	132
108	Effect of Control System Lags on F-5E Case 5 With Augmenter, Gaussian Turbulence	133
109	Effect of Control System Lag on F-5E Case 5 Without Augmenter, Gaussian Turbulence	133
110	Effect of Control System Lags on F-5E Case 8 With Augmenter, Gaussian Turbulence	134
111	Effect of Control System Lags on F-5E Case 9 With Augmenter, Gaussian Turbulence	134
112	Effect of Control System Lags on F-5E Case 9 Without Augmenter, Gaussian Turbulence	135
113	Definition of Step Target Tracking Task	140
114	Configuration 1A Step Tracking Response	142
115	Configuration 1B Step Tracking Response	142
116	Configuration 1D Step Tracking Response	143
117	Configuration 1E Step Tracking Response	143
118	Configuration 1F Step Tracking Response	144
119	Configuration 1G Step Tracking Response	144
120	Configuration 2A Step Tracking Response	145

ILLUSTRATIONS (continued)

Figure		Page
121	Configuration 2C Step Tracking Response	145
122	Configuration 2D Step Tracking Response	146
123	Configuration 2E Step Tracking Response	146
124	Configuration 2F Step Tracking Response	147
125	Configuration 2H Step Tracking Response	147
126	Configuration 2J Step Tracking Response	148
127	Configuration 3A Step Tracking Response	148
128	Configuration 3B Step Tracking Response	149
129	Configuration 3C Step Tracking Response	149
130	Configuration 3D Step Tracking Response	150
131	Configuration 3E Step Tracking Response	150
132	Configuration 4A Step Tracking Response	151
133	Configuration 4B Step Tracking Response	151
134	Configuration 4C Step Tracking Response	152
135	Configuration 4D Step Tracking Response	152
136	Configuration 4E Step Tracking Response	153
137	Configuration 5A Step Tracking Response	153
138	Configuration 5B Step Tracking Response	154
139	Configuration 5C Step Tracking Response	154
140	Configuration 5D Step Tracking Response	155
141	Configuration 5E Step Tracking Response	155
142	Configuration 6A Step Tracking Response	156
143	Configuration 6B Step Tracking Response	156
144	Configuration 6C Step Tracking Response	157
145	Configuration 6D Step Tracking Response	157
146	Configuration 6E Step Tracking Response	158
147	Configuration 6F Step Tracking Response	158
148	Configuration 7A Step Tracking Response	159
149	Configuration 7B Step Tracking Response	159
150	Configuration 7C Step Tracking Response	160
151	Configuration 7D Step Tracking Response	160
152	Configuration 7E Step Tracking Response	161
153	Configuration 7F Step Tracking Response	161

ILLUSTRATIONS (continued)

Figure		Page
154	Configuration 7G Step Tracking Response	162
155	Configuration 7H Step Tracking Response	162
156	Correlation of rms θ_e With Pilot Ratings	164
157	Correlation of Time-On-Target With Pilot Ratings	164
158	Pilot Ratings as Functions of rms θ_e and Time-On-Target	165
159	Control Configuration for Step Target Tracking	167
160	F-5E Case 1 Step Target Tracking Response	169
161	F-5E Case 1 Step Target Tracking Response	169
162	F-5E Case 2 Step Target Tracking Response	170
163	F-5E Case 2 Step Target Tracking Response	170
164	F-5E Case 3 Step Target Tracking Response	171
165	F-5E Case 3 Step Target Tracking Response	171
166	F-5E Case 4 Step Target Tracking Response	172
167	F-5E Case 4 Step Target Tracking Response	172
168	F-5E Case 5 Step Target Tracking Response	173
169	F-5E Case 5 Step Target Tracking Response	173
170	F-5E Case 6 Step Target Tracking Response	174
171	F-5E Case 6 Step Target Tracking Response	174
172	F-5E Case 7 Step Target Tracking Response	175
173	F-5E Case 7 Step Target Tracking Response	175
174	F-5E Case 8 Step Target Tracking Response	176
175	F-5E Case 8 Step Target Tracking Response	176
176	F-5E Case 9 Step Target Tracking Response	177
177	F-5E Case 9 Step Target Tracking Response	177
178	F-5E Validation of Step Target Prediction Method	178
179	Tracking Degradation as a Function of Side Task Urgency	183
180	Reserve Attention as a Function of Side Task Urgency	184
181	High and Low Pilot Workload as Functions of Tracking Degradation and Reserve Attention	185
182	Reserve Attention for F-5E Case 1 With Augmenter	187
183	Reserve Attention for F-5E Case 1 Without Augmenter	188
184	Reserve Attention for F-5E Case 2 With Augmenter	188
185	Reserve Attention for F-5E Case 2 Without Augmenter	189

ILLUSTRATIONS (continued)

Figure		Page
186	Reserve Attention for F-5E Case 3 With Augmenter	189
187	Reserve Attention for F-5E Case 4 With Augmenter	190
188	Reserve Attention for F-5E Case 5 With Augmenter	190
189	Reserve Attention for F-5E Case 5 Without Augmenter	191
190	Reserve Attention for F-5E Case 8 With Augmenter	191
191	Reserve Attention for F-5E Case 9 With Augmenter	192
192	Reserve Attention for F-5E Case 9 Without Augmenter	192
193	Attention Allocation Logic for Side Tasks	195
194	Classification of Housekeeping Side Tasks	196
195	Interpretations of Pilot Workload	197
196	Bank Angle Errors Versus Pilot Rating for Normal Mode F-5 and A-7 Airplanes for All Gust Levels	210
197	NT-33 BB2.3 Average Pilot Rating	212
198	Average NT-33 Pilot Ratings as Functions of Tracking Error	212
199	F-5 Case 1 Without Augmenter Average Pilot Rating	213
200	F-5 Turbulence Data Showing Poor Correlation of Average Pilot Rating With Tracking Error	213
201	NT-33 Turbulence Data Showing Influence of Motion Cues on Pilot Ratings	214
202	F-5 Turbulence Data Showing Influence of Motion Cues on Pilot Ratings	214
203	Flight Simulation to Determine Critical Side Task	216
204	Pilot Rating as a Function of Critical Task λ_c	216
205	Pitch Angle Tracking Errors as Functions of Side Task	218
206	Bank Angle Tracking Errors as Functions of Side Task	219
207	Reserve Attentions as Functions of Side Task	220
208	Bank Angle Rates as Functions of Side Task	221
209	Organization of Major Program Elements	225
210	Program Input Format	227
211	F-5E Stability Augmentation System	232
212	Program COMMON Blocks	234
213	Program Flow Chart	238
214	Sample Data Set	240

TABLES

Table		Page
1	Stability Derivatives for Attitude Stabilization in Turbulence	33
2	Single-Axis Turbulence Stabilization Pilot Model Data	39
3	Single-Axis Turbulence Stabilization Flight Simulation Data	39
4	Two-Axis Turbulence Stabilization Pilot Model Data	43
5	Two-Axis Turbulence Stabilization Flight Simulation Data	44
6	Pilot Model Data for Command Tracking Task	79
7	Dwell Fraction and Mean Dwell Time Data	80
8	Command Tracking Flight Simulation and Model Data	81
9	Numerical Data for Visual Delay of 1.5 Units	95
10	Numerical Data for Visual Delay of 6.5 Units	95
11	Target Tracking Pilot Model Data	97
12	F-5E Configurations Simulated	102
13	F-5E Dimensional Stability Derivatives – Lateral (Body Axes)....	103
14	F-5E Dimensional Stability Derivatives – Longitudinal (Body Axes) ..	104
15	F-5E SAS Gains	105
16	F-5E Open Loop Attitude Errors in Gaussian Turbulence	108
17	Flight Simulation Data — Attitude Stabilization in Gaussian Turbulence	108
18	Pilot Model Data — Attitude Stabilization in Gaussian Turbulence..	109
19	F-5E Open Loop Attitude Errors in Reeves Turbulence	115
20	Flight Simulation Data — Attitude Stabilization in Reeves Turbulence	115
21	Pilot Model Data — Attitude Stabilization in Reeves Turbulence...	116
22	Flight Simulation Data — Attitude Stabilization in Gaussian Turbulence, 0.05 Sec Control Lags	124
23	Flight Simulation Data — Attitude Stabilization in Gaussian Turbulence, 0.1 Sec Control Lags	125
24	Pilot Model Data — Attitude Stabilization in Gaussian Turbulence, 0.05 Sec Control Lags	126

TABLES (continued)

Table		Page
25	Pilot Model Data — Attitude Stabilization in Gaussian Turbulence, 0.1 Sec Control Lags	127
26	F-5E Reserve Attention Data	186

LIST OF SYMBOLS

D	duration of target acquisition phase in step tracking (sec)
e	tracking error
g	gravity acceleration constant (32.2 ft/sec^2)
I_{xx}, I_{yy}, I_{zz}	aircraft moments of inertia (ft-lb-sec^2)
I_{xy}, I_{xz}, I_{yz}	aircraft products of inertia (ft-lb-sec^2)
I_1	$(I_{yy} - I_{zz})/I_{xx}$
I_2	$(I_{zz} - I_{xx})/I_{yy}$
I_3	$(I_{xx} - I_{yy})/I_{zz}$
K	pilot model gain
K_A, K_V, K_Y	F-5E control augmenter gains
L	perturbed rolling moment (ft-lb)
L_v	$\frac{1}{I_{xx}} \frac{\partial L}{\partial v}$ (1/ft-sec)
L_p	$\frac{1}{I_{xx}} \frac{\partial L}{\partial p}$ (1/sec)

L_r	$\frac{1}{I_{xx}} \frac{\partial L}{\partial r}$ (1/sec)
$L_{\delta a}$	$\frac{1}{I_{xx}} \frac{\partial L}{\partial \delta a}$ (1/sec^2)
$L_{\delta r}$	$\frac{1}{I_{xx}} \frac{\partial L}{\partial \delta r}$ (1/sec^2)
L'_i	$\left(L_i + \frac{I_{xz}}{I_{xx}} N_i\right) \Big/ \left(1 - \frac{I_{xz}^2}{I_{xx} I_{zz}}\right)$, $i = \beta, p, r, \delta a$
M	perturbed pitching moment (ft-lb)
M_u	$\frac{1}{I_{yy}} \frac{\partial M}{\partial u}$ (1/ft-sec)
M_w	$\frac{1}{I_{yy}} \frac{\partial M}{\partial w}$ (1/ft-sec)
$M_{\dot{w}}$	$\frac{1}{I_{yy}} \frac{\partial M}{\partial \dot{w}}$ (1/ft)
M_q	$\frac{1}{I_{yy}} \frac{\partial M}{\partial q}$ (1/sec)
$M_{\delta e}$	$\frac{1}{I_{yy}} \frac{\partial M}{\partial \delta e}$ (1/sec^2)
m	aircraft mass (lb-sec^2/ft); meter
N	perturbed yawing moment (ft-lb)
N_v	$\frac{1}{I_{zz}} \frac{\partial N}{\partial v}$ (1/ft-sec)
N_p	$\frac{1}{I_{zz}} \frac{\partial N}{\partial p}$ (1/sec)
N_r	$\frac{1}{I_{zz}} \frac{\partial N}{\partial r}$ (1/sec)
$N_{\delta a}$	$\frac{1}{I_{zz}} \frac{\partial N}{\partial \delta a}$ (1/sec^2)
$N_{\delta r}$	$\frac{1}{I_{zz}} \frac{\partial N}{\partial \delta r}$ (1/sec^2)

N'_i	$\left(N_i + \frac{I_{xz}}{I_{zz}} L_i\right) \Big/ \left(1 - \frac{I_{xz}^2}{I_{xx} I_{zz}}\right)$, $i = \beta, p, r, \delta a$
p	perturbed roll rate (rad/sec)
PIO	pilot induced oscillation
PR	pilot rating
q	perturbed pitch rate (rad/sec)
r	perturbed yaw rate (rad/sec); radial error
RA	pilot reserve attention, percent
s	Laplace variable
t	time (sec)
T_L	pilot model lead (sec)
TOT	time-on-target (sec)
U	urgency function
u	perturbed longitudinal velocity (ft/sec)
v	perturbed lateral velocity (ft/sec)
w	perturbed normal velocity (ft/sec)
X	perturbed longitudinal force (lb)
X_u	$\frac{1}{m} \frac{\partial X}{\partial u}$ (1/sec)
X_w	$\frac{1}{m} \frac{\partial X}{\partial w}$ (1/sec)
$X_{\dot{w}}$	$\frac{1}{m} \frac{\partial X}{\partial \dot{w}}$
X_q	$\frac{1}{m} \frac{\partial X}{\partial q}$ (ft/sec)
$X_{\delta e}$	$\frac{1}{m} \frac{\partial X}{\partial \delta e}$ (ft/sec^2)
Y	perturbed lateral force (lb)
Y_v	$\frac{1}{m} \frac{\partial Y}{\partial v}$ (1/sec)

Y_p	$\frac{1}{m}\frac{\partial Y}{\partial p}$ (ft/sec)
Y_r	$\frac{1}{m}\frac{\partial Y}{\partial r}$ (ft/sec)
$Y_{\delta a}$	$\frac{1}{m}\frac{\partial Y}{\partial \delta a}$ (ft/sec^2)
$Y_{\delta r}$	$\frac{1}{m}\frac{\partial Y}{\partial \delta r}$ (ft/sec^2)
Z	perturbed normal force (lb)
Z_u	$\frac{1}{m}\frac{\partial Z}{\partial u}$ (1/sec)
Z_w	$\frac{1}{m}\frac{\partial Z}{\partial w}$ (1/sec)
$Z_{\dot{w}}$	$\frac{1}{m}\frac{\partial Z}{\partial \dot{w}}$
Z_q	$\frac{1}{m}\frac{\partial Z}{\partial q}$ (ft/sec)
$Z_{\delta e}$	$\frac{1}{m}\frac{\partial Z}{\partial \delta e}$ (ft/sec^2)
α	urgency function coefficient; flight simulation display scaling
β	urgency function coefficient; sideslip angle (rad)
δa	aileron command (rad)
δe	elevator command (rad)
δr	rudder command (rad)
$\Delta\epsilon$	tracking error degradation, percent
ϵ	tracking error
θ	pitch angle (rad)
λ	critical task parameter
μ	urgency function coefficient; flight simulation display scaling
ν	urgency function coefficient
σ	standard deviation
τ	time delay or lag (sec)

ϕ	roll angle (rad)
ψ	heading angle (rad)

Subscripts

c	command; critical
F	final
g	gust
H	horizontal
I	initial
IC	integral control
P	pitch
R	roll
ST	side task
V	vertical
o	threshold value; trim value

Superscripts

$\cdot$	time derivative
$\wedge$	observed value
$-$	average

SECTION I

INTRODUCTION

Modern high-performance tactical aircraft have required increased design and development costs in an effort to produce crucial improvements in performance of precision flight tasks such as terminal control and weapon delivery. Since analysis of these precision tracking problems depends heavily on the integration of the pilot and aircraft, it is essential to consider the pilot's dynamics in the development of analytical methods to support and augment flight test and flight simulation programs. With accurate and reliable pilot - aircraft performance analysis and specification methods, the following benefits in the design and development of tactical aircraft can be realized:

- Improved weapon delivery effectiveness.
- Safer operation during critical flight conditions.
- Improved pilot acceptance.
- Reduced system costs through improved design efficiency.

A. SCOPE AND PURPOSE OF REPORT

In order to help realize these benefits, Northrop has developed and validated a time-domain multiaxis pilot model for predicting and evaluating precision flying qualities. This model is now developed to the point that it may be reliably employed by the Air Force as well as other governmental and industrial users. There are five objectives for this report:

- Document the Urgency Decision Pilot Model.
- Develop a comprehensive approach to the prediction, evaluation and specification of closed loop multiaxis flying qualities.
- Illustrate this new methodology through applications.
- Formulate the method in a readily employed manner for a wide range of user applications.
- Suggest further areas of application and research.

In this way, the report will constitute an account of the time-domain multiaxis pilot modeling approach to flying qualities analysis and provide numerous problem demonstrations. New research performed under contract includes prediction of pilot

reserve attention, the evaluation of the effects of control system lags on multiaxis precision tracking, and a comparison of Gaussian and Reeves non-Gaussian turbulence models employed in two-axis attitude stabilization tasks. Fixed-base flight simulations have been performed to validate the model for these problems, and complete simulation data is presented along with a computer program user guide.

B. PRECISION PILOTED FLYING QUALITIES

Although there are numerous examples of precision flight — ranging from air-to-ground attack to in-flight refueling to landing — it will be shown that all such piloted tasks can be classified according to the nature of the command to the pilot, the control configuration he must adopt, and the criteria by which he and the flying qualities analyst judge his performance. These piloted tasks constitute the most critical aspects of the tactical fighter mission as performed by skilled and motivated pilots.

The analysis of the dynamics of the pilot considered as part of the total aircraft system is the objective of employing mathematical descriptions of the human pilot. There have been several valuable approaches to this subject via frequency-domain and optimal control theory. Nevertheless, there have been limitations and drawbacks that needed to be overcome, namely:

- Lack of generality in aircraft description.
- Lack of models for pilot decision and time-varying abilities.
- Difficult mathematical procedures for exercising the models.

These limitations have been overcome by use of time-history simulation as a model context, and the development of pilot decision logics that are directly mechanized. This is the basis of the Urgency Decision Pilot Model.

C. URGENCY DECISION PILOT MODEL

Owing to the complexity of current tactical fighter control systems, it is necessary to model the system by digital simulation for control analysis and design. This is now a common and accepted practice. This approach must also be taken to study the piloted aircraft, so that it is necessary to develop simulation pilot models. Fortunately, describing-function pilot models work well in simulations of single-axis time-invariant tracking problems. The problem then becomes: Can single-axis pilot models be extended to realistic multiaxis tracking, and if so, is anything gained?

The answer to both questions is yes. It is well known that pilots share their attention between lateral and longitudinal tracking tasks, and in addition allocate attention for instrument scanning and other cockpit chores. This allocation of activity can be characterized in terms of relative task urgency, and the development of these "urgency functions" is the key to the urgency decision model. In addition to providing a simple method that can be used in conjunction with existing aircraft models and flight simulators, the method has identified important flying qualities dynamic effects related to the interference of one task by the attention demands of another. For this reason, multiaxis flying qualities – which studies the complete piloted task – is a larger and more comprehensive subject than the study of single-axis time-invariant problems.

D. PREDICTION AND EVALUATION OF FLYING QUALITIES

Analysis and flight simulation data for a number of precision flight tasks are illustrated in the following Sections of the report. In each case (with the exception of the YF-17 validation study where the aircraft model cannot be reported) the discussion is complete in model description so the reader who wants to become familiar with the use of this method can easily recalculate the model predictions. In particular, the following items have been selected:

- Single- and two-axis attitude stabilization in turbulence.
- Analysis of relative display sensitivity on two-axis tasks.
- Analysis of task interference effects.
- Self-generated VTOL hover task.
- Two-axis command tracking with varied plant dynamics.
- Two-axis command tracking with unstable plant.
- Target tracking with visual delays and side task.
- Prediction of critical task performance.
- Prediction of pilot reserve attention.
- Prediction of step target tracking performance.
- Analysis of control system lags in two-axis tracking tasks.
- Comparison of Gaussian and non-Gaussian (Reeves) turbulence.

In addition to the discussion of these problems, there is analysis of the nature of pilot workload, and the demonstration that pilot ratings are highly correlated with multi-dimensional performance measures. These examples will illustrate the

application of the urgency decision model to the analysis of all precision piloted flying qualities that can be comprehensively classified by the scheme mentioned above.

E. SPECIFICATION OF FLYING QUALITIES

In order for a candidate specification item to be accepted into MIL-F-8785B, it must satisfy a number of conditions that guarantee unbiased yet discriminating ability of the item to ensure performance as well as pilot acceptance. There are two methods presented for flying qualities specification that meet these criteria:

- Specification of target tracking by means of step target tracking.
- Specification of pilot reserve attention capacity.

F. A READER'S GUIDE TO THE REPORT

Although a thorough reading of the report is required for the reader to obtain a working knowledge of the Urgency Decision Pilot Model and its application to flying qualities, it is useful to suggest a more modest introduction to these methods. The following suggested Sections will provide this:

	Section	Page
I.	Introduction	1
II.	Precision Piloted Flying Qualities	5
III.	The Urgency Decision Pilot Model	11
IV F.	Target Tracking with Visual Delays and Side Task	91

The background provided by these Sections is sufficient for an understanding of all other applications in the report. A summary of all topics discussed is presented in Section VIII, page 201.

SECTION II

PRECISION PILOTED FLYING QUALITIES

One of the objectives of this report is to present a comprehensive approach to the prediction, evaluation, and specification of closed loop multiaxis flying qualities. To do this, it is necessary to classify precision piloted tasks in a way that lends itself to straightforward applications of the Urgency Decision Pilot Model. This Section will postulate such a classification, and Section III will present the general model that can be adapted to any precision task that falls into the classification.

A. PRECISION PILOTED TASKS IN FLYING QUALITIES EVALUATION

Precision piloted tasks are the most important mission components of tactical aircraft. Landing, in-flight refueling, and dive bombing are obvious examples, and although combat maneuvering may not count as a precision tracking task, accurate weapon delivery, once conversion has been achieved, is the intended mission objective. Since these tasks are all performed under conditions where survival and safety are of great concern, only pilots that are highly trained undertake them. And when they do so, they are highly motivated to perform their best. For this reason, it is important to develop pilot-aircraft analysis methods that represent this well-trained and motivated pilot behavior. Consider these examples in closer detail:

Landing: To perform this task, the pilot must control a number of system variables including altitude, rate of descent, heading, touchdown point, angle of attack, and airspeed. In addition, there are other cockpit duties that must be performed. Control strategies are adopted by the pilot for each of these control requirements, and his performance is measured in terms of the precision with which the intended glide path is maintained.

In-Flight Refueling: To be successful, the pilot must maintain fixed position relative to the tanker aircraft. Thus he must track a point moving in front of him, often in the presence of turbulence and pilot induced disturbances. Performance is measured in terms of the probability of staying within a certain distance of the commanded point.

Dive Bombing: Once a target has been identified, the pilot must establish a glide slope, and track a number of dynamic and geometric variables to arrive at the correct release point and flight condition. During

the few seconds of precise tracking, the pilot may adopt time-varying control strategies. Performance is measured by circular impact error, or by an error prediction formula in simulation and analysis studies.

There are three aspects that these examples have in common. First of all, the pilot identifies a number of geometric or dynamic quantities that have to be controlled: glide slope errors must be zeroed, a spatial position error must be corrected, or a bomb release condition variable such as airspeed must be reached. This points out that in a given mission, there may be a number of simultaneous control tasks that the pilot must perform. The second aspect is a consequence of the first. Once the control tasks have been identified, the pilot must adopt control strategies that allow him to meet all objectives. During landing, for example, changes in heading are produced by rolling the aircraft, but at the same time roll angle must itself be stabilized. The final aspect concerns mission performance evaluation. There are two distinct methods. The first is to obtain subjective evaluation from the pilot in terms of Cooper-Harper pilot ratings and associated pilot comments. The second is to monitor geometric and dynamic variables and record statistics based upon them.

B. CLASSIFICATION OF PRECISION PILOTED FLIGHT TASKS

It is postulated here that all precision flight tasks can be classified by means of the above three characteristics. For convenience, they are summarized in Figure 1.

1) TASK - This is defined to be the complete set of mission objectives expressed in terms of geometric or dynamic variables that the pilot manipulates attempting to minimize certain quantities, reach specified values, or satisfy inequality constraints.

2) CONTROL - This is defined to be the complete set of control strategies that the pilot adopts in order to meet each objective as specified in the TASK.

3) EVALUATION - This is defined to be the set of all data that determines how well the TASK has been performed using a given CONTROL. This data may include subjective pilot opinion as well as control and performance statistics. Interpretation of these data then can be used to evaluate how well the CONTROL performed the TASK.

Figure 1. Characteristics of Precision Flight Tasks

Any flight phase that can be characterized in terms of the items defined in Figure 1 is called a precision flight task. To see in more detail the range of TASK, CONTROL, and EVALUATION, a comprehensive outline of tactical applications

is presented next. The items listed in the outline are generic characteristics that can be used to classify any particular precision flight task. This is given in Figure 2.

The classification of Figure 2 can be used in the following way: Given a flying qualities evaluation problem to be studied through the predictive analysis methods presented in the next Section, every aspect of the pilot's activity can be classified. Once the problem is fully described in these terms, the model can then be applied. In this way, the model constitutes a unified and comprehensive prediction and evaluation method for precision flying qualities as defined above.

In order to demonstrate the diversity of the flying qualities applications covered in this report, the classification characteristics of the list presented in the Introduction are given in Figure 3.

TASK

- Command or Pursuit Tracking
  - Random command
  - Discrete or deterministic command
  - Maneuvering target
  - Terminal control target
  - Finite tracking time
- Stabilization
  - Gaussian turbulence
  - Non-Gaussian turbulence
  - Aerodynamic disturbances
  - Pilot-induced disturbances
- Monitoring
  - Instrument scan
  - Cockpit chores

CONTROL

- Single-Axis Tracking
- Multiaxis Tracking
- Side Task (Tracking)
- Side Task (Diversion)
- Time-Varying Control
- Human Factors Effects
  - Perception
  - Motion cues
  - Controller actuation
  - Acceleration environment

EVALUATION

- Pilot Subjective Data
  - Cooper-Harper pilot ratings
  - Pilot comments
- Mean and rms Statistics
- Integral Average Error
- Statistics of Derived Performance Measures
  - Dive bombing error impact equation
  - Air-to-air gunnery miss distance estimation
  - Pilot rating estimators
  - Time-on-target, -on-glideslope, etc.
- Pilot Model Parameters
  - Compensation gain and lead
  - Task dwell fractions
  - Task mean control period
- Task Interference Effects
- Multi-Parameter Flying Qualities Evaluation

Figure 2. Generic Classification of Precision Task Components

CLASSIFICATION \ APPLICATIONS IN THIS REPORT	SINGLE-AXIS TURBULENCE STABILIZATION	TWO-AXIS TURBULENCE STABILIZATION	RELATIVE DISPLAY SENSITIVITY	VTOL HOVER	TWO-AXIS COMMAND TRACKING	TARGET TRACKING	CRITICAL TASK	PILOT RESERVE ATTENTION	STEP TARGET TRACKING	CONTROL SYSTEM LAG	COMPARISON OF TURBULENCE MODELS
TASK											
TRACKING COMMAND											
RANDOM COMMAND					X		X				
MANEUVERING TARGET						X					
DISCRETE MANEUVERING TARGET									X		
FINITE TRACKING TIME									X		
STABILIZATION											
GAUSSIAN TURBULENCE	X	X	X					X		X	X
NON-GAUSSIAN TURBULENCE											X
PILOT GENERATED DISTURBANCES				X		X					
CONTROL											
SINGLE-AXIS TRACKING	X				X			X	X	X	X
MULTIAXIS TRACKING		X	X	X	X	X	X			X	X
SIDE TASK (TRACKING)					X		X				
SIDE TASK (DIVERSION)						X		X			
TIME-VARYING CONTROL									X		
EVALUATION											
RMS STATISTICS	X	X	X	X	X	X	X	X	X	X	X
INTEGRAL AVERAGE ERROR					X						
DWELL FRACTIONS		X	X	X	X					X	X
MEAN CONTROL PERIOD				X	X						X
TIME-ON-TARGET									X		
TASK INTERFERENCE EFFECTS		X	X				X	X		X	X
VISUAL PERCEPTION EFFECTS		X		X							
MULTI-PARAMETER EVALUATION		X	X						X	X	X

Figure 3. Classifications of Applications in This Report

SECTION III

THE URGENCY DECISION PILOT MODEL

Section II was devoted to the definition and classification of precision piloted tasks. Before the Urgency Decision Pilot Model is presented, it is necessary first to define what pilot models are, and indicate exactly what aspects of pilot activity they are purported to model.

A. DEFINITION OF STATISTICAL AND DYNAMICAL PILOT MODELS

There are three main reasons why methods of analyzing piloted aircraft are of use: 1) to increase the likelihood that an aircraft being designed or developed has good flying qualities, 2) to improve or study the modification of existing aircraft, and 3) to aid in identifying and correcting specific flying qualities deficiencies. Flight test and flight simulation are also employed for these purposes, but analytical methods have several advantages. Large analytical surveys can be carried out to screen candidate aircraft at much lower cost than experimental methods, and in addition can lead to measurements that are difficult to obtain from piloted flight or flight simulation.

In order to understand how an analytical method can substitute for or reinforce experimental testing, consider a given precision flying qualities problem classified as discussed in Section II in terms of TASK, CONTROL, and EVALUATION. In the test program, the TASK and the EVALUATION parameters are assigned; the human pilot supplies the CONTROL. For an analytical pilot model — aircraft approach, the same TASK and EVALUATION parameters must be used, but a mathematical description of the CONTROL must be supplied. This CONTROL description is what is meant by a pilot model. Since the pilot is a self-adjusting and self-motivating part of the piloted aircraft, adjustment and operation methods must also be included in the pilot model — aircraft analysis method. One of the main topics of this report is the application of the Urgency Decision Pilot Model to a number of flying qualities problems, but in order to see how this model constitutes a comprehensive analysis method, the following definition is offered:

Definition: The Urgency Decision Pilot Model is a rule that, given a simulation model of an aircraft along with the pilot's TASK and an EVALUATION as defined in Section II, assigns the following three items:

1) The system configuration of multiaxis pilot CONTROL.
2) The method for adjusting the CONTROL model coefficients.
3) The method for obtaining the performance indices required by the EVALUATION.

In this way, the Urgency Decision Pilot Model can be thought of as a function that maps flying qualities problems into numbers that measure the performance of the pilot model — aircraft system. The usefulness of this method depends on its practicality and utility. More specifically, it will be shown that:

- The model is extremely easy to program and append to existing simulations.
- All nonlinearities and time-varying quantities can be modeled without resort to equivalent models.
- The Urgency Decision Pilot Model will assign a specific model for any combination of TASK and EVALUATION classified in Figure 2.
- The model is validated for a large number of TASK and EVALUATION generic descriptions as shown in Figure 3.

It is natural to compare the Urgency Decision Pilot Model with the frequency-domain and optimal control pilot models. The use of the time-history simulation context not only allows greater flexibility in the aircraft descriptions, but also as discussed next, allows the examination of many pilot decision and dynamic activities. These advantages are further enhanced by the ability to generate many kinds of performance measures that are based on inequality tests and nonlinear functions. These advantages are briefly summarized in Figure 4.

In order to see the advantages of this generality of the pilot model, it is necessary to discuss the extent of pilot activity that the models are intended to represent. From the above definitions it should be clear that the modeling is generated by the TASK and the EVALUATION, and depending on the problem at hand, the model may be either statistical or dynamical.

If the EVALUATION items refer only to statistics of the aircraft motions during the performance of the TASK, the model generates statistical data that predicts what actual piloted performance can be expected to result. In such problems, there is no

	TIME HISTORY URGENCY DECISION PILOT MODEL
PILOT MODEL	MODELS ALL FORMS OF ATTENTION ALLOCATION ACTIVITY ALONG WITH NONLINEAR PERCEPTION, CONTROLLER ACTUATION CHARACTERISTICS AND RAPIDLY CHANGING PILOT CONTROL STRATEGIES.
ERROR CRITERIA	EASILY HANDLES ALL CRITERIA INCLUDING ROOT-MEAN-SQUARE, ABSOLUTE ERROR, INTEGRAL TIME ABSOLUTE ERROR, ARBITRARILY WEIGHTED ERROR, TIME SPENT WITHIN LIMITS.
GROSS SYSTEM NONLINEARITIES	CAN ALWAYS DIRECTLY MODEL NONLINEAR AERODYNAMICS, EXOTIC CONTROL SYSTEMS, HUMAN FACTORS EFFECTS.
PROCESS	GAUSSIAN AND NONGAUSSIAN SUCH AS DISCRETE COMMANDS, "OPEN LOOP" MANEUVERS, REEVES OR JONES NONGAUSSIAN TURBULENCE.
DISCRETE MANEUVERS	COMMANDED TRAJECTORIES AND MANEUVERS CAN ALWAYS BE MODELED.
UNCORRELATED INPUTS	UNCORRELATED P, V, W, AND U GUSTS ARE EASILY GENERATED ALONG WITH UNCORRELATED MODELS OF PILOT REMNANT, BUFFET, GUN REACTION, AND SENSOR NOISE AS REQUIRED.
COMPUTING	INEXPENSIVE TO COMPUTE AND EASY TO PROGRAM FOR A LARGE VARIETY OF PROBLEMS.

Figure 4. Urgency Decision Pilot Model Advantages

concern about whether the pilot model actually represents the physical and logical processes that a human pilot actually adopts in his selected CONTROL. Such models are called <u>statistical</u>.

On the other hand, it frequently is of interest to examine how the pilot carries out the flight phase. For such problems, the EVALUATION selected by the flying qualities analyst will contain items relating to the pilot's compensation: demands of

competing tasks for his attention in terms of how long on the average he controls each, to what extent the tasks interfere with one another, and what margin of attention reserve the pilot has available for emergency operation. These evaluation items refer not just to the aircraft motions, but to numerically definable and measureable quantities that correspond to the pilot's actual physical and mental activity. Such models are referred to as dynamical even though they are exercised to produce statistical measures of pilot activity.

Such definition of statistical and dynamical can also be applied to specific programming components of the full multiaxis pilot model. If a component represents the physical activity of the pilot then the model can be used to examine the dynamic characteristics of that activity and will be called a dynamical pilot model component. If the programming only leads to good statistical predictions of the closed loop performance, then that part of the model is called a statistical pilot model component. In this way, the full models that are discussed later in this report consist of both dynamical and statistical model components.

If one wishes, for example, to evaluate how well a pilot will perform glide slope control using a small cathode ray tube (CRT) display, a statistical model could be used that injects noise to model visual perception limitations of the pilot. If the effects of visual perception limitations such as visual deadband on glideslope tracking are to be analyzed, then the deadband must be dynamically modeled using decision logic to represent whether or not the pilot and hence the pilot model observe the tracking errors. Dynamic modeling of pilot CONTROL is most important for multiaxis tracking tasks. The use of decision logic incorporated into the pilot models assigned by the Urgency Decision Pilot Model, References 1-3, is the model feature that will be most prominent in the application examples presented in this report.

B. PRINCIPLES OF HUMAN OPTIMALITY AND HUMAN DYNAMIC LIMITATIONS

The discussion above has been limited to the definition of pilot models and their dynamical and statistical attributes. It is the purpose of this Subsection to state the principles by which pilot model components are derived along with the way in which they are adjusted.

The most fundamental aspect of manual control concerns the performance of highly trained and motivated pilots. A large amount of data dating back many years supports the proposition that pilots perform in an optimum manner with respect to specified performance measures, subject to limitations of plant dynamics and human

capability. The exact interpretation of "optimum" depends on the context of the model. In frequency-domain models "optimum" is interpreted as optimum gain, lead, and lag for a continuous linear control compensation subject to an inherent human time delay and neuromuscular lag. In this case, model predictions are obtained by optimizing the model coefficients with respect to some performance measure based on tracking error. For continuous single-axis time-invariant tasks, frequency-domain methods can be used to validate these statistical models and show that not only rms tracking scores, but also gain and phase characteristics obtained through spectral analysis agree well between the model and the flight simulation data.

Further refinement in modeling the "optimum" performance of the human pilot was made with the development of the optimal control approach to pilot modeling. Optimal control techniques are employed to calculate the optimal performance with respect to quadratic performance measures. Again, this approach agrees well with flight test and simulation data from which the human pilot's dynamics have been recovered using parameter identification methods. These frequency-domain describing-function and optimal control models are described in References 4 and 5.

In both the frequency-domain describing-function and the optimal control pilot models, the optimization of the model is through the choice of coefficients that determine the optimum linear control compensation. In other words, the optimum compensation is obtained by choosing from a set of linear functions. When it comes to the consideration of TASKS that consist of a number of tracking tasks, instrument scanning, and other chores, the dynamic description of the pilot becomes much more complicated than the linear continuous models.

For such general problems, limitations exist in the pilot's capacity to observe many quantities, calculate appropriate control corrections, and carry out the control procedures simultaneously. This forces the pilot to adopt a method of attention sharing in which he passes from task to task, devoting his attention where it is most required. In this way, decision logic and measures of task urgency become involved in the model description of CONTROL. Much data presented in Section IV indicates that these measures of task urgency are nonlinear in nature, thus the optimization of the pilot model must be made over a more general set of functions than linear continuous compensation. The span of this set of functions is yet to be determined, but indications from available flight simulation and model data justify the following principle:

Principle of Human Optimality Given a precision flight TASK and EVALUATION, the human pilot with training and motivation will adopt an optimized CONTROL composed of one or more of the following:

1) Linear piecewise-continuous compensation of specific state variables.

2) Nonlinear piecewise-continuous compensation of specific state variables.

3) Discrete control inputs including "no operation" and "control hold."

4) Pulse or bang-bang control.

5) Instrument scanning and other required activities which are selected according to decision processes based on subjective measures of task urgency, and available control strategy.

To utilize this principle as stated for the human pilot as a means of suggesting the forms of pilot models along with their rules of adjustment and use, it is necessary to examine the restrictions that limit human performance. The above principle implicitly incorporates these restrictions, for the trained and motivated human has adopted ways of minimizing these limitations:

Principle of Human Dynamic Limitations Given a precision flight TASK and EVALUATION, the human CONTROL contains at least the following limitations:

1) Limited visual resolution.

2) Visual position and rate thresholds.

3) Visual fixation time.

4) Visual image perception delay.

5) Proprioceptive perception threshold and resolution.

6) Delay during information processing that includes all decision, estimation, and control correction generation.

7) Limited motor information channel restricting simultaneous control output.

8) Neuromuscular dynamics, response time, and resolution.

The implementation of these two principles is best done by means of time-history simulation in order to preserve for examination the flying qualities effects of the pilot's numerous nonlinearities, time-varying compensation, and decision logic. To

this end the Urgency Decision Pilot Model has been developed along the lines of dynamic modeling as defined above. The specific model components that achieve this will be presented in the next few Subsections.

C. SINGLE-AXIS PILOT MODELS

Although this Subsection will consider only precision tasks in which the pilot is tracking only one variable, the information presented here will be applicable to the complete model. (The urgency decision multiaxis model will perform tracking tasks sequentially, each of which can be controlled by single-axis models during their allocated control periods.)

As pointed out above, there are two kinds of pilot model components, dynamical and statistical. The importance of dynamic components depends on the nature of the TASK and the EVALUATION; for many problems it is sufficient to employ statistical components. This is the case for many single-axis problems as well as for single-axis compensations employed in the modeling of a multiaxis CONTROL.

For single-axis problems where the EVALUATION is concerned with the statistics of the aircraft's performance — target tracking error or excursions from a commanded attitude in turbulence, for example — describing-function pilot models have been shown to be accurate. Perhaps the best general reference is the survey by McRuer and Krendel, Reference 4, with which the reader who intends to apply the methods of this report should become acquainted. Data to support the hypothesis that describing-function pilot models are accurate predictors of aircraft motion statistics is presented frequently in Section IV whenever single-axis continuous tracking data is discussed.

It is the authors' belief that dynamic consideration of single-axis flying qualities is of importance. Much simulation data indicates that in multiloop control the pilot may operate in a time-varying manner, probably involving decision logic. This possibility and others relating to pilot subjective evaluation have been considered by Ralph Smith, Reference 6. It is likely that his approach to single-axis continuous problems will provide important dynamic models that can be incorporated into the Urgency Decision Pilot Model presented in this study. Since the topics covered in Sections IV-VII are concerned mainly with statistical tracking performance EVALUATION of the multiaxis task, there is no penalty for the use of describing-function compensation on each task, and in fact, this is the practical way to study these problems. This assumption that the statistical gain-lead-delay compensation components do not significantly interfere with the dynamic multiaxis components is consistent with the data presented in Sections IV — VII.

There are three parts to the single-axis pilot model to be discussed: visual and motion perception effects, the generation of the control command, and the actuation of the controller.

Visual and Motion Perception Effects

Statistical models for visual and proprioceptive perception effects are frequently employed. This is done by adding Gaussian white noise to the pilot model input, which is the tracking error. The amount of this noise, which often is taken to include controller and processing noise, varies with the problem. If the display or the controller has poor resolution for the pilot, then the amount of this noise, called remnant in most references, is significant and must be calibrated by an experimental procedure, or estimated from existing data. If a pilot model has been validated for the problem, then the remnant level can be estimated by matching the model to the data.

There is another method for remnant calibration that is useful where pilot remnant is the only disturbance. The method is essentially Archimedean, and the way it was developed is as follows: If a pilot's actual remnant were an accessible quantity, the remnant amplitude could be altered. Thus one could determine the unknown remnant level simply by turning it down until the system error vanishes; the amount of reduction would be equal to the original remnant. A second glance reveals that one doesn't need to turn the pilot's remnant down — the slope of the line and the point of the unaltered performance will suffice to determine the intercept at zero tracking error. At this point it becomes apparent that the pilot's remnant can be increased experimentally by adding noise of the right spectral shape to his output, then by measuring the change in tracking performance, the slope can be found. This method is diagrammed in Figure 5. Actual data obtained by this method is reported in Reference 1.

Where visual error and error rate indifference thresholds dominate, these thresholds can be programmed into the model as logical tests. If ϵ represents error and $\dot{\epsilon}$ error rate, then the visual model is represented by the following test based on the threshold values ϵ_o and $\dot{\epsilon}_o$:

$$\hat{\epsilon}: \begin{cases} \text{If } \epsilon > \epsilon_o, \text{ then } \epsilon \text{ is observed by the model.} \\ \text{If } \epsilon \leq \epsilon_o, \text{ then no error is observed by the model.} \end{cases}$$

$$\hat{\dot{\epsilon}}: \begin{cases} \text{If } \dot{\epsilon} > \dot{\epsilon}_o, \text{ then } \dot{\epsilon} \text{ is observed by the model.} \\ \text{If } \dot{\epsilon} \leq \dot{\epsilon}_o, \text{ then no error rate is observed by the model.} \end{cases}$$

where "observed by the model" will be made clear shortly. An example of error threshold is presented in the discussion of the validation of the model, Section IV B. If the display is such that there are significant errors in reading or estimating the correct value, then a statistical distribution of error can be added to the value observed by the pilot model; the standard deviation of the reading error must be experimentally determined or estimated from existing data.

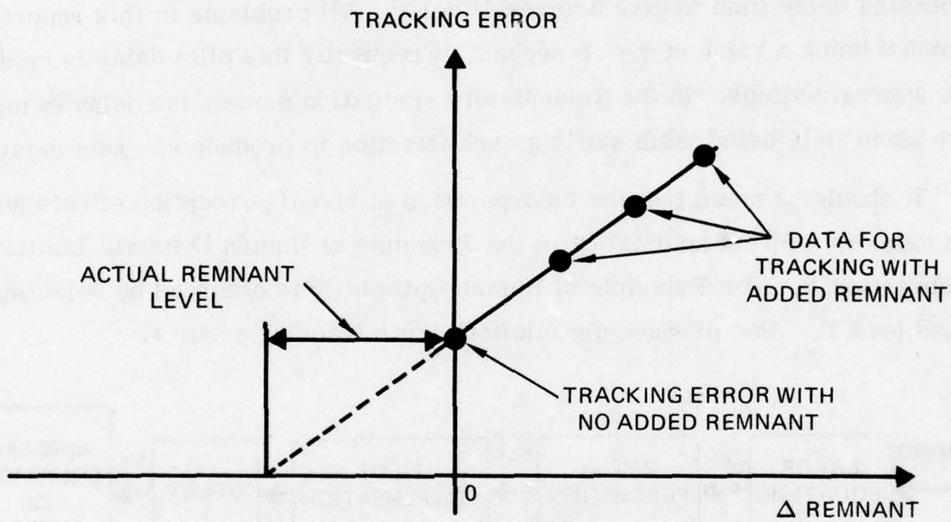

Figure 5. Remnant Model Calibration Method

The dynamic characteristics of physical motion can also be incorporated into the model in a manner similar to the visual perception effects. Reference 7 presents motion cue models first identified by Young. There is much current research into motion effects; when complete it should furnish the components to extend the model presented here to include visual, proprioceptive, and kinesthetic cues.

Pilot Control Compensation

The discussion presented here will consider statistical models of a particularly simple kind, the fixed-form gain-lead-delay describing function model. If $\hat{\epsilon}$ represents observed ϵ, and $\hat{\dot{\epsilon}}$ represents observed $\dot{\epsilon}$, then the basic model is of the form shown in Figure 6. It defines a single-loop control command δ_ϵ at time t:

$$\delta_\epsilon(t) \equiv (\text{delay } \tau) \left\{ K_\epsilon \left(\hat{\epsilon}(t) + T_{L_\epsilon} \hat{\dot{\epsilon}}(t) \right) \right\}$$

where K_ϵ = pilot model gain

T_{L_ϵ} = pilot model lead time constant

τ = pilot model delay time constant

For a single-loop task, this is the complete model for a large variety of problems. However, for plants consisting of gain alone, it is necessary to include pilot lag compensation. In the present model, neuromuscular lag has been lumped together with processing delay time to give an overall delay. All problems in this report have been computed using a value of $\tau = .3$ second. Frequently this pilot delay is modeled using Padé approximations. In the time-history simulation model, the delay is modeled more accurately using table shifting each iteration to produce an exact delay.

It should be noted that the incorporation of visual perception effects and the pilot time delay is a direct application of the Principle of Human Dynamic Limitations stated in Subsection B. The Principle of Human Optimality is enforced by selecting the gain K_ϵ and lead T_{L_ϵ} that produce the minimum rms tracking error ϵ.

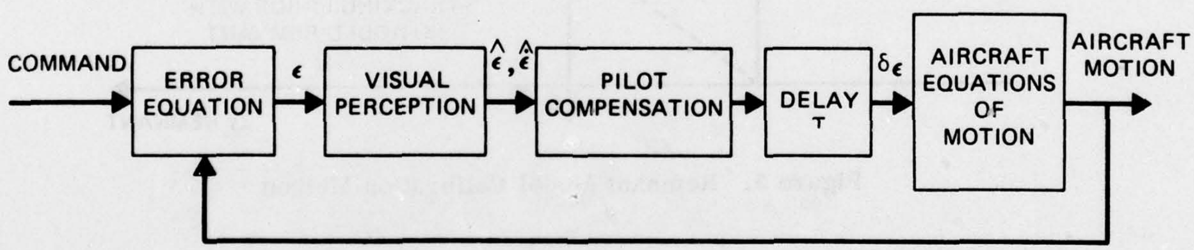

Figure 6. Single-Loop Pilot Model

In order to present the essentials of a multiloop compensation model, consider a heading command task in which the pilot is subject to visual threshold effects of magnitudes ψ_o and ϕ_o. The system configuration is shown in Figure 7.

The pilot model equations are then given by:

$$\text{If } \psi_e > \psi_o,\ \hat{\psi}_e = \psi_e. \quad \text{Otherwise } \hat{\psi}_e = 0$$

$$\text{If } \phi > \phi_o,\ \hat{\phi} = \phi. \quad \text{Otherwise } \hat{\phi} = 0$$

$$\delta a = (\text{delay } \tau) \left\{ K_\psi \left(\hat{\psi}_e + T_{L_\psi} \hat{\dot{\psi}} \right) + K_\phi \left(\hat{\phi} + T_{L_\phi} \hat{\dot{\phi}} \right) \right\}$$

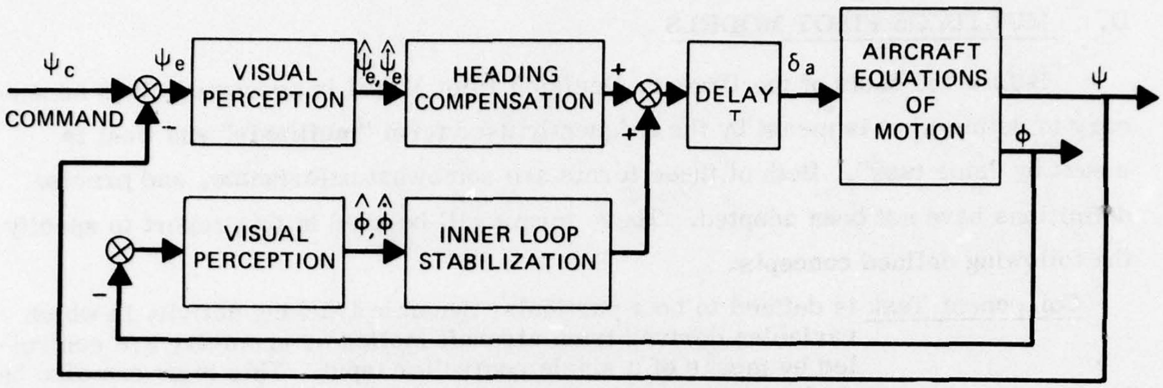

Figure 7. Heading Command Task

By the Principle of Human Optimality, the gains K_ψ and K_ϕ along with the leads $T_{L\psi}$ and $T_{L\phi}$ are adjusted to produce the minimum rms ψ_e for an "acceptable" amount of bank angle rms ϕ. Other examples of multiloop compensation can be found in Subsections IV C and IV F.

Controller Actuation Effects

Remnant models for controller actuation effects can be used to account statistically for imprecise positioning of the stick, rudder, throttle, or other controllers. Since pilot induced oscillation (PIO) depends on stick force breakout and gradient forces, it is important to provide for dynamic modeling of the neuromuscular-controller system. In these problems, perceived controller position is subject to error, threshold, and hysteresis effects that can be directly implemented in a manner similar to the incorporation of visual effects. In the examples considered in this report, controller effects have been minimized by using light breakout and gradient forces along with sensitivities selected by the subject using the controller.

Generalization of the Single-Axis Model

The above brief account of the statistical single-axis model is intended for use in flying qualities problems where the EVALUATION consists mainly of performance statistics. Since the context of the model is time-history simulation, advances in understanding of the dynamic nature of human compensation can be incorportated into the model in a way that preserves all decision and nonlinear aspects of human control.

D. MULTIAXIS PILOT MODELS

Before the basis of the Urgency Decision Pilot Model is presented, it is necessary to define what is meant by the frequently used term "multiaxis" and what is meant by "side task". Both of these terms are somewhat unfortunate, and precise definitions have not been adopted. These terms will be used in this report to specify the following defined concepts:

Component Task is defined to be a particular dynamic tracking activity in which variables derived from aircraft motion or geometry are controlled by means of a single controller input. This term can also be applied to any other required physical activity of the pilot.

Multiaxis Task is defined to be a collection of at least two component tasks. If a complete description of the piloted mission is encompassed by the multiaxis task, then a complete TASK has been described.

There is frequent mention of "side task" in current literature. The following definition may not cover all usage of this term, but will be adhered to in this report:

Side Task is defined to be a component task whose performance is not measured or optimized by an EVALUATION requirement. Performance is instead evaluated in terms of maintaining control, performing the task when no other multiaxis task component requires attention, or other non-metric or subjective conditions.

The objective now is to postulate the nature of the pilot's CONTROL for a multiaxis TASK, and to present a method for implementing this CONTROL in the pilot model.

That a pilot's performance of a component task is degraded when performed as part of a multiaxis task has been widely recognized. There have been several attempts to demonstrate statistical multiaxis pilot models, which do not attempt dynamically to allocate model attention, but rely on several methods to degrade the compensation modeled for each task with respect to single-axis control. These statistical methods are:

1) Increased time delay to account for periods of inattention.
2) Decreased model gain to a specified sub-optimum value.
3) Filtered white Gaussian noise injection.

Although References 8 and 9 show that these statistical models prove to be accurate for certain classes of problems, there are advantages to using dynamic models of attention allocation. It will be demonstrated in the applications detailed in

Section IV that the following benefits are obtained using the dynamic allocation of attention using the Urgency Decision Pilot Model:

1) Total time allocated to each task is automatically generated and predicted by the model.
2) Mean control period for each component task is directly predicted by the model.
3) The influence of any variation in aircraft dynamics, control system, TASK, or EVALUATION on any performance statistic — including allocation time and mean control period of each component task — can be predicted.
4) Flying qualities effects concerning the interference of component tasks can be predicted.

The basis of the urgency decision dynamic allocation of pilot attention can be seen by observing pilot stick activity during a multiaxis task that requires lateral and longitudinal tracking control. One of the first reports to identify exclusive attention allocation, Reference 10, was written by one of the authors of this report in 1966. It was this study that first considered allocation models based on measures of task urgency. The exclusive allocation of attention was noted during simulation flights of a difficult VTOL hover problem. A crossplot of lateral and longitudinal stick commands clearly showed that the pilot flew the simulation by performing a sequence of exclusive lateral and longitudinal control episodes. Figure 8, reproduced from Reference 10, was obtained during a simulator flight test and demonstrates this sequential control behavior.

This 1966 study attempted to model the VTOL hover task by means of the following model characteristics:

1) Generation of the model dynamics by real-time simulation using analog computers.
2) Continuous generation of urgency functions as measures of relative need for control action. These functions were nonlinear functions of the aircraft state variables.
3) Switching control between the two component tasks according to the magnitude of the urgency functions.
4) There was no external disturbance other than pilot induced errors and control inattention. The induced errors consisted of inadvertent control crossfeed and remnant.
5) The use of gain-lead-delay pilot model components for the compensation during each control episode.

There were two limitations to the analysis presented in Reference 10: analog computer resolution and accuracy which were poor compared to those of digital computers, and inability to develop the correct structure to incorporate error rate

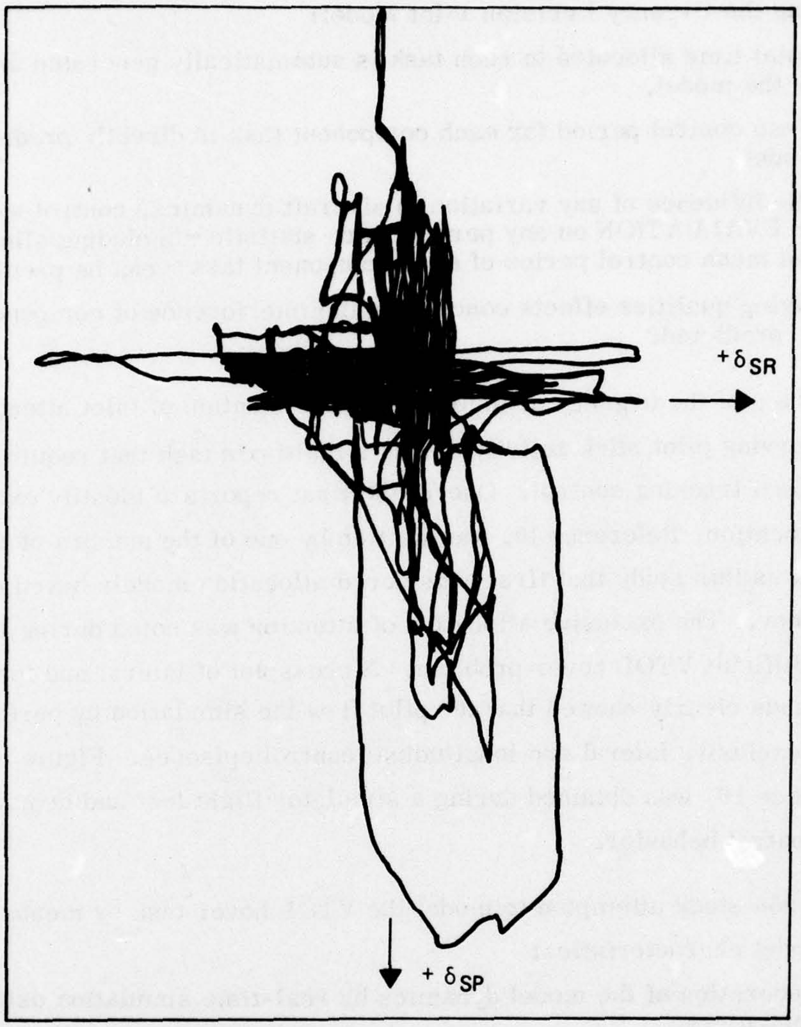

Figure 8. Demonstration of Pilot Attention Allocation by Cross Plot of Lateral and Longitudinal Stick Commands During Hover Task

terms in the urgency functions, again the result of the computer limitation. A correct and complete account of this VTOL hover problem using the model presented in this Section can be found in Subsection IV C.

Urgency Decision Pilot Model Postulates

There are three postulates that characterize the Urgency Decision Pilot Model:

1) Exclusive Attention Allocation

Control changes are initiated on only one component task at a time. No two component tasks are performed simultaneously.

2) <u>Urgency Decision</u>

Attention is allocated according to the greatest of the urgency decision measures. The form of these measures is postulated below. The component task with the greatest urgency is controlled; the control inputs to the other tasks are either held constant or set to trim.

3) <u>Compensation</u>

The compensation of a component tracking task is identical in form to the compensation for that component task under continuous control as presented in Subsection III B. The optimization of the pilot model coefficients is performed while the complete multiaxis model is operating.

These postulates were first developed during the VTOL hover problem discussed above, and further attempts to use the urgency decision model in other applications have led to the conclusion that these postulates apply with great generality. The presentation of other applications is the objective of Section IV.

To present the postulated form of the urgency function, consider a single-loop component tracking task. The third postulate states that the compensation for this task is of the form presented in Subsection III B. It remains to define the form and the adjustment of the urgency functions. Let ϵ be the tracking error corresponding to the component task. Then the urgency is a measure of how bad the tracking error is at a given moment, weighted by whether the error is increasing or decreasing. If the error is decreasing, little or no control correction may be warranted; but if the error is increasing, the situation may be critical. For this reason, the magnitude of the urgency function is reduced if the error is decreasing and increased if the error is getting larger.

The simplest function U_ϵ that takes this into account is given by the following formula in terms of observed error $\hat{\epsilon}$ and error rate $\hat{\dot{\epsilon}}$:

$$U_\epsilon = \left| \alpha_\epsilon |\hat{\epsilon}| + \beta_\epsilon \frac{\hat{\epsilon} \quad \hat{\dot{\epsilon}}}{|\hat{\epsilon}|} \right|$$

$$= \left| \alpha_\epsilon |\hat{\epsilon}| + \beta_\epsilon \operatorname{sign}(\hat{\epsilon})\, \hat{\dot{\epsilon}} \right|$$

The coefficients α_ϵ and β_ϵ in this expression are positive numbers that are either dictated by the task description, or are subject to optimization along with the compensation coefficients. The specific method for adjusting and optimizing the urgency functions is illustrated in the demonstrations of the Urgency Decision Pilot Model in the next Sections.

Decision Delay and Parallel Compensation

There are two further dynamic aspects to the multiaxis urgency decision model that are essential to the applications detailed in Section IV, but these are not nearly as firmly established as the above postulates.

The first aspect concerns implementation of the attention diversion algorithm. It is natural to expect that the human pilot cannot instantaneously divert attention to another task. The time delay involved, called the urgency time delay, has been uniformly employed in all calculations of this report with a value of .15 second. In most cases, the omission of this delay leads to model calculations that do not agree well with simulation data. Beyond this, nothing is known about the accuracy of this constant, or whether this value is independent of TASK.

The second aspect involves the way in which the model shifts its attention and calculates its control compensation. For each dynamic component task, the model computes a control input generated from observed error and error rate information. This control input is then delayed by the .3 second human compensation delay. It is important to consider whether the delay table of a task control compensation is zeroed when the task is abandoned, or whether just the output of the table is set to zero. In the first case, return to the task would require the sum of the urgency delay together with the human compensation delay – a total of .45 second – before control activity is resumed. Simulation data indicates that such a large delay is not the case. Model computations in which the compensation delay tables are zeroed for abandoned tasks support this since it leads to performance predictions that are badly degraded. The alternative is to assume that the pilot generates estimates of his required control inputs simultaneously, but is unable to effect parallel controller actuation. This is the basis of the seventh item of the Principle of Human Dynamic Limitations which postulates a limited motor information channel that restricts simultaneous control output. Figure 9 shows the mechanization of a two-axis tracking task consisting of a single-loop task (1), a multiloop task (2), and a diversion side task.

Incorporation of Side Tasks

There are two classes of side tasks, diversion and dynamic. In both cases attention is shifted to the side task when the side task urgency exceeds the urgency of all other tasks; the classes differ in how the urgency is computed. In the case of the dynamic side task, the urgency is computed as for any other tracking task. However, the

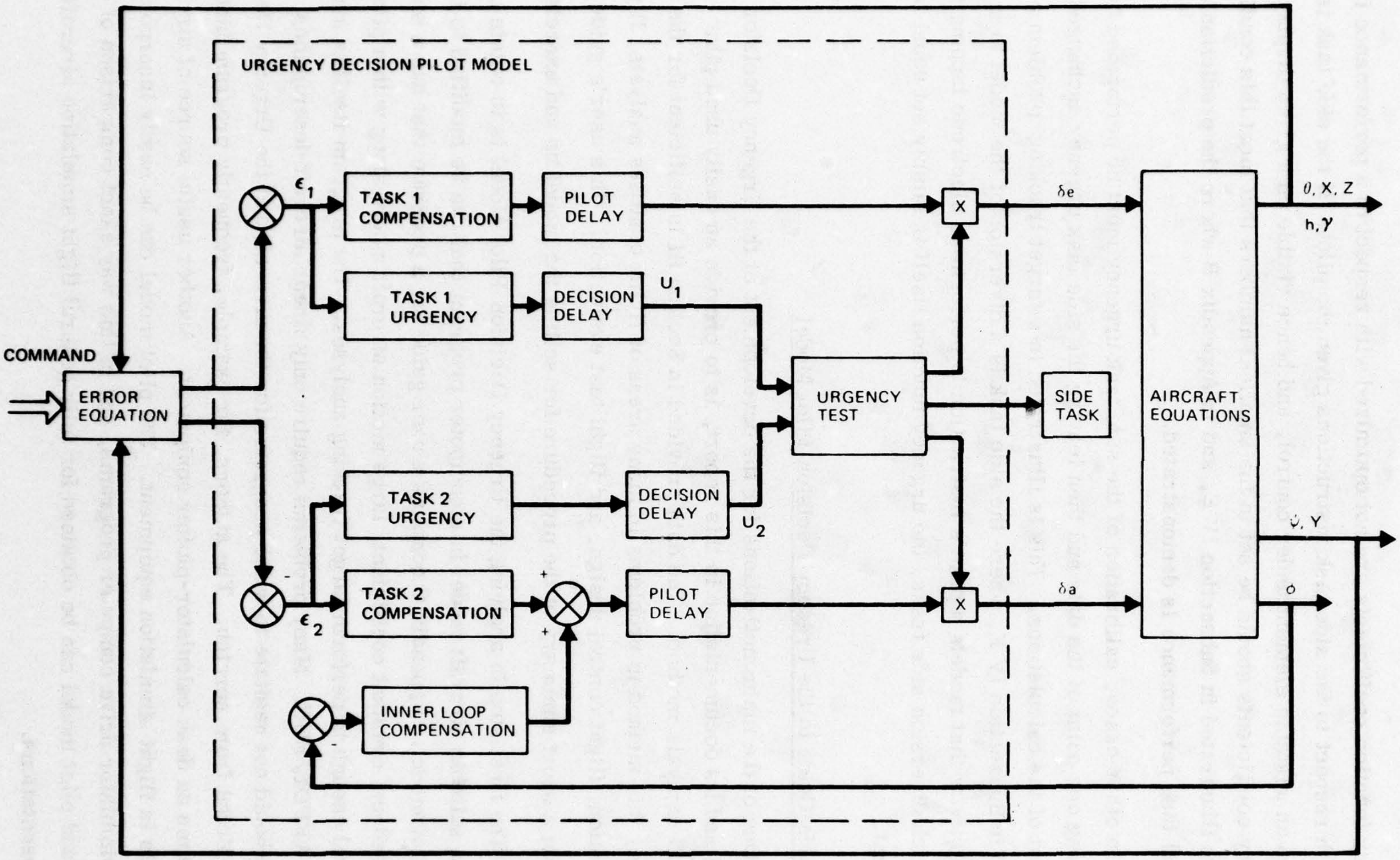

Figure 9. Urgency Decision Pilot Model Structure

urgency function coefficients are not optimized with respect to a performance index, but with respect to the side task instructions given the pilot. If the side task is simply to keep an unstable element under control, and hence visible on a given display, the urgency coefficients should be set to the smallest numbers that meet this condition. This is illustrated in Subsection IV E, and in Appendix B where the prediction of critical task performance is demonstrated.

In other cases, calibration of the side task urgency must be performed by matching one point of the data and then leaving the side task urgency unchanged for the rest of the calculations. This is illustrated in a target tracking problem presented in Subsection IV F, where the side task is a diversion of the model to a state of no activity that models a pilot's instruction to perform an electrode tapping task. For such diversion side tasks, the urgency function itself is simply set equal to a constant.

A User's Guide to the Urgency Decision Pilot Model

One of the main motivations for the development of the Urgency Decision Pilot Model and its documentation in this report, is to provide an easily used pilot - aircraft analysis method. The data provided in Section III is sufficient for the reader to apply this method to problems in many areas of flying qualities analysis, flight simulation, flight control design, and flight test evaluation. This user's guide will provide a short summary of the procedure for setting the model up and exercising it.

The first step in applying the Urgency Decision Pilot Model is to obtain or produce a suitable aircraft model in a computer program that can be modified to include the pilot model. Appendix C contains a user guide for a program that has a six degree-of-freedom, constant coefficient, large motion aircraft model along with a pilot model general enough to perform target tracking analyses. The program itself is available from AFFDL/FGC. Many problems require only linear aircraft descriptions, and the user should not hesitate to write programs for the aircraft and the Urgency Decision Pilot Model from scratch. The authors, for example, frequently program independent problems on desk calculator-plotter equipment. Another useful source of aircraft models is flight simulation equipment. The pilot model can be easily incorporated into simulator drive computer programs, and in this way exact comparison of human pilot and pilot model can be obtained for fully general flight simulation aircraft representations.

If the reader will consult the demonstrations of Section IV and V, he will see that it is a simple matter to set the model up for any particular problem that falls into the classification of Section II. Briefly the steps are as follows:

1) Identify the complete TASK that is to be studied, develop an analytic description of it, and model the TASK commands or disturbances.

2) Identify each component task, including dynamic and diversion side tasks.

3) Determine if perception models are relevant to the problem, and if so produce a description of them.

4) Mechanize a representation of all component task tracking errors and error rates; and, using the perception models, calculate the observed errors and error rates.

5) For each component tracking task, program the gain-lead-time delay compensation.

6) Program the urgency functions and the urgency function delays.

7) Program the urgency test logic: the output of all compensation time delay tables except the one for the task with the greatest urgency is set to trim for stabilization tasks about trim values; in all other cases, the compensation is held at its last value until the associated urgency again becomes greatest.

8) Program all EVALUATION data items including tracking error statistics, dwell fractions and times, time-on-target defined by allowable error and other relevant items.

9) Optimize the compensation gain and lead of each component dynamic task in a single-axis mode by setting the other urgency coefficients temporarily to zero.

10) Using the full model, optimize or calibrate the urgency functions. This may be done as illustrated in Section IV A, B, and F.

11) Check by perturbation the optimization of the compensation coefficients. It is common that the single-axis optimum gains may be too high, and the leads too low.

12) Using the optimized model, exercise the pilot — aircraft model to obtain data in the same manner that it is obtained in flight test or flight simulation testing.

SECTION IV

PREDICTION OF PILOTED AIRCRAFT PERFORMANCE

Although the full pilot model as postulated in the previous section may appear unwieldy, its application to specific problems is simple and direct. To illustrate both the versatility and the utility of the multiaxis time-domain analysis method, a number of demonstrations will be presented next. Each is supported by agreement with flight simulation data, and several new results of importance to flying qualities research are also discussed.

A. ATTITUDE STABILIZATION IN TURBULENCE

It is natural to inquire about applications of the pilot model to representative tactical fighter dynamics. Attitude stabilization in the presence of low-level turbulence is an almost ever-present flying qualities consideration. A study of the dynamics of this task will serve as a guide to how the model is set up and exercised. This problem will be discussed first with aircraft descriptions that emphasize display and task interference aspects of the multiaxis control. Validation data obtained using the fully general YF-17 aircraft model as mechanized on the Northrop moving-base flight simulator will be presented in the next Subsection.

There were four important aspects of this problem to be investigated:

1) Accuracy and standardization of the method.
2) The effects of attention sharing on pilot compensation.
3) The effects of relative display gains.
4) Task interference effects.

In order to do this, two lateral and three longitudinal tactical aircraft linear descriptions were employed. Figure 10 shows the linear equations of motion used to compute the aircraft dynamics, and Table 1 gives the dimensional stability derivatives using primed notation, as defined in the List of Symbols.

$$\dot{w} = \frac{1}{1 - Z_{\dot{w}}}\left(u_o + Z_q\right) q + Z_{\delta e}\ \delta e + Z_w\left(w + w_g\right)$$

$$\dot{q} = M_{\dot{w}}\ \dot{w} + M_q\ q + M_{\delta e}\ \delta e + M_w\left(w + w_g\right)$$

$$\dot{\theta} = q$$

$$\dot{r} = N'_r\ r + N'_p\ p + N'_{\delta a}\ \delta a + N'_{\delta r}\ \delta r + N'_{\beta}\left(\beta + \beta_g\right)$$

$$\dot{\beta} = Y^*_p\ p - r(1 - Y^*_r) + \frac{g\phi}{u_o} + Y^*_{\delta a}\ \delta a + Y^*_{\delta r}\ \delta r + Y_v\left(\beta + \beta_g\right)$$

$$\dot{p} = L'_p\ p + L'_r\ r + L'_{\delta a}\ \delta a + L'_{\delta r}\ \delta r + L'_{\beta}\left(\beta + \beta_g\right)$$

$$\dot{\phi} = p$$

Figure 10. Equations of Motion

In this way a matrix of six aircraft descriptions was obtained as shown in Figure 11.

LONGITUDINAL \ LATERAL	A	B
1	1A	1B
2	2A	2B
3	3A	3B

Figure 11. Matrix of Aircraft Configurations

To isolate attention diversion effects for study in this example, visual perception and controller effects were minimized. The flight simulation was performed at Northrop using a fixed-base facility. The dynamics were generated digitally, the subject sat in a chair fitted with a side-arm controller, and the display was presented to him on a large CRT.

The simulation display consisted of a bright dot against a dimly illuminated background grid with prominent vertical and horizontal center lines as shown in Figure 12. The actual scaling of the dot displacement for each test point was determined experimentally by going to the most sensitive gain settings K which would accommodate all dot excursions. These μ and α scalings resulted in a dot displacement of αK centimeters per degree of bank angle and μK centimeters per degree of pitch angle.

TABLE 1. STABILITY DERIVATIVES FOR ATTITUDE STABILIZATION IN TURBULENCE

LONGITUDINAL DERIVATIVES

	1	2	3
Z_w	-1.3	-1.3	-1.3
$Z_{\dot{w}}$	0.0	0.0	0.0
M_w	-.004	-0.008153	-.003
$M_{\dot{w}}$	-8.103×10^{-6}	-8.103×10^{-6}	-8.103×10^{-6}
Z_q	-4.596	-4.596	-4.596
M_q	-1.0	-1.5	-2.0
$Z_{\delta e}$	72.023	72.023	72.023
$M_{\delta e}$	-10.503	-10.503	-10.503
u_o	718.0	718.0	718.0

LATERAL DERIVATIVES

	A	B
N'_r	-1.5	-1.5
N'_p	0.00705	0.00705
$N'_{\delta a}$	0.0352	0.0352
N'_β	2.0	3.0
Y_v	-0.5002	-0.5002
L'_p	-1.0	-1.0
L'_r	0.4045	0.4045
$L'_{\delta a}$	2.023	2.023
L'_β	-29.06	-29.06

All other derivatives are zero.

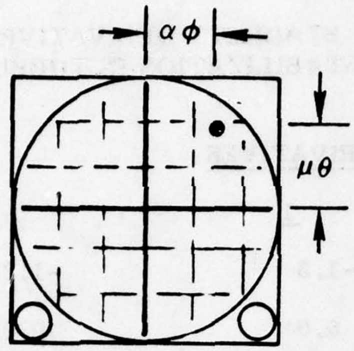

Figure 12. Two-Axis Flight Simulation Display

Provision was made to simulate with the ratios of μ and α given in Figure 13.

μ	α	Task
0	1	Continuous Lateral Only
8	1	Two axis, $\mu/\alpha = 8$
16	1	Two axis, $\mu/\alpha = 16$
1	0	Continuous Longitudinal Only

Figure 13. Display Ratios Tested

The pilot was instructed to keep the dot as close to the center of the screen as he could for each given display ratio. As this μ/α ratio is increased from zero (continuous lateral tracking), the pilot was forced to pay greater and greater attention to the longitudinal task. In this way, the μ/α ratio greatly influences the way in which the pilot allocates his attention between the lateral and longitudinal tracking tasks. The pilot optimizes his performance with respect to the distance of the dot from the center of the scope. This is called the radial tracking error, denoted by $r(\phi, \theta)$, and is given by

$$r(\phi, \theta) = \sqrt{(\alpha\phi)^2 + (\mu\theta)^2}$$

The task proved difficult to fly, and about ten hours were required for asymptotic training. Data were collected for test periods of 30 seconds, and simulation sessions were held to two hours maximum to avoid fatigue effects. The turbulence simulation used Dryden spectra obtained by filtering digitally generated Gaussian white noise as specified in MIL-F-8785B, where an airspeed of 718 fps and an altitude of 1750 feet

were used. In order to diminish low-frequency effects during the short test periods, the gusts were precomputed and the sequence adjusted to zero mean and 10 ft/sec rms intensity. The hand controller had light breakout and gradient forces; both the sensitivity and the polarity were selected by the subject.

With this description of the simulation complete, it is now possible to apply the generalized pilot model as given in Section III. Figure 14 shows the multiaxis pilot-aircraft control configuration. Since the high-frequency turbulence stabilization task requires no pilot lag compensation, only a gain and lead must be selected for each axis.

The compensations are simply gain, lead, and delay describing-function models. Expressed in terms of the familiar s-plane notation these are:

$$\delta a = [K_\phi (T_{L_\phi} s + 1) e^{-\tau s}] \phi_e$$

$$\delta e = [K_\theta (T_{L_\theta} s + 1) e^{-\tau s}] \theta_e$$

In terms of time-domain notation they become:

$$\delta a = (\text{Delay}\ \tau) \left\{ K_\phi (\phi_e + T_{L_\phi} \dot{\phi}_e) \right\}$$

$$\delta e = (\text{Delay}\ \tau) \left\{ K_\theta (\theta_e + T_{L_\theta} \dot{\theta}_e) \right\}$$

However, since commanded ϕ and θ are identically zero,

$$\dot{\phi}_e = \frac{d}{dt} (\phi_c - \phi)$$

$$= -\dot{\phi}$$

$$= -p$$

Similarly

$$\dot{\theta}_e = -q$$

Thus, for this problem, the error rate lead terms can be mechanized by numerical differentiation or by use of attitude rate terms from the aircraft equations of motion.

The pilot delays are simply mechanized by shifting a table of values once each iteration. Padé approximation formulas need never be used.

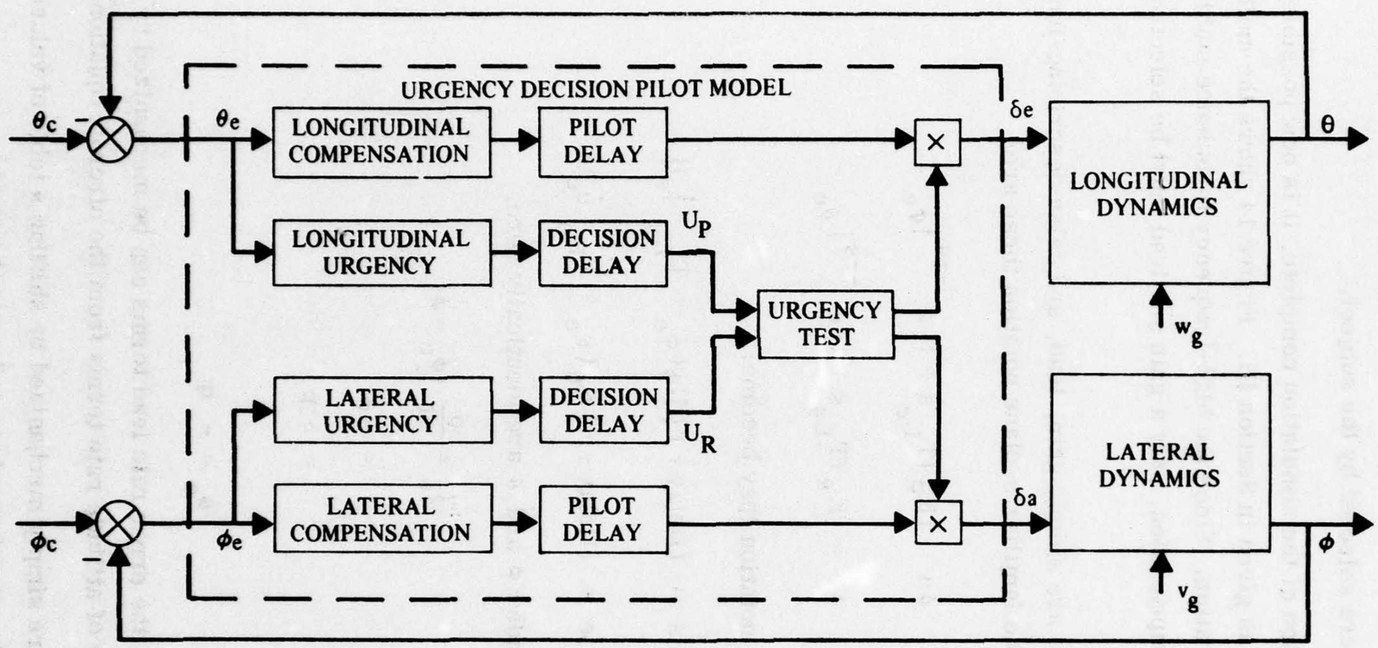

Figure 14. Control Configuration for Turbulence Task

The digital mechanization for the compensation is shown in Figure 15.

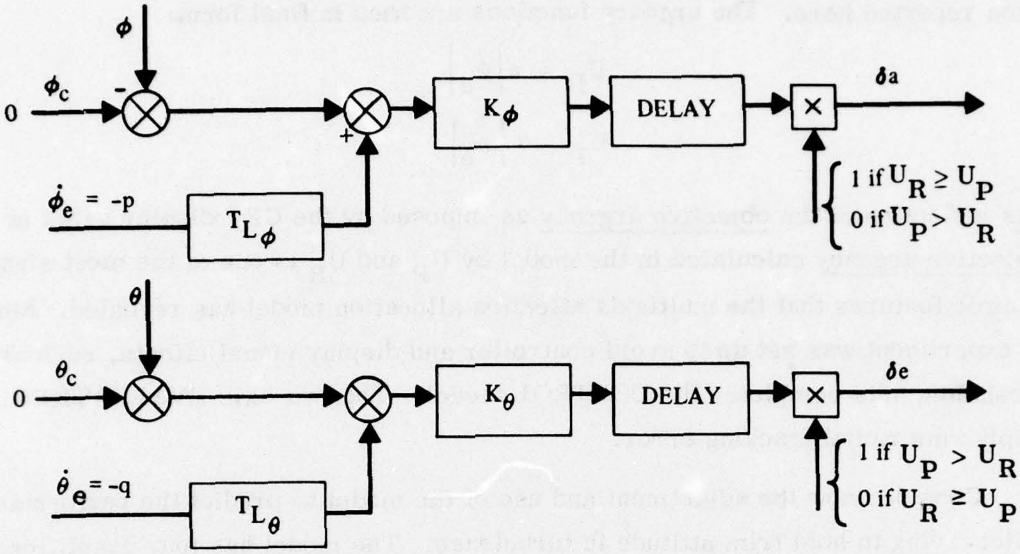

Figure 15. Lateral and Longitudinal Pilot Compensation for Attitude Stabilization in Turbulence

A pilot delay of 0.3 sec was adopted, and U_P and U_R are delayed by 0.15 sec. The urgency test logic becomes:

$$\begin{cases} \text{If } U_R \geq U_P \text{ then } \delta_e = 0 & \text{and lateral axis controlled} \\ \text{If } U_R < U_P \text{ then } \delta_a = 0 & \text{and longitudinal axis controlled} \end{cases}$$

For this problem, the optimum control requires the stick command of the axis not controlled to be returned to trim, in this case zero. The only part of the model not yet discussed is the form and adjustment of the urgency functions for each axis. Their general form is given by

$$U_R = \left| \alpha \left| \phi_e \right| + \beta \frac{\phi_e}{|\phi_e|} \dot{\phi}_e \right|$$

$$U_P = \left| \mu \left| \theta_e \right| + \nu \frac{\theta_e}{|\theta_e|} \dot{\theta}_e \right|$$

where β and ν are often zero in single-loop control problems, a fact which was easily verified in this case by perturbing these quantities about zero. The use of the symbols μ and α for both the display gains and the urgency coefficients will not cause any confusion, for the display weighting is exactly accounted for by using those same numbers to weight the relative urgencies of the two component tasks. This result, discussed

in Reference 3, is substantiated by the data obtained for the analysis and flight simulation reported here. The urgency functions are then in final form:

$$U_R = \alpha \left| \phi_e \right|$$

$$U_P = \mu \left| \theta_e \right|$$

This reflection of the objective urgency as imposed by the CRT display gains in the subjective urgency calculated in the model by U_P and U_R is one of the most significant dynamic features that the multiaxis attention allocation model has revealed. Since the experiment was set up to avoid controller and display visual effects, such as thresholds, this completes the CONTROL model. The two-axis EVALUATION is simply rms radial tracking error.

Consider now the adjustment and use of the model to predict the performance of a pilot trying to hold trim attitude in turbulence. The model has four quantities to be adjusted, the gain, K_ϕ, and lead, T_{L_ϕ}, of the lateral task and the gain, K_θ, and lead, T_{L_θ}, of the longitudinal task.

For most representative tactical aircraft multiaxis problems, the correct gains and leads are near the correct values for each continuous task separately and serve as a good starting point to find the multiaxis values. Taking the roll task first, the simulation can be exercised for the bank angle task alone by simply setting the pitch urgency coefficient μ to zero. The optimization principle of pilot modeling then asserts that K_ϕ and T_{L_ϕ} must be adjusted to minimize the rms radial tracking error, which is just rms ϕ since dot motions in the corresponding flight simulation occur only along the horizontal axis of the CRT display. A useful starting value for T_L is 0.5 sec. This value may be required for stability in some aircraft, and represents a weighting of error rate to error that pilots can generate with little difficulty. With this value of T_{L_ϕ}, the gain K_ϕ can be perturbed to find the optimum for this initial guess of lead. Once this is done, the lead can again be varied, and the process repeated until an optimum has been reached. This steepest ascent procedure could be directly mechanized on the computer; however it has been the experience of the authors that such methods are not necessary for most analyses.

In the case of the lateral and longitudinal configurations defined by Table 1, the gains and leads are as shown in Table 2 along with the rms tracking errors for a turbulence level of 10 ft/sec. These data were obtained by calculating the pilot — aircraft response for a series of 30-second runs totaling 1200 seconds of real-time

using an integration step of 0.05 second. The mean and standard deviation refer to these sets of 30-second rms tracking errors.

TABLE 2. SINGLE-AXIS TURBULENCE STABILIZATION PILOT MODEL DATA

	K	T_L	rms tracking errors (deg)	
			mean	s.d.
A continuous ϕ	3.5	0.5	3.17	0.461
B continuous ϕ	3.5	0.5	3.31	0.517
1 continuous θ	-0.5	0.6	0.196	0.0208
2 continuous θ	-0.5	0.7	0.319	0.0366
3 continuous θ	-0.8	0.5	0.118	0.0152

The flight simulation of this task led to the data shown in Table 3 where 20 flights of 30 seconds duration were obtained for each test point.

TABLE 3. SINGLE-AXIS TURBULENCE STABILIZATION FLIGHT SIMULATION DATA

	rms tracking errors (deg)	
	mean	s.d.
A continuous	3.12	0.508
open loop	10.1	1.25
B continuous	3.22	0.407
open loop	7.19	0.670
1 continuous	0.196	0.0276
open loop	0.484	0.0180
2 continuous	0.315	0.0388
open loop	0.565	0.0115
3 continuous	0.118	0.0149
open loop	0.293	0.0146

A comparison of the pilot model data with the flight simulation results is shown in Figure 16.

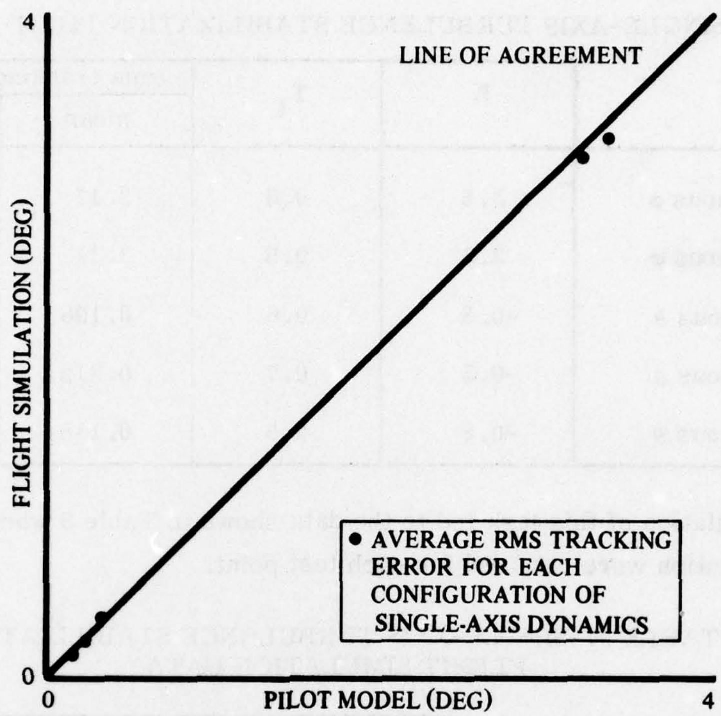

Figure 16. Comparison of Pilot Model with Flight Simulation Tracking Error Data for Single-Axis Turbulence Stabilization

It is clear from these statistics that the model has agreed well with the flight simulation. Since no information from the flight simulation was used in the analysis, the predictive capability of the model has been demonstrated. Ground rules for data acquisition shown in Figure 17 have been consistently employed.

MODEL: Using the optimum pilot model, a series of runs is obtained using the run length corresponding to the flight simulation. The series is taken consecutively. No rejection of data is allowed.

FLIGHT SIMULATION: Data is obtained in a series of 10 to 20 consecutive flights. Series may be kept or rejected to allow for training and subject daily variation, but a series must be kept or rejected in its entirety. No series may be rejected which is the best obtained.

Figure 17. Rules for Data Acquisition

In addition to providing careful control over the collection of comparison data, the procedure of exactly repeating the individual simulation test items reveals additional information. During a flight of finite time, there will be two kinds of fluctuations in the task: disturbance intensity and disturbance power spectrum. These fluctuations represent aspects of the task environment that are encountered in actual flight and, as such, are useful to evaluate. For purposes of identifying pilot dynamics and validating pilot model components, the statistical fluctuations that result can be severely limiting. The data of Tables 2 and 3 were obtained by using a method for reducing the intensity fluctuation without changing the nature of the defined flight task. By precomputing each complete 30-second history of turbulence, the mean and rms values for the turbulence can be obtained. The series is then adjusted by shifting the mean to zero and the rms intensity to a specified level, in this case 10 ft/sec. The task as presented to the pilot and the pilot model thus avoids problems of unsettled low-frequency statistics and display limiting.

A comparison of the standard deviations of these data reveals that there is a similar scatter to the series of 30-second runs obtained from the simulator and from the pilot model. This is shown in Figure 18.

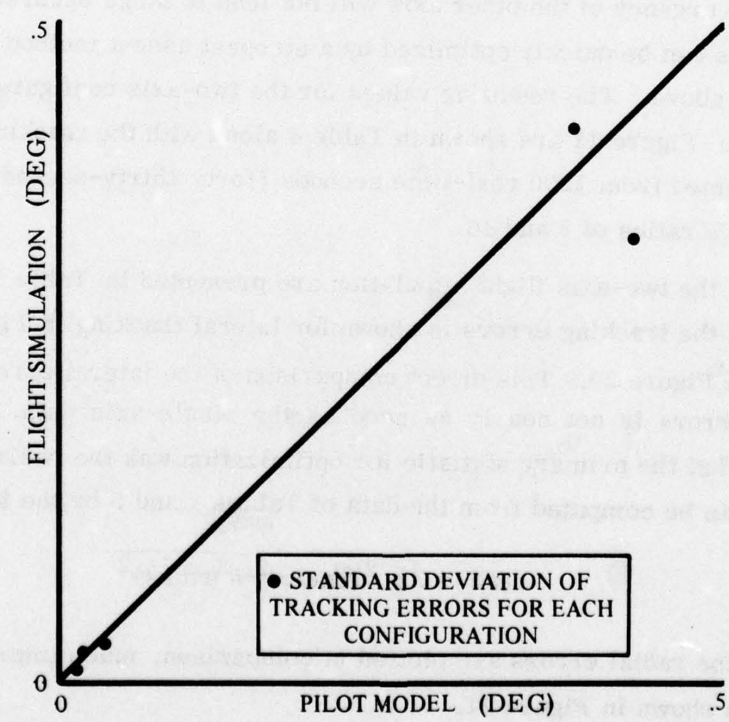

Figure 18. Comparison of Standard Deviations of Pilot Model and Flight Simulation Tracking Error Data for Single-Axis Turbulence Stabilization Task

Correlation of standard deviations frequently occurs in comparisons between model and flight simulation data, and appears in this case to be the result of fluctuations in the power spectra during the 30-second flight period. For command tracking tasks, this power spectra fluctuation can be eliminated by using sums of sinusoids to generate the command, but the idea of using such a method for turbulence is apparently untried. In any event the standard deviations here are small enough to allow a meaningful comparison of the average rms tracking errors.

Consider the two-axis task of attempting to hold zero (trim) attitude in turbulence. The urgency coefficients are fixed by the experimental choice of display scalings so that the only adjustments of the model to optimize its radial error performance concern the compensation gains and leads. The diversion of attention in both the pilot and the pilot model results in attitude rates (that may have been generated during the initial phase of correcting an attitude error) being left uncancelled. For this reason, the optimum lead and gain of the single-axis continuous task may be not optimum in the two-axis task. Indeed, the gains of the two-axis problem are generally lower, and the leads higher, thus reflecting the added requirement for keeping the attitude rates more closely controlled so that an interruption of the task by the urgency of the other axis will not lead to large excursions. The gains and leads can be quickly optimized by a steepest ascent method similar to the one described above. The resulting values for the two-axis configurations described in the matrix of Figure 11 are shown in Table 4 along with the tracking error statistics obtained from 1200 real-time seconds (forty thirty-second runs), each exercised at μ/α ratios of 8 and 16.

Data for the two-axis flight simulation are presented in Table 5, and a comparison of the tracking errors is shown for lateral tracking in Figure 19, and longitudinal in Figure 20. This direct comparison of the lateral errors and the longitudinal errors is not nearly as good as the single-axis data. It must be remembered that the primary statistic for optimization was the radial tracking error which can be computed from the data of Tables 4 and 5 by the formula:

$$r(\phi,\theta) = \sqrt{\alpha^2(\text{rms}\,\phi)^2 + \mu^2(\text{rms}\,\theta)^2}$$

Now if the radial errors are plotted in comparison, much improved agreement is obtained as shown in Figure 21.

TABLE 4. TWO-AXIS TURBULENCE STABILIZATION
PILOT MODEL DATA

	μ/α	K_ϕ	T_{L_ϕ}	K_θ	T_{L_θ}	rms ϕ (deg) mean	rms ϕ (deg) s.d.	rms θ (deg) mean	rms θ (deg) s.d.
1A	8	2.0	1.1	-0.4	1.0	4.33	0.610	0.306	0.0482
1A	16	2.0	1.1	-0.4	1.0	5.00	0.823	0.275	0.0450
1B	8	1.5	1.6	-0.4	0.9	4.11	0.514	0.302	0.0476
1B	16	1.5	1.6	-0.4	0.9	4.73	0.776	0.273	0.0406
2A	8	2.0	1.1	-0.4	1.0	4.59	0.664	0.388	0.0406
2A	16	2.0	1.1	-0.4	1.0	5.30	0.652	0.365	0.0460
2B	8	1.5	1.5	-0.4	1.0	4.28	0.554	0.381	0.0378
2B	16	1.5	1.5	-0.4	1.0	5.06	0.785	0.361	0.0396
3A	8	2.0	1.2	-0.6	0.9	3.93	0.529	0.174	0.0232
3A	16	2.0	1.2	-0.6	0.9	4.43	0.810	0.158	0.0215
3B	8	1.5	1.6	-0.6	0.9	3.69	0.481	0.177	0.0250
3B	16	1.5	1.6	-0.6	0.9	4.10	0.561	0.158	0.0237

The agreement this figure shows indicates that optimum performance can be obtained with some even tradeoff between the attention allocated to the two tracking tasks. It is apparent that the pilot adopted weightings slightly different from the exact μ/α ratio; however, the use of μ and α for the urgency function coefficients led to the correct predictions for the radial error statistic, the primary checkpoint for agreement. In fact, the agreement over these twelve cases averages only 9.3% error.

Data for direct comparison of the control periods and dwell fractions of the attention allocation were not obtained from the flight simulation. However, the division of control between the roll and pitch tasks can be clearly seen in terms of elevator and aileron activity on strip chart traces obtained during the manned simulation. Figure 22 from Reference 3 shows an apparent switching curve imposed on a sample strip chart trace. This record is for 20 seconds of configuration

TABLE 5. TWO-AXIS TURBULENCE STABILIZATION FLIGHT SIMULATION DATA

	μ/α	rms ϕ (deg) mean	rms ϕ (deg) s.d.	rms θ (deg) mean	rms θ (deg) s.d.
1A	8	3.59	.537	.380	.0508
1A	16	4.00	.620	.294	.0346
1B	8	3.23	.420	.364	.0428
1B	16	3.76	.545	.286	.0360
2A	8	3.68	.397	.430	.0321
2A	16	4.11	.528	.369	.0308
2B	8	3.46	.710	.399	.0376
2B	16	3.88	.474	.323	.0226
3A	8	3.07	.438	.217	.0333
3A	16	3.20	.433	.161	.0145
3B	8	3.60	.621	.253	.0260
3B	16	3.71	.574	.210	.0329

1B flown at a μ/α ratio of 16. If the reader will follow the record as it evolves from left to right, the episodic nature of the control and the task demands that initiate attention shifting will be readily seen. In only one marked control episode is there conspicuous simultaneous control, and in that case the aileron is held constant rather than returned to trim.

To evaluate task interference effects, the continuous performance of each of the five single-axis dynamics can be compared to the two-axis tracking errors. Plotted on a linear scale for easy visibility, longitudinal task interference of lateral tracking is shown in Figure 23, while a similar plot of lateral task interference of longitudinal tracking is shown in Figure 24.

The order of degradation of the lateral tasks - 3A, 1A, 2A and 3B, 1B, 2B - corresponds to the ranking of the continuous longitudinal tracking errors - 3, 1, 2 - which simply indicates that a more demanding longitudinal task in a two-axis problem

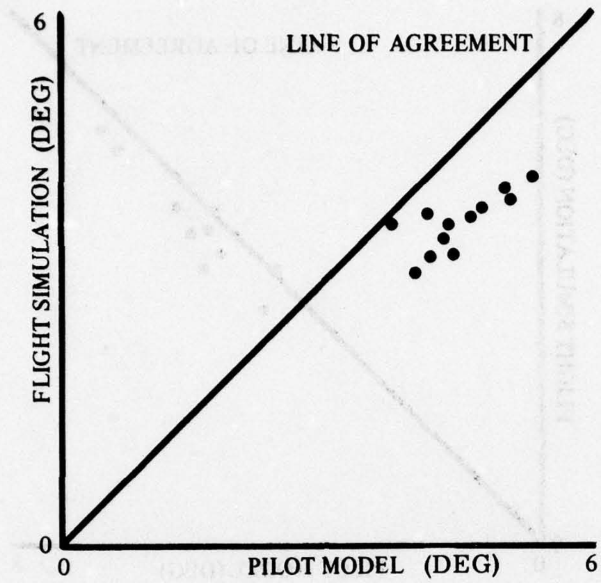

Figure 19. Comparison of Two-Axis Bank Angle Tracking Error

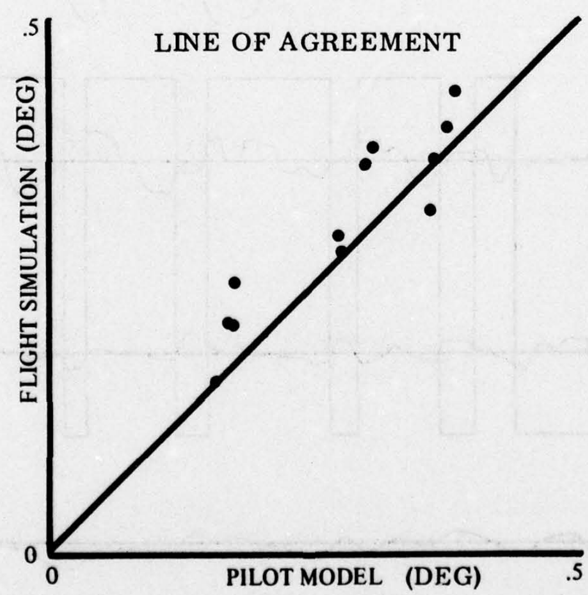

Figure 20. Comparison of Two-Axis Pitch Angle Tracking Error

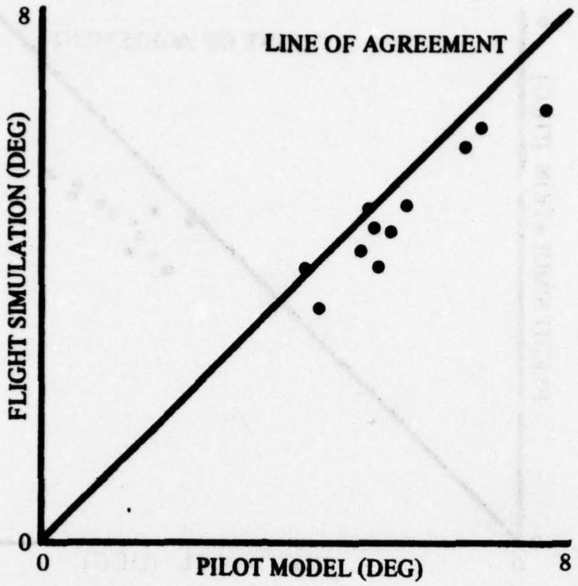

Figure 21. Comparison of Radial Errors for Turbulence Stabilization

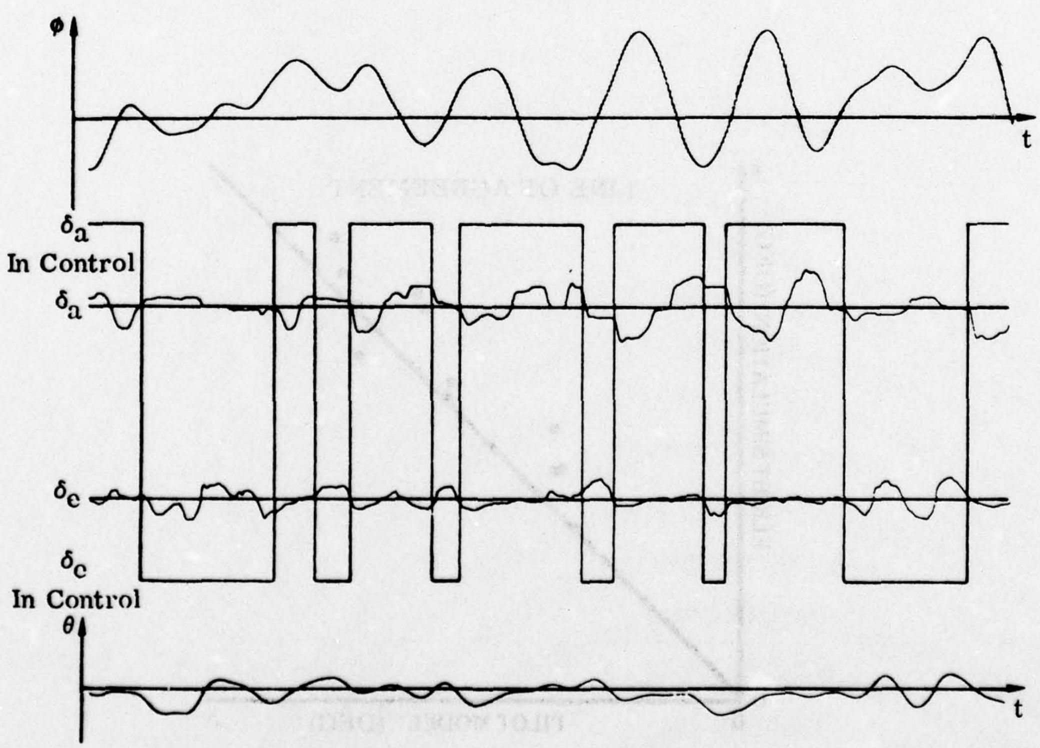

Figure 22. Attention Shifting Episodes From Flight Simulation

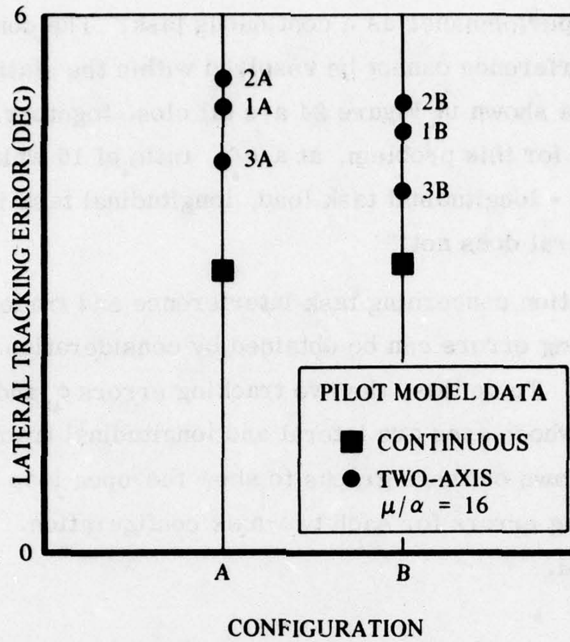

Figure 23. Longitudinal Task Interference

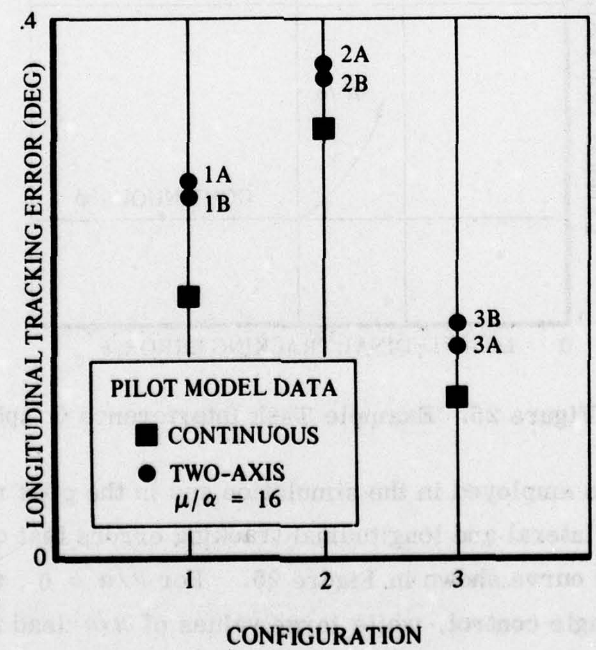

Figure 24. Lateral Task Interference

is one that has worse performance as a continuous task. The converse question about lateral task interference cannot be resolved within the statistics of the data since the two-axis data shown in Figure 24 are all close together. It can be concluded, however, that for this problem, at a μ/α ratio of 16 which represents nearly an even lateral - longitudinal task load, longitudinal task interference has significance while lateral does not.

Further information concerning task interference and tradeoff between lateral and longitudinal tracking errors can be obtained by consideration of the two dimensional nature of the problem. To do this, the two tracking errors ϕ_e and θ_e will be plotted as a point on a graph whose axes are lateral and longitudinal tracking error. Furthermore, lines will be drawn on these graphs to show the open loop responses and continuous θ and ϕ tracking errors for each two-axis configuration. Figure 25 shows an example of this method.

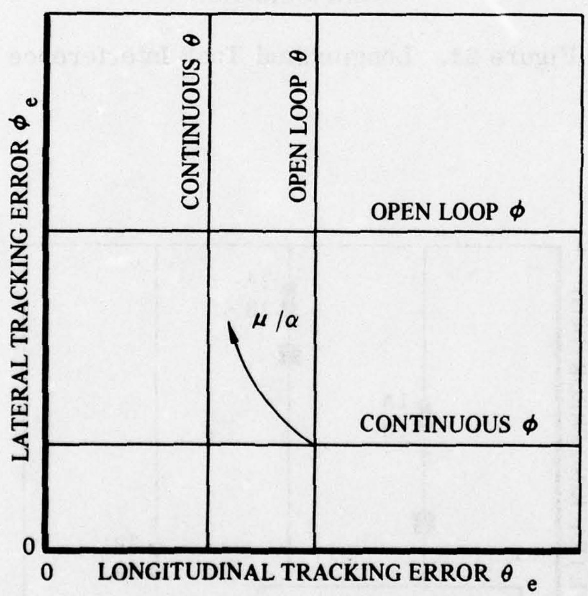

Figure 25. Example Task Interference Graph

The μ/α ratios employed in the simulation and in the pilot model lead to a tradeoff between the lateral and longitudinal tracking errors that qualitatively resembles the example curve shown in Figure 25. For $\mu/\alpha = 0$, the problem reduces to continuous bank angle control, while large values of μ/α lead to continuous pitch control. For intermediate values, the two-axis task is characterized by tracking degradation compared to the continuous cases, and this degradation is exactly what

is shown by the μ/α curve. The tradeoff between these two tracking errors for a nearly optimum radial tracking error will be manifested by two-axis tracking data points that lie along such a curve. Using the data in Tables 2 through 5, these data can be compared on the task interference graph for the flight simulation and the pilot-aircraft model, Figures 26 through 31, where the open loop and continuous data are from the flight simulation.

At this point it is necessary to consider further the effects of fluctuations in the turbulence intensity that characterize experience in actual flight. The method of precomputing the turbulence and adjusting the means to zero and the rms values to 10 ft/sec used in obtaining the simulation data summarized in Figures 27 through 31 eliminates whatever effects might be associated with random weighting of the turbulence towards one axis or the other. Consider a single-axis task, say lateral. Since the piloted system represents a linear open loop dynamical system with turbulence input and bank angle output, it is clear that every dynamical variable in the pilot-aircraft system will scale with the actual turbulence intensity. Thus, for example, if the intensity of the turbulence were to be doubled, the pilot would see a doubling of the excursions of the display during his control. If the display gain were now halved, the pilot would not be able to distinguish visually the final configuration from the original problem presented to him.

This consideration illustrates that for the two-axis stabilization task, fluctuations in turbulence intensity and display gain selection combine to form a single variation in task intensity that the pilot perceives. Reference 3 reports data for this task where the gusts were not precomputed. At the time this work was performed at Northrop, it was found that the turbulence intensities would vary between 8 and 14 ft/sec when the filter gains were set to produce a long-term average of 10 ft/sec. In this way, a factor of up to two must be either multiplied by or divided into the display gain ratios. Thus the effective task ratios in this earlier study effectively varied from 4 to 32. The data from individual simulation flights are distributed or dispersed along the μ/α curves of the task interference graphs for a large part of the curve, depending on the sensitivity of the curve to these μ/α ratios.

The clearest example of task interference effects can be seen in the 1B and 3B configurations of Figures 27 and 31. Individual flight data, presented in Reference 3 and reproduced here as Figures 32 and 33, reveals a great difference in lateral B performance resulting from the selection of the longitudinal dynamics 1 or 3. In the pilot model analysis, the optimum lateral gains and leads for these two cases turned out to be

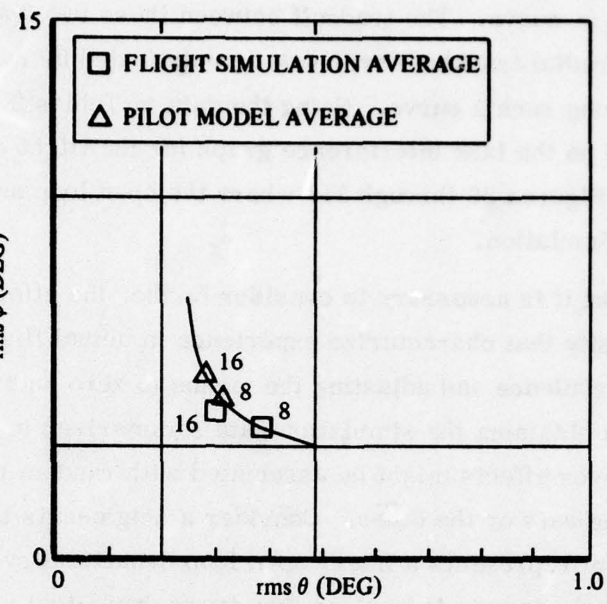

Figure 26. Task Interference Graph for Configuration 1A

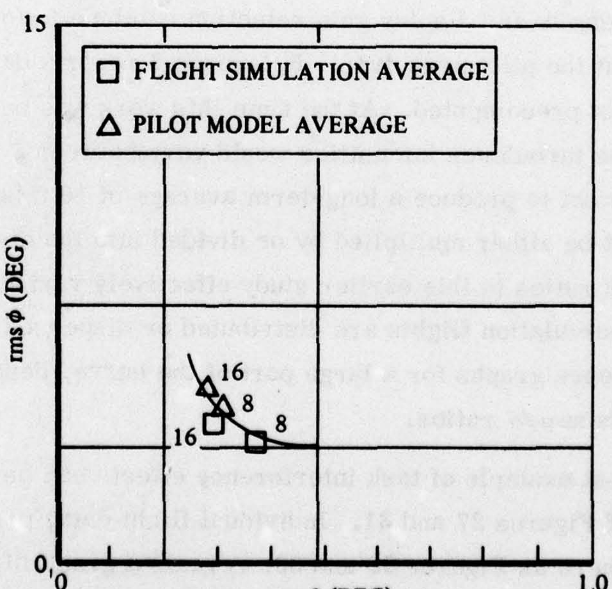

Figure 27. Task Interference Graph for Configuration 1B

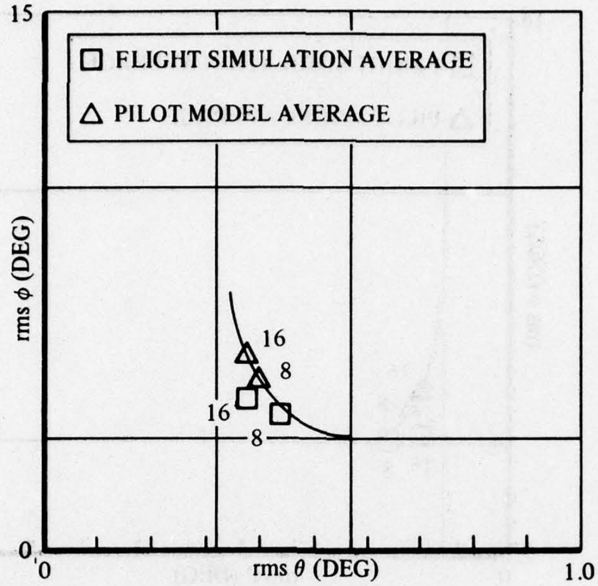

Figure 28. Task Interference Graph for Configuration 2A

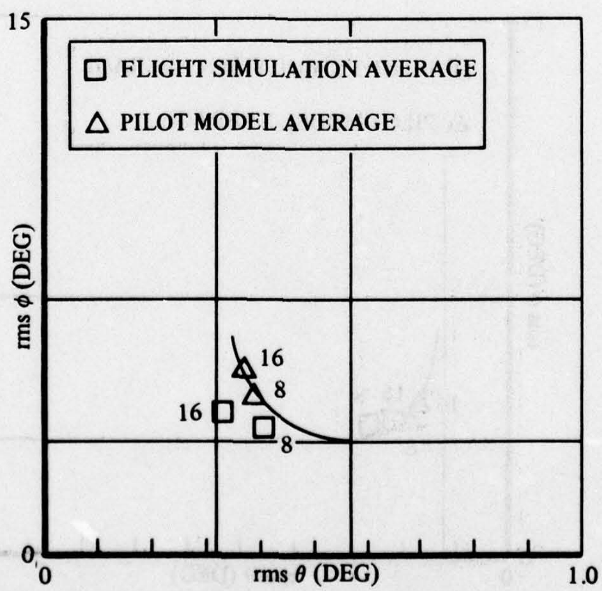

Figure 29. Task Interference Graph for Configuration 2B

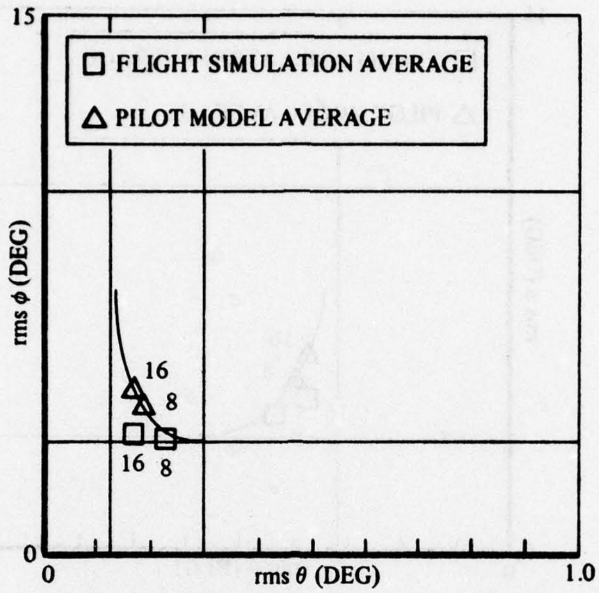

Figure 30. Task Interference Graph for Configuration 3A

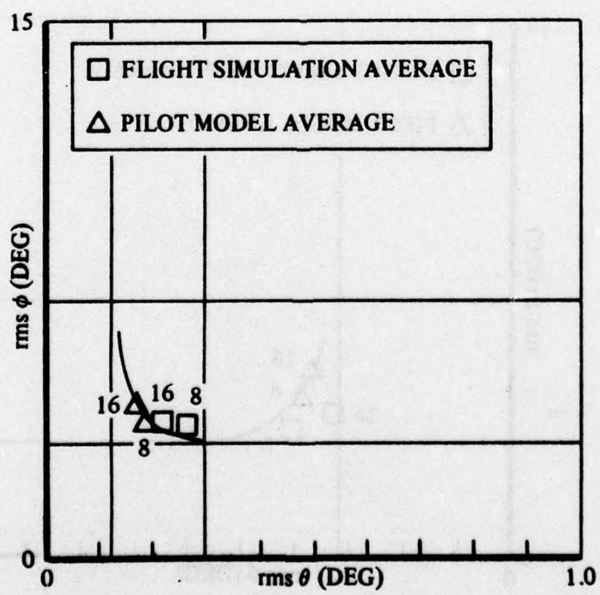

Figure 31. Task Interference Graph for Configuration 3B

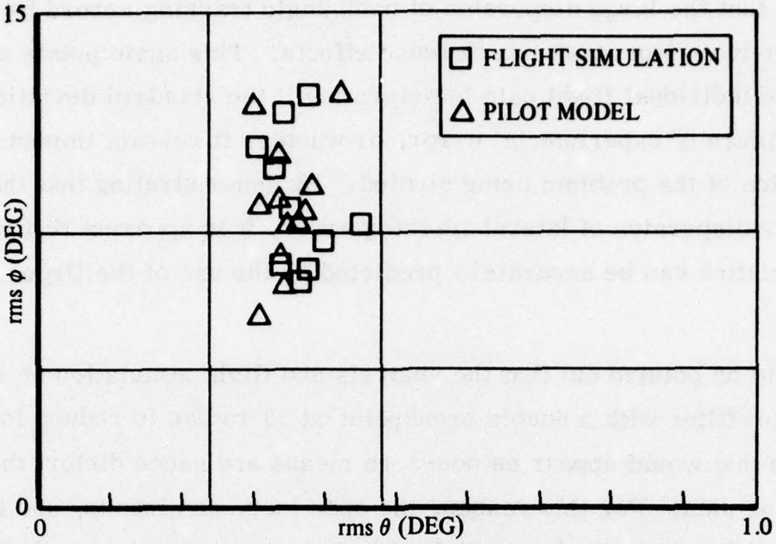

Figure 32. Pilot Model and Flight Simulation Data Dispersion for 30-Second Flights of Configuration 1B at μ/α = 16.

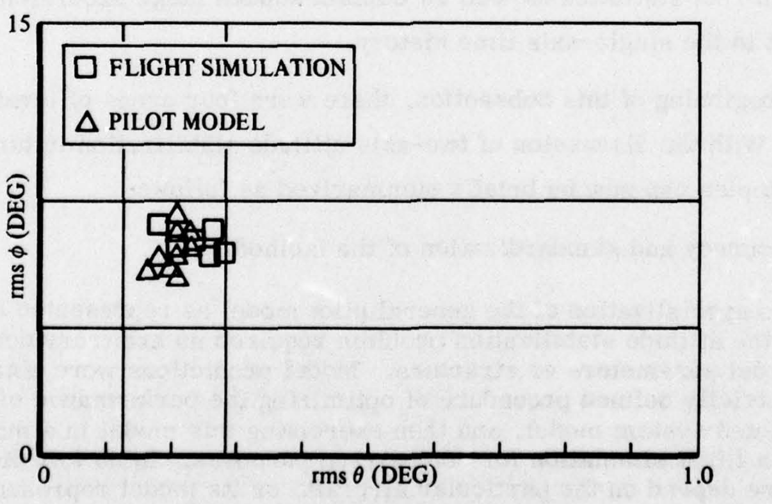

Figure 33. Pilot Model and Flight Simulation Data Dispersion for 30-Second Flights of Configuration 3B at μ/α = 16.

identical, so that the large dispersion of bank angle tracking errors for configuration 1B derives exclusively from task interference effects. This again points out the utility of examining the individual flight data to determine if the standard deviation statistic is simply a measure of experimental error, or whether it reveals important dynamic characteristics of the problem being studied. By demonstrating that the model produces similar dispersion of lateral tracking error, it is apparent that the mismatched 1B characteristics can be accurately predicted by the use of the Urgency Decision Pilot Model.

It should be pointed out that the analysis and flight simulation of Reference 3 employed a prefilter with a double breakpoint at .3 radian to reduce low-frequency disturbances that would appear as non-zero means and hence distort the normalized tracking error data. For this reason, the open loop, continuous, and two-axis tracking data are different from those obtained by the pre-computing method since no prefilter was employed in the current study.

The use of time-history simulation to generate the specific episodic histories of these control dynamics allows insight into an aspect of piloted flying qualities of importance to a wide range of practical problems ranging from landing safety to weapon delivery accuracy. To illustrate the severity of this task interference in configuration 1B, Figure 34 reproduces time histories from Reference 3 that show 225 seconds of model control for single-axis B lateral bank angle compared to bank angle as part of the two-axis task 1B. It can be seen that 30-second segments of the two-axis record vary widely in rms statistics as well as contain sudden large excursions which are totally absent in the single-axis time history.

At the beginning of this Subsection, there were four areas of investigation to be considered. With the discussion of two-axis attitude stabilization in turbulence complete, these topics can now be briefly summarized as follows:

1) Accuracy and standardization of the method.

   The specialization of the general pilot model as represented in Section III to the attitude stabilization problem required no arbitrary decisions of model parameters or structure. Model predictions were obtained through a strictly defined procedure of optimizing the performance of the total piloted system model, and then exercising this model in a manner similar to a flight simulation for comparison purposes. In no way did this procedure depend on the particular aircraft, or its model representation. Consequently, the pilot model could be used in conjunction with fully general nonlinear and time-varying aircraft models in conjunction with aircraft

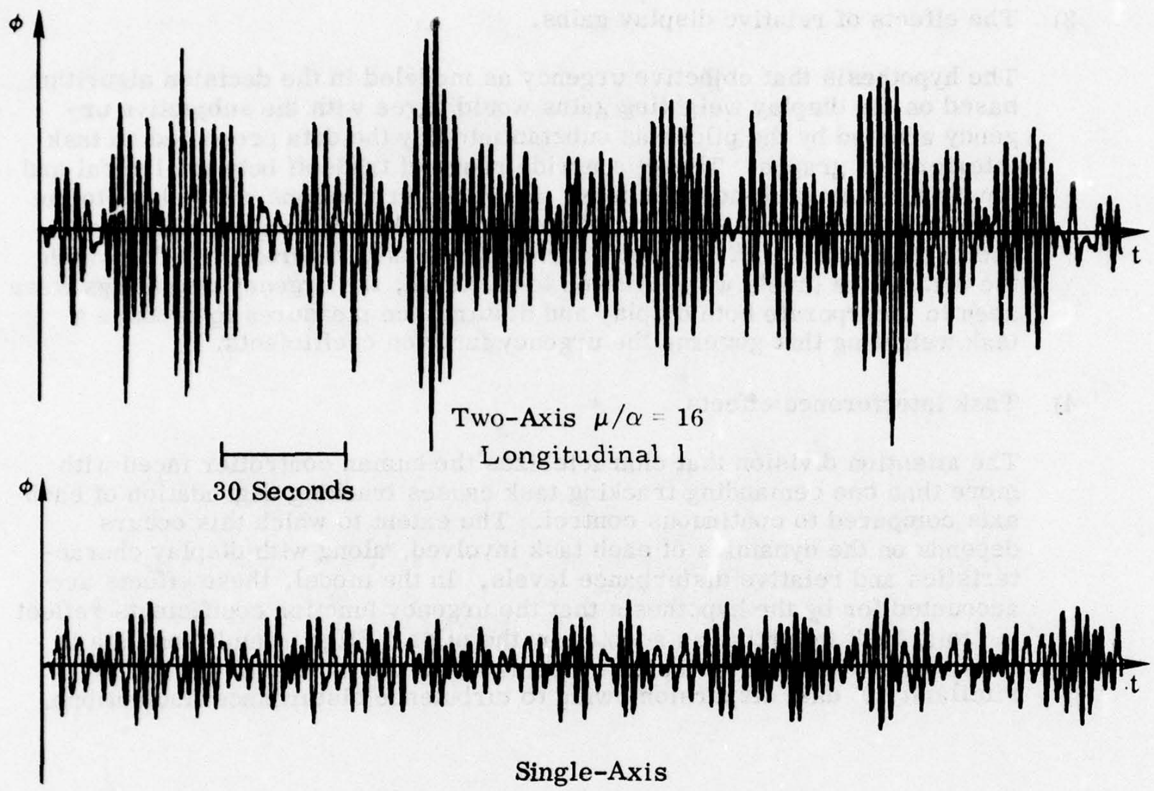

Figure 34. Lateral Time Histories for Single- and Two-Axis Turbulence Stabilization of Configuration B Lateral Dynamics

simulations, or incorporated into large flight simulator drive computer programs. The accuracy of the model for the two-axis radial tracking errors proved to be 9.3%, much smaller than the range of radial tracking errors of various configurations, thus giving useful resolution in the comparative flying qualities of the configurations.

2) The effects of attention sharing on pilot compensation.

Optimum compensation in terms of pilot gain and lead differed significantly between the single- and two-axis tracking tasks. In general, divided attention results in optimum compensation that generates lower attitude rates to avoid the possibility that they may have to be left unattended through diversion to the other task. For this reason the gains are lower and the leads greater for the two-axis task, as compared to single-axis continuous tracking.

3) The effects of relative display gains.

The hypothesis that objective urgency as modeled in the decision algorithm based on the display weighting gains would agree with the subjective urgency adopted by the pilot was substantiated by the data presented on task interference graphs. There is a wide range of tradeoff between lateral and longitudinal control; nevertheless, the model predictions were close to the flight simulation data in terms of the optimized performance quantity, radial tracking error. By considering previously reported data for which the turbulence levels were allowed to fluctuate, the urgency weightings were seen to incorporate both display and disturbance measures to produce a task weighting that governs the urgency function coefficients.

4) Task interference effects.

The attention division that characterizes the human controller faced with more than one demanding tracking task causes tracking degradation of each axis compared to continuous control. The extent to which this occurs depends on the dynamics of each task involved, along with display characteristics and relative disturbance levels. In the model, these effects are accounted for by the hypothesis that the urgency function coefficients reflect the total task weighting as adopted by the pilot. Flight simulation data is consistent with this hypothesis in terms of overall statistics as well as similarity of data dispersion owing to turbulence disturbance fluctuations.

B. VALIDATION OF THE MODEL FOR TWO-AXIS ATTITUDE STABILIZATION

The first data, Reference 3, to demonstrate the nature of two-axis attitude stabilization in turbulence was obtained in the summer of 1974. In the following April, the model was validated for this problem using the moving-base Northrop Large Amplitude Simulator, Wide Angle Visual System (LAS/WAVS) facility. Although the basic comparison between the model and the moving-base flight simulation was presented in graphical form in Reference 3, a full account of this validation study is appropriate here.

The piloted tasks are similar to the problem discussed in the previous Subsection, but with one important difference: the display was not a CRT, it was the external view projected by the earth-sky projector of the WAVS onto the hemisphere that surrounds the pilot in the simulator. This being the case, there was no natural μ/α ratio to use in the urgency functions of the pilot model. The horizon appeared as mountainuous terrain, which induced visual thresholds. The aircraft model used in the study was the fully general nonlinear YF-17 description including all table look-ups for the aerodynamic descriptions and control system gain schedules as mechanized on digital computers. The cockpit arrangement and stick force characteristics also corresponded to the YF-17 aircraft. Dryden spectra turbulence was employed according to flight condition for lateral v- and longitudinal w-gusts. Six flight conditions shown in Figure 35 were flown by a former U.S. Navy test pilot.

	ALTITUDE (FT)	5K	10K	30K	40K	60K
MACH						
0.4		X		X		
0.8		X			X	
0.9						X
1.1			X			

Figure 35. YF-17 Flight Conditions Surveyed

By having the pilot attempt to fly the simulator in still air back to trim theta and zero phi from an initial condition, visual thresholds for the external display were evaluated. Short control periods were flown so that heading changes induced by residual non-zero bank angles could not be used as a bank angle indication. The result of this calibration simulation was the identification of a four-degree threshold in bank

angle, and no discernible threshold in theta, an anticipated result since the horizon could be viewed across the edge of a head-up gunsight. This visual threshold was directly incorporated into the pilot model mechanized on the simulator drive computers in the following way:

$$\text{If } \phi > 4°,\ \phi \text{ observed} = \phi$$

$$\text{If } \phi \leq 4°,\ \phi \text{ observed} = 0$$

Comparisons of the model with the flight simulation for single-axis tasks were performed in a manner similar to that described in the previous Subsection. Since the description of the complete YF-17 cannot be released, data will not be presented in tables, but only in graphical form. These comparisons for the single-axis stabilization task were obtained by suppressing the turbulence first on the lateral, and then on the longitudinal axis. Figure 36 shows the comparison for bank angle stabilization where the model and simulation data are averaged from 30-second flights.

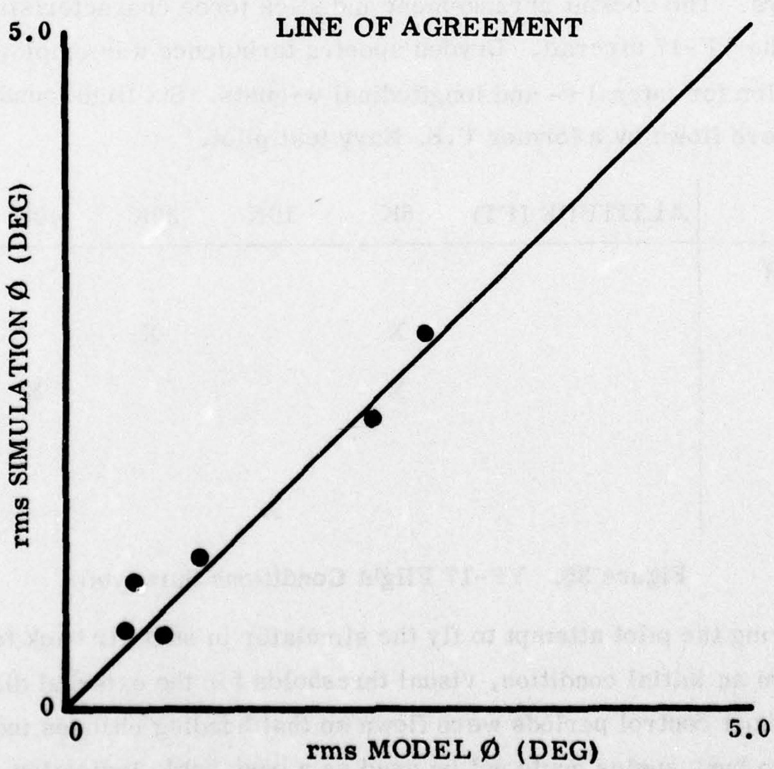

Figure 36. Lateral Stabilization of the YF-17 Single-Axis

Comparison of the model with the simulation for the single-axis longitudinal task is given in Figure 37.

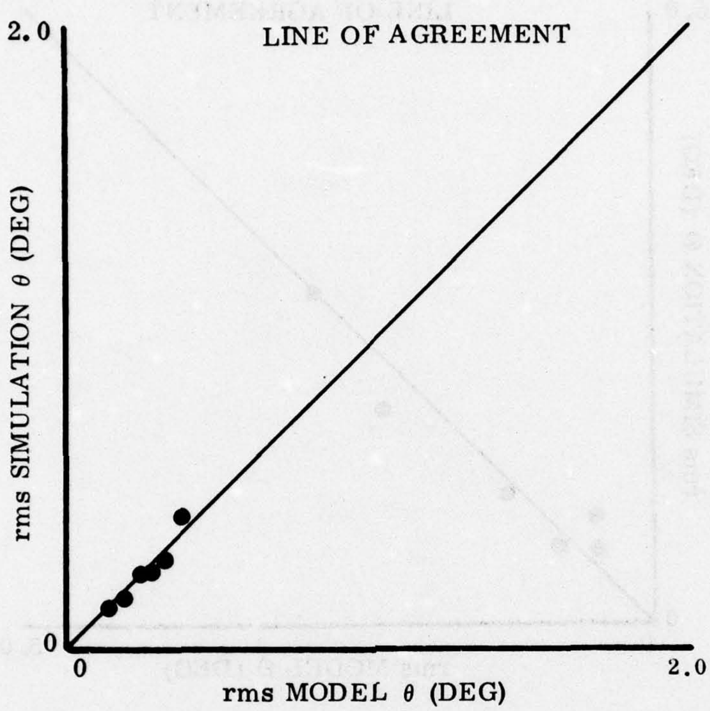

Figure 37. Longitudinal Stabilization of the YF-17 Single-Axis

Since the external display does not lead to a natural selection of the urgency coefficients, some method of calibration must be employed. The way in which this was done depended on the observation that for the model, dwell fraction on an axis is a monotonic function of the urgency of that axis. After selecting a flight condition - 5000 ft. at Mach 0.8 - for calibration, the dwell fractions adopted by the pilot were estimated using x-y plots of stick activity. The model was then exercised to determine the urgency coefficients that produced this dwell fraction. The urgency functions determined by this method were then held constant for the other flight conditions. The urgency functions for this problem are given by:

$$U_R = \left|\phi_e\right|$$

$$U_P = 4\left|\theta_e\right|$$

Agreement between the model exercised in this manner and the flight simulation is shown for the lateral axis in Figure 38. Longitudinal comparison is shown in Figure 39.

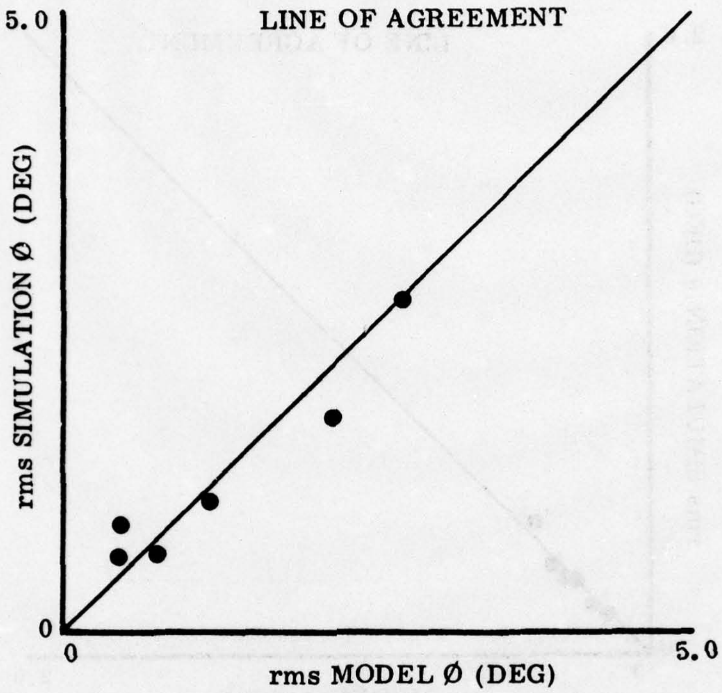

Figure 38. Lateral Stabilization of the YF-17 Two-Axis

It should be pointed out that the incorporation of the visual threshold was essential; without it, model predictions for the three highest dynamic pressure flight conditions showed poor agreement with the flight simulation data.

To see what task interference effects might be shown in this study, task interference graphs are presented for individual flights of the model and the pilot in Figures 40-45.

Task interference effects are apparent as large data dispersion in low dynamic pressure flight conditions such as shown in Figures 41 and 44. Unlike the case of the 1B configuration of Figure 32 the worst of the individual flights at these conditions are bounded by the open loop values for the YF-17. Again it should be emphasized that this dispersion which statistically would be reported as a large standard deviation represents important information beyond the usual interpretation of standard deviations.

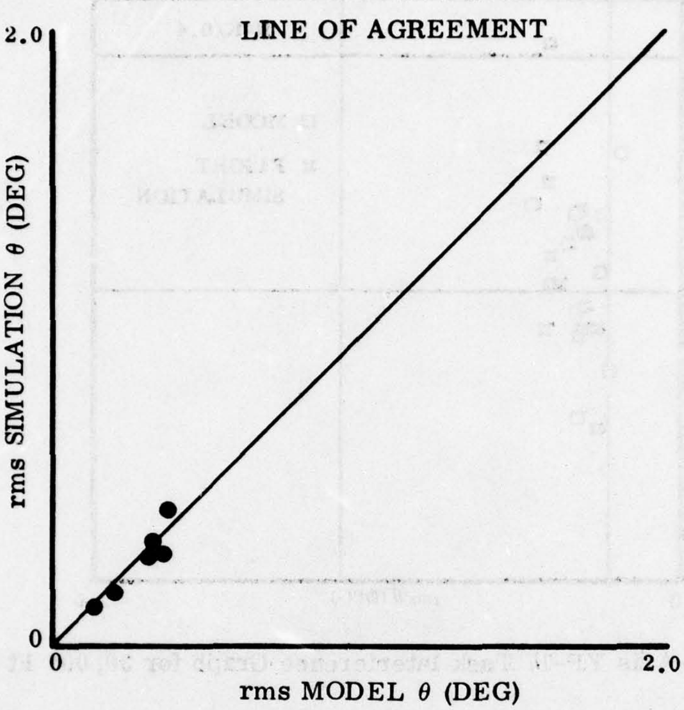

Figure 39. Longitudinal Stabilization of the YF-17 Two-Axis

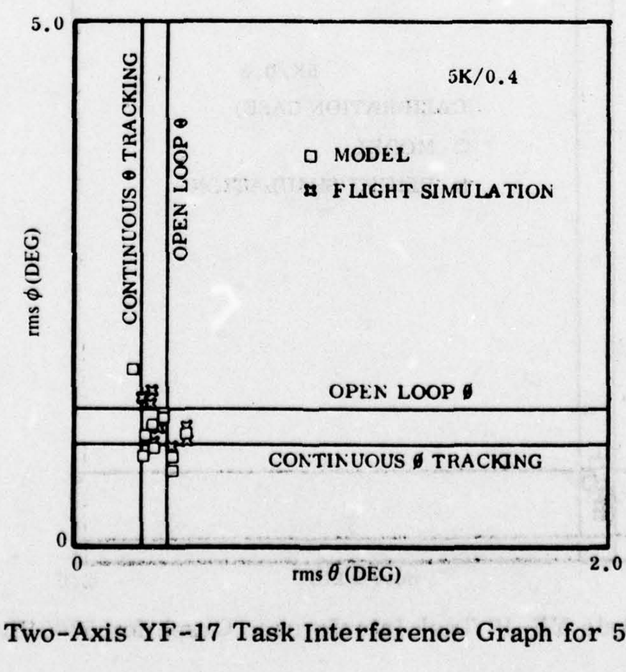

Figure 40. Two-Axis YF-17 Task Interference Graph for 5000 Ft at Mach 0.4

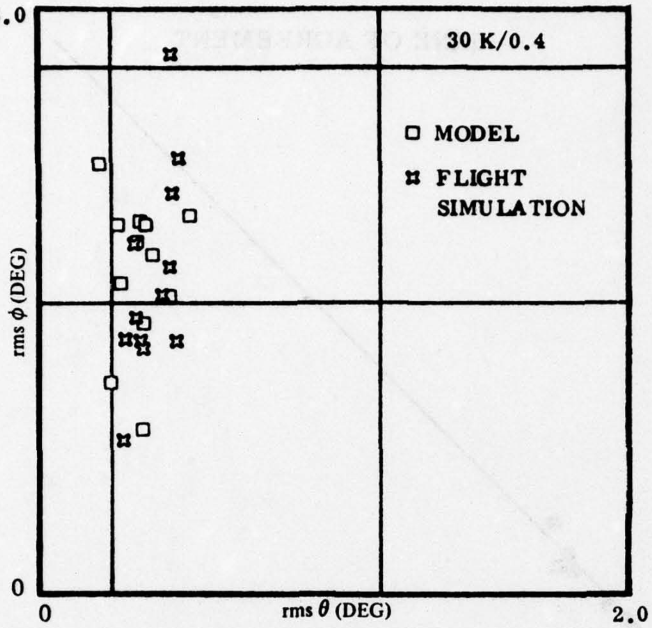

Figure 41. Two-Axis YF-17 Task Interference Graph for 30,000 Ft at Mach 0.4

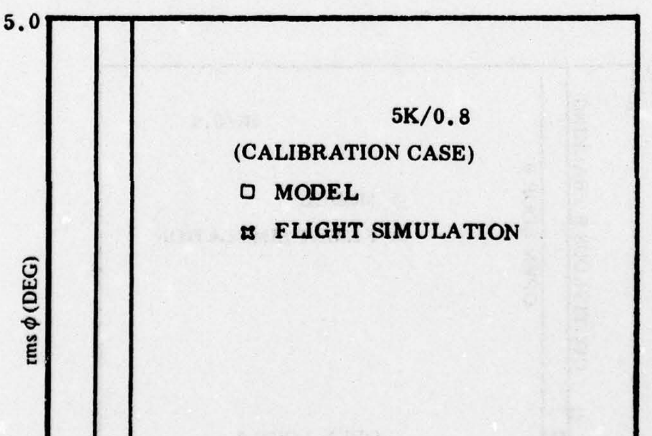

Figure 42. Two-Axis YF-17 Task Interference Graph for 5000 Ft at Mach 0.8

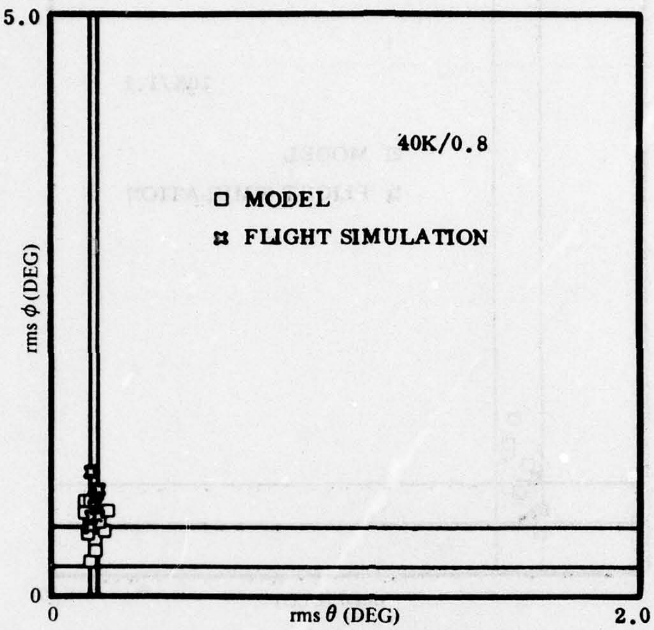

Figure 43. Two-Axis YF-17 Task Interference Graph for 40,000 Ft at Mach 0.8

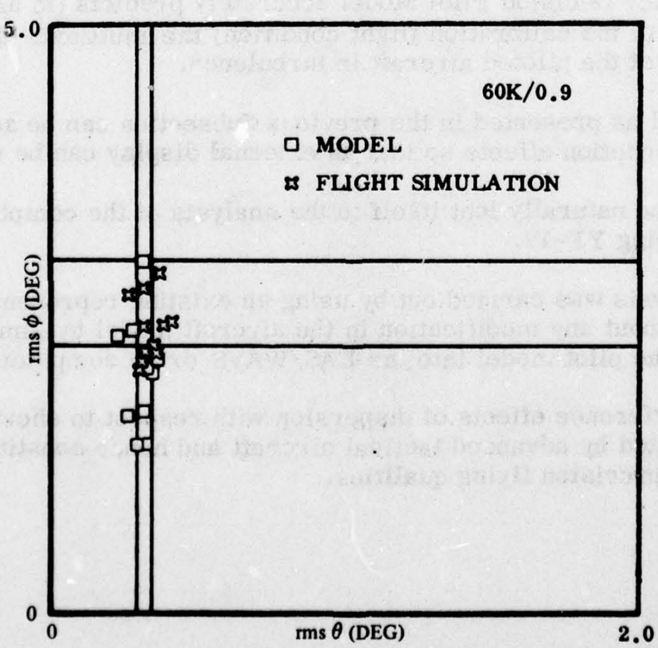

Figure 44. Two-Axis YF-17 Task Interference Graph for 60,000 Ft at Mach 0.9

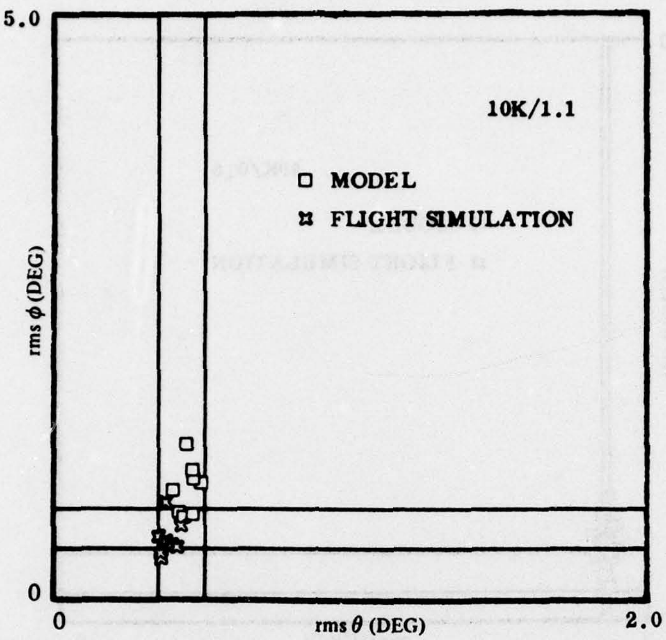

Figure 45. Two-Axis YF-17 Task Interference Graph for 10,000 Ft at Mach 1.1

There are six conclusions to be drawn from the study of the YF-17 in turbulence:

1) The Urgency Decision Pilot Model accurately predicts (in all cases with the exception of the calibration flight condition) the multiaxis disturbance statistics of the piloted aircraft in turbulence.

2) The model as presented in the previous Subsection can be adapted to include visual perception effects so that an external display can be modeled.

3) The method naturally lent itself to the analysis of the complete nonlinear time-varying YF-17.

4) This analysis was carried out by using an existing representation of the YF-17 without any modification in the aircraft model by simply incorporating the pilot model into the LAS/WAVS drive computers.

5) Task interference effects of dispersion with respect to short tracking times are exhibited by advanced tactical aircraft and hence constitute an important aspect of precision flying qualities.

The sixth conclusion is most important to users of this approach to piloted flying qualities:

6) The Urgency Decision Pilot Model is fully validated by the YF-17 study for use in aircraft simulations to evaluate the flying qualities of attitude stabilization in turbulence.

C. A SELF-GENERATED VTOL HOVER TASK

The examples of the preceding Subsections have considered flight control tasks that were single-loop on each axis and required holding attitude in the presence of turbulence disturbances. To demonstrate the versatility of the full Urgency Decision Pilot Model, these problem characteristics will be generalized.

Consider a VTOL aircraft model first. Each axis consists of inner loop attitude and outer loop position dynamics as shown in Figure 46.

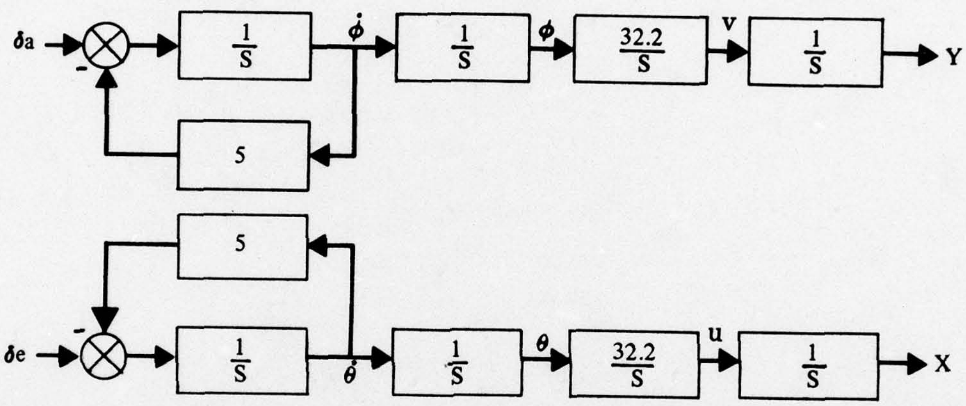

Figure 46. VTOL Aircraft System Dynamics

The pilot's task is to hover over the ground position 0, 0 in the presence of pilot induced disturbances only, as described later. It is assumed that the pilot has a display from which he can read position X, Y; translation velocity u, v; attitude θ, ϕ; and attitude rate $\dot{\theta}$, $\dot{\phi}$.

These fourth-order dynamics require pilot model compensation on both attitude and position control for each axis as shown in Figure 47. The subscript "P" denotes longitudinal (pitch), and "R" lateral (roll). The stick command δa goes into the aircraft dynamics if the urgency condition for lateral control is met. A similar model is implemented for longitudinal control.

According to the general pilot model as presented in Section III, the urgency functions will take the forms shown in Figure 48, where α, β, γ, δ are the constant urgency function coefficients.

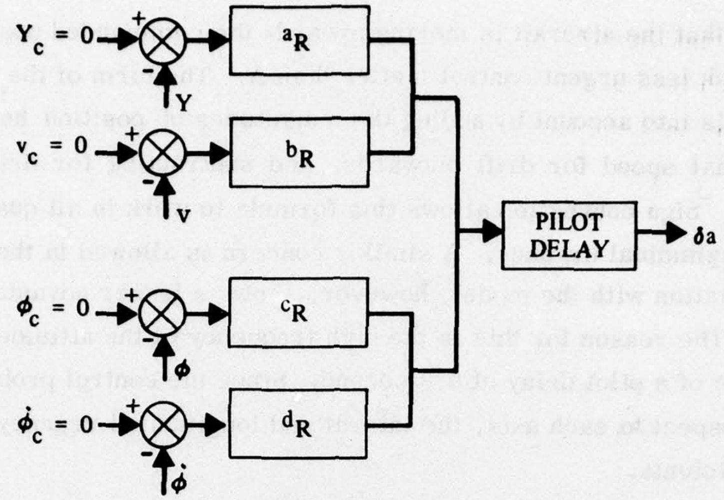

Figure 47. VTOL Pilot Model Compensation for Lateral Control

$$U_R = \left| \alpha_R |Y| + \beta_R \frac{vY}{|Y|} + \gamma_R |\phi| + \delta_R \frac{\dot{\phi}\,\phi}{|\phi|} \right|$$

$$U_P = \left| \alpha_P |X| + \beta_P \frac{uX}{|X|} + \gamma_P |\theta| + \delta_P \frac{\dot{\theta}\,\theta}{|\theta|} \right|$$

Figure 48. Urgency Functions for the VTOL Hover Task

It is easy to see the effects of the α and β terms of these urgency functions. Consider the lateral urgency of the two cases diagrammed in Figure 49.

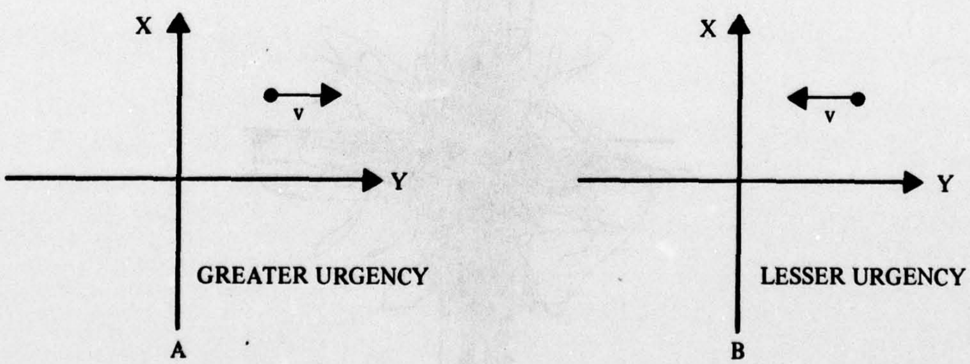

Figure 49. Interpretation of VTOL Urgency Functions

In case A, there is a lateral position hovering error Y, and a translational speed v taking the aircraft away from the commanded position. In case B, the same speed is reducing the identical hovering position error as in A. However, in this

case, the fact that the aircraft is moving towards the commanded position clearly makes B a much less urgent control matter than A. The form of the α and the β terms takes this into account by adding the magnitudes of position hovering error and translational speed for drift outwards, and subtracting for drift in the correct direction. Sign convention allows this formula to work in all quadrants for both lateral and longitudinal urgency. A similar concern is allowed in the γ and δ terms. Calculation with the model, however, shows a lesser advantage in using the δ terms. The reason for this is the high frequency of the attitude control loop in the presence of a pilot delay of 0.3 second. Since the control problem is symmetric with respect to each axis, the lateral and longitudinal urgency functions have identical coefficients.

An important objective of this example was to demonstrate the ability of the model to match performance statistics with a flight simulation in which the only input disturbance was pilot inaccuracy. There are two distinct sources of this for the multiaxis task. The first is observation, estimation, and control actuation noise, which is modeled using an additive white noise superimposed on the stick commands. The second source of pilot induced error arises from the operation of the side-arm controller used in the flight simulation.

Figure 50 shows an X-Y plot of lateral versus longitudinal stick obtained from the flight simulation.

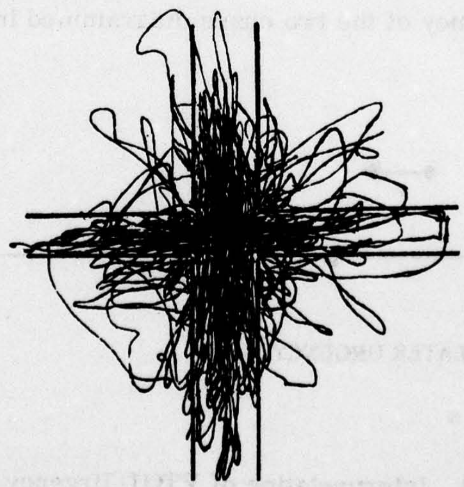

Figure 50. X-Y Plot of Lateral Versus Longitudinal Stick for VTOL Hover

This figure clearly shows the division of control activity between the two axes, but this division is not free from errors. If it were the trace would lie only on the

control axes. The failure for this to be the case shows that for the controller equipped with low gradients and breakout forces, the stick was not precisely centered nor moved exactly parallel to the control axes. These control actuation errors, called control crossfeed, References 1 and 2, are diagrammed in Figure 51. They consist of <u>bias</u>, the failure of the stick to be centered, and <u>skewness</u>, the failure of the stick to be moved parallel to the control axis. Data such as that shown in Figure 50 indicates that during any control episode, a particular value of bias and skewness applies. In this figure, boundaries have been superimposed to indicate the range of most of the crossfeed.

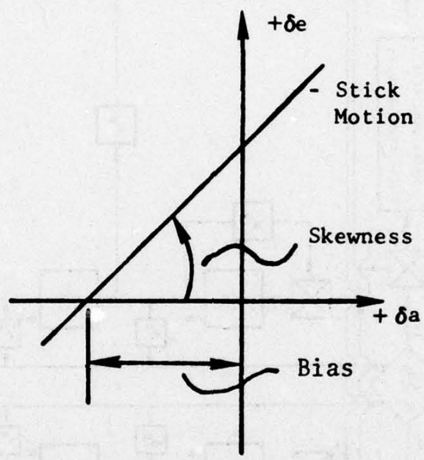

Figure 51. Definition of Crossfeed, Bias, and Skewness

Uniformly distibuted white noise was used to model these sources of pilot induced error. Estimates of the correct amplitudes were obtained from flight simulation data, and the model was optimized for minimum hovering error. A complete system diagram for the piloted hover problem is given in Figure 52.

The flight simulation was performed in 1973 on a Northrop fixed-base simulator similar to the one described in Subsection IV A. Position error was displayed as a point and attitude was presented as a line whose inclination represented bank angle, and whose elevation showed pitch. This display is shown in Figure 53.

The subject, a former Navy test pilot, determined the optimum control sensitivities and was asymptotically trained. Data were taken for a total of twenty trials of 100 seconds duration. The data from the simulation described in Reference 1 are tightly clustered and show only a slight learning trend during the final ten trials.

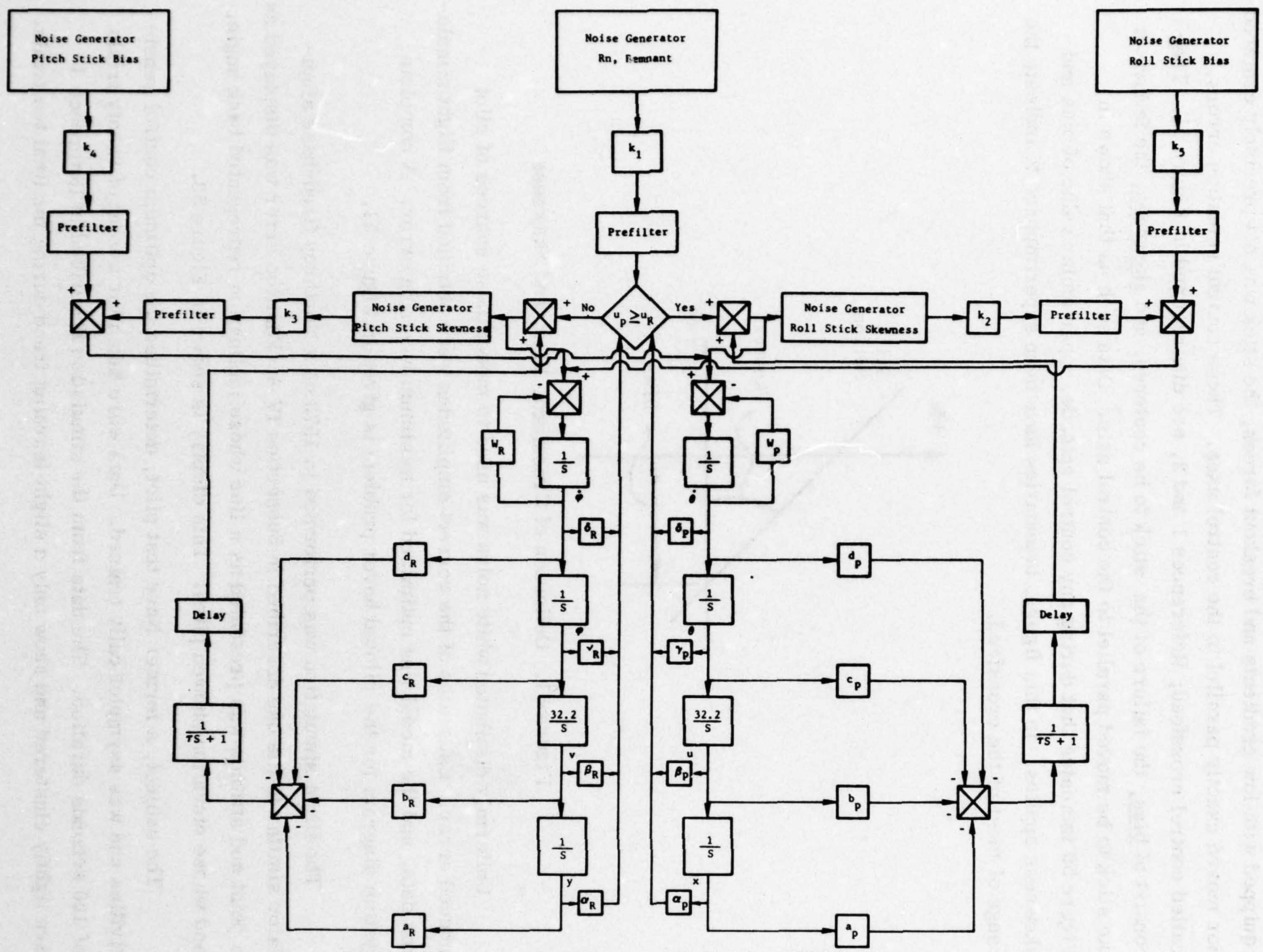

Figure 52. Complete System Model for VTOL Hover

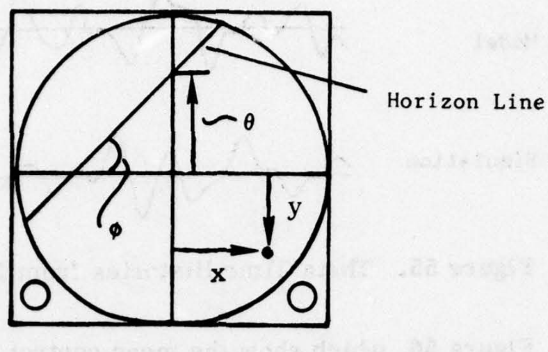

Figure 53. VTOL Flight Simulation Display

A comparison between the model and the simulation ground paths is shown in Figure 54, each drawn to the same scale.

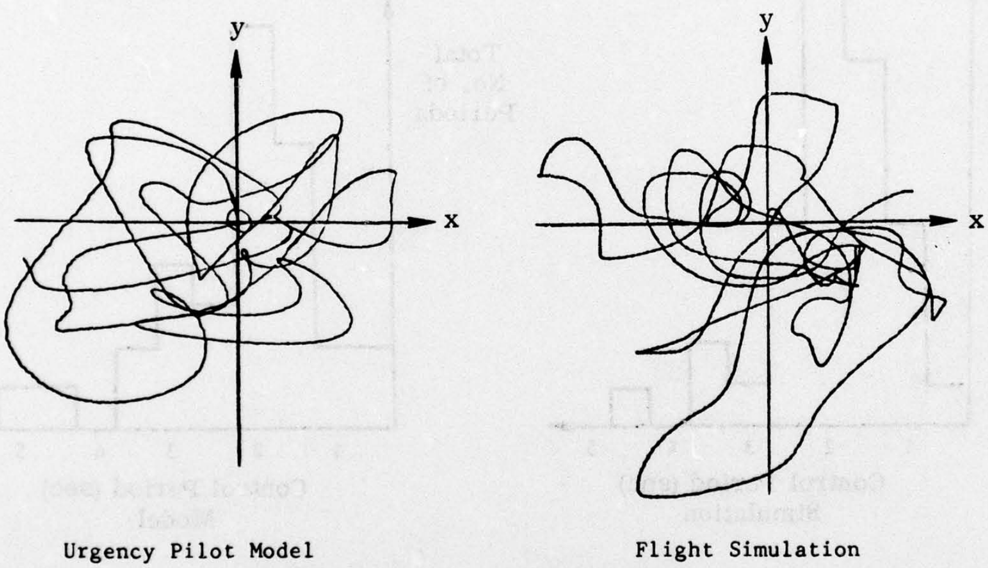

Figure 54. Model and Flight Simulation Ground Paths for VTOL Hover

These ground path traces show many similar qualitative features, absent in the non-optimum model, such as the sharp points and tight turns where the pilot nearly stops the translation of the airplane in order to initiate a better velocity vector. The similar size and shape of the loops indicate similar spectral content. Figure 55 shows a segment of the time history of pitch angle as generated by the model and by the simulation.

The switching times produced by the model and by estimation from the strip chart recording of the lateral and longitudinal stick are compared in the following

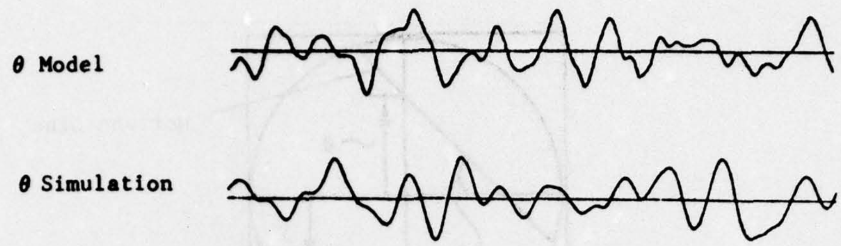

Figure 55. Theta Time Histories from Model and Simulation

histograms, Figure 56, which show the mean control period to be between 1.5 and 2.0 seconds. These statistics are combined from lateral and longitudinal data since the dynamics of the two axes are identical.

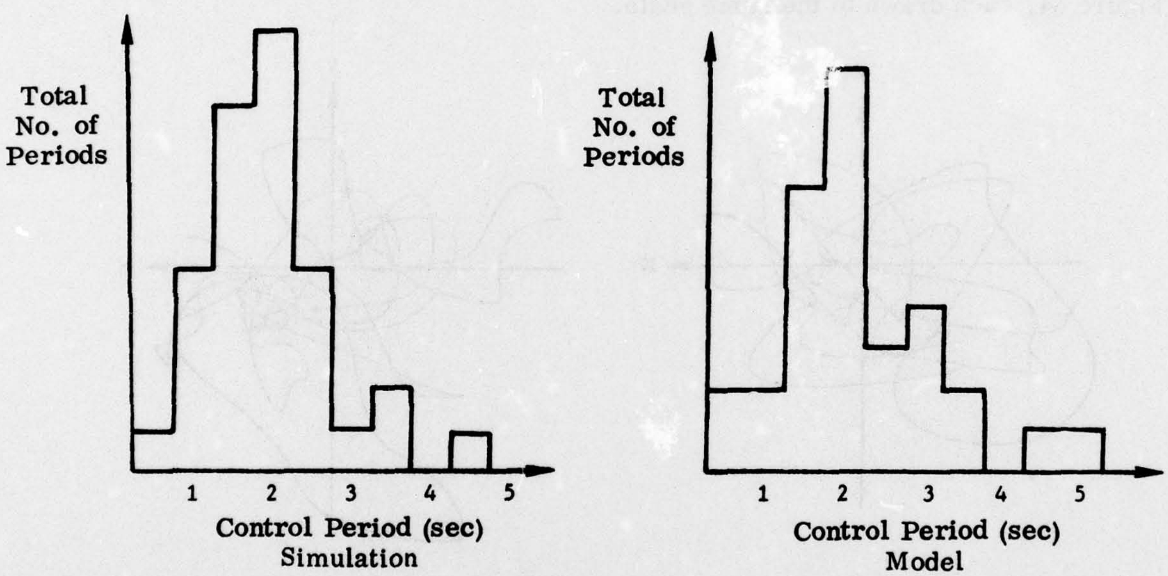

Figure 56. Histograms of Pilot Switching

The most discriminating comparison of the urgency function model and the flight simulation is in the statistics. These are shown in Figure 57. This agreement of the model and the simulation completes the comparisons for the VTOL example.

The optimum pilot model coefficients are given in Figure 58.

	Flight Simulation Data (rms)	2-Axis Model Predictions (rms)
X (ft)	.221	.225
Y (ft)	.217	.172
u (ft/sec)	.065	.084
v (ft/sec)	.074	.082
θ (deg)	.057	.153
ϕ (deg)	.120	.151
$\dot{\theta}$ (deg/sec)	.198	.256
$\dot{\phi}$ (deg/sec)	.440	.261

Figure 57. Comparison of Model and Simulation Statistics

Compensation	Urgency	Disturbances
$a = -0.02$	$\alpha = 5$	$k_1 = 0.1$
$b = -0.215$	$\beta = 40$	$k_2 = k_3 = 0.2$
$c = -8.0$	$\gamma = 10$	$k_4 = k_5 = 0.04$
$d = 2.0$	$\delta = 0$	

Figure 58. Optimum VTOL Pilot Model Parameters

D. ERROR RATE INFORMATION IN ATTENTION ALLOCATION PILOT MODELS

The postulated form of the urgency functions in the Northrop Urgency Decision Pilot Model has provision for both error and error rate terms. It was the purpose of the present study 1) to apply the optimized complete model with urgency function error rate terms to marginally stable and unstable second-order system dynamics, and 2) to examine the characteristics of the performance of the optimized incomplete model without urgency function error rate terms. In this way, the importance of the error rate terms in achieving optimum performance can be assessed by examining the control strategy the model adopts to compensate for the lack of error rate information in its attention shifting algorithm.

The postulated form of the urgency functions has led to correct predictions in VTOL hover, attitude stabilization in turbulence, and air-to-air target tracking analyses as discussed elsewhere in this Section. In the attitude stabilization in turbulence problem, which is single-loop on each axis, it was found that the error rate terms were not needed; in the air-to-air target tracking problem, it will be found that while error rate terms are needed on both axes, the rate coefficient required on the multi-loop axis is two orders of magnitude larger than that required on the single-loop axis. These results raise two fundamental questions:

1) Are urgency function error rate terms ever required for single-loop component tasks?

2) If so, how do they improve pilot model performance?

To answer these questions, a two-axis compensatory tracking task was simulated. The command tracking signals were generated from uniformly distributed white noise as shown in Figure 59. Identical filters were used for each command.

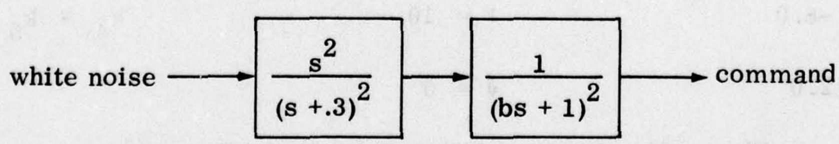

Figure 59. Command Tracking Signal Generation

Two sets of dynamics and two command tracking filter bandwidths were combined to produce six two-axis configurations as shown in Figure 60. Both symmetric and asymmetric combinations were used.

Configuration	Lateral Dynamics	Longitudinal Dynamics	b
1	$\frac{1}{s^2}$	$\frac{1}{s^2}$	8
2	$\frac{1}{s^2}$	$\frac{1}{s^2}$	4
3	$\frac{1}{s^2}$	$\frac{1}{s(s-1)}$	8
4	$\frac{1}{s^2}$	$\frac{1}{s(s-1)}$	4
5	$\frac{1}{s(s-1)}$	$\frac{1}{s(s-1)}$	8
6	$\frac{1}{s(s-1)}$	$\frac{1}{s(s-1)}$	4

Figure 60. Configurations Simulated for Command Tracking Task

A flow diagram of the total piloted system appears in Figure 61. The pilot compensations were modeled using a gain K, lead T_L, and delay τ on each axis and programmed as follows:

$$\delta a = (\text{Delay } \tau)\left\{K_\phi(\phi_e + T_{L_\phi} \dot{\phi}_e)\right\}$$

$$\delta e = (\text{Delay } \tau)\left\{K_\theta(\theta_e + T_{L_\theta} \dot{\theta}_e)\right\}$$

The delays were fixed at $\tau = 0.3$ second, and the gains and leads were chosen to produce optimum model tracking statistics.

The urgency functions for this problem are of the form:

$$U_\phi = \left| \alpha_\phi \left|\phi_e\right| + \beta_\phi \frac{\phi_e}{\left|\phi_e\right|} \dot{\phi}_e \right|$$

$$U_\theta = \left| \alpha_\theta \left|\theta_e\right| + \beta_\theta \frac{\theta_e}{\left|\theta_e\right|} \dot{\theta}_e \right|$$

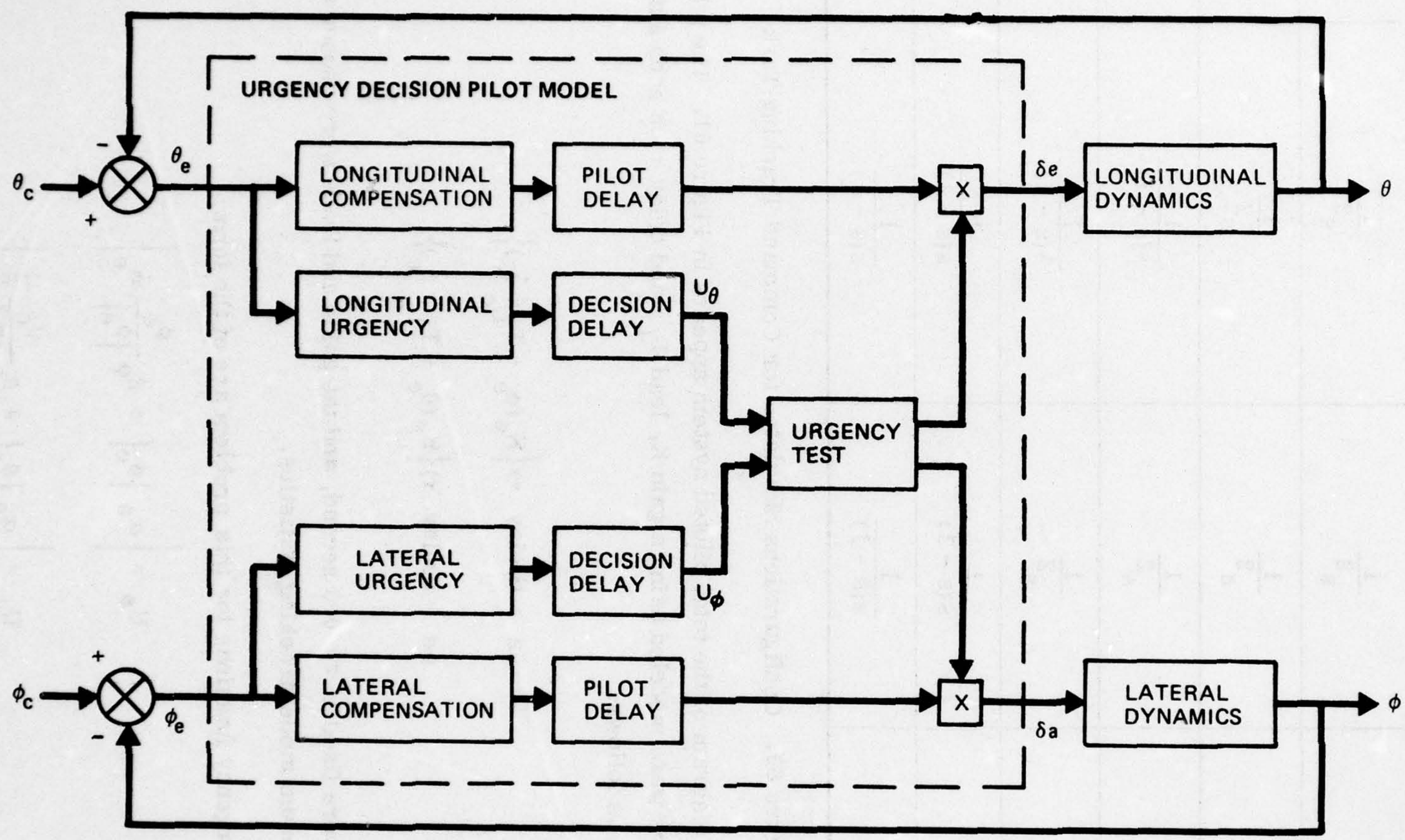

Figure 61. Control Configuration for Command Tracking Task

AD-A056 983 NORTHROP CORP HAWTHORNE CA AIRCRAFT GROUP F/G 5/8
PREDICTION, EVALUATION, AND SPECIFICATION OF CLOSED LOOP AND MU--ETC(U)
FEB 78 E D ONSTOTT, W H FAULKNER F33615-77-C-3008
UNCLASSIFIED NOR-77-162 AFFDL-TR-78-3 NL

2 OF 3
AD
A056983

Since the planned simulation called for identical display gains on each axis, the relative position urgencies as perceived by the pilot are equal, so that α_ϕ and α_θ can be set to unity. The reflection of objective urgency as presented to the pilot by the display, in the subjective urgency adopted by the pilot is addressed in Reference 3. For the analysis of the complete model, the rate coefficients β_ϕ and β_θ are optimized along with the compensation gains and leads.

In order to discuss how the model is optimized for this problem, it is first necessary to describe the display used in the flight simulation. The CRT display consisted of a bright dot against a darkened background containing white crosshairs. Vertical displacement of the dot away from the origin represented θ_e, while horizontal displacement indicated ϕ_e. The pilot was instructed to keep the dot as close to the center as possible. This radial tracking error

$$r(t) = \sqrt{\alpha^2 \phi_e^2(t) + \mu^2 \theta_e^2(t)}$$

is shown in Figure 62.

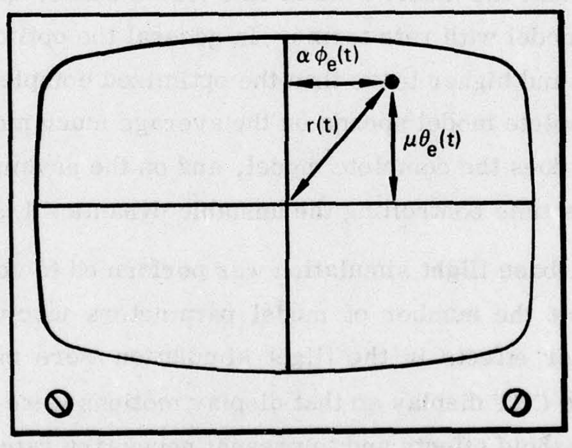

Figure 62. Flight Simulation Display

Explicitly, the quantity that the pilot and the pilot model optimized is given by

$$\bar{r} = \frac{1}{T}\int_0^T r(t)\, dt$$

In order to gain insight into the role played by error rate terms in the urgency functions, the model was optimized using a perturbation method to select K_ϕ, K_θ, T_{L_ϕ},

$T_{L\theta}$, β_ϕ, and β_θ. The resulting tracking performance then could be compared with the model performance obtained by setting the β_ϕ and β_θ urgency rate coefficients to zero and optimizing by selecting K_ϕ, K_θ, $T_{L\phi}$, and $T_{L\theta}$.

Since it was planned that the pilot in the subsequent fixed-base flight simulation would fly a series of twenty thirty-second runs for a total of 600 seconds of data for each configuration, the model was optimized with respect to the average radial error for the same test schedule. To reduce statistical fluctuations of the command tracking signal, the command tracking signal sequence for each of the short runs was computed and scaled beforehand to produce a zero mean and unit standard deviation, i.e., unit command intensity.

The averaged optimum model tracking scores and the corresponding model parameters for each of the six configurations with and without error rate terms in the urgency functions are given in Table 6. Averaged data on dwell fractions (the percentages of time the model controls each axis) and mean dwell times (the average length of individual control episodes) are presented in Table 7.

Table 6 shows that the model without rate terms cannot approach the tracking performance of the model with rate terms. In general the optimized incomplete model employs lower gains and higher leads than the optimized complete model. Table 7 shows that the incomplete model spends on the average much more time on each control episode than does the complete model, and on the asymmetric tasks spends a greater portion of its time controlling the unstable dynamics $1/s(s - 1)$.

A piloted fixed-base flight simulation was performed to verify the pilot model predictions. To limit the number of model parameters involved in the problem, display and controller effects in the flight simulation were minimized. This was done by using a large CRT display so that display motions were amplified enough to eliminate visual threshold effects and to present necessary rate information; controller effects were reduced by using a side-arm controller that had low force gradients and low but conspicuous breakout forces. The same computer programs, running on the same digital computers, were used for the simulation that were used for the model analysis work. For the flight simulation, the program operated in real-time and branched around the pilot model routine, reading the pilot's stick commands through analog-to-digital converters.

The pilot was instructed to keep the dot as close to the center of the screen as possible. This proved to be a difficult task, requiring several hours of training before

TABLE 6. PILOT MODEL DATA FOR COMMAND TRACKING TASK

Configuration	Model with Error Rate Terms								Model without Error Rate Terms							
	$\bar{r}$	σ_r	K_ϕ	T_{L_ϕ}	β_ϕ	K_θ	T_{L_θ}	β_θ	$\bar{r}$	σ_r	K_ϕ	T_{L_ϕ}	β_ϕ	K_θ	T_{L_θ}	β_θ
1	0.299	0.0744	2.0	2.6	1.0	2.0	2.6	1.0	0.554	0.171	1.6	2.4	0	1.6	2.4	0
2	0.374	0.0866	1.8	2.6	1.0	1.8	2.6	1.0	0.726	0.211	1.4	2.4	0	1.4	2.4	0
3	0.464	0.122	2.2	2.0	1.0	2.0	2.0	1.0	1.20	0.452	1.4	2.4	0	1.6	2.2	0
4	0.578	0.138	2.2	2.0	1.0	2.0	2.0	1.0	1.60	0.491	1.2	2.6	0	1.6	2.4	0
5	0.647	0.178	2.2	1.8	1.0	2.2	1.8	1.0	5.81	3.29	0.4	8.0	0	0.4	8.0	0
6	0.725	0.158	2.6	2.0	4.0	2.6	2.0	4.0	6.80	2.79	0.4	8.0	0	0.4	8.0	0

TABLE 7. DWELL FRACTION AND MEAN DWELL TIME DATA

Configuration	Model with Error Rate Terms				Model without Error Rate Terms			
	Dwell Fractions		Mean Dwell Times (seconds)		Dwell Fractions		Mean Dwell Times (seconds)	
	lat.	long.	lat.	long.	lat.	long.	lat.	long.
1	0.509	0.491	0.392	0.372	0.501	0.499	0.770	0.748
2	0.496	0.504	0.383	0.383	0.486	0.514	0.812	0.836
3	0.422	0.578	0.371	0.503	0.317	0.683	0.505	1.06
4	0.414	0.586	0.362	0.505	0.316	0.684	0.475	0.998
5	0.490	0.510	0.439	0.451	0.522	0.478	1.46	1.26
6	0.495	0.505	0.388	0.394	0.479	0.521	1.31	1.38

the pilot achieved his optimum performance. It also required much experimentation with the controller and display scalings to arrive at a combination for each configuration that allowed the pilot to perform optimally.

The pilot flew thirty-second runs, in sets of ten or twenty. For each configuration, the best set of twenty (or the best pair of sets of ten) was saved, giving a total of 600 seconds of data. On the asymmetric configurations, the pilot flew ten runs with $1/s^2$ lateral and $1/s(s - 1)$ longitudinal, and ten with $1/s^2$ longitudinal and $1/s(s - 1)$ lateral.

The pilot's averaged tracking scores for the six configurations, along with the averaged scores for the complete model with urgency function error rate terms, are given in Table 8. The excellent agreement between the tracking scores predicted by the complete model with the flight simulation tracking scores is shown in Figure 63.

TABLE 8. COMMAND TRACKING FLIGHT SIMULATION AND MODEL DATA

Configuration	Pilot		Model	
	$\bar{r}$	σ_r	$\bar{r}$	σ_r
1	0.311	0.0250	0.299	0.0744
2	0.420	0.0619	0.374	0.0866
3	0.506	0.0778	0.464	0.122
4	0.609	0.0678	0.578	0.138
5	0.565	0.0882	0.647	0.178
6	0.650	0.0952	0.725	0.158

A few comments concerning the large standard deviations σ_r in Table 7 are in order. The precomputing and scaling of each command tracking signal sequence removed one source of variability from the runs by fixing the mean of ϕ_c and θ_c at zero with a standard deviation of one. However, this did nothing to standardize the frequency content of the command tracking signals. Owing to the short length of each run, the spectral content of the command sequences varied widely from run to run.

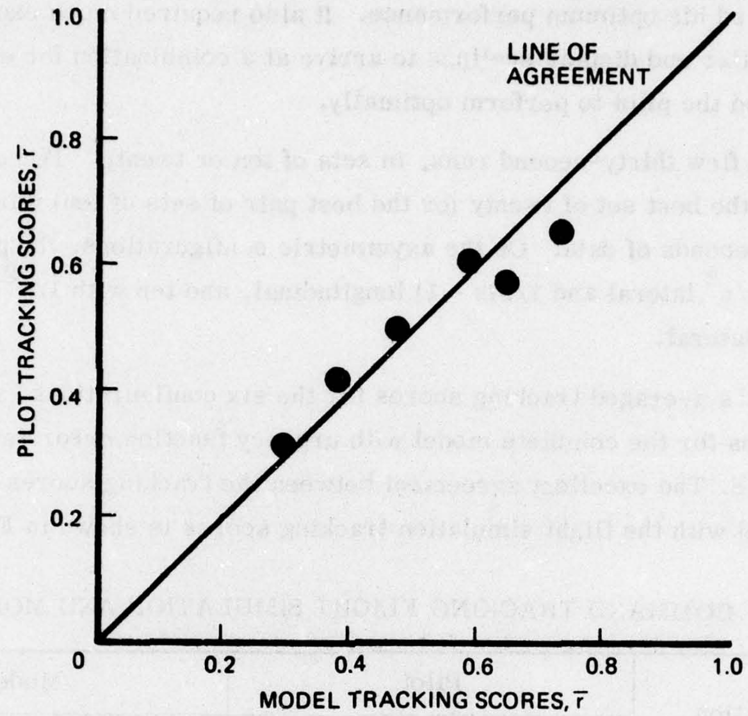

Figure 63. Agreement of Model and Flight Simulation Tracking Scores

This is illustrated by Figure 64, which presents time histories of two command tracking sequences for the simulation; each sequence represents thirty seconds of real time. It is likely that this contributed to the variability in both pilot and model performance.

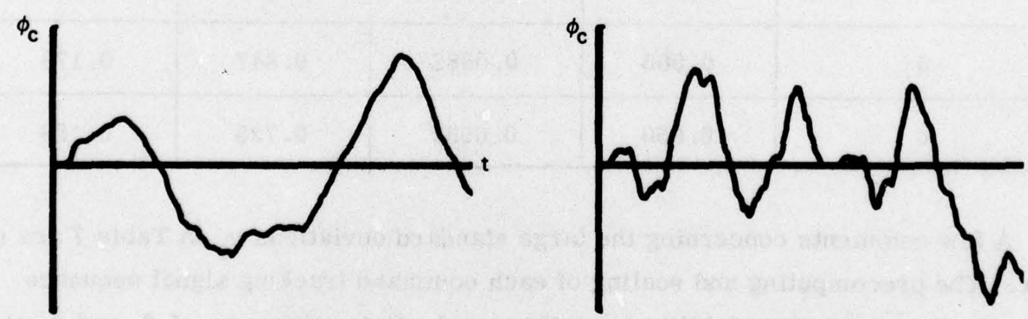

Figure 64. Sample Tracking Command Time Histories

It can also be seen in Table 8 that the standard deviations for the model are generally larger than those for the pilot. It was sometimes the case that initial transient command tracking errors and rates were of such a nature that the pilot had

to abort a run shortly after it began (e.g., the dot started near the edge of the screen and quickly went out of sight). Such runs were not counted, and no statistics were kept for them. However, the model did not have this luxury and had to fly every command sequence that came along. It is likely that a few of these runs with large initial transients in each set increased the standard deviations of the model's tracking scores.

The Northrop Urgency Decision Pilot Model was applied to a compensatory tracking task involving marginally stable and unstable second order system dynamics in an effort to answer two fundamental questions concerning the model's urgency functions:

1) Are urgency function error rate terms ever required for single-loop tasks?

2) If so, how do they improve pilot model performance?

Comparison of the flight and pilot model simulations demonstrated the complete model's ability to predict the pilot's tracking statistics, just as it demonstrated that the incomplete model was incapable of such performance. Analysis using the pilot model with and without the benefit of error rate information in the urgency functions demonstrated the importance of this error rate information in the following ways:

1) The complete model agreed well with the flight simulation, whereas the incomplete model without urgency function rate terms had badly degraded performance not seen in the flight simulation.

2) The error rate information in the complete model led to attention shifting rates necessary to control the unstable systems, while the incomplete model was not able to initiate corrective action promptly enough to maintain low error rates.

3) Since large rates built up, the incomplete model was forced in most cases to adopt higher leads to control them, while adopting lower gains to avoid overcontrolling the system.

4) In asymmetric tasks, the incomplete model was forced to spend a disproportionate amount of time trying to control the rates generated by the less stable dynamics.

From the results of this study, it is reasonable to conclude that urgency function error rate terms are required for analysis of any unstable or marginally stable system or, in general, for any system capable of evolving appreciable error rates.

E. COMPARISON OF THE MULTIAXIS PILOT MODEL WITH WANAMAKER-SOWER DATA

The problem described in the previous Subsection is similar to a study performed by Wanamaker and Sower at the Air Force Institute of Technology, Reference 8. Their thesis contains the complete description of a command tracking flight simulation analyzed by means of linear reconstruction theory and measured mean control periods to predict the tracking errors. Since the urgency decision multiaxis pilot model generates its own information concerning sample periods, it is of interest to compare the mean sample data the model generates with the experimental values which were obtained through the use of a split display and eye electrodes. The model was exercised in a manner identical to that just described in Subsection IV D. The following data is taken from Reference 1. Figure 65 shows a sample of time histories for the tracking command and the two tracking errors for 20 seconds of flight as generated by the model. In this case one of the axes was unstable, called the side task in the thesis. For all combinations of dynamics and commands, only the longitudinal task was given a command tracking history; the lateral command was the constant zero. Since all lateral dynamics were unstable, inadvertent control inputs modeled by small initial errors were sufficient to initiate the lateral task.

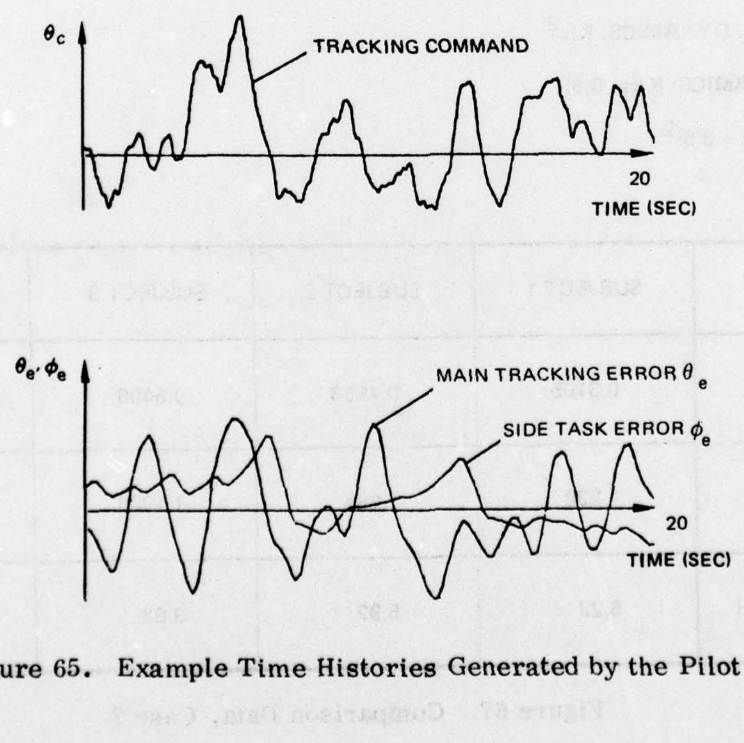

Figure 65. Example Time Histories Generated by the Pilot Model

Data for six combinations of system dynamics and command bandwidths are given in Figures 66-71 for Cases 1 - 6.

LONGITUDINAL DYNAMICS: K/(s - 1)

LATERAL DYNAMICS: K/(s - 1.5)

COMMAND: $K/(s + 0.5)^2$

	SUBJECT 1	SUBJECT 2	SUBJECT 3	NORTHROP 2-AXIS MODEL
σ / σ_c (RMS)	0.2742	0.3696	0.3697	0.4161
MEAN CONTROL PERIOD (SEC)	0.9509	0.9271	0.9277	1.110
ERROR BANDWIDTH (RAD/SEC)	3.83	3.61	3.71	4.20

Figure 66. Comparison Data, Case 1

LONGITUDINAL DYNAMICS: K/s^2

LATERAL DYNAMICS: K/(s - 0.5)

COMMAND: $K/(s + 0.5)^2$

	SUBJECT 1	SUBJECT 2	SUBJECT 3	NORTHROP 2-AXIS MODEL
σ / σ_c (RMS)	0.3195	0.4553	0.5406	0.3825
MEAN CONTROL PERIOD (SEC)	1.238	1.285	1.1006	1.32
ERROR BANDWIDTH (RAD/SEC)	6.22	5.92	3.66	3.8

Figure 67. Comparison Data, Case 2

LONGITUDINAL DYNAMICS: K/s

LATERAL DYNAMICS: K/(s - 1.5)

COMMAND: $K/(s + 1.5)^2$

	SUBJECT 1	SUBJECT 2	NORTHROP 2-AXIS MODEL
σ / σ_c (RMS)	0.6249	0.6156	0.6159
MEAN CONTROL PERIOD (SEC)	1.22	1.17	1.11
ERROR BANDWIDTH (RAD/SEC)	4.87	3.54	4.6

Figure 68. Comparison Data, Case 3

LONGITUDINAL DYNAMICS: K/(s - 1)

LATERAL DYNAMICS: K/(s - 1.5)

COMMAND: $K/(s + 1.5)^2$

	SUBJECT 1	SUBJECT 2	NORTHROP 2-AXIS MODEL
σ / σ_c (RMS)	0.8454	0.8838	0.8598
MEAN CONTROL PERIOD (SEC)	1.077	1.008	1.041
ERROR BANDWIDTH (RAD/SEC)	4.3	3.1	4.1

Figure 69. Comparison Data, Case 4

LONGITUDINAL DYNAMICS: K/s^2

LATERAL DYNAMICS: $K/(s - 1.5)$

COMMAND: $K/(s + 1.5)^2$

	SUBJECT 1	SUBJECT 2	NORTHROP 2-AXIS MODEL
σ / σ_c (RMS)	0.8201	1.0556	0.8991
MEAN CONTROL PERIOD (SEC)	1.551	1.944	1.923
ERROR BANDWIDTH (RAD/SEC)	7.04	5.13	4.9

Figure 70. Comparison Data, Case 5

LONGITUDINAL DYNAMICS: K/s

LATERAL DYNAMICS: $K/(s - 1.5)$

COMMAND: $K/(s + 0.5)^2$

	SUBJECT 1	SUBJECT 2	SUBJECT 3	NORTHROP 2-AXIS MODEL
σ / σ_c (RMS)	0.2029	0.2781	0.2465	0.2335
MEAN CONTROL PERIOD (SEC)	1.093	1.1515	0.8939	1.031
ERROR BANDWIDTH (RAD/SEC)	3.83	3.32	3.62	3.8

Figure 71. Comparison Data, Case 6

Graphical comparison of the model with the simulation data can be made for both the tracking errors and the mean sample periods. This is done in Figures 72 and 73.

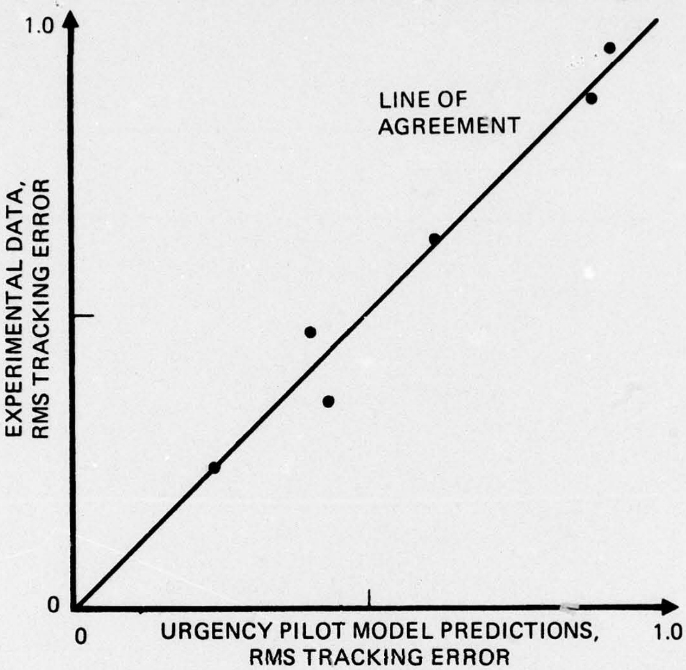

Figure 72. Comparison of Tracking Errors

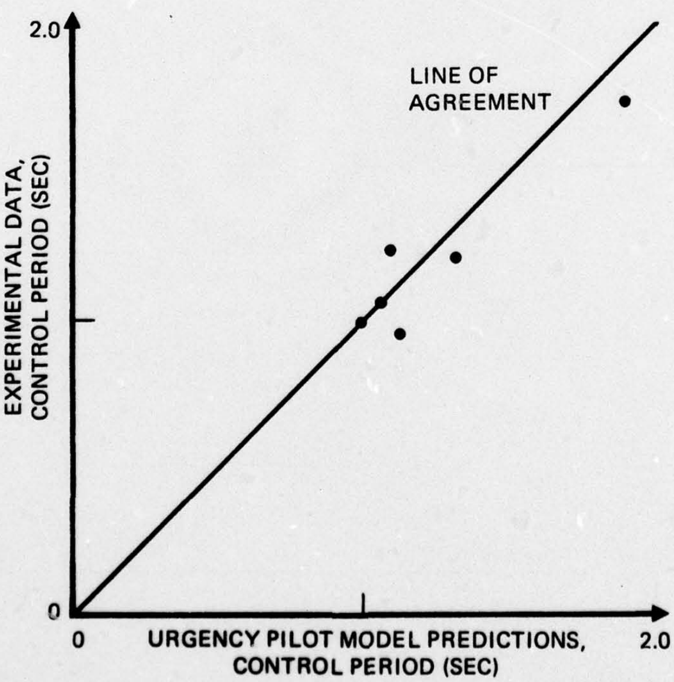

Figure 73. Comparison of Mean Control Periods

This data again shows the accuracy of the model in predicting the tracking errors of a multiaxis task, and in addition, generating the mean control periods observed in the flight simulation performed at AFIT.

F. TARGET TRACKING WITH VISUAL DELAYS AND SIDE TASK

In 1975, M. J. Queijo and D. R. Riley of NASA LRC performed a flight simulation study to determine the effect of time delays in visual cues on pilot tracking performance, as reported in Reference 11. The subjects controlled a five degree-of-freedom aircraft tracking a target that maneuvered by slow altitude oscillations in the vertical plane. By delaying the visual CRT display, evaluation of flight simulator time delays was obtained. In addition to vertical and horizontal tracking statistics, workload information was obtained by use of a side task which consisted of using an electrical stylus to tap alternately on two electrodes separated by a barrier and strapped to the subject's leg. The general availability and completeness of the reported experiment make this problem a useful one for the demonstration of the Northrop Urgency Decision Pilot Model.

The pilot's specific tasks were as follows:

1) Track the target vertically. The target oscillated at a frequency of 0.21 radian/sec with an amplitude of ±100 feet at a distance of 600 feet ahead of the tracking aircraft.

2) Track the target horizontally. The target did not oscillate horizontally; inadvertent pilot input provided the lateral task.

3) Whenever possible, perform the side task of tapping the electrodes strapped to the leg. This tapping rate was postulated to measure pilot reserve attention capacity for the target tracking task.

The following assumptions are made to establish the dynamic form of the multiaxis pilot model:

1) The pilot tracks vertically and horizontally, not in azimuth and elevation.

2) The vertical tracking, horizontal tracking, and side tasks are performed one at a time depending on the relative urgencies U_V, U_H, U_{ST} of these tasks.

3) The side task represents a constant urgency diversion from the vertical and horizontal tasks:

$$U_{ST} = \text{Constant}$$

These pilot model assumptions can then be implemented by programming a time-domain simulation of the pilot compensations for each task along with the urgency functions and their associated decision logic. Figure 74 shows a diagram of the complete simulation model.

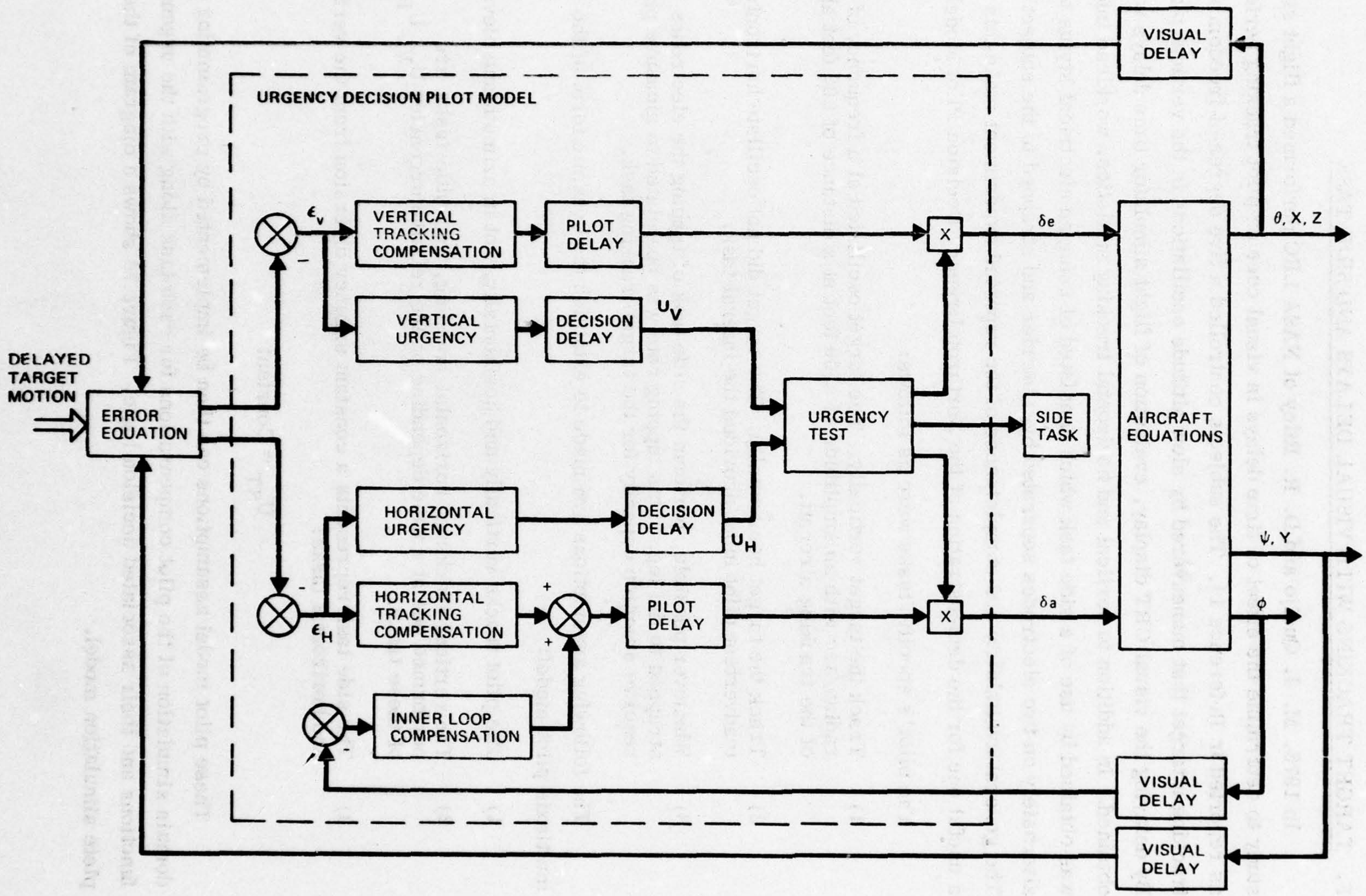

Figure 74. Control Configuration for Target Tracking Task

Consider the vertical task first. Here the tracking task is essentially to point the aircraft, so that this pilot closure is a single-loop pitch tracking task. Now if ϵ, K, and T_L denote tracking error, pilot model gain, and pilot model lead, with the subscripts V and H denoting the vertical and horizontal tasks, the fixed-form compensation of the vertical task can be written:

$$\begin{cases} \delta e = (\text{Delay } \tau) \left\{ K_V \left(\epsilon_V + T_{L_V} \dot{\epsilon}_V \right) \right\} \\ \delta a = 0 \end{cases}$$

The associated urgency function of this single-loop control task is then dictated by the general formulation of the Urgency Decision Pilot Model to be of the form:

$$U_V = \left| \alpha_V \left| \epsilon_V \right| + \beta_V \frac{\epsilon_V \dot{\epsilon}_V}{\left| \epsilon_V \right|} \right|$$

When the model is in horizontal control, it is required to track the target through changes in the heading of the tracking aircraft. This multiloop task is modeled through an inner loop attitude stabilization and an outer loop heading command tracking closure. These take the forms:

$$\delta a_1 = (\text{Delay } \tau) \left\{ K_\phi \left(\phi + T_{L\phi} \dot{\phi} \right) \right\}$$

$$\delta a_2 = (\text{Delay } \tau) \left\{ K_H \left(\epsilon_H + T_{L_H} \dot{\epsilon}_H \right) \right\}$$

$$\begin{cases} \delta a = \delta a_1 + \delta a_2 \\ \delta e = 0 \end{cases}$$

The horizontal urgency function takes the form:

$$U_H = \left| \alpha_H \left| \epsilon_H \right| + \beta_H \frac{\epsilon_H \dot{\epsilon}_H}{\left| \epsilon_H \right|} \right|$$

Of the various pilot model parameters, only four can be assigned typical values prior to optimizing the model performance. These values are given in Figure 75.

$\tau = 0.3$ second
$T_{L_V} = 0.5$ second
$T_{L\phi} = 0.5$ second
$T_{L_H} = 1.5$ second

Figure 75. Pre-assigned Pilot Model Parameters for Target Tracking Task

To demonstrate the predictive capabilities of the model, it is necessary to make clear the procedure for obtaining the other model parameters by optimization, and the method for calibrating the side task urgency. There were three steps involved in doing this:

1) Optimize by individual parameter variation the quantities

$$K_V,\ \alpha_V,\ \beta_V,\ K_\phi,\ K_H,\ \alpha_H,\ \beta_H$$

for minimum target miss distance

$$\epsilon = \sqrt{\epsilon_V^{\,2} + \epsilon_H^{\,2}}$$

using no side task,

$$U_{ST} = 0$$

2) Using these optimized values, vary U_{ST} until ϵ_V matches ϵ_V reported for the minimum visual delay for one simulation test datum.

3) Holding all quantities including U_{ST} constant for each simulation test case, vary the visual time delay by retarding the pilot model input to obtain model data.

It should be clear from the above description that the model was adjusted by optimization, with only one statistic of one test case matched to the simulation data for the calibration of the side task urgency.

Two test cases, 5 and 6, were investigated. Each unit of visual delay equaled 0.03125 second. Table 9 shows the rms comparison data for pilot model and flight simulation for a visual delay of 1.5 units. It can be seen that not only do the tracking errors agree, but the average stick amplitude and stick rate statistics agree as well. Table 10 presents the data for a visual delay of 6.5 units. Tracking error is given in meters, and stick displacement and stick rates are given in rad and rad/sec, respectively.

For case 5, Figures 76 and 77 present the pilot model data for the vertical and horizontal tracking errors in comparison with means and standard deviations from simulation data. Pilot model data are presented in Table 11.

TABLE 9. NUMERICAL DATA FOR VISUAL DELAY OF 1.5 UNITS

	CASE 5		CASE 6	
	Simulation	Model	Simulation	Model
ϵ_V	3.53*	3.42	3.72	3.60
ϵ_H	1.94	1.97	2.68	2.06
$\overline{\delta a}$	0.029	0.030	0.049	0.042
$\overline{\delta e}$	0.0057	0.0044	0.0089	0.0097
$\overline{\delta \dot{a}}$	0.093	0.26	0.154	0.36
$\overline{\delta \dot{e}}$	0.025	0.017	0.035	0.047

*matched data point for side task urgency calibration

TABLE 10. NUMERICAL DATA FOR VISUAL DELAY OF 6.5 UNITS

	CASE 5		CASE 6	
	Simulation	Model	Simulation	Model
ϵ_V	4.09	4.29	5.05	5.82
ϵ_H	2.39	2.09	3.45	2.32
$\overline{\delta a}$	0.035	0.032	0.061	0.051
$\overline{\delta e}$	0.0067	0.006	0.011	0.02
$\overline{\delta \dot{a}}$	0.098	0.26	0.169	0.375
$\overline{\delta \dot{e}}$	0.027	0.021	0.038	0.09

A combined comparison of cases 5 and 6 vertical and horizontal tracking errors is presented in Figure 78 for the data furnished in Tables 9 and 10.

It is useful to examine a plot of tracking error versus time as it would be viewed in the sight by the pilot. Figure 79 was obtained from the pilot model, with the pilot model control episodes shown by symbols as indicated.

There are two important observations that can be made concerning the side task. By examination of many time histories such as Figure 9, it was clear that the side task

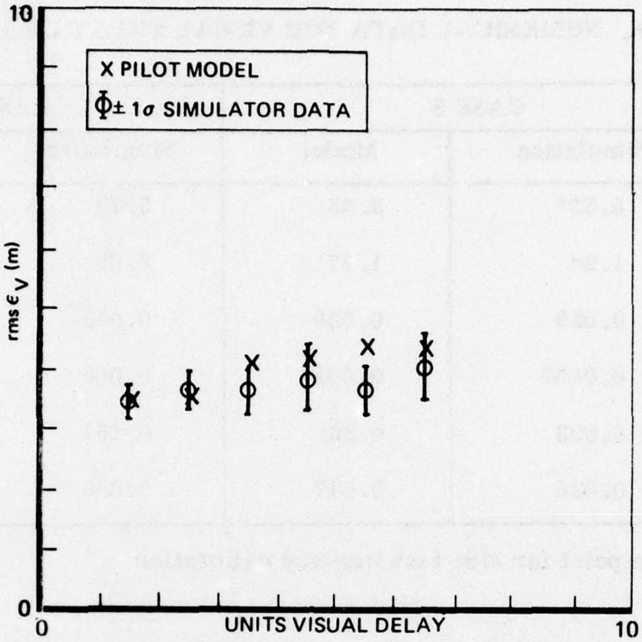

Figure 76. Case 5 Vertical Tracking Data

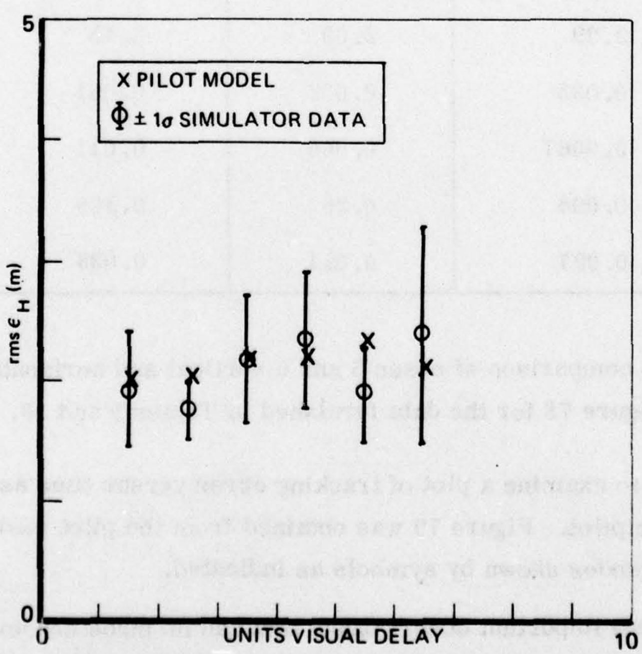

Figure 77. Case 5 Horizontal Tracking Data

TABLE 11. TARGET TRACKING PILOT MODEL DATA

	Case 5	Case 6
K_V	-0.002	-0.004
α_V	2.0	2.0
β_V	0.1	0.1
K_H	0.015	0.02
α_H	3.0	3.0
β_H	10.0	10.0
K_ϕ	0.6	0.6
U_{st}	5.5	5.5
Initial ϵ_H	0.5 m	0.5 m

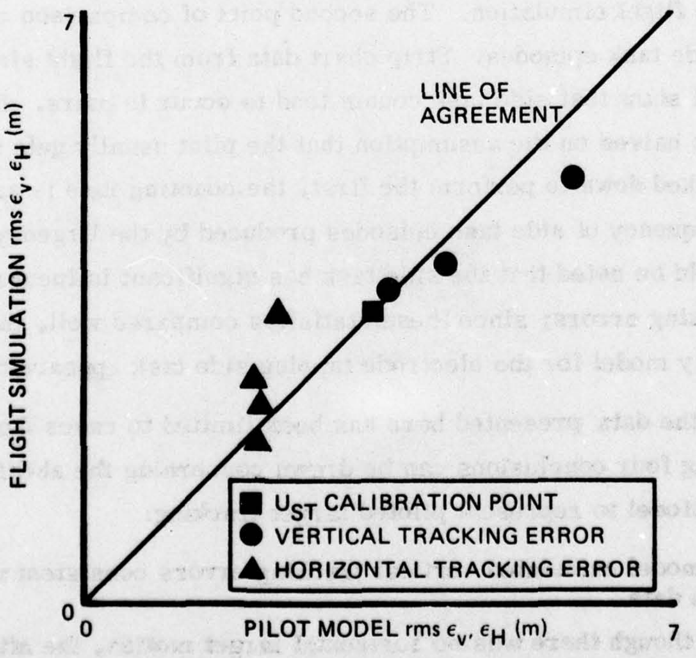

Figure 78. Comparison of Flight Simulation and Pilot Model Target Tracking Errors.

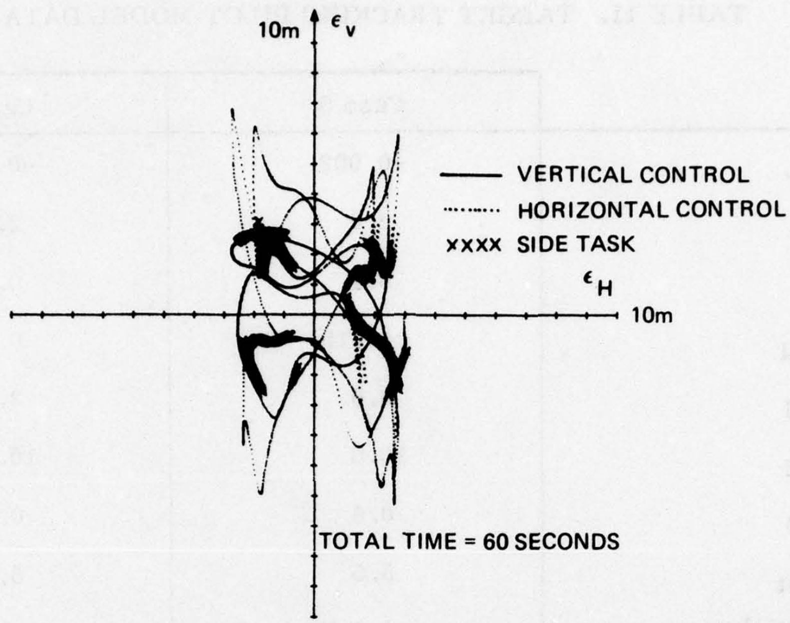

Figure 79. Time History of Pilot Model Control Episodes

was performed by the model only when the tracking error was less than four meters. Since the simulation pilots were reported not to perform side tasks unless the error was less than one wing semi-span of the target, this model side task behavior is consistent with the flight simulation. The second point of comparison concerns the frequency of side task episodes. Strip chart data from the flight simulation reported in Reference 11 show that side task counts tend to occur in pairs. If the side task counting rate is halved on the assumption that the pilot usually gets the second count once he has looked down to perform the first, the counting rate is approximately equal to the frequency of side task episodes produced by the Urgency Decision Pilot Model. It should be noted that the side task has significant influence on vertical and horizontal tracking errors; since these statistics compared well, the assumption of a constant urgency model for the electrode tapping side task appears to be justified.

Although the data presented here has been limited to cases 5 and 6 of Reference 11, the following four conclusions can be drawn concerning the ability of the Urgency Decision Pilot Model to represent piloted target tracking:

1) The model calculated vertical tracking errors consistent with simulation data.

2) Even though there was no horizontal target motion, the attention diversion in the pilot and in the pilot model led to horizontal tracking errors of nearly the same size.

3) The assumption that the electrode tapping side task used in the flight simulation could be represented as a constant urgency task was justified by a) the vertical and horizontal tracking errors, b) the occurrence of side task episodes only for tracking errors less than 4 meters, and c) the frequency of side task episodes.

These results justify the last conclusion:

4) The Urgency Decision Pilot Model can be used to predict tracking error performance and pilot workload for maneuvering targets by straightforward application of the fixed form model adjusted through optimization and side task urgency calibration involving only one data point.

SECTION V

COMPARISON OF TURBULENCE MODELS AND CONTROL SYSTEM LAG EFFECTS

The preceding Sections have discussed the classification of precision piloted flight tasks and have shown how the general Urgency Decision Pilot Model can be used to address a wide variety of piloted tasks. The remainder of the report will consider further applications of the model to the following problems:

- Comparison of Gaussian and Reeves non-Gaussian turbulence models.
- Evaluation of the effects of control system lags on two-axis attitude stabilization performance.
- Evaluation and specification of flying qualities by means of step target tracking.
- Prediction of pilot reserve attention capacity as a measure of pilot workload.

In order to demonstrate the applicability of the methods to general aircraft models, nonlinear six degree-of-freedom aircraft equations will be employed. The aircraft to be studied is the F-5E in a clean configuration at nine flight conditions, with and without flight control system augmentation. Since these aircraft descriptions will be used for each of the above applications, an account of these F-5E configurations will be presented next.

A. AIRCRAFT DESCRIPTIONS AND EQUATIONS OF MOTION

For the analyses discussed above, nine F-5E configurations were chosen from the aircraft's primary operating envelope, shown in Figure 80. The flight conditions simulated are given in Table 12, and corresponding dimensional stability derivatives appear in Tables 13 and 14.

PRECEDING PAGE BLANK-NOT FILMED

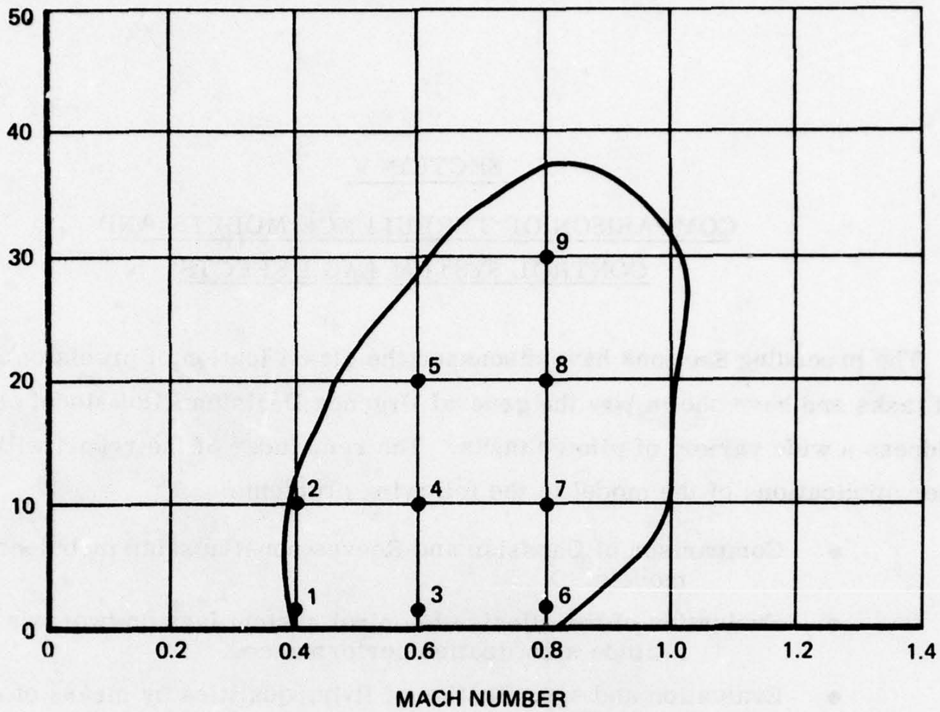

Figure 80. F-5E Primary Operating Envelope

TABLE 12. F-5E CONFIGURATIONS SIMULATED

Case	Mach No.	Altitude (ft)	u_o (ft/sec)	w_o (ft/sec)	θ_o (deg)
1	0.4	1750.	445.	35.8	4.60
2	0.4	10000.	428.	49.2	6.56
3	0.6	1750.	669.	25.7	2.20
4	0.6	10000.	646.	34.6	3.07
5	0.6	20000.	620.	48.6	4.48
6	0.8	1750.	893.	21.0	1.35
7	0.8	10000.	861.	27.8	1.85
8	0.8	20000.	829.	38.1	2.63
9	0.8	30000.	794.	54.4	3.92

I_{xx} = 3600 ft-lb-sec^2 $\quad$ I_{zz} = 47000 ft-lb-sec^2

I_{yy} = 44200 ft-lb-sec^2 $\quad$ $I_{xy} = I_{xz} = I_{yz} = 0$

TABLE 13. F-5E DIMENSIONAL STABILITY DERIVATIVES – LATERAL (BODY AXES)

	Case 1	Case 2	Case 3	Case 4	Case 5	Case 6	Case 7	Case 8	Case 9
Y_v	-0.2434	-0.1762	-0.3557	-0.2559	-0.1804	-0.4698	-0.3366	-0.2358	-0.1611
Y_p	-0.5254	-0.3807	-0.7719	-0.5543	-0.3896	-1.022	-0.7312	-0.5112	-0.3482
Y_r	2.216	1.598	3.275	2.346	1.643	4.344	3.105	2.166	1.471
$Y_{\delta a}$	-1.904	-1.110	-5.081	-3.295	-1.987	-9.534	-6.354	-4.034	-2.381
$Y_{\delta r}$	22.30	15.25	50.53	34.66	23.07	90.05	61.84	41.23	26.54
L_v	-0.07703	-.06422	-0.08809	-0.06987	-0.05650	-0.1045	-0.07990	-0.06136	-0.04789
L_p	-3.546	-2.329	-5.829	-4.022	-2.644	-8.013	-5.609	-3.785	-2.428
L_r	1.538	1.266	1.867	1.444	1.130	2.282	1.713	1.284	0.9697
$L_{\delta a}$	15.01	9.646	34.06	23.35	15.52	60.73	41.69	27.78	17.87
$L_{\delta r}$	4.032	2.582	9.837	6.574	4.187	17.97	12.16	7.924	4.904
N_v	0.01370	0.009882	0.01967	0.01425	0.01015	0.02582	0.01857	0.01308	0.009025
N_p	0.06054	0.04496	0.08612	0.06258	0.04482	0.1126	0.08118	0.05737	0.03976
N_r	-0.2629	-0.1928	-0.3803	-0.2747	-0.1948	-0.5005	-0.3594	-0.2526	-0.1735
$N_{\delta a}$	0.1961	0.1071	0.4889	0.3243	0.2038	0.8992	0.6062	0.3924	0.2400
$N_{\delta r}$	-2.680	-1.843	-6.032	-4.148	-2.771	-10.72	-7.374	-4.928	-3.184

TABLE 14. F-5E DIMENSIONAL STABILITY DERIVATIVES – LONGITUDINAL (BODY AXES)

	Case 1	Case 2	Case 3	Case 4	Case 5	Case 6	Case 7	Case 8	Case 9
X_u	-0.01303	-0.007238	-0.02187	-0.01499	-0.009732	-0.03021	-0.02109	-0.01416	-0.008984
X_w	0.05524	0.02091	0.08296	0.05907	0.04100	0.1108	0.07886	0.05470	0.03682
$X_{\dot{w}}$	-4.782×10^{-10}	-7.633×10^{-11}	-5.189×10^{-10}	7.768×10^{-10}	1.283×10^{-10}	-1.395×10^{-9}	-1.790×10^{-10}	-6.047×10^{-10}	3.028×10^{-11}
X_q	4.847×10^{-8}	7.828×10^{-6}	4.636×10^{-7}	-3.391×10^{-7}	1.808×10^{-6}	-3.315×10^{-7}	1.286×10^{-6}	5.417×10^{-7}	-1.268×10^{-6}
$X_{\delta e}$	13.74	9.214	31.84	21.66	14.22	57.18	39.09	25.87	16.46
Z_u	-0.06377	-0.06756	-0.03890	-0.04238	-0.04593	-0.02508	-0.02910	-0.03238	-0.03536
Z_w	-0.9966	-0.7120	-1.491	-1.063	-0.7396	-1.987	-1.417	-0.9842	-0.6638
$Z_{\dot{w}}$	-0.001389	-9.242×10^{-4}	-0.001556	-0.001105	-7.446×10^{-4}	-0.001615	-0.001167	-8.134×10^{-4}	-5.375×10^{-4}
Z_q	-2.098	-1.484	-3.176	-2.256	-1.558	-4.249	-3.022	-2.092	-1.402
$Z_{\delta e}$	-75.48	-53.21	-164.6	-114.5	-77.92	-289.3	-200.3	-135.2	-88.88
M_u	4.318×10^{-4}	4.288×10^{-4}	3.188×10^{-4}	3.136×10^{-4}	3.125×10^{-4}	2.634×10^{-4}	2.557×10^{-4}	2.501×10^{-4}	2.473×10^{-4}
M_w	-0.005367	-0.003728	-0.008297	-0.005849	-0.003990	-0.01118	-0.007918	-0.005445	-0.003609
$M_{\dot{w}}$	-1.421×10^{-4}	-9.430×10^{-5}	-1.596×10^{-4}	-1.132×10^{-4}	-7.618×10^{-5}	-1.657×10^{-4}	-1.197×10^{-4}	-8.337×10^{-5}	-5.502×10^{-5}
M_q	-0.3862	-0.2792	-0.5690	-0.4082	-0.2864	-0.7538	-0.5392	-0.3766	-0.2562
$M_{\delta e}$	-8.036	-5.649	-17.59	-12.22	-8.297	-30.95	-21.41	-14.44	-9.471

The aircraft was simulated both with and without augmenter, thus giving a total of eighteen test points. A description of the F-5E stability augmentation system is presented in Appendix C; the SAS gains for each of the nine flight conditions are given in Table 15.

TABLE 15. F-5E SAS GAINS

Case	K_A	K_V	K_Y
1	-0.24	0.19	1.1
2	-0.36	0.19	1.4
3	0.042	0.089	0.73
4	-0.084	0.15	0.87
5	-0.22	0.19	1.1
6	0.064	0.077	0.58
7	0.064	0.077	0.62
8	0.0056	0.11	0.78
9	-0.15	0.19	0.98

The coupled, nonlinear, six degree-of-freedom, constant coefficient, perturbation equations of motion used are shown in Figure 81. Kinematic, gravity orientation, and inertial nonlinearities are included. The equations are written about the aircraft body axes, and only one nonstandard assumption was made: that I_{XZ} can be neglected. For the configurations studied, I_{XZ} was zero.

The reader should note that in the equations of Figure 81, all dynamic variables are perturbed about trim values. The only non-zero trim values are u_o, w_o, and θ_o.

$$\dot{u} = g\,[\sin\theta_o\,(1-\cos\theta\cos\psi) - \cos\theta_o\,\sin\theta] - q(w_o + w) + rv$$
$$+ X_u\,(u+u_g) + X_w\,(w+w_g) + X_{\dot{w}}\,\dot{w} + X_q\,(q+q_g) + X_{\delta e}\delta e$$

$$\dot{w} = \frac{1}{1-Z_{\dot{w}}}\left\{ g[\cos\theta_o\,(\cos\theta\cos\phi - 1) - \sin\theta_o\,(\cos\psi\sin\theta\cos\phi + \sin\psi\sin\phi)] \right.$$
$$\left. + q(u_o+u) - pv + Z_u\,(u+u_g) + Z_w\,(w+w_g) + Z_q\,(q+q_g) + Z_{\delta e}\delta e \right\}$$

$$\dot{q} = I_2 pr + M_u\,(u+u_g) + M_w\,(w+w_g) + M_{\dot{w}}\dot{w} + M_q\,(q+q_g) + M_{\delta e}\delta e$$

$$\dot{r} = I_3 pq + N_v\,(v+v_g) + N_p\,(p+p_g) + N_r\,(r+r_g) + N_{\delta a}\delta a + N_{\delta r}\delta r$$

$$\dot{v} = g[\cos\theta_o\cos\theta\sin\phi - \sin\theta_o\,(\cos\psi\sin\theta\sin\phi - \sin\psi\cos\phi)]$$
$$- r\,(u_o+u) + p\,(w_o+w)$$
$$+ Y_v\,(v+v_g) + Y_p\,(p+p_g) + Y_r\,(r+r_g) + Y_{\delta a}\delta a + Y_{\delta r}\delta r$$

$$\dot{p} = I_1 qr + L_v\,(v+v_g) + L_p\,(p+p_g) + L_r\,(r+r_g) + L_{\delta a}\delta a + L_{\delta r}\delta r$$

$$\dot{\theta} = q\cos\phi - r\sin\phi$$

$$\dot{\phi} = p + \frac{\sin\theta}{\cos\theta}\,(q\sin\phi + r\cos\phi)$$

$$\dot{\psi} = (r\cos\phi + q\sin\phi)\,\frac{1}{\cos\theta}$$

Figure 81. Aircraft Equations of Motion

B. COMPARISON OF GAUSSIAN AND REEVES NON-GAUSSIAN TURBULENCE

Two-Axis Attitude Stabilization in Gaussian Turbulence

A simulation of two-axis attitude stabilization in turbulence was performed using the F-5E aircraft descriptions. This simulation was intended to serve two purposes. It was a base case for comparison with the subsequent non-Gaussian turbulence and control system lag simulations. It also served as a further validation of the Urgency Decision Pilot Model in problems involving more general equations of motion and more complete aircraft and control system descriptions.

The TASK in the simulation was stabilization of roll angle ϕ and pitch angle θ in the presence of uncorrelated u-, v-, and w-gusts. For Gaussian turbulence, white noise was filtered to produce the Dryden spectra specified in Reference 12.

The experimental setup for the fixed-base flight simulation was similar to that described in Section IV A. The CRT scalings chosen resulted in a horizontal dot displacement of 2.5 centimeters per degree of roll angle and a vertical dot displacement of 10 centimeters per degree of pitch angle, for a θ/ϕ scaling ratio of four to one.

For each aircraft configuration, ten thirty-second runs were made, giving a total of five minutes of data for each test point. In order to diminish low-frequency effects during the short runs and remove one source of variability in the data, each gust sequence was precomputed and scaled to zero mean and ten ft/sec rms. Further information on the precomputing procedure is contained in Appendix C.

The Urgency Decision Pilot Model applied to this problem was of the same form as described in Section IV A, with one major difference: in the current simulation, error rate terms in the urgency functions were required for optimum model performance. This was necessary even though the component tasks were both single-loop. The error rate coefficients were chosen along with the gains and leads in the model optimization process. Since the θ/ϕ display scaling ratio was four to one throughout the flight simulation, the longitudinal urgency function error coefficient was fixed at four, while the lateral urgency function error coefficient was fixed at one.

For some of the configurations, it was discovered that the open loop attitude errors in turbulence were the best that could be obtained; neither the pilot nor the model could improve on the open loop errors. Hence, these configurations (Cases 3 and 4 without augmenter; Cases 6 and 7; Case 8 without augmenter) were not used in the three simulations discussed in this Section.

Open loop attitude errors for all eighteen F-5E configurations are presented in Table 16. Complete flight simulation and model data for the eleven usable configurations are given in Tables 17 and 18. The mean and standard deviation values shown throughout the remainder of the report were calculated for sets of ten rms errors. It should be noted that the standard deviations of the rms errors are strong functions of run length, in this case 30 seconds. The close agreement between the model's scores and the pilot's scores — in terms of both mean and standard deviation — is shown in Figures 82 through 86, plotted from Tables 17 and 18.

TABLE 16. F-5E OPEN LOOP ATTITUDE ERRORS IN GAUSSIAN TURBULENCE

Case		Lateral error rms (deg)		Longitudinal error rms (deg)	
		mean	s.d.	mean	s.d.
1	With augmenter	2.77	0.531	0.886	0.160
	Without augmenter	2.90	0.680	1.59	0.291
2	With augmenter	3.67	0.674	1.10	0.232
	Without augmenter	3.52	0.783	1.82	0.341
3	With augmenter	1.46	0.248	0.561	0.0518
	Without augmenter	1.93	0.364	0.878	0.0778
4	With augmenter	1.99	0.334	0.569	0.0595
	Without augmenter	2.46	0.487	1.05	0.0813
5	With augmenter	2.72	0.432	0.633	0.0805
	Without augmenter	3.00	0.626	1.23	0.140
6	With augmenter	0.962	0.147	0.374	0.0196
	Without augmenter	1.58	0.338	0.631	0.113
7	With augmenter	1.29	0.204	0.450	0.0270
	Without augmenter	2.11	0.340	0.813	0.158
8	With augmenter	1.78	0.276	0.484	0.0341
	Without augmenter	2.37	0.423	0.906	0.106
9	With augmenter	2.42	0.350	0.482	0.0437
	Without augmenter	2.91	0.530	1.05	0.114

TABLE 17. FLIGHT SIMULATION DATA — ATTITUDE STABILIZATION IN GAUSSIAN TURBULENCE

Case		Tracking Errors, rms (deg)				
		Lateral		Longitudinal		Radial
		mean	s.d.	mean	s.d.	mean
1	With augmenter	1.73	0.302	0.249	0.0382	1.99
	Without augmenter	2.20	0.581	0.344	0.0454	2.60
2	With augmenter	2.01	0.390	0.273	0.0560	2.28
	Without augmenter	2.29	0.544	0.287	0.0340	2.56
3	With augmenter	1.24	0.143	0.214	0.0285	1.51
4	With augmenter	1.52	0.210	0.196	0.0324	1.71
5	With augmenter	1.62	0.211	0.216	0.0319	1.84
	Without augmenter	2.41	0.493	0.298	0.0436	2.69
8	With augmenter	1.33	0.254	0.190	0.0208	1.53
9	With augmenter	1.65	0.266	0.180	0.0203	1.80
	Without augmenter	2.42	0.346	0.291	0.0362	2.69

TABLE 18. PILOT MODEL DATA — ATTITUDE STABILIZATION IN GAUSSIAN TURBULENCE

Case		Tracking Errors, rms (deg)					Model Parameters					
		Lateral		Longitudinal		Radial	Lateral			Longitudinal		
		mean	s.d.	mean	s.d.	mean	K	T_L	β	K	T_L	β
1	With augmenter	1.61	0.272	0.233	0.0302	1.86	0.38	1.3	0.5	-1.2	0.50	4
	Without augmenter	2.38	0.437	0.325	0.0485	2.71	0.32	1.3	0.5	-0.84	0.80	4
2	With augmenter	2.01	0.395	0.249	0.0322	2.24	0.40	1.3	0.5	-1.4	0.50	4
	Without augmenter	2.43	0.499	0.313	0.0442	2.73	0.40	1.3	0.5	-1.0	0.80	4
3	With augmenter	1.16	0.176	0.218	0.0267	1.45	0.18	1.3	0.5	-0.67	0.50	4
4	With augmenter	1.46	0.227	0.211	0.0205	1.68	0.19	1.3	0.5	-0.84	0.50	4
5	With augmenter	1.70	0.291	0.213	0.0263	1.90	0.27	1.3	0.5	-1.1	0.50	4
	Without augmenter	2.58	0.468	0.319	0.0365	2.88	0.27	1.3	0.5	-0.70	0.80	4
8	With augmenter	1.33	0.180	0.207	0.0200	1.56	0.20	1.3	0.5	-0.75	0.50	4
9	With augmenter	1.58	0.250	0.186	0.0210	1.74	0.24	1.3	0.5	-1.1	0.50	4
	Without augmenter	2.64	0.316	0.314	0.0225	2.92	0.22	1.3	0.5	-0.55	0.80	4

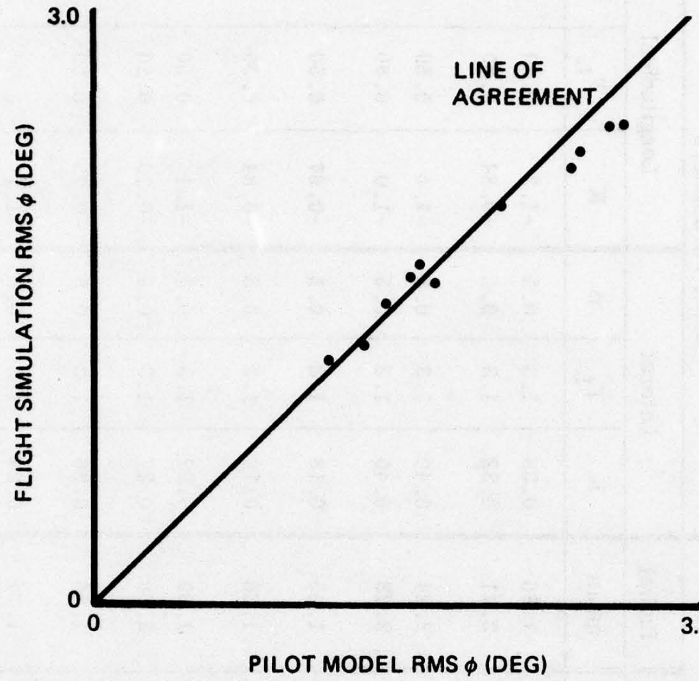

Figure 82. Agreement of Pilot Model and Flight Simulation Data for F-5E Lateral Tracking Errors, Gaussian Turbulence

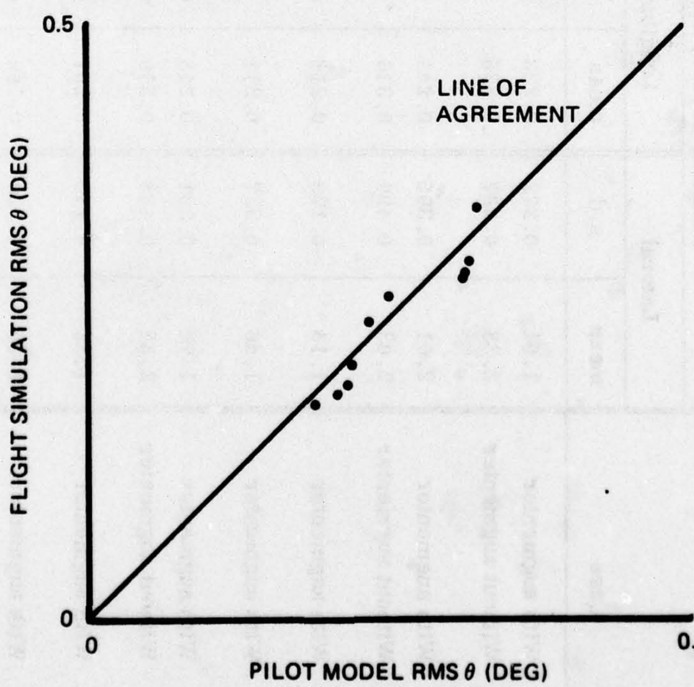

Figure 83. Agreement of Pilot Model and Flight Simulation Data for F-5E Longitudinal Tracking Errors, Gaussian Turbulence

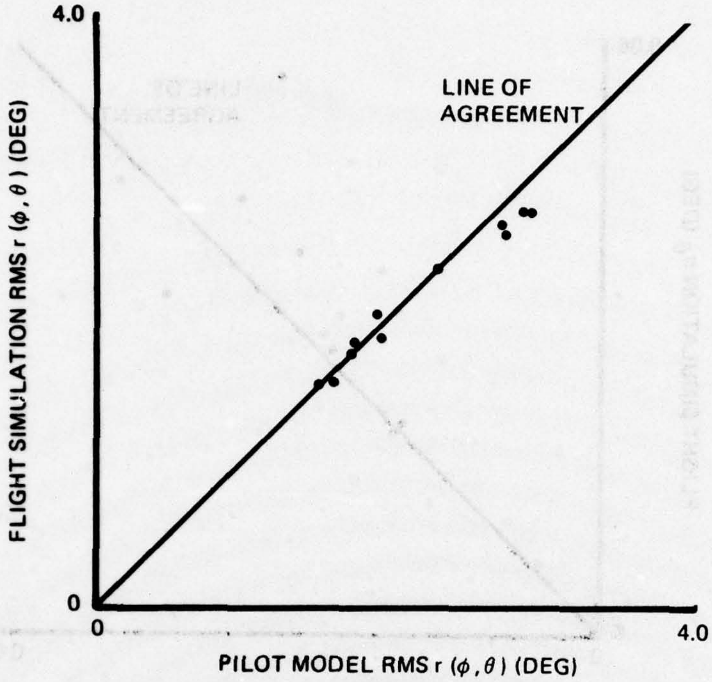

Figure 84. Agreement of Pilot Model and Flight Simulation Data for F-5E Radial Tracking Errors, Gaussian Turbulence

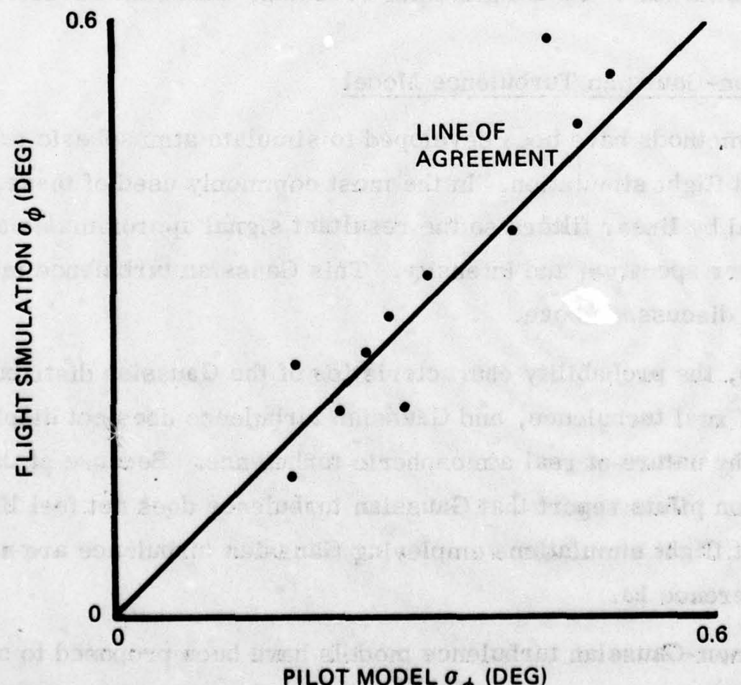

Figure 85. Agreement of Pilot Model and Flight Simulation Standard Deviation Data for F-5E Lateral Tracking, Gaussian Turbulence

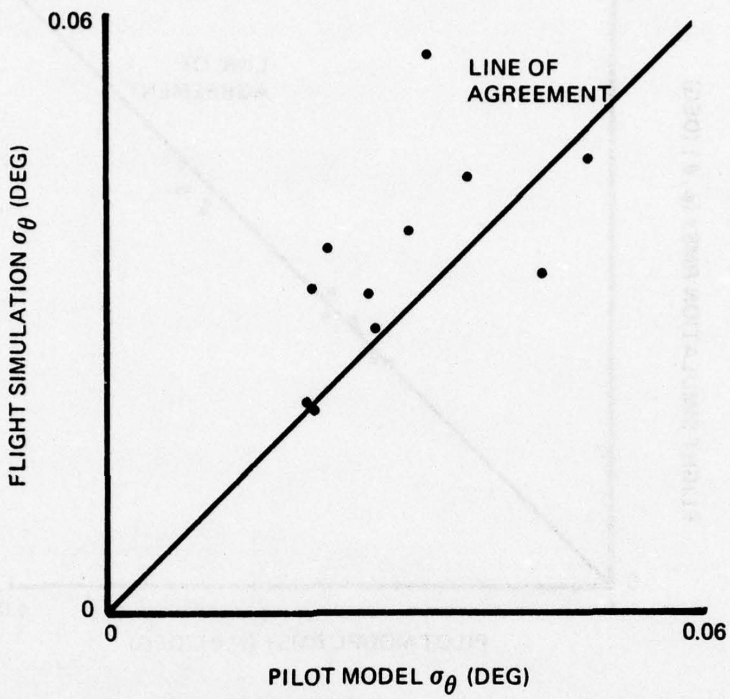

Figure 86. Agreement of Pilot Model and Flight Simulation Standard Deviation Data for F-5E Longitudinal Tracking, Gaussian Turbulence

The Reeves Non-Gaussian Turbulence Model

Several methods have been developed to simulate atmospheric turbulence for use in analysis and flight simulation. In the most commonly used of these, Gaussian white noise is shaped by linear filters so the resultant signal approximates atmospheric turbulence in power spectrum and intensity. This Gaussian turbulence model was used in the simulation discussed above.

However, the probability characteristics of the Gaussian distribution do not match those of real turbulence, and Gaussian turbulence does not display the large gusts and patchy nature of real atmospheric turbulence. Because of these shortcomings, simulation pilots report that Gaussian turbulence does not feel like real turbulence, and that flight simulations employing Gaussian turbulence are not sufficiently realistic, Reference 13.

Several non-Gaussian turbulence models have been proposed to overcome defects in the traditional Gaussian model. One such model was developed by P. M. Reeves,

Reference 13. Basically, the Reeves model employs Gaussian white noise sources and linear filters as shown in Figure 87 to produce each gust component.

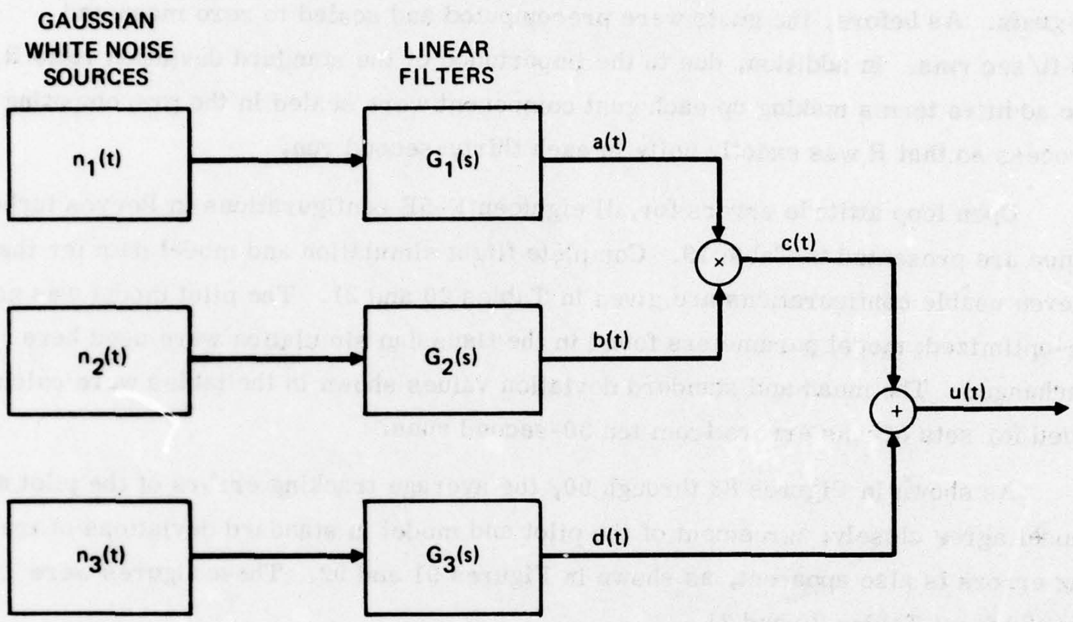

Figure 87. Reeves Non-Gaussian Turbulence Simulation

In Figure 87, a(t), b(t), and d(t) are all Gaussian processes, while c(t), the product of two Gaussian processes, is a Modified Bessel process. The final gust term is thus the sum of a Gaussian process and a Modified Bessel process.

The standard deviation ratio, $R = \sigma_c / \sigma_d$, determines the probability distribution and patchy character of the gust, u(t). If R is very small, the contribution of c(t) can be neglected, and u(t) is a Gaussian process. If R is very large, then the contribution of d(t) can be neglected, and u(t) is a Modified Bessel process. Reeves reported that an R value of approximately unity provides the best mix, producing turbulence that closely matches atmospheric turbulence in frequency content, probability characteristics, and patchiness.

<u>Two-Axis Attitude Stabilization in Reeves Turbulence</u>

A fixed-base flight simulation and model analysis similar to those reported above were performed to assess what effects non-Gaussian turbulence might have on the

tracking performance of both a human pilot and the pilot model. The only difference was that now Reeves turbulence was used instead of Gaussian turbulence.

The Reeves model was programmed to generate uncorrelated u-, v-, and w-gusts. As before, the gusts were precomputed and scaled to zero mean and 10 ft/sec rms. In addition, due to the importance of the standard deviation ratio R, the additive terms making up each gust component were scaled in the precomputing process so that R was exactly unity in each thirty-second run.

Open loop attitude errors for all eighteen F-5E configurations in Reeves turbulence are presented in Table 19. Complete flight simulation and model data for the eleven usable configurations are given in Tables 20 and 21. The pilot model was not re-optimized; model parameters found in the Gaussian simulation were used here unchanged. The mean and standard deviation values shown in the tables were calculated for sets of rms errors from ten 30-second runs.

As shown in Figures 88 through 90, the average tracking errors of the pilot and model agree closely; agreement of the pilot and model in standard deviations of tracking errors is also apparent, as shown in Figures 91 and 92. These figures were plotted from Tables 20 and 21.

TABLE 19. F-5E OPEN LOOP ATTITUDE ERRORS IN REEVES TURBULENCE

Case		Lateral error rms (deg)		Longitudinal error rms (deg)	
		mean	s.d.	mean	s.d.
1	With augmenter	2.65	0.308	0.756	0.0971
	Without augmenter	2.72	0.339	1.29	0.181
2	With augmenter	3.46	0.404	0.911	0.140
	Without augmenter	3.35	0.407	1.49	0.214
3	With augmenter	1.39	0.126	0.512	0.0289
	Without augmenter	1.80	0.276	0.784	0.0763
4	With augmenter	1.91	0.185	0.515	0.0329
	Without augmenter	2.33	0.295	0.927	0.124
5	With augmenter	2.60	0.264	0.560	0.0403
	Without augmenter	2.80	0.319	1.04	0.137
6	With augmenter	0.920	0.0679	0.355	0.0126
	Without augmenter	1.33	0.224	0.569	0.0465
7	With augmenter	1.23	0.0958	0.422	0.0173
	Without augmenter	1.68	0.232	0.661	0.0743
8	With augmenter	1.71	0.147	0.450	0.0204
	Without augmenter	2.30	0.295	0.830	0.140
9	With augmenter	2.33	0.209	0.439	0.0240
	Without augmenter	2.74	0.339	0.938	0.147

TABLE 20. FLIGHT SIMULATION DATA — ATTITUDE STABILIZATION IN REEVES TURBULENCE

Case		Tracking Errors, rms (deg)				
		Lateral		Longitudinal		Radial
		mean	s.d	mean	s.d.	mean
1	With augmenter	1.89	0.371	0.232	0.0396	2.10
	Without augmenter	2.21	0.228	0.342	0.0420	2.60
2	With augmenter	2.02	0.265	0.257	0.0388	2.27
	Without augmenter	2.43	0.275	0.334	0.0344	2.77
3	With augmenter	1.20	0.164	0.219	0.0211	1.48
4	With augmenter	1.43	0.123	0.222	0.0352	1.68
5	With augmenter	1.63	0.177	0.202	0.0201	1.82
	Without augmenter	2.36	0.604	0.312	0.0780	2.67
8	With augmenter	1.28	0.186	0.212	0.0272	1.53
9	With augmenter	1.59	0.127	0.184	0.0330	1.76
	Without augmenter	2.25	0.343	0.264	0.0352	2.49

TABLE 21. PILOT MODEL DATA — ATTITUDE STABILIZATION IN REEVES TURBULENCE

		Tracking Errors, rms (deg)					Model Parameters					
		Lateral		Longitudinal		Radial	Lateral			Longitudinal		
Case		mean	s.d.	mean	s.d.	mean	K	T_L	β	K	T_L	β
1	With augmenter	1.56	0.221	0.255	0.0288	1.86	0.38	1.3	0.5	-1.2	0.50	4
	Without augmenter	2.09	0.252	0.372	0.132	2.57	0.32	1.3	0.5	-0.84	0.80	4
2	With augmenter	1.97	0.208	0.255	0.00808	2.22	0.40	1.3	0.5	-1.4	0.50	4
	Without augmenter	2.28	0.264	0.314	0.0159	2.60	0.40	1.3	0.5	-1.0	0.80	4
3	With augmenter	1.07	0.0991	0.228	0.0239	1.41	0.18	1.3	0.5	-0.67	0.50	4
4	With augmenter	1.35	0.118	0.221	0.0163	1.61	0.19	1.3	0.5	-0.84	0.50	4
5	With augmenter	1.60	0.158	0.218	0.0119	1.82	0.27	1.3	0.5	-1.1	0.50	4
	Without augmenter	2.17	0.282	0.316	0.0260	2.51	0.27	1.3	0.5	-0.70	0.80	4
8	With augmenter	1.20	0.119	0.212	0.0174	1.47	0.20	1.3	0.5	-0.75	0.50	4
9	With augmenter	1.49	0.104	0.189	0.0144	1.67	0.24	1.3	0.5	-1.1	0.50	4
	Without augmenter	2.21	0.269	0.296	0.0234	2.51	0.22	1.3	0.5	-0.55	0.80	4

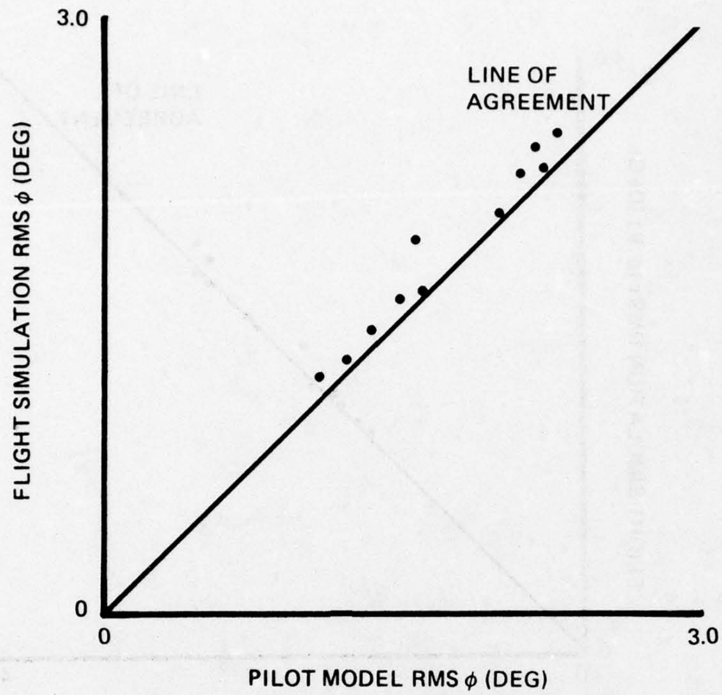

Figure 88. Agreement of Pilot Model and Flight Simulation Data for F-5E Lateral Tracking Errors, Reeves Turbulence

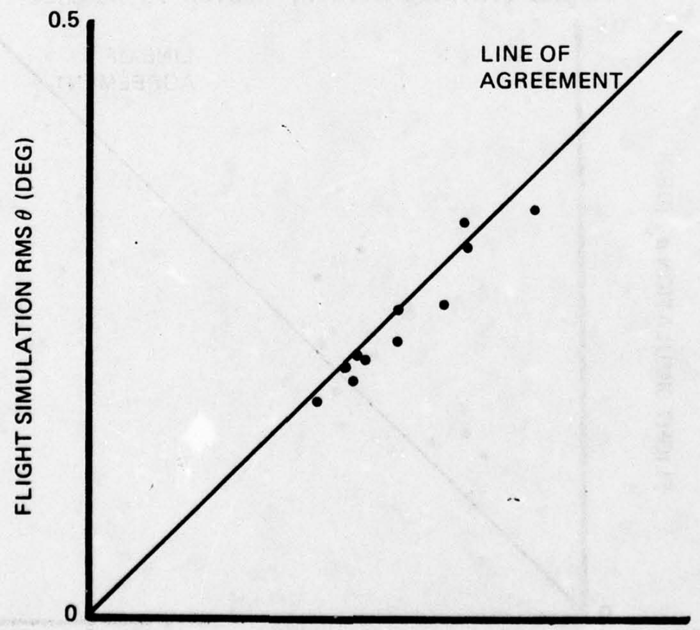

Figure 89. Agreement of Pilot Model and Flight Simulation Data for F-5E Longitudinal Tracking Errors, Reeves Turbulence

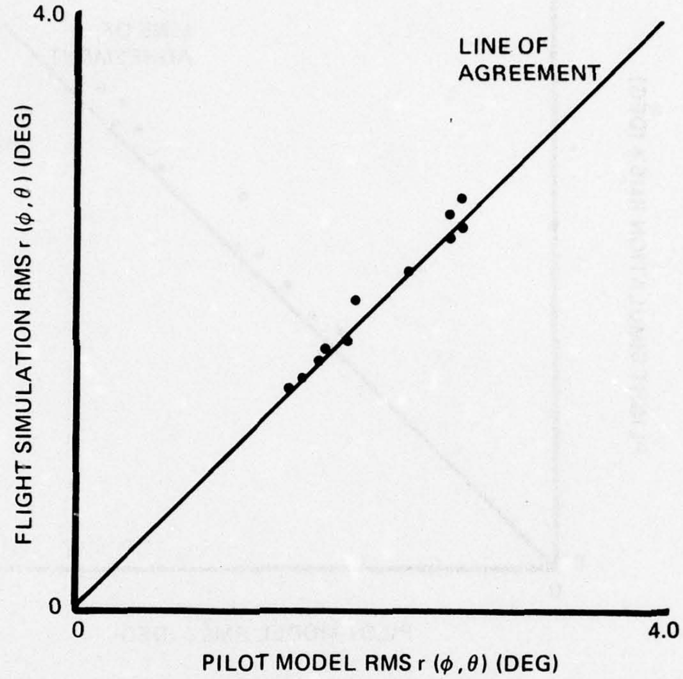

Figure 90. Agreement of Pilot Model and Flight Simulation Data for F-5E Radial Tracking Errors, Reeves Turbulence

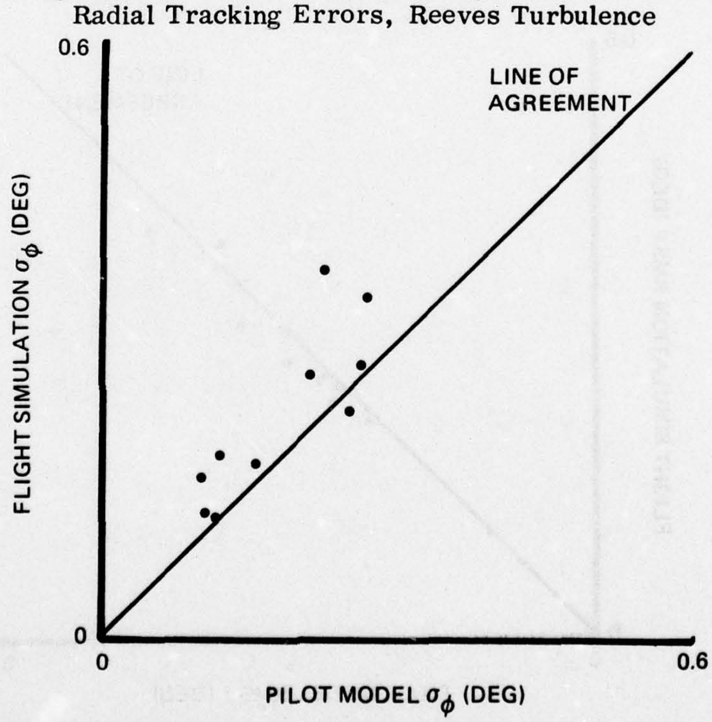

Figure 91. Agreement of Pilot Model and Flight Simulation Standard Deviation Data for F-5E Lateral Tracking, Reeves Turbulence

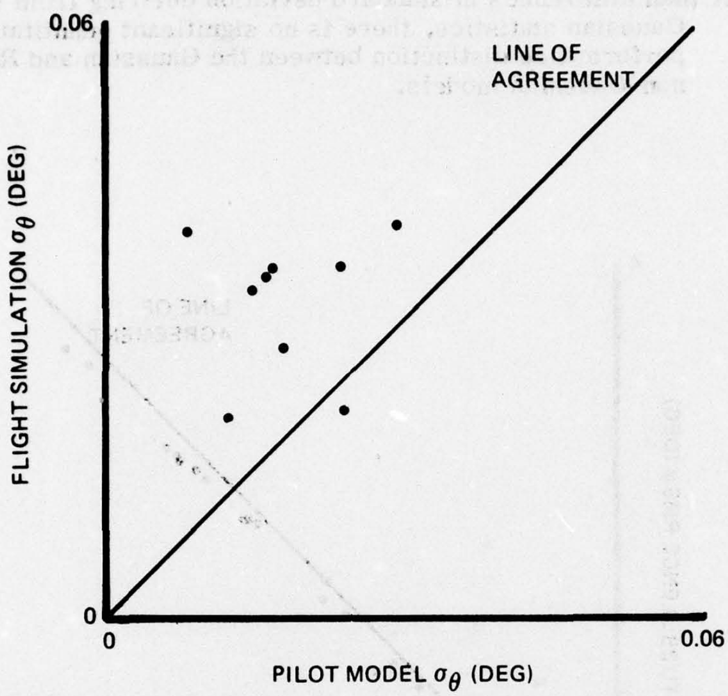

Figure 92. Agreement of Pilot Model and Flight Simulation Standard Deviation Data for F-5E Longitudinal Tracking, Reeves Turbulence

Comparison of Gaussian and Reeves Non-Gaussian Simulations

Gaussian and Reeves turbulence models differ somewhat in spectral content and more significantly in probability distribution. This is the probable cause of the small but noticeable disagreement in the F-5E open loop attitude errors shown in Figures 93 and 94. The average tracking scores achieved by the pilot and model shown in Figures 95 through 97 do not exhibit any marked trend. Figures 98 and 99 show that the standard deviations of the pilot's and model's tracking scores are generally somewhat smaller for the Reeves turbulence model than for the Gaussian turbulence model.

As a result of the above discussion, the following conclusions regarding the use of the Urgency Decision Pilot Model in the analysis of flying qualities in turbulence can be drawn:

- The model is validated for a general nonlinear aircraft representation.
- The model is accurate for prediction with the non-Gaussian Reeves turbulence model, and can therefore be expected to be accurate with other non-Gaussian turbulence sources.

- Other than differences in standard deviation deriving from the non-Gaussian statistics, there is no significant quantitative performance distinction between the Gaussian and Reeves non-Gaussian models.

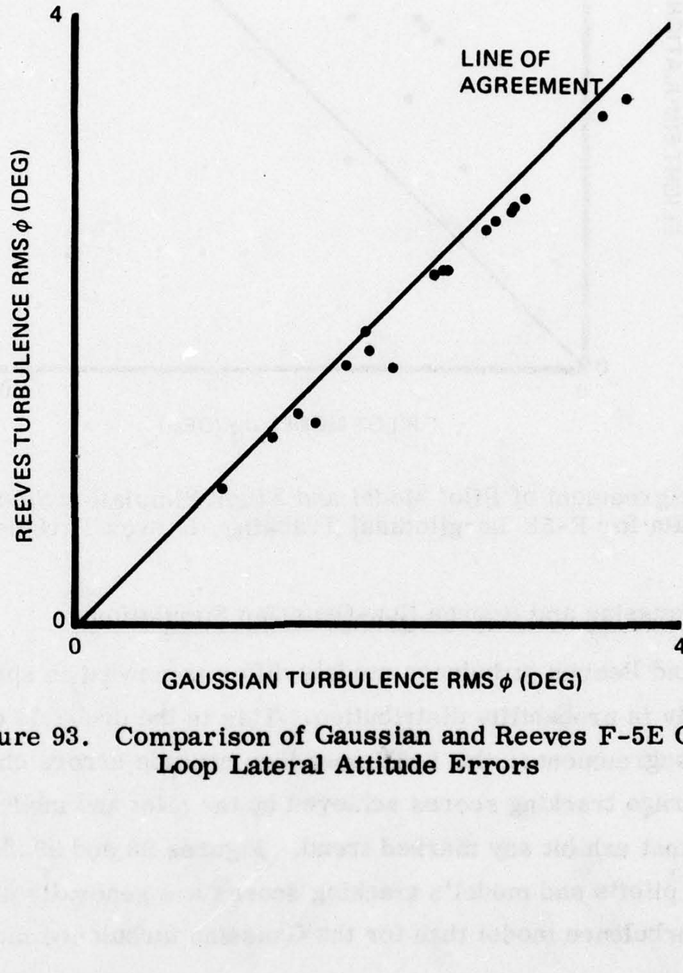

Figure 93. Comparison of Gaussian and Reeves F-5E Open Loop Lateral Attitude Errors

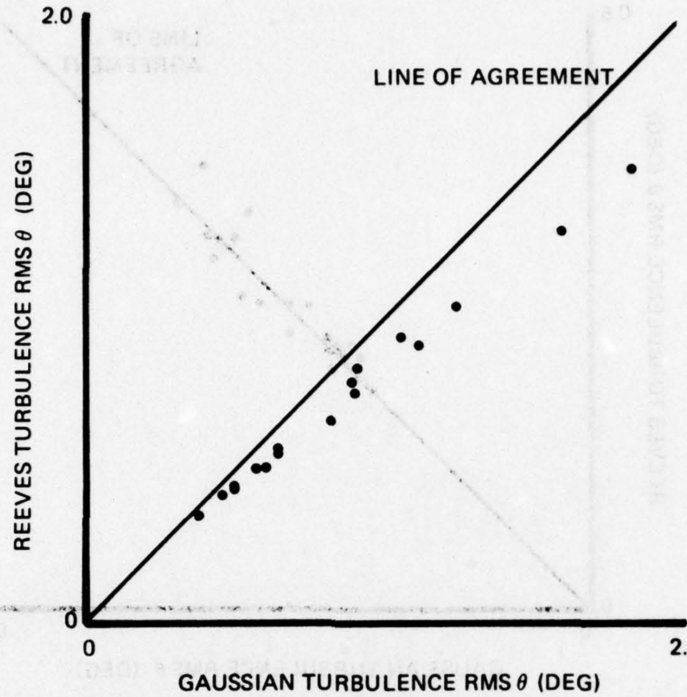

Figure 94. Comparison of Gaussian and Reeves F-5E Open Loop Longitudinal Attitude Errors

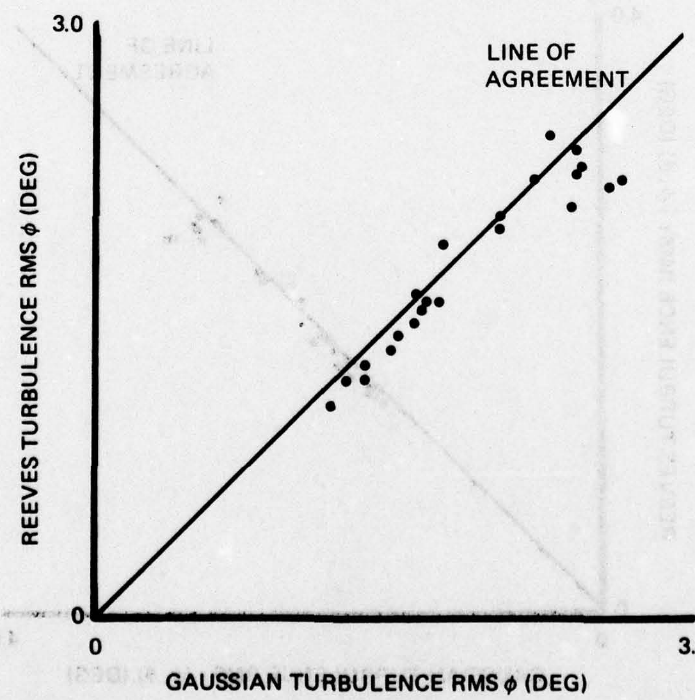

Figure 95. Comparison of Gaussian and Reeves F-5E Lateral Tracking Errors, Pilot Model and Flight Simulation Data

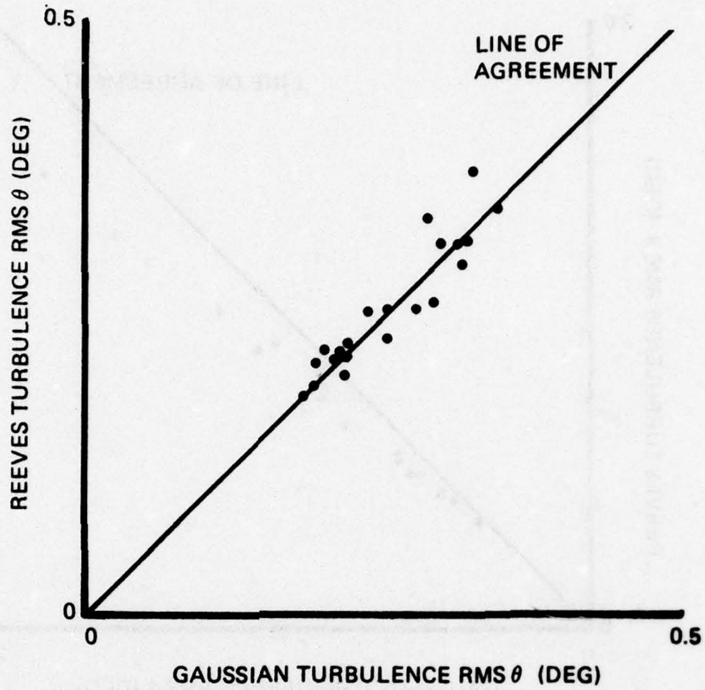

Figure 96. Comparison of Gaussian and Reeves F-5E Longitudinal Tracking Errors, Pilot Model and Flight Simulation Data

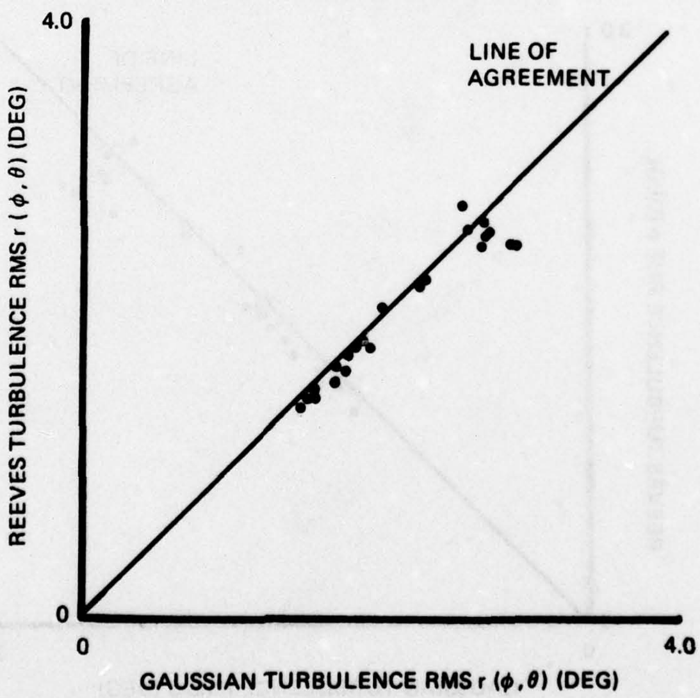

Figure 97. Comparison of Gaussian and Reeves F-5E Radial Tracking Errors, Pilot Model and Flight Simulation Data

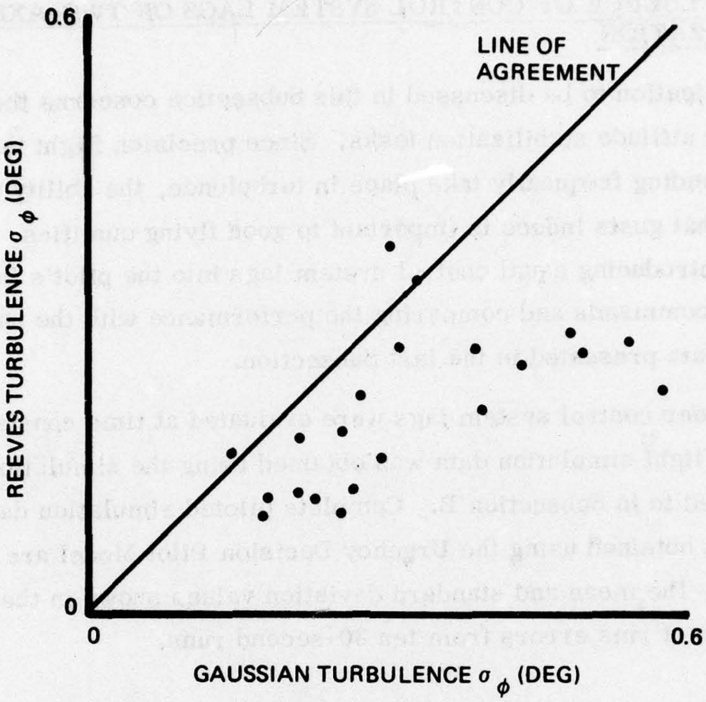

Figure 98. Comparison of Gaussian and Reeves F-5E Lateral Tracking Error Standard Deviations, Pilot Model and Flight Simulation Data

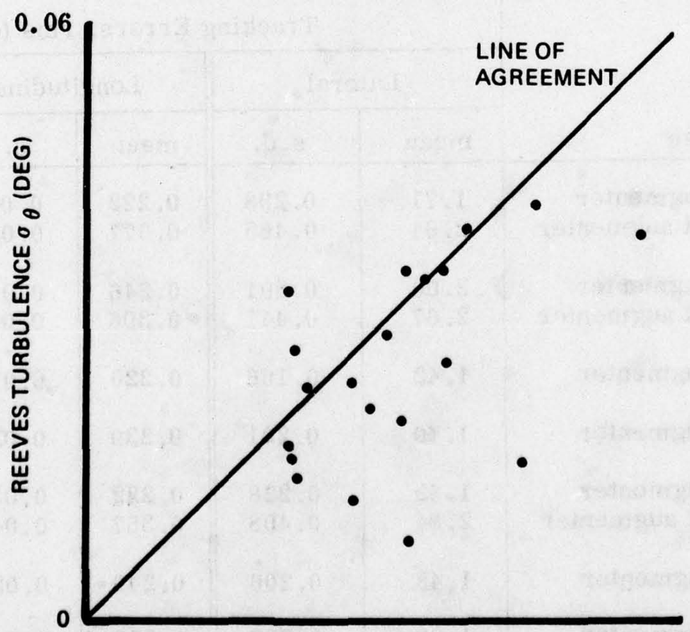

Figure 99. Comparison of Gaussian and Reeves F-5E Longitudinal Tracking Error Standard Deviations, Pilot Model and Flight Simulation Data

C. THE INFLUENCE OF CONTROL SYSTEM LAGS ON TWO-AXIS ATTITUDE STABILIZATION

The application to be discussed in this Subsection concerns the allowable control system lag for attitude stabilization tasks. Since precision flight tasks such as weapon delivery and landing frequently take place in turbulence, the ability to eliminate the disturbances that gusts induce is important to good flying qualities. This will be evaluated by introducing equal control system lags into the pilot's lateral and longitundinal stick commands and comparing the performance with the unmodified F-5E performance data presented in the last Subsection.

First-order control system lags were evaluated at time constants of 0.05 and 0.1 second. Flight simulation data was obtained using the simulation procedure and facility referred to in Subsection B. Complete piloted simulation data and performance prediction data obtained using the Urgency Decision Pilot Model are presented in Tables 22-25. The mean and standard deviation values shown in the tables were calculated for sets of rms errors from ten 30-second runs.

TABLE 22. FLIGHT SIMULATION DATA — ATTITUDE STABILIZATION IN GAUSSIAN TURBULENCE, 0.05 SEC CONTROL LAGS

		Tracking Errors, rms (deg)				
		Lateral		Longitudinal		Radial
Case		mean	s.d.	mean	s.d.	mean
1	With augmenter	1.71	0.298	0.222	0.0262	1.92
	Without augmenter	2.64	0.465	0.377	0.0655	3.04
2	With augmenter	2.00	0.291	0.246	0.0467	2.23
	Without augmenter	2.67	0.441	0.306	0.0652	2.94
3	With augmenter	1.42	0.166	0.220	0.0166	1.67
4	With augmenter	1.70	0.221	0.239	0.0273	1.95
5	With augmenter	1.82	0.228	0.222	0.0345	2.03
	Without augmenter	2.84	0.408	0.357	0.0474	3.18
8	With augmenter	1.48	0.206	0.249	0.0288	1.78
9	With augmenter	1.88	0.320	0.222	0.0418	2.08
	Without augmenter	2.74	0.274	0.292	0.0357	2.98

TABLE 23. FLIGHT SIMULATION DATA — ATTITUDE STABILIZATION IN GAUSSIAN TURBULENCE, 0.1 SEC CONTROL LAGS

Case		Tracking Errors, rms (deg)				
		Lateral		Longitudinal		Radial
		mean	s.d.	mean	s.d.	mean
1	With augmenter	2.01	0.303	0.274	0.0481	2.28
	Without augmenter	2.60	0.350	0.366	0.0440	2.99
2	With augmenter	2.35	0.344	0.296	0.0350	2.63
	Without augmenter	3.19	0.519	0.407	0.0713	3.58
3	With augmenter	1.49	0.178	0.249	0.0298	1.80
4	With augmenter	1.71	0.217	0.283	0.0452	2.05
5	With augmenter	1.98	0.300	0.252	0.0529	2.22
	Without augmenter	3.16	0.470	0.402	0.0627	3.55
8	With augmenter	1.76	0.253	0.254	0.0403	2.03
9	With augmenter	2.09	0.221	0.239	0.0346	2.30
	Without augmenter	3.05	0.455	0.458	0.0528	3.56

TABLE 24. PILOT MODEL DATA — ATTITUDE STABILIZATION IN GAUSSIAN TURBULENCE, 0.05 SEC CONTROL LAGS

Case		Tracking Errors, rms (deg)					Model Parameters					
		Lateral		Longitudinal		Radial	Lateral			Longitudinal		
		mean	s.d	mean	s.d.	mean	K	T_L	β	K	T_L	β
1	With augmenter	1.97	0.350	0.243	0.0276	2.20	0.31	1.3	0.5	-1.1	0.50	8
	Without augmenter	2.74	0.532	0.350	0.0630	3.07	0.30	1.3	0.5	-0.73	0.80	8
2	With augmenter	2.23	0.417	0.262	0.0405	2.46	0.40	1.3	0.5	-1.4	0.50	4
	Without augmenter	2.67	0.568	0.339	0.0443	2.99	0.39	1.3	0.5	-1.0	0.80	4
3	With augmenter	1.41	0.224	0.240	0.0245	1.70	0.18	1.3	0.5	-0.51	0.50	8
4	With augmenter	1.79	0.313	0.232	0.0416	2.01	0.19	1.3	0.5	-0.84	0.50	8
5	With augmenter	1.94	0.322	0.234	0.0294	2.15	0.24	1.3	0.5	-1.0	0.50	4
	Without augmenter	2.89	0.474	0.356	0.0480	3.22	0.24	1.3	0.5	-0.65	0.80	4
8	With augmenter	1.53	0.224	0.228	0.0275	1.78	0.16	1.3	0.5	-0.67	0.50	4
9	With augmenter	1.84	0.276	0.207	0.0206	2.02	0.23	1.3	0.5	-1.0	0.50	4
	Without augmenter	2.97	0.395	0.344	0.0498	3.27	0.20	1.3	0.5	-0.55	0.80	4

TABLE 25. PILOT MODEL DATA — ATTITUDE STABILIZATION IN GAUSSIAN TURBULENCE, 0.1 SEC CONTROL LAGS

		Tracking Errors, rms (deg)					Model Parameters					
		Lateral		Longitudinal		Radial	Lateral			Longitudinal		
Case		mean	s.d.	mean	s.d.	mean	K	T_L	β	K	T_L	β
1	With Augmenter	2.16	0.360	0.275	0.0473	2.42	0.31	1.3	0.5	-1.1	0.50	8
	Without augmenter	2.92	0.501	0.400	0.0325	3.33	0.30	1.3	0.5	-0.64	0.80	8
2	With augmenter	2.50	0.459	0.290	0.0435	2.75	0.40	1.3	0.5	-1.4	0.50	4
	Without augmenter	3.02	0.569	0.410	0.0834	3.44	0.39	1.3	0.5	-0.90	0.80	4
3	With augmenter	1.53	0.241	0.258	0.0228	1.84	0.18	1.3	0.5	-0.51	0.50	8
4	With augmenter	1.85	0.341	0.242	0.0270	2.08	0.19	1.3	0.5	-0.77	0.50	8
5	With augmenter	2.07	0.354	0.250	0.0212	2.30	0.24	1.3	0.5	-1.0	0.50	4
	Without augmenter	3.19	0.555	0.416	0.0545	3.60	0.24	1.3	0.5	-0.55	0.80	4
8	With augmenter	1.65	0.248	0.241	0.0344	1.91	0.16	1.3	0.5	-0.64	0.50	4
9	With augmenter	2.00	0.318	0.218	0.0230	2.18	0.20	1.3	0.5	-1.0	0.50	4
	Without augmenter	3.05	0.566	0.406	0.0626	3.45	0.10	1.3	0.5	-0.45	0.80	4

The accuracy of the model in predicting the effects of the control lags is demonstrated by comparing the data along lines of agreement. Figure 100 shows the comparison of the data for the bank angle tracking errors for turbulence intensities of 10 ft/sec, and Figure 101 presents the data for pitch angle tracking errors for the same intensity of turbulence. It is clear that the agreement is good for a variation of tracking errors exceeding 100 percent.

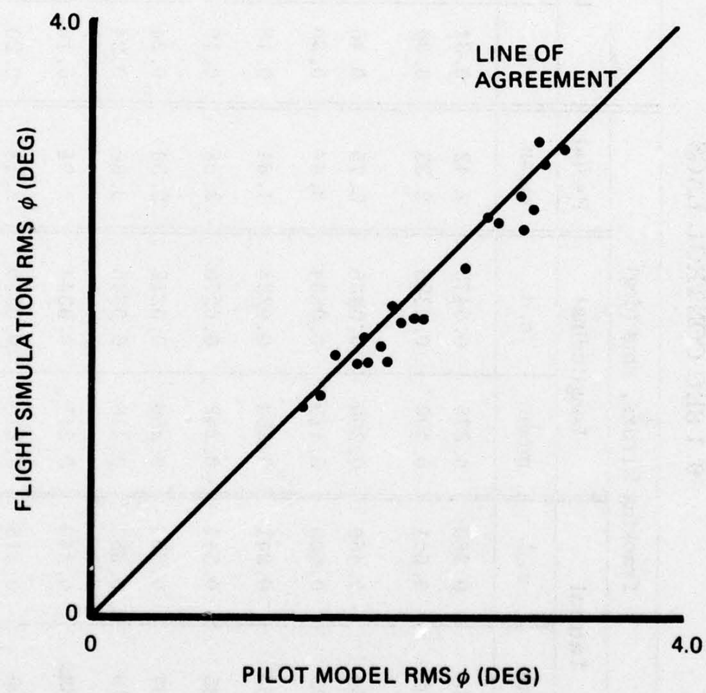

Figure 100. Agreement of Pilot Model and Flight Simulation Data for F-5E Lateral Tracking Errors, Gaussian Turbulence With Control System Lags

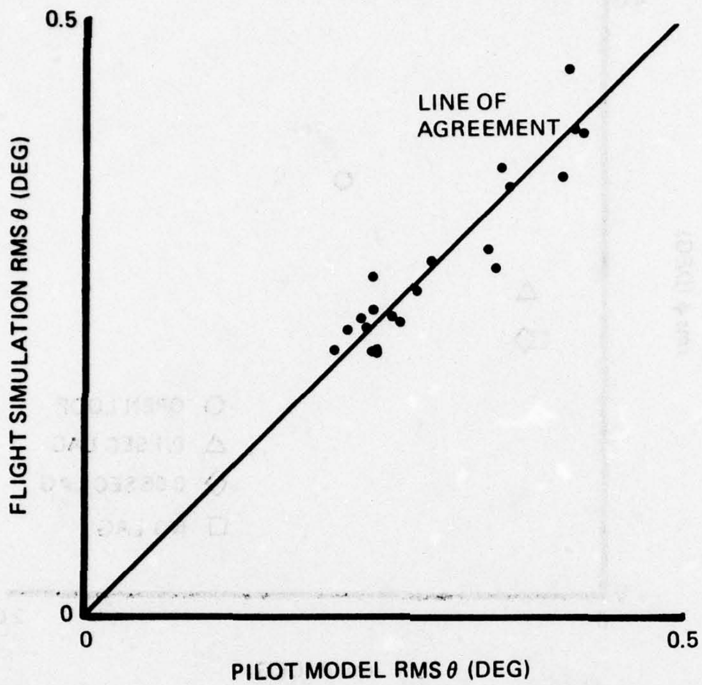

***Figure 101.** Agreement of Pilot Model and Flight Simulation Data for*
F-5E Longitudinal Tracking Errors, Gaussian Turbulence
With Control System Lags

Graphs that are similar to the task interference figures of Section IV A will be used to show the influence of the control lags on the two-axis attitude stabilization task performance. Performance of the two-axis tasks is plotted as a point with coordinates of bank angle and pitch angle tracking errors. Thus, the F-5E with control system lags can be compared to the unaltered F-5E flown optimally by the simulation pilot, and also to the open loop aircraft. These data are presented in Figures 102 to 112 for the eleven flight conditions/configurations studied in Subsection V B.

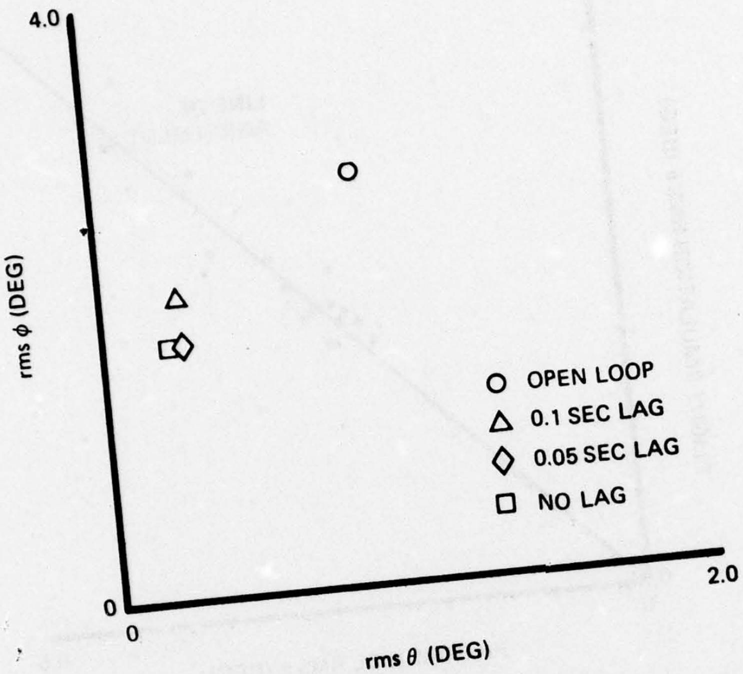

Figure 102. Effect of Control System Lags on F-5E Case 1 With Augmenter, Gaussian Turbulence

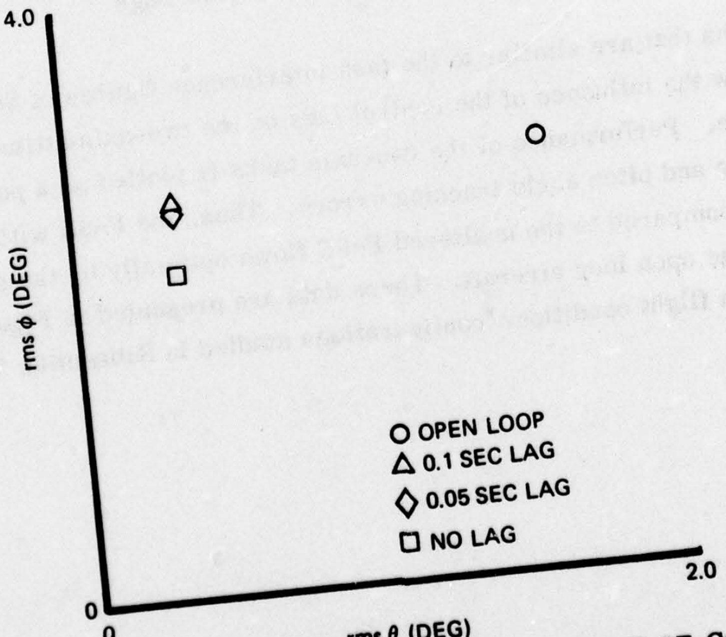

Figure 103. Effect of Control System Lags on F-5E Case 1 Without Augmenter, Gaussian Turbulence

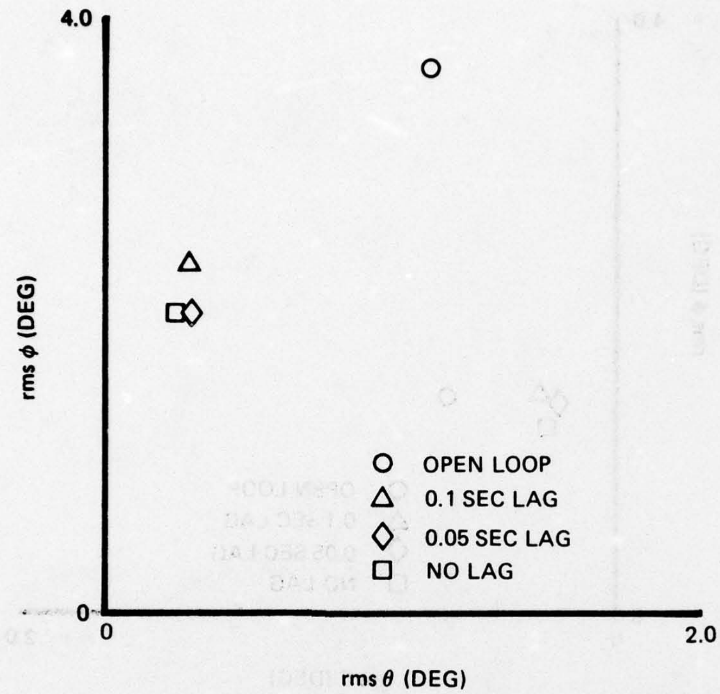

Figure 104. Effect of Control System Lags on F-5E Case 2 With Augmenter, Gaussian Turbulence

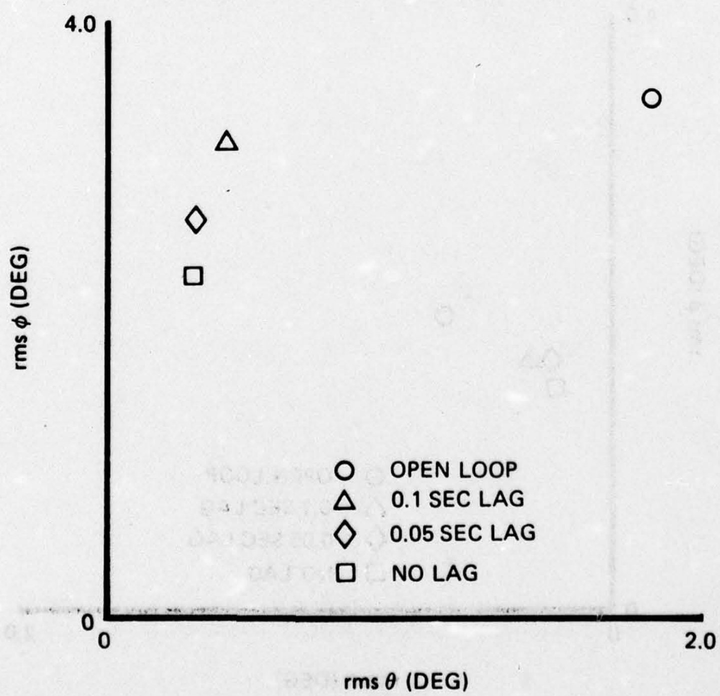

Figure 105. Effect of Control System Lags on F-5E Case 2 Without Augmenter, Gaussian Turbulence

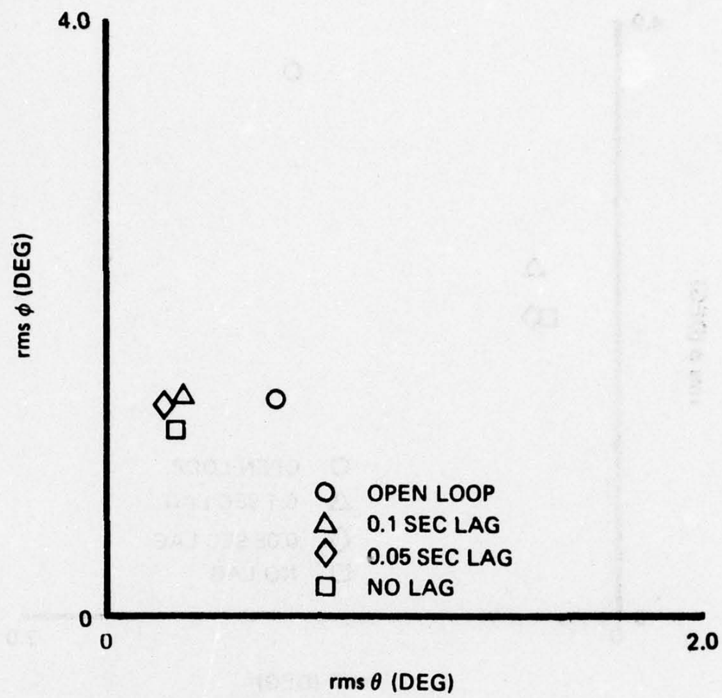

Figure 106. Effect of Control System Lags on F-5E Case 3 With Augmenter, Gaussian Turbulence

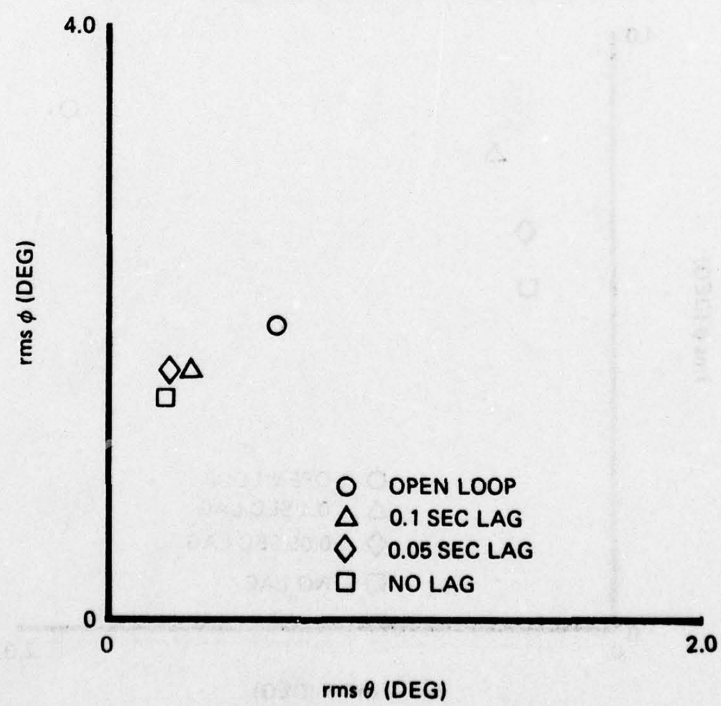

Figure 107. Effect of Control System Lags on F-5E Case 4 With Augmenter, Gaussian Turbulence

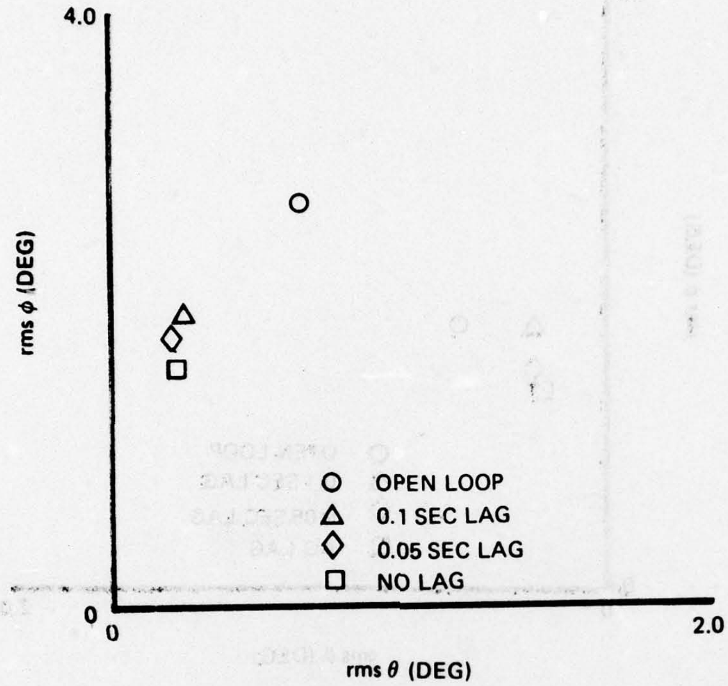

Figure 108. Effect of Control System Lags on F-5E Case 5 With Augmenter, Gaussian Turbulence

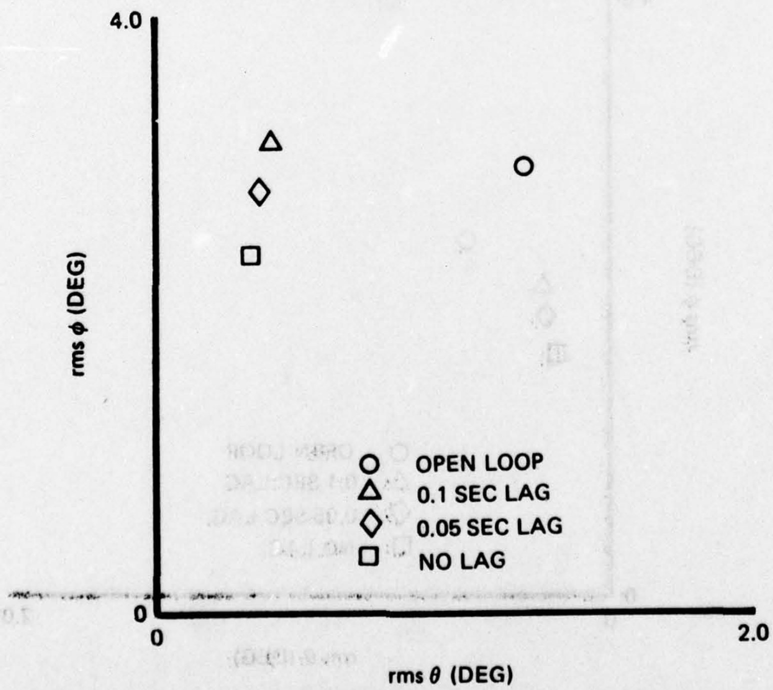

Figure 109. Effect of Control System Lag on F-5E Case 5 Without Augmenter, Gaussian Turbulence

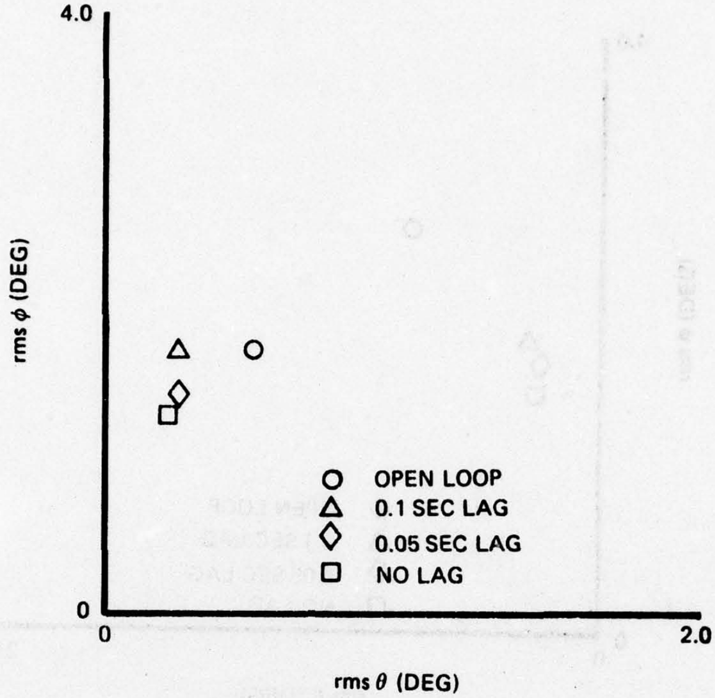

Figure 110. Effect of Control System Lags on F-5E Case 8 With Augmenter, Gaussian Turbulence

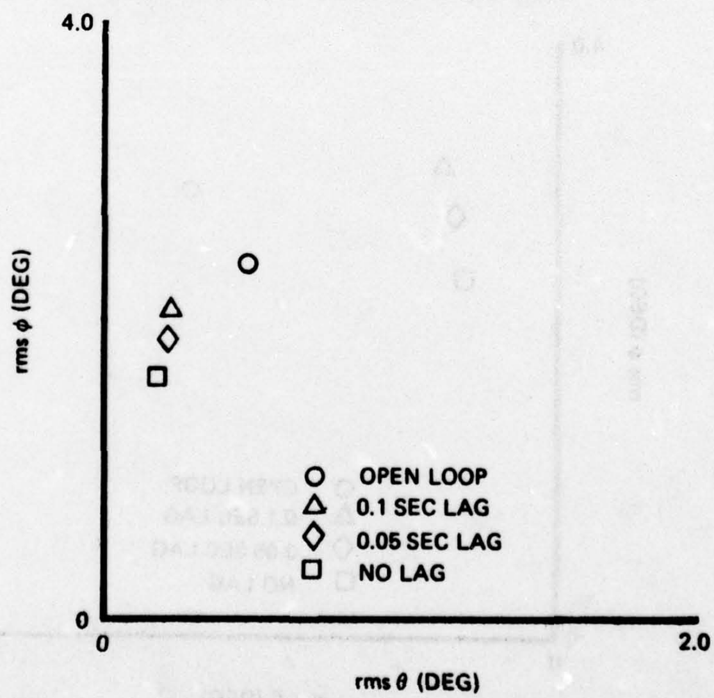

Figure 111. Effect of Control System Lags on F-5E Case 9 With Augmenter, Gaussian Turbulence

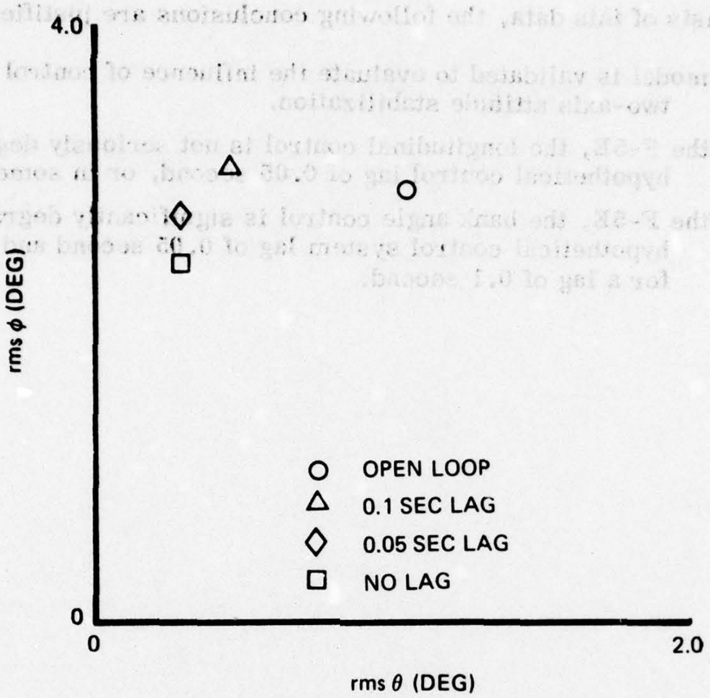

Figure 112. Effect of Control System Lags on F-5E Case 9
Without Augmenter, Gaussian Turbulence

First of all, it is apparent by inspection of Figures 102 through 112 that no significant deterioration of longitudinal tracking ability takes place at either value of lag, whether or not the augmentation is being used. However, the trends at the 0.1 sec lag value that show in cases 2 and 9 without augmenter indicate that acceptable performance in pitch attitude tracking may be degraded by lags larger than 0.1 sec. The overall conclusion is that for the attitude stabilization in turbulence task, the pilot can perform longitudinal stabilization in the F-5E with control system lags of the order of 0.1 second.

On the other hand, bank angle stabilization is quite sensitive to control system lags. In cases 1 and 2 with augmenter no degradation is noted for a lag of 0.05 second. In cases 3, 4, 5, 8 and 9 with augmenter, there is noticeable degradation in performance with lags of 0.05 second. For lags of 0.1 second, there is significant tracking degradation, in some cases resulting in essentially open loop performance. This is evident in cases 3, 8, and 9 with augmenter, and cases 1, 2, 5, and 9 without augmenter. *From this it is clear that a control lag of 0.1 second in the lateral control system is unacceptable for the F-5E in attitude stabilization tasks.*

On the basis of this data, the following conclusions are justified:

- The model is validated to evaluate the influence of control system lag on two-axis attitude stabilization.
- For the F-5E, the longitudinal control is not seriously degraded for a hypothetical control lag of 0.05 second, or in some cases, 0.1 sec.
- For the F-5E, the bank angle control is significantly degraded for a hypothetical control system lag of 0.05 second and badly degraded for a lag of 0.1 second.

SECTION VI

STEP TARGET TRACKING ANALYSIS AND PERFORMANCE SPECIFICATION

The previous two Sections have demonstrated the application of the Urgency Decision Pilot Model to predictions of statistical performance measures of precision flight tasks. These time-invariant problems represent long-term performance averages. In contrast, this Section will consider a transient tracking problem in which the pilot model may change its form and coefficients as a function of time in order to perform optimally during a short tracking period. Associated with this TASK is an EVALUATION that consists of not only rms tracking error but also the nonlinear measure of time-on-target as defined by a given pipper size.

In order to see the motivation of analyzing discrete maneuver target tracking, it is necessary to consider current specification procedures for tactical aircraft.

A. COORDINATION OF FLYING QUALITIES ANALYSIS WITH FLIGHT TEST AND SIMULATION

MIL-F-8785B, "Military Specification, Flying Qualities of Piloted Airplanes," Reference 14, presents boundaries of acceptance in terms of such quantities as short period frequency and damping. These criteria have been obtained through operational experience with large numbers of past and current aircraft, and through analysis and simulation – both ground-based and in variable-stability airplanes. Even though many of these aircraft have employed stability augmentation, their responses to control inputs and disturbances generally could be characterized in terms of an equivalent unaugmented "bare" airframe. Values of airframe parameters are then correlated with pilot ratings on a revised Cooper-Harper scale, Reference 12.

However, there is an increasing tendency to add compensation and adopt forms of control which may change the character of the response. Then to the extent that no equivalent classical "bare" airframe can be found to match the response, these requirements lose validity. Even if nothing more than a time delay needs to be added, one can easily leave the data base behind.

Since these criteria are no longer sufficient or comprehensive, there has been considerable research into 1) the nature of pilot ratings, 2) the dynamics of closed loop piloted flight as predicted using dynamic models of pilot control compensation, and 3) innovative simulation and flight test procedures. There has been considerable success in these three areas. Pilot ratings deriving from different rating systems can now be related to one another, Reference 15, and the relation of ratings to certain performance measures has been demonstrated.

On the other hand, flight test and flight simulation — both in-flight and ground-based — have not been subject to mathematical constraints that have limited the generality and scope of the analytical methods. Consequently, some test methods have evolved along lines of discrete test maneuvers evaluated by measures that have not been readily computed by the use of analytic models.

It is unfortunate that these three areas of activity have not led to an integrated, consistent, and comprehensive approach to the evaluation and specification of piloted aircraft flying qualities. The problem is this: as aircraft dynamics become more complex, pilot ratings and comments become more difficult to relate to widely used frequency-domain or optimal control pilot models. Furthermore, many flight test procedures such as wind-up turns and step target tracking have not been analyzed owing to their nonlinear time-varying descriptions which are not easily incorporated into pilot-aircraft models.

Pilot ratings and pilot comments often refer to two basic kinds of evaluation: 1) How well can the aircraft be made to perform? 2) How hard is the task to carry out? Since these two questions are asked simultaneously by the Cooper-Harper decision tree employed by the pilot in assigning a rating, performance and pilot workload are combined into a single scalar quantity, the rating. Pilot rating prediction formulas have been developed that weight normalized statistical performance, usually an rms tracking error, Reference 15, along with an assumed correlate of pilot workload, such as the pilot lead compensation constant. Although these methods have correlated well with steady state tracking data, the predictive and practical aspects of this approach have yet to be demonstrated, especially in view of the simplifications required in task descriptions and system models. One basic problem with these approaches is that pilot model parameters of lead, reserve attention as defined by additional task requirements on the pilot, or other identifiable pilot characteristics are difficult to relate quantitatively to pilot comments. Furthermore, the limitation of pilot model analysis to steady state statistics of a linearized pilot-aircraft model

precludes analysis of discrete flight test maneuvers such as wind-up turns and step target tracking.

The object of this Section is to present a simple method for coordinating these areas of flying qualities research through the use of the Urgency Decision Pilot Model which can be used to model discrete maneuvers and fully general aircraft. This approach predicts tracking error and time-on-target statistics for step target tracking in a way that is directly related to both pilot ratings and pilot comments. As an illustration of this technique, the definitive in-flight simulation study of longitudinal flying qualities performed by Neal and Smith, Reference 16, will be analyzed in terms of step target tracking.

B. PILOT – AIRCRAFT ANALYSIS OF LONGITUDINAL STEP TARGET TRACKING

One of the most familiar and widely employed guides to longitudinal flying qualities is the data obtained by Neal and Smith of Cornell Aeronautical Laboratory (now called Calspan) during an in-flight simulation sponsored by the Air Force Flight Dynamics Laboratory in 1970. The test matrix included variations in short period frequency, damping, and control system parameters. Flight test evaluation included pitch angle tracking of both random and step commands. The reported pilot ratings and pilot comments cover stick forces, predictability of response, attitude control/tracking capability, normal acceleration control, effects of random disturbances, and IFR problems. Most pilot comments deal with initial response ("predictability of response") or precision attitude tracking control ("attitude control/tracking capability").

It is clear that the objectives of quick initial response and precise tracking once the target is acquired are to some degree opposed. If the pilot pulls the airplane toward the target too rapidly, unwanted overshoot and oscillation about the target may result. On the other hand, pulling too slowly to the target may lead to steady tracking but with a penalty of unacceptably slow target acquisition. The ability to investigate this compromise and predict how well the overall task can be achieved for a given aircraft is the primary advantage of using the time-domain pilot model to investigate step target tracking.

Consider a target that suddenly appears above steady-state trim pitch for the tracking aircraft. The pilot sees the target and initiates a pull-up. At some point, say D seconds into the maneuver, he will possibly change the nature of his control to initiate precision tracking and reduce steady-state errors. By repeatedly flying this

maneuver, he will learn just how much he can force a quick initial response without producing overshoot and oscillation. The performance of this step target tracking task can then be measured by rms tracking error and time-on-target for a given pipper size and total tracking time.

The pilot model is set up to perform this tracking task in just the way the pilot does it as described above. This is shown in Figure 113. There will be two forms for the pilot compensation elevator command δe: one which provides the initial target acquisition, and the other after time D has passed which controls final precision tracking and eliminates steady state errors. These are of the form:

ACQUISITION

$$\text{time} < D, \quad \delta e_I = (\text{Delay } \tau) \left\{ K_{p_I} \left(\theta_e(t) + T_{L_I} \dot{\theta}_e(t) \right) \right\}$$

TRACKING

$$\text{time} \geq D, \quad \delta e_F = (\text{Delay } \tau) \left\{ K_{p_F} \left(\theta_e(t) + T_{L_F} \dot{\theta}_e(t) + K_{IC} \int_0^t \theta_e(s)\, ds \right) \right\}$$

where θ_e is pitch angle tracking error and the subscripts I and F refer to initial acquisition and final tracking, respectively. The K_{IC} term represents a pilot's avoidance of steady state error by means of integral control. A pilot delay of $\tau = 0.3$ sec will be used.

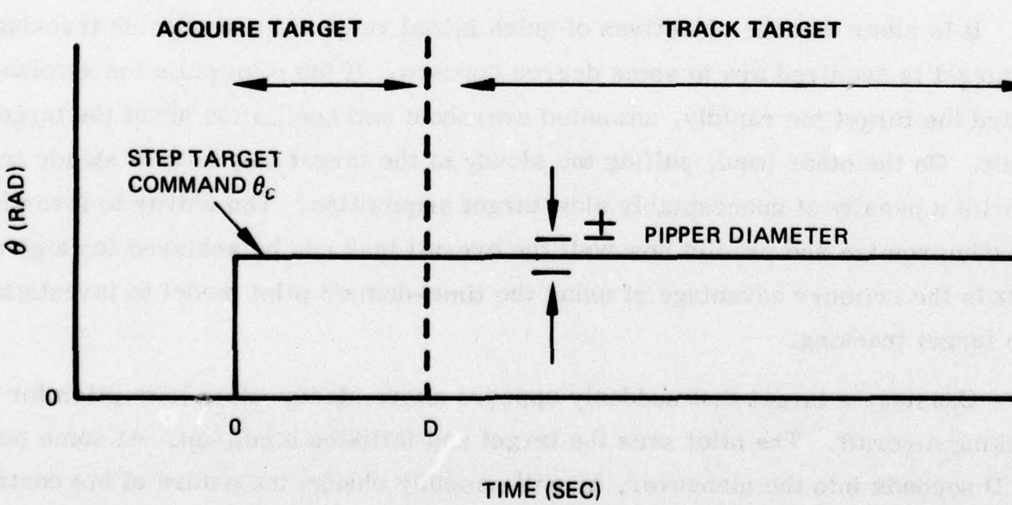

Figure 113. Definition of Step Target Tracking Task

The following quantities must now be adjusted in order to perform a simulation of this step tracking task for the evaluation of a given aircraft configuration:

$$K_{P_I},\ T_{L_I},\ D,\ K_{P_F},\ T_{L_F},\ K_{IC}$$

This adjustment will be performed using the optimization principle. For the analysis of step target tracking, it will be assumed that the pilot optimizes time-on-target and that this leads to the best compromise of rapid target acquisition and steadiness of target tracking. The adjustment rule for the pilot model is thus: choose the parameters any way that leads to a maximum time-on-target. In practice, it is easiest to use the following procedure:

1) Select a pipper size and a total tracking time, T_F.

2) Set $D = T_F$. Increase K_{P_I} and T_{L_I} as required to obtain the most rapid acquisition of target with moderate overshoot and oscillation.

3) With K_{P_I} and T_{L_I} fixed, set D to that time where θ is approximately 80% of the step command.

4) Vary K_{P_F} and T_{L_F} and K_{IC} to increase time-on-target.

Steps 1 - 4 result in an initial guess for the parameters. Final optimization requires use of a gradient method which obtains the partial derivatives of time-on-target with respect to all model parameters, including the time D. Once the model is adjusted, a matter that is easy in practice, rms tracking error and time-on-target can be obtained. Data for the Neal and Smith aircraft configurations, computed in this manner, will be presented next.

Equations for the Neal and Smith configurations were programmed as described in their report, Reference 16, with the exception that the high-frequency second-order control dynamics were omitted. Forty-two configurations, Series 1 through 7, were calculated with the aid of a programmable desk calculator and plotter, and the reader who is interested in applying this method is encouraged to repeat the analysis of the Neal and Smith configurations. A pipper diameter of 0.005 radian, a step size of 0.2 radian, and total tracking time of 5 seconds have been adopted. Since the system is linear, any choice of step and pipper size that preserves the 40 to 1 ratio will lead to the same time-on-target and normalized rms θ_e statistics. Complete data for these configurations are given in Figures 114-155, where rms θ_e is normalized by the 0.2 radian step size. The pilot ratings shown are the best obtained by Neal and Smith for each configuration.

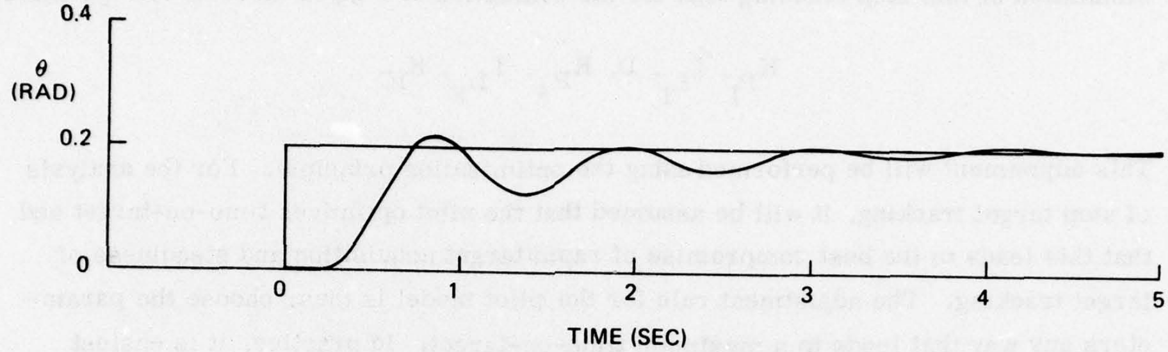

K_{PI}	=	5.0	K_{PF}	=	4.5	TOT	=	1.9
T_{LI}	=	.3	T_{LF}	=	.3	$RMS\theta_e$	=	.34
D	=	.3	K_{IC}	=	.2	PR	=	2.0

Figure 114. Configuration 1A Step Tracking Response

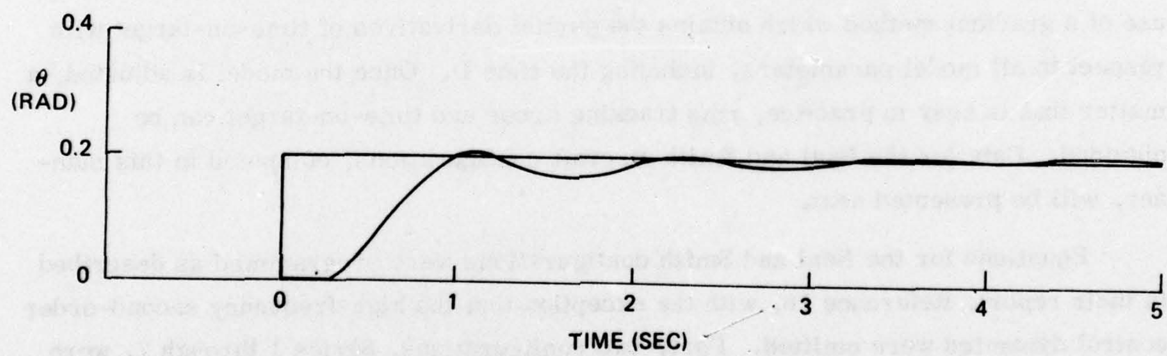

K_{PI}	=	5.75	K_{PF}	=	10.5	TOT	=	2.55
T_{LI}	=	.1	T_{LF}	=	.2	$RMS\theta_e$	=	.35
D	=	.75	K_{IC}	=	.15	PR	=	3.0

Figure 115. Configuration 1B Step Tracking Response

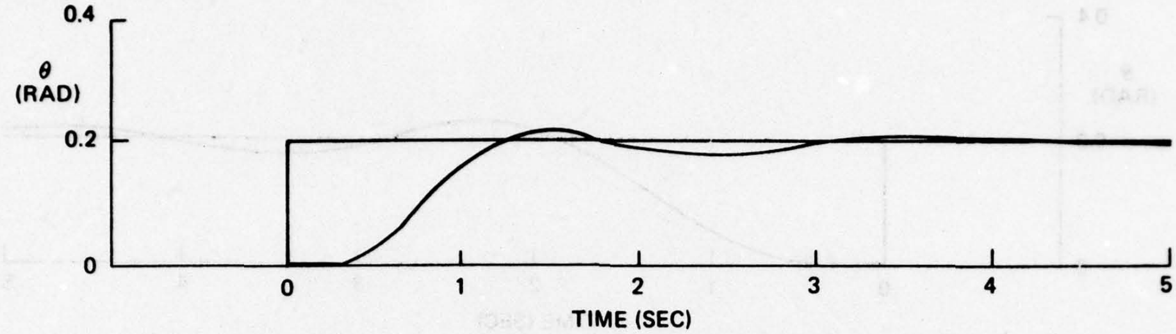

K_{PI}	=	5.75	K_{PF}	=	7.0	TOT	=	2.20
T_{LI}	=	.10	T_{LF}	=	.25	$RMS\theta_e$	=	.38
D	=	.75	K_{IC}	=	.15	PR	=	3.0

Figure 116. Configuration 1D Step Tracking Response

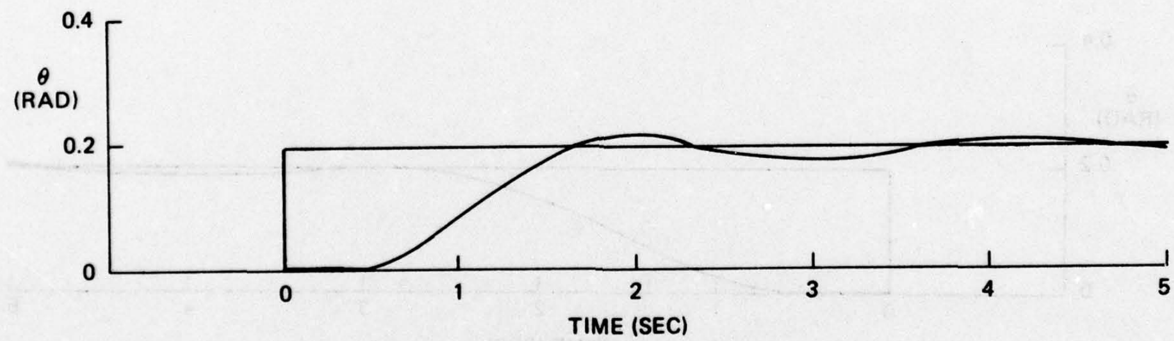

K_{PI}	=	4.6	K_{PF}	=	8.0	TOT	=	1.35
T_{LI}	=	.2	T_{LF}	=	.5	$RMS\theta_e$	=	.43
D	=	2.0	K_{IC}	=	.4	PR	=	6.0

Figure 117. Configuration 1E Step Tracking Response

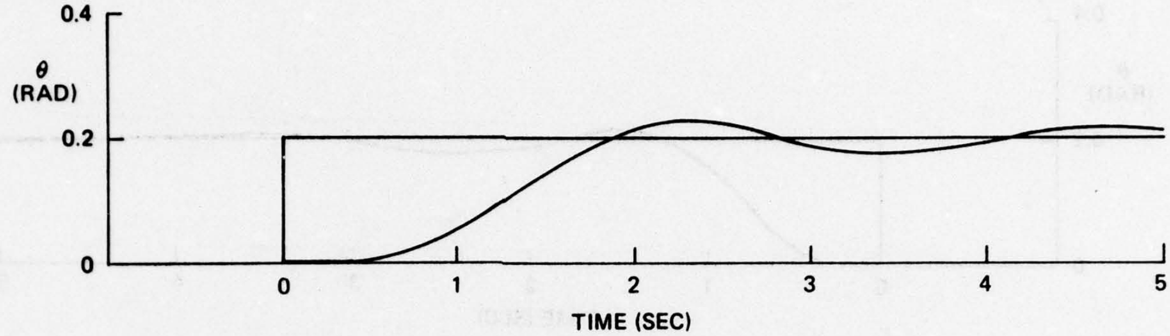

K_{PI}	=	4.6	K_{PF}	=	7.0	TOT	=	.4
T_{LI}	=	.2	T_{LF}	=	.5	RMSθ_e	=	.47
D	=	1.5	K_{IC}	=	0	PR	=	8.0

Figure 118. Configuration 1F Step Tracking Response

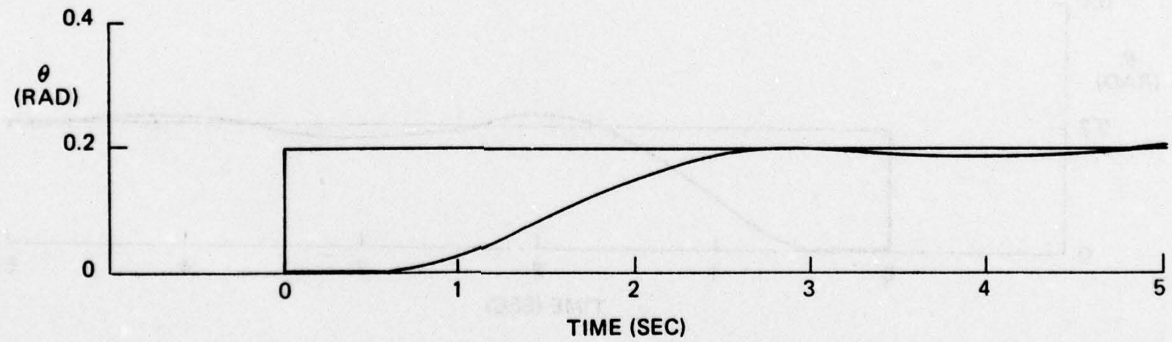

K_{PI}	=	8.0	K_{PF}	=	10.0	TOT	=	1.2
T_{LI}	=	1.0	T_{LF}	=	1.25	RMSθ_e	=	.52
D	=	2.25	K_{IC}	=	0	PR	=	8.5

Figure 119. Configuration 1G Step Tracking Response

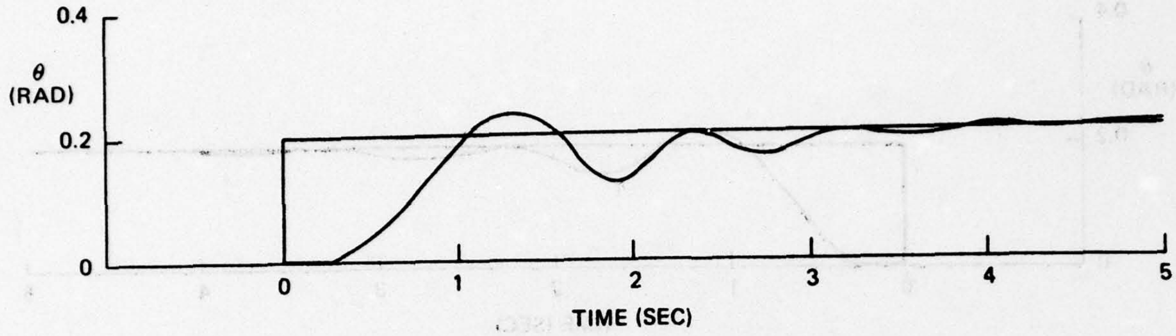

K_{PI} = 5.5	K_{PF} = 17.0	TOT = 1.45
T_{LI} = -1.6	T_{LF} = .15	$RMS\theta_e$ = .38
D = 1.3	K_{IC} = .4	PR = 4.0

Figure 120. Configuration 2A Step Tracking Response

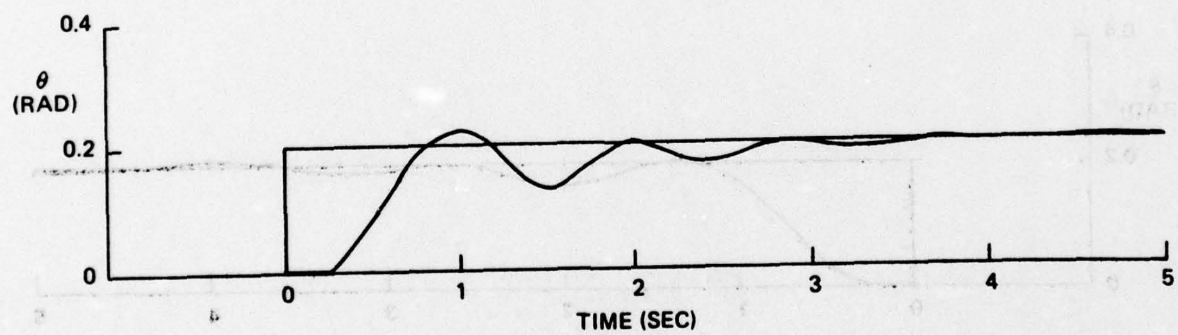

K_{PI} = 15	K_{PF} = 28.0	TOT = 2.15
T_{LI} = -.35	T_{LF} = .10	$RMS\theta_e$ = .34
D = .9	K_{IC} = .18	PR = 3.0

Figure 121. Configuration 2C Step Tracking Response

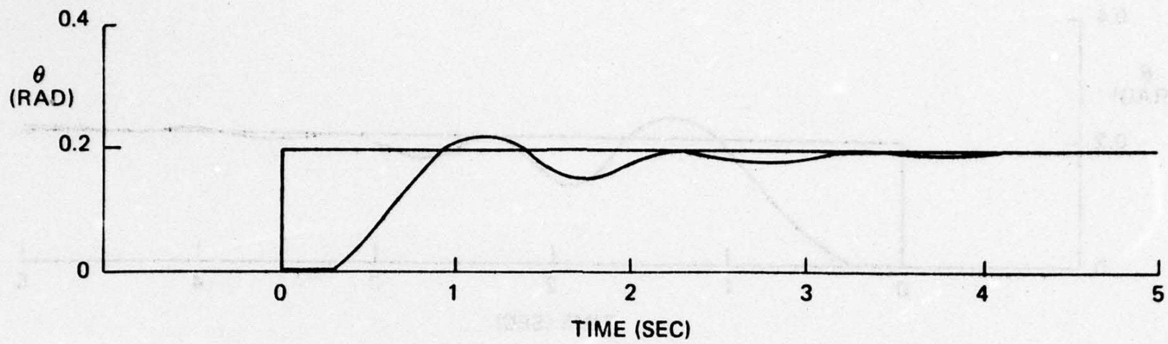

K_{PI}	=	17.0	K_{PF}	=	27.0	TOT	=	2.15
T_{LI}	=	-.3	T_{LF}	=	.15	$RMS\theta_e$	=	.35
D	=	1.0	K_{IC}	=	.15	PR	=	2.5

Figure 122. Configuration 2D Step Tracking Response

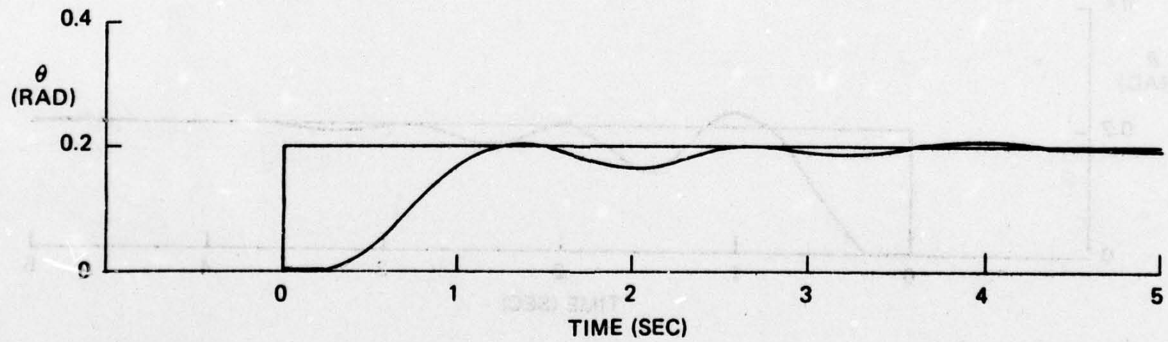

K_{PI}	=	15.0	K_{PF}	=	25.0	TOT	=	2.25
T_{LI}	=	-.3	T_{LF}	=	.15	$RMS\theta_e$	=	.38
D	=	1.25	K_{IC}	=	.3	PR	=	4.0

Figure 123. Configuration 2E Step Tracking Response

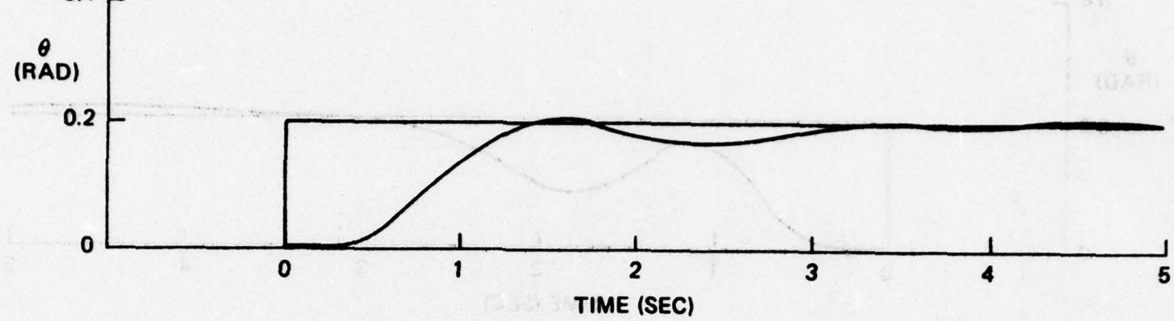

K_{PI}	=	15.0	K_{PF}	=	25.0	TOT	=	2.35
T_{LI}	=	-.3	T_{LF}	=	.15	$RMS\theta_e$	=	.40
D	=	1.65	K_{IC}	=	.3	PR	=	3.0

Figure 124. Configuration 2F Step Tracking Response

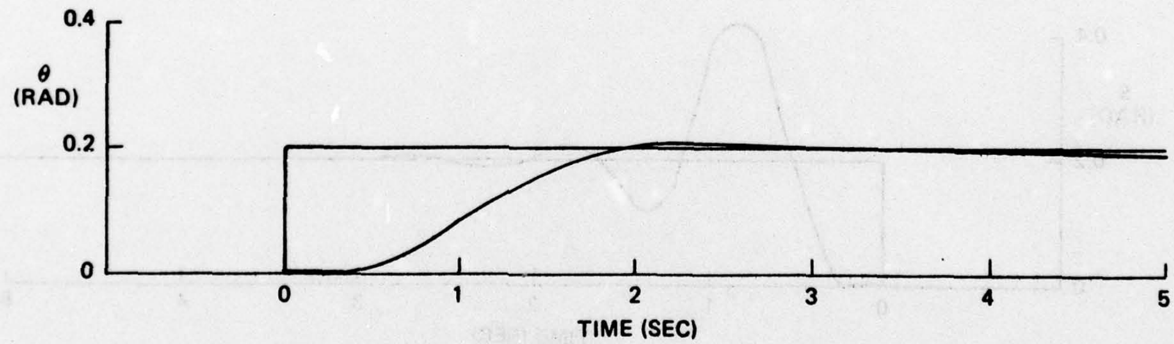

K_{PI}	=	15.0	K_{PF}	=	4.0	TOT	=	2.45
T_{LI}	=	-.3	T_{LF}	=	.12	$RMS\theta_e$	=	.44
D	=	2.0	K_{IC}	=	0	PR	=	5.0

Figure 125. Configuration 2H Step Tracking Response

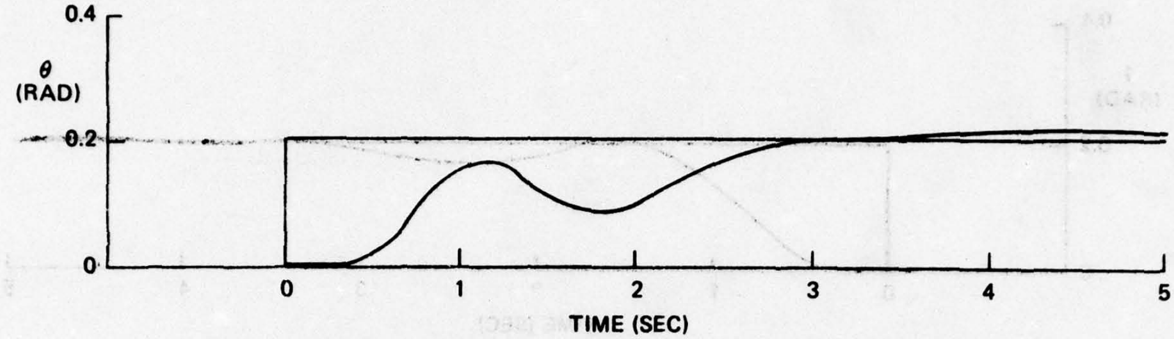

K_{PI}	=	100.0	K_{PF}	=	50.0	TOT	=	.70
T_{LI}	=	1.0	T_{LF}	=	.5	$RMS\theta_e$	=	.44
D	=	1.0	K_{IC}	=	0	PR	=	6.0

Figure 126. Configuration 2J Step Tracking Response

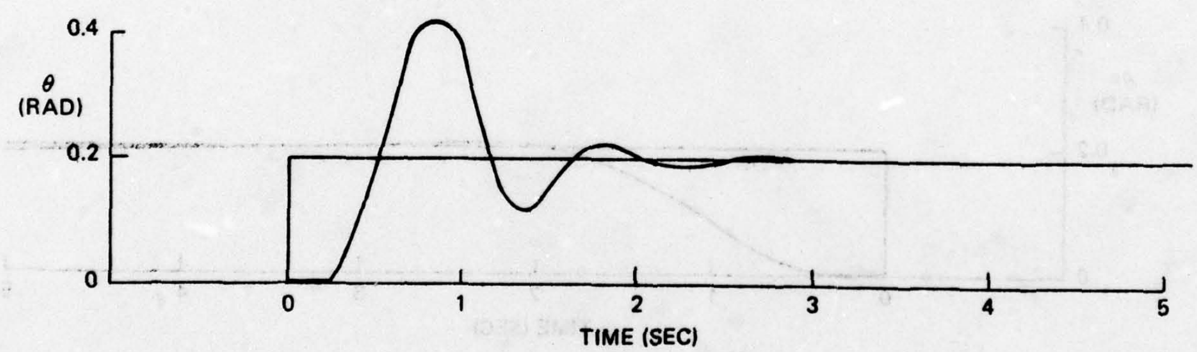

K_{PI}	=	100.0	K_{PF}	=	40.0	TOT	=	2.7
T_{LI}	=	-.3	T_{LF}	=	0	$RMS\theta_e$	=	.42
D	=	.7	K_{IC}	=	0	PR	=	4.0

Figure 127. Configuration 3A Step Tracking Response

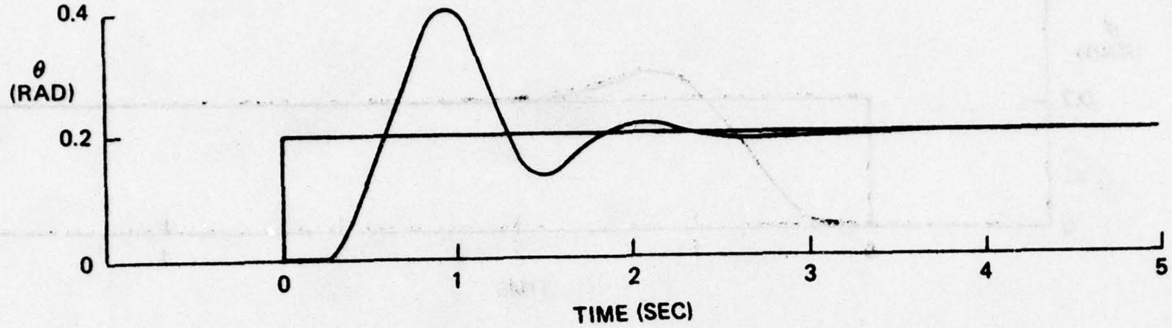

K_{PI}	=	100.0	K_{PF}	=	40.0	TOT	=	2.35
T_{LI}	=	-.3	T_{LF}	=	0	RMSθ_e	=	.40
D	=	.7	K_{IC}	=	0	PR	=	4.5

Figure 128. Configuration 3B Step Tracking Response

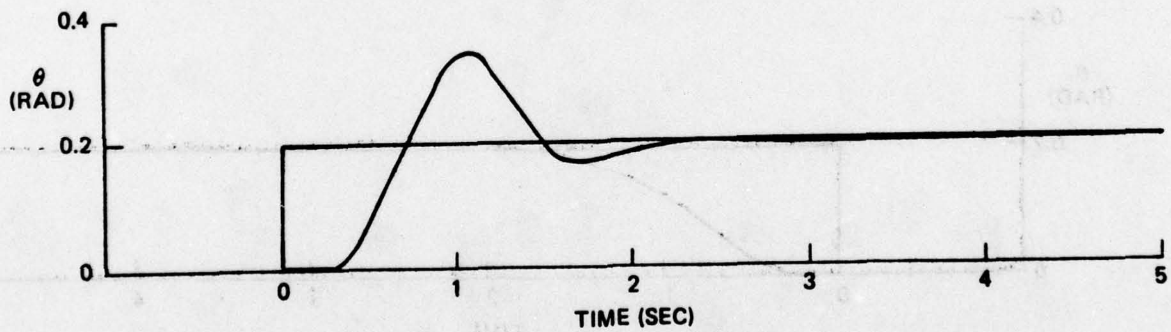

K_{PI}	=	100.0	K_{PF}	=	40.0	TOT	=	2.4
T_{LI}	=	-.3	T_{LF}	=	0	RMSθ_e	=	.38
D	=	.7	K_{IC}	=	0	PR	=	3.0

Figure 129. Configuration 3C Step Tracking Response

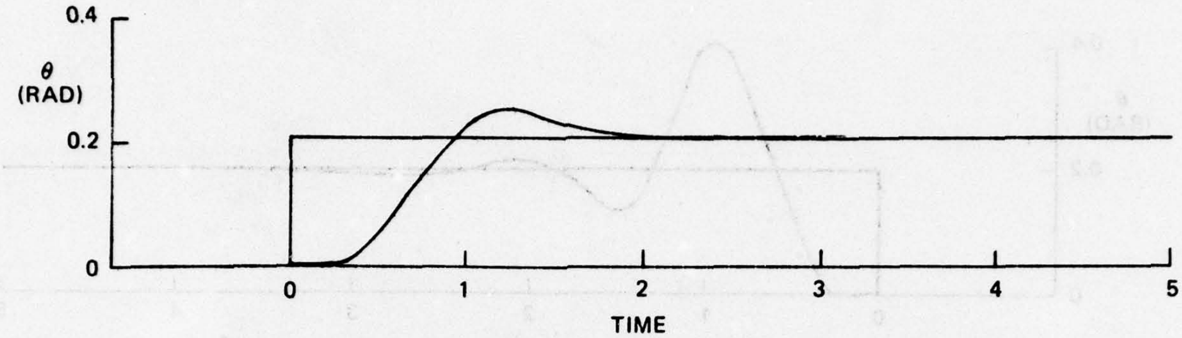

K_{PI} = 100.0 K_{PF} = 40.0 TOT = 3.00
T_{LI} = -.3 T_{LF} = 0 $RMS\theta_e$ = .36
D = .7 K_{IC} = 0 PR = 4.0

Figure 130. Configuration 3D Step Tracking Response

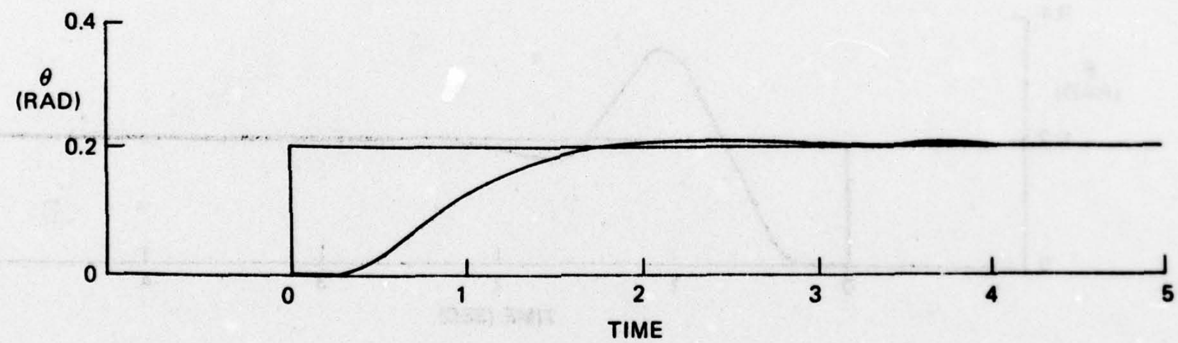

K_{PI} = 200.0 K_{PF} = 500.0 TOT = 1.9
T_{LI} = .3 T_{LF} = .4 $RMS\theta_e$ = .40
D = 1.0 K_{IC} = 0 PR = 4.0

Figure 131. Configuration 3E Step Tracking Response

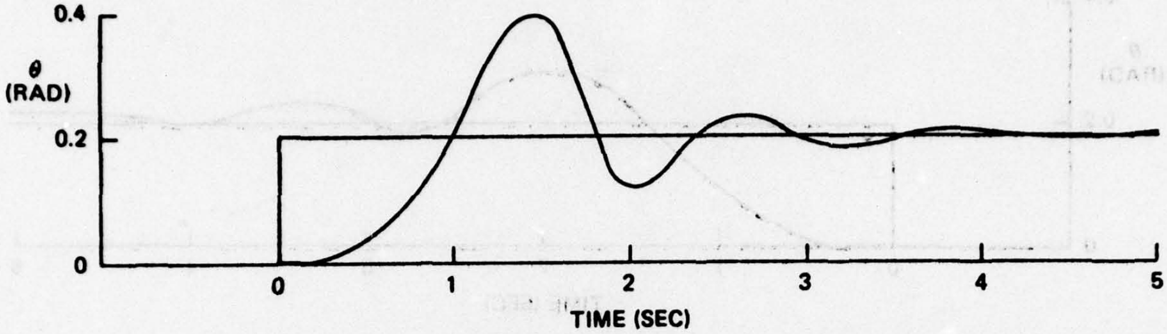

K_{PI}	=	6.75	K_{PF}	=	.35	TOT	=	1.40
T_{LI}	=	-2.0	T_{LF}	=	2.5	$RMS\theta_e$	=	.46
D	=	1.10	K_{IC}	=	-2	PR	=	5.0

Figure 132. Configuration 4A Step Tracking Response

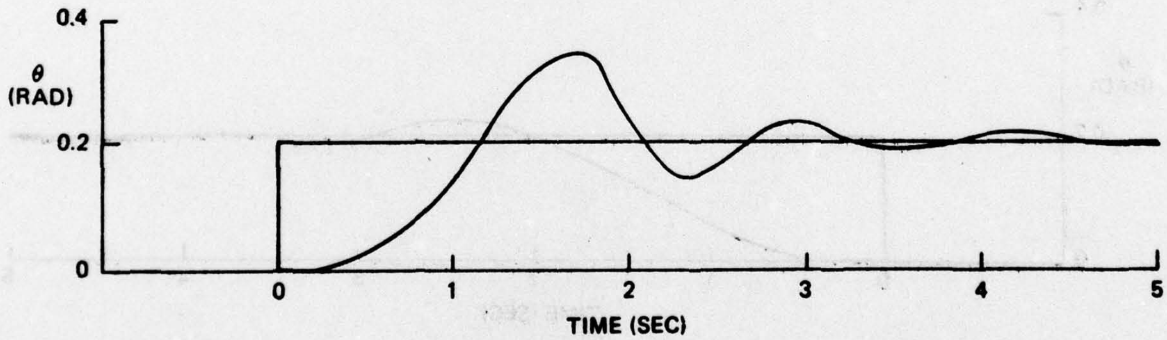

K_{PI}	=	6.75	K_{PF}	=	.35	TOT	=	1.05
T_{LI}	=	-2.0	T_{LF}	=	2.50	$RMS\theta_e$	=	.45
D	=	1.35	K_{IC}	=	0	PR	=	7.0

Figure 133. Configuration 4B Step Tracking Response

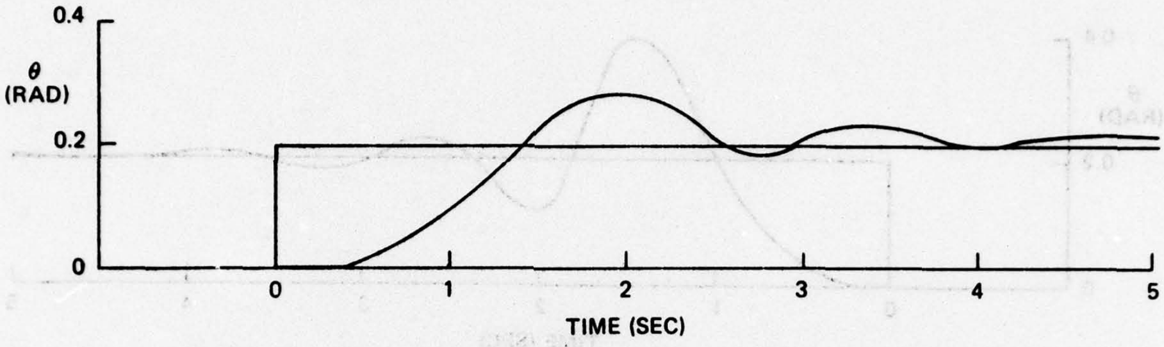

K_{PI}	= 6.75	K_{PF}	= .35	TOT	= .90
T_{LI}	= -2.0	T_{LF}	= 2.50	$RMS\theta_e$	= .44
D	= 1.75	K_{IC}	= 0	PR	= 8.5

Figure 134. Configuration 4C Step Tracking Response

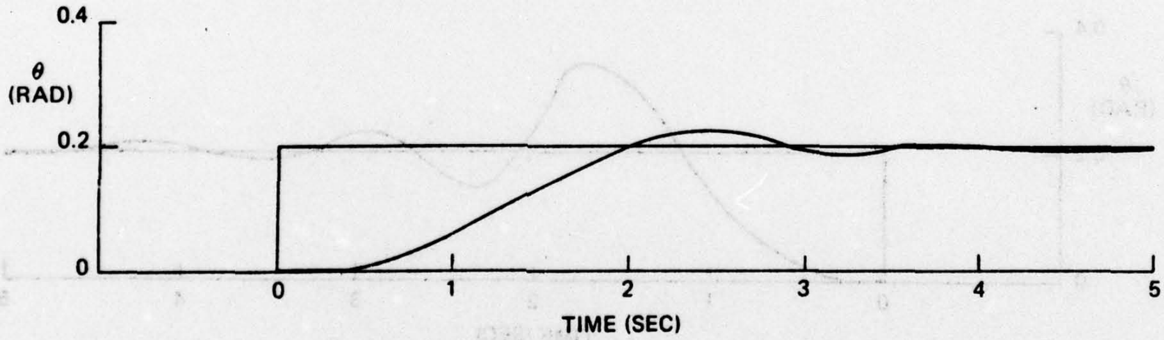

K_{PI}	= 7.10	K_{PF}	= 1.0	TOT	= 1.4
T_{LI}	= -2.0	T_{LF}	= 2.5	$RMS\theta_e$	= .47
D	= 2.0	K_{IC}	= 0	PR	= 8.0

Figure 135. Configuration 4D Step Tracking Response

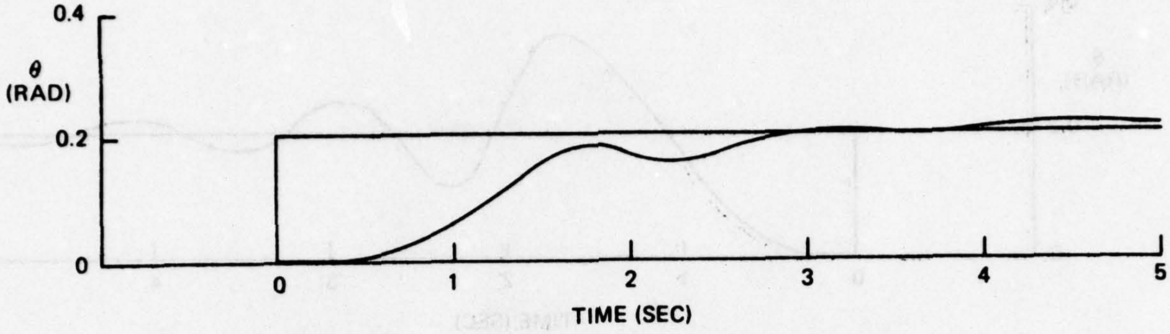

K_{PI}	=	20.0	K_{PF}	=	5.0	TOT	=	1.10
T_{LI}	=	-2.5	T_{LF}	=	2.50	$RMS\theta_e$	=	.47
D	=	1.0	K_{IC}	=	0	PR	=	7.5

Figure 136. Configuration 4E Step Tracking Response

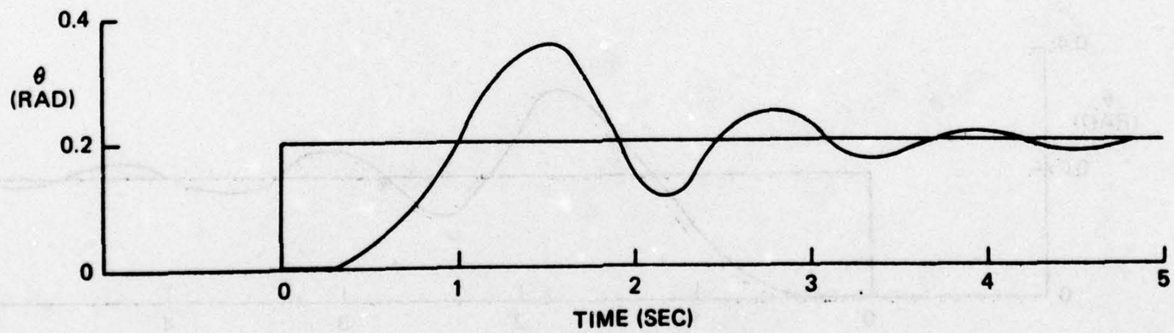

K_{PI}	=	6.12	K_{PF}	=	.20	TOT	=	.55
T_{LI}	=	-2.0	T_{LF}	=	3.5	$RMS\theta_e$	=	.45
D	=	1.35	K_{IC}	=	0	PR	=	5.0

Figure 137. Configuration 5A Step Tracking Response

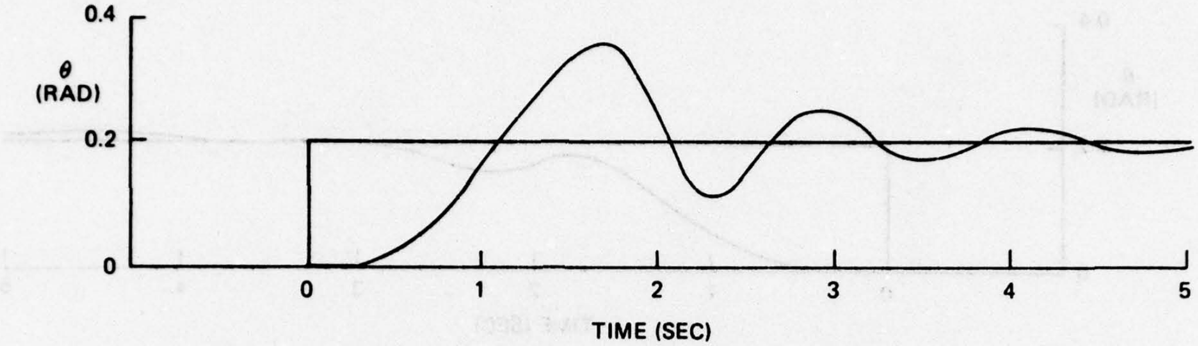

K_{PI}	=	6.75	K_{PF}	=	.2	TOT	=	.4
T_{LI}	=	-2.0	T_{LF}	=	3.50	RMSθ_e	=	.47
D	=	1.35	K_{IC}	=	0	PR	=	7.0

Figure 138. Configuration 5B Step Tracking Response

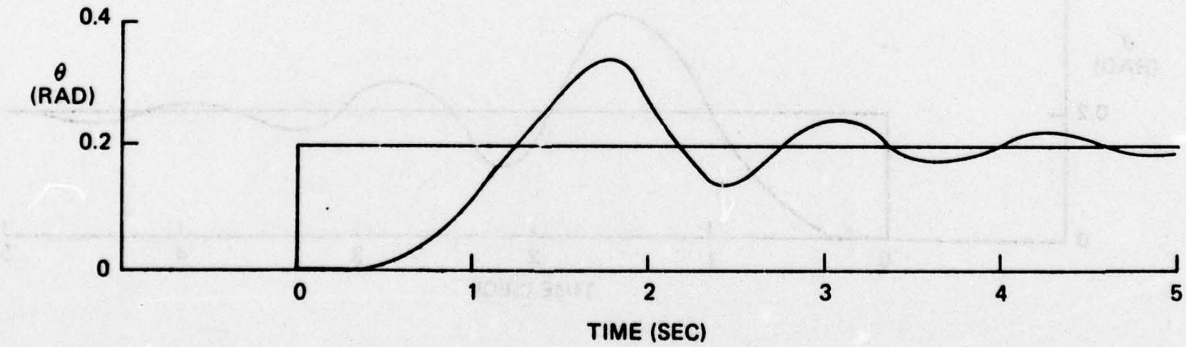

K_{PI}	=	7.5	K_{PF}	=	.2	TOT	=	.45
T_{LI}	=	-2.0	T_{LF}	=	3.5	RMSθ_e	=	.46
D	=	1.35	K_{IC}	=	0	PR	=	7.0

Figure 139. Configuration 5C Step Tracking Response

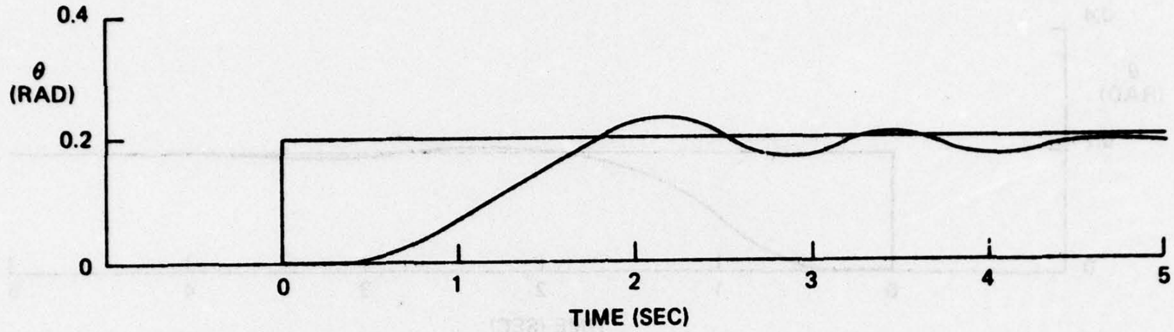

K_{PI}	=	7.5	K_{PF}	=	1.0	TOT	=	.90
T_{LI}	=	-2.0	T_{LF}	=	3.5	$RMS\theta_e$	=	.46
D	=	1.75	K_{IC}	=	0	PR	=	8.5

Figure 140. Configuration 5D Step Tracking Response

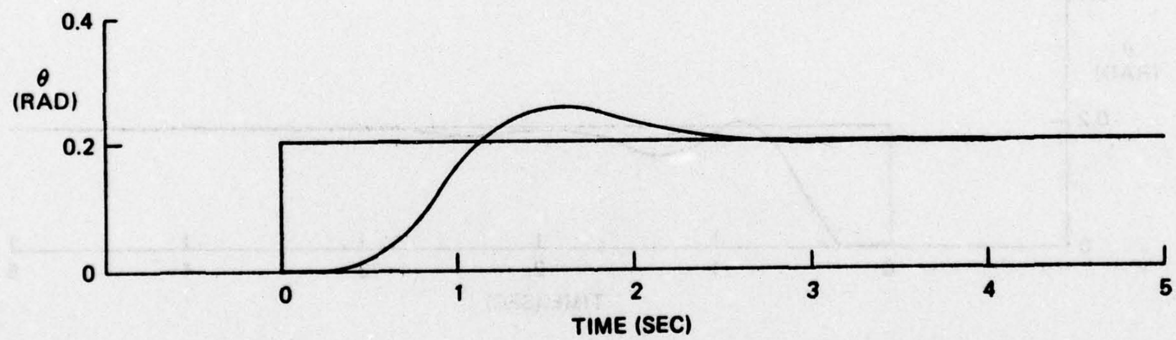

K_{PI}	=	60.0	K_{PF}	=	110	TOT	=	2.0
T_{LI}	=	0	T_{LF}	=	0	$RMS\theta_e$	=	.40
D	=	1.4	K_{IC}	=	0	PR	=	8.0

Figure 141. Configuration 5E Step Tracking Response

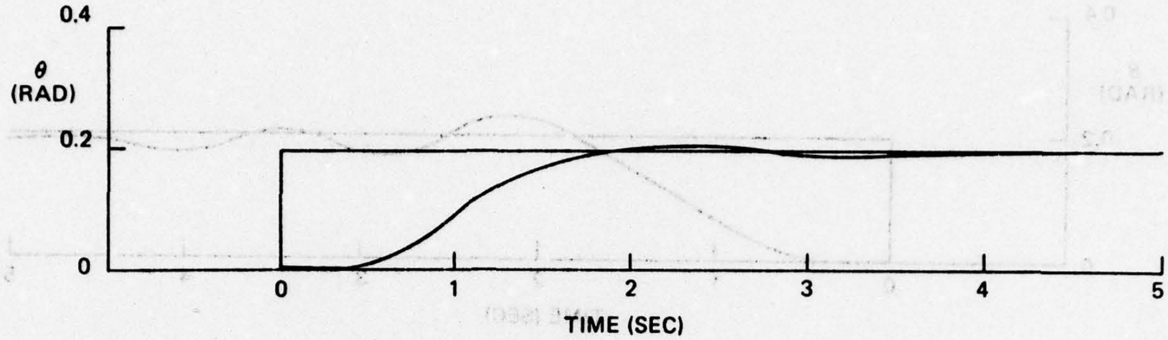

K_{PI}	=	10.0	K_{PF}	=	10.0	TOT	=	3.15
T_{LI}	=	0	T_{LF}	=	0	RMSθ_e	=	.42
D	=	1.0	K_{IC}	=	0	PR	=	5.0

Figure 142. Configuration 6A Step Tracking Response

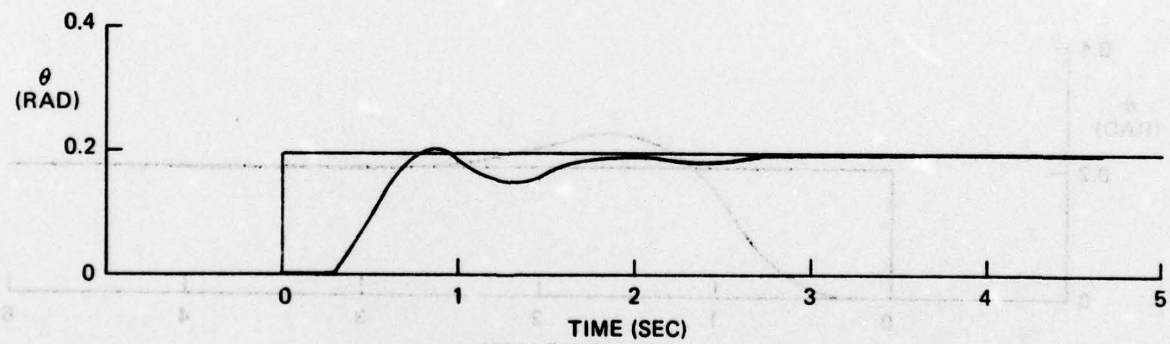

K_{PI}	=	22.0	K_{PF}	=	10.0	TOT	=	2.75
T_{LI}	=	.2	T_{LF}	=	0	RMSθ_e	=	.32
D	=	6.0	K_{IC}	=	0	PR	=	1.0

Figure 143. Configuration 6B Step Tracking Response

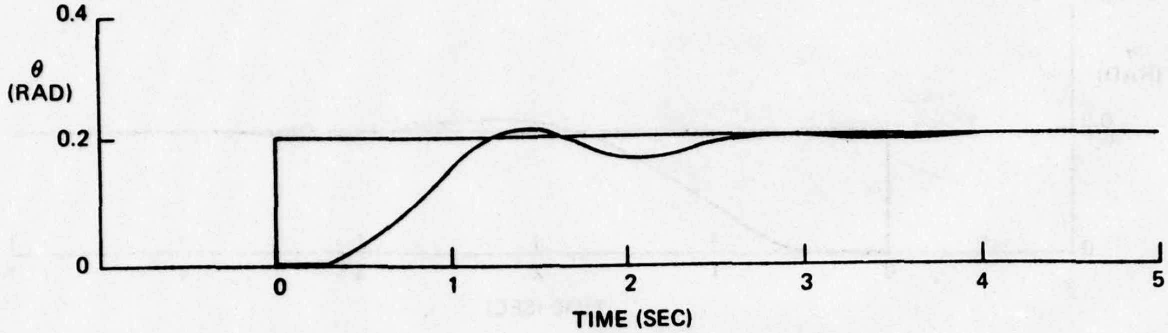

K_{PI}	=	12.0	K_{PF}	=	20.0	TOT	=	2.65
T_{LI}	=	-.1	T_{LF}	=	.3	$RMS\theta_e$	=	.38
D	=	1.0	K_{IC}	=	0	PR	=	2.5

Figure 144. Configuration 6C Step Tracking Response

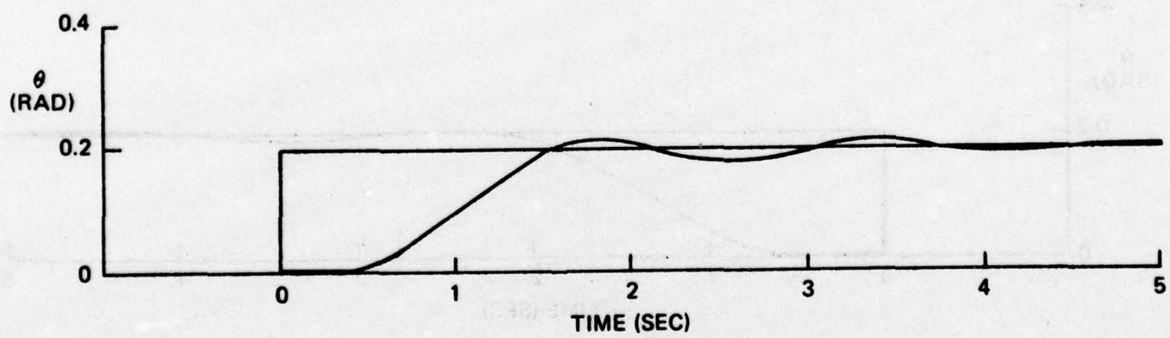

K_{PI}	=	10.0	K_{PF}	=	18.0	TOT	=	1.70
T_{LI}	=	-.1	T_{LF}	=	.3	$RMS\theta_e$	=	.42
D	=	1.25	K_{IC}	=	0	PR	=	5.5

Figure 145. Configuration 6D Step Tracking Response

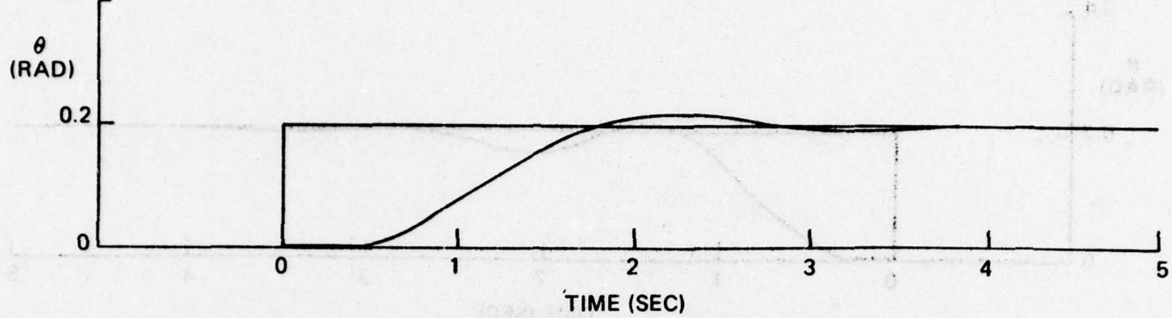

K_{PI}	=	10.0	K_{PF}	=	10.0	TOT	=	1.95
T_{LI}	=	0	T_{LF}	=	.2	RMSθ_e	=	.45
D	=	1.5	K_{IC}	=	0	PR	=	5.5

Figure 146. Configuration 6E Step Tracking Response

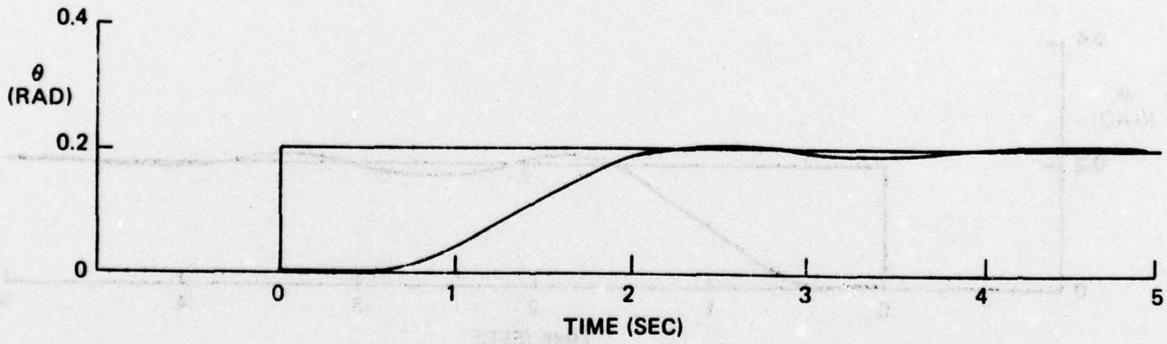

K_{PI}	=	16.0	K_{PF}	=	20.0	TOT	=	1.90
T_{LI}	=	.50	T_{LF}	=	1.0	RMSθ_e	=	.49
D	=	1.5	K_{IC}	=	0	PR	=	6.0

Figure 147. Configuration 6F Step Tracking Response

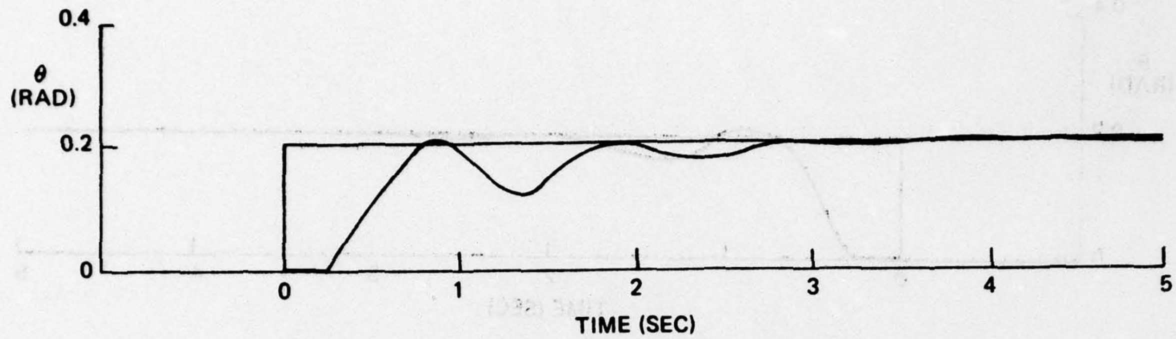

K_{PI}	=	40.0	K_{PF}	=	50.0	TOT	=	2.60
T_{LI}	=	-.3	T_{LF}	=	0	$RMS\theta_e$	=	.33
D	=	.7	K_{IC}	=	.15	PR	=	2.0

Figure 148. Configuration 7A Step Tracking Response

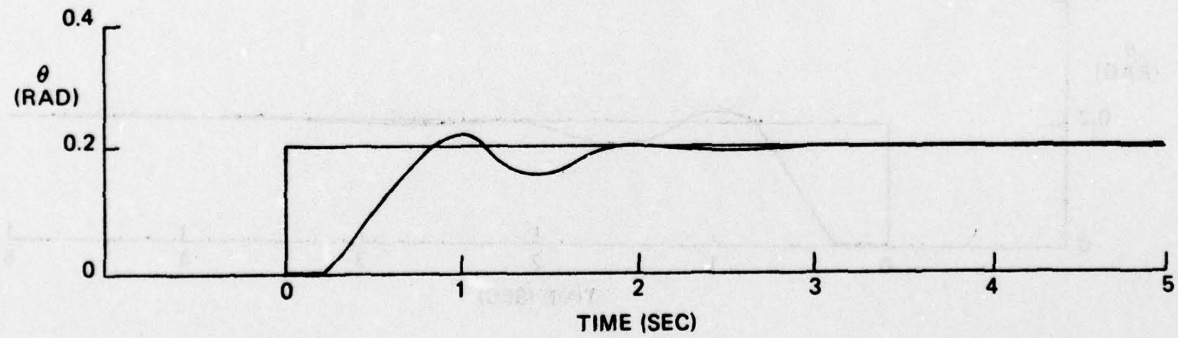

K_{PI}	=	40.0	K_{PF}	=	65.0	TOT	=	2.65
T_{LI}	=	-.45	T_{LF}	=	0	$RMS\theta_e$	=	.33
D	=	.75	K_{IC}	=	0	PR	=	3.0

Figure 149. Configuration 7B Step Tracking Response

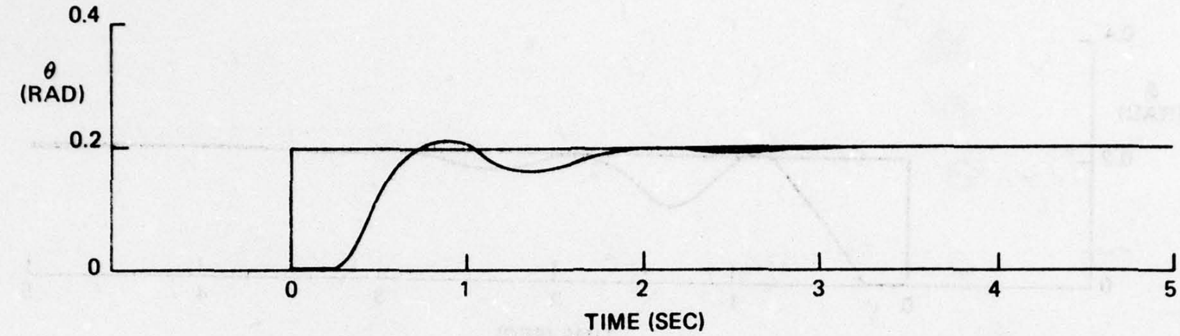

K_{PI}	=	70.0	K_{PF}	=	65.0	TOT	=	2.80
T_{LI}	=	-.05	T_{LF}	=	0	$RMS\theta_e$	=	.32
D	=	.5	K_{IC}	=	0	PR	=	1.5

Figure 150. Configuration 7C Step Tracking Response

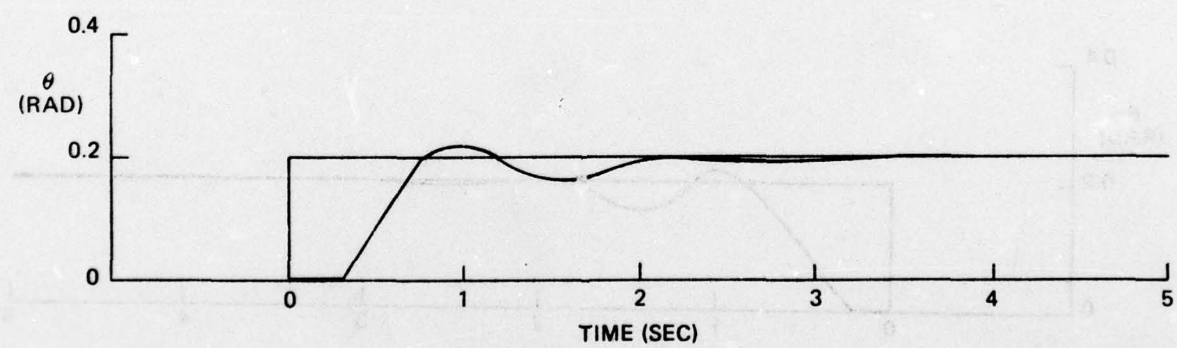

K_{PI}	=	70.0	K_{PF}	=	65.0	TOT	=	2.9
T_{LI}	=	-.05	T_{LF}	=	0	$RMS\theta_e$	=	.33
D	=	.5	K_{IC}	=	0	PR	=	5.5

Figure 151. Configuration 7D Step Tracking Response

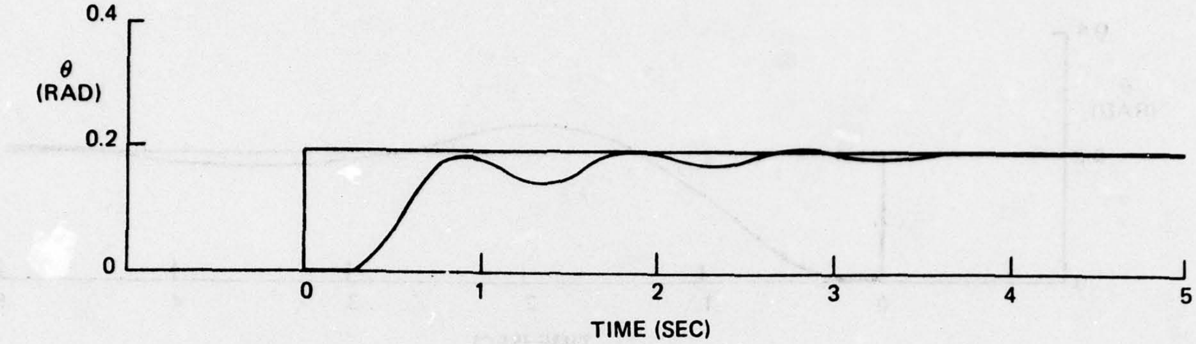

K_{PI}	=	80.0	K_{PF}	=	65.0	TOT	=	2.15
T_{LI}	=	.2	T_{LF}	=	.3	$RMS\theta_e$	=	.35
D	=	.75	K_{IC}	=	0	PR	=	5.0

Figure 152. Configuration 7E Step Tracking Response

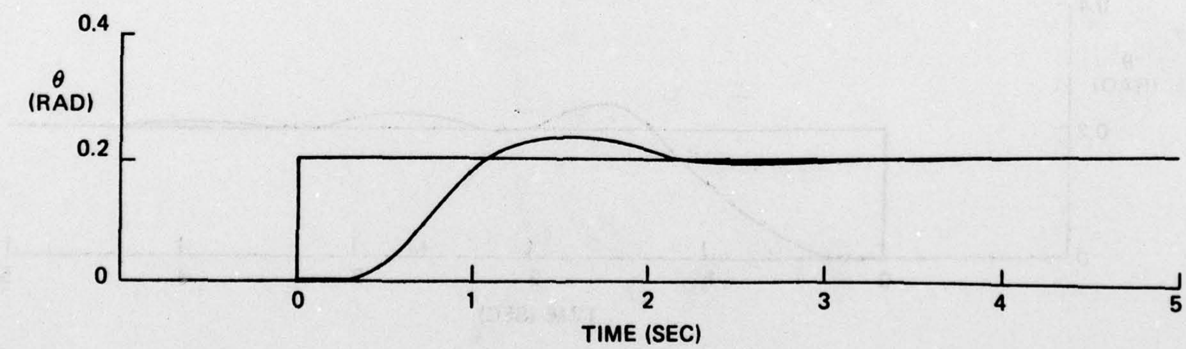

K_{PI}	=	70.0	K_{PF}	=	65.0	TOT	=	2.35
T_{LI}	=	-.05	T_{LF}	=	0	$RMS\theta_e$	=	.37
D	=	.5	K_{IC}	=	0	PR	=	3.0

Figure 153. Configuration 7F Step Tracking Response

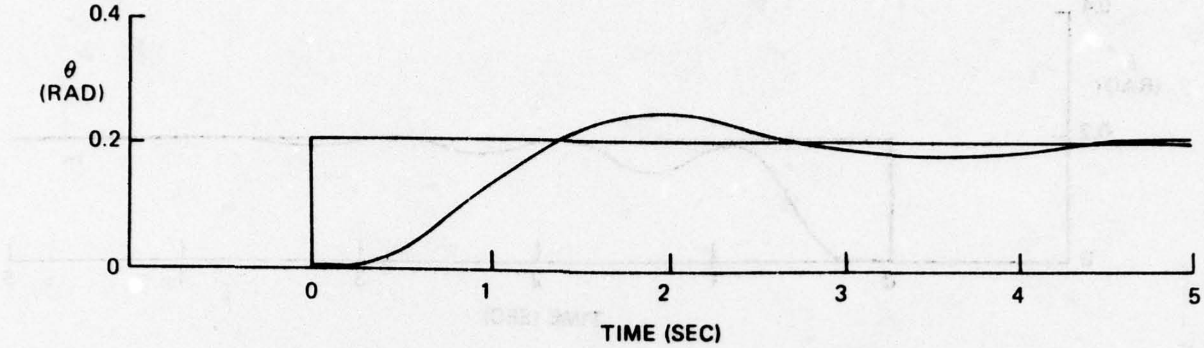

K_{PI}	=	60.0	K_{PF}	=	9[illegible]	TOT	=	1.20
$T_{[illegible]}$	=	-.05	T_{LF}	=	0	$RMS\theta_e$	=	.41
D	=	1.0	K_{IC}	=	0	PR	=	5.0

Figure 154. Configuration 7G Step Tracking Response

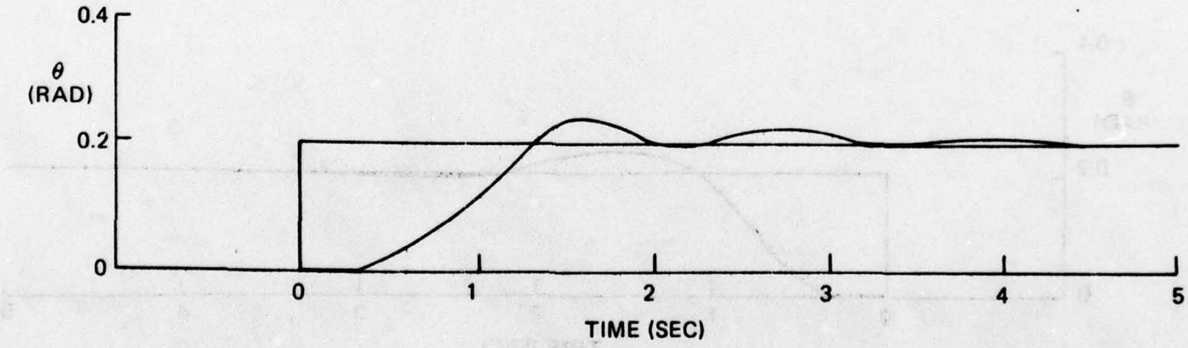

K_{PI}	=	100.0	K_{PF}	=	110.0	TOT	=	1.55
T_{LI}	=	-.30	T_{LF}	=	1.0	$RMS\theta_e$	=	.42
D	=	1.0	K_{IC}	=	0	PR	=	5.0

Figure 155. Configuration 7H Step Tracking Response

Figure 150 shows the optimized step tracking response of one of the better configurations surveyed, 7C, which was given a rating of PR = 1.5. In this case, the rapid acquisition of the target leads to low rms θ_e while the steadiness of the precision tracking results in large time-on-target. On the other hand, Figure 118 shows a poor configuration, 1F (PR = 8) that has sluggish response indicated by high rms θ_e. Even worse is the inability of this configuration to settle out on the target so that the time-on-target is mostly achieved during target crossings. Other configurations show a wide range of specific handling qualities problems: aircraft that exhibit great overshoot and others with a steady state error that is difficult to overcome even with the use of the integral control compensation.

C. CORRELATION OF PILOT RATINGS WITH STEP TARGET DATA

The military flying qualities specification, MIL-F-8785B, establishes numerical criteria that define Levels of flying qualities performance which in general correspond to Cooper-Harper pilot ratings:

Level 1 – PR 1 – 3.5

Level 2 – PR 3.5 – 6.5

Level 3 – PR 6.5 – 9.5

It is useful to examine the correlations with pilot ratings of the rms θ_e and time-on-target data obtained for the Neal and Smith configurations. The normalized rms θ_e data is presented in Figure 156. The expected result of increasing pilot rating number with increasing rms θ_e is clearly shown. However, vertical lines are needed on the figure at specific rms θ_e values in order to specify the performance as Level 1, 2, or 3. But no lines can be drawn that do not also include many points from the wrong Levels. This failure of rms θ_e to correlate with pilot ratings sufficiently well for specification purposes has been frequently noted, and attempts to weight other quantities along with it to produce stronger correlations were referenced earlier. From the above description of the piloted task, it is clear that the rms θ_e statistic is incidental, time-on-target being the primary performance measure. If time-on-target is plotted against pilot ratings, there is again a strong correlation as shown in Figure 157. Unfortunately, this correlation is even less able to furnish specification boundaries than the rms θ_e versus pilot rating data.

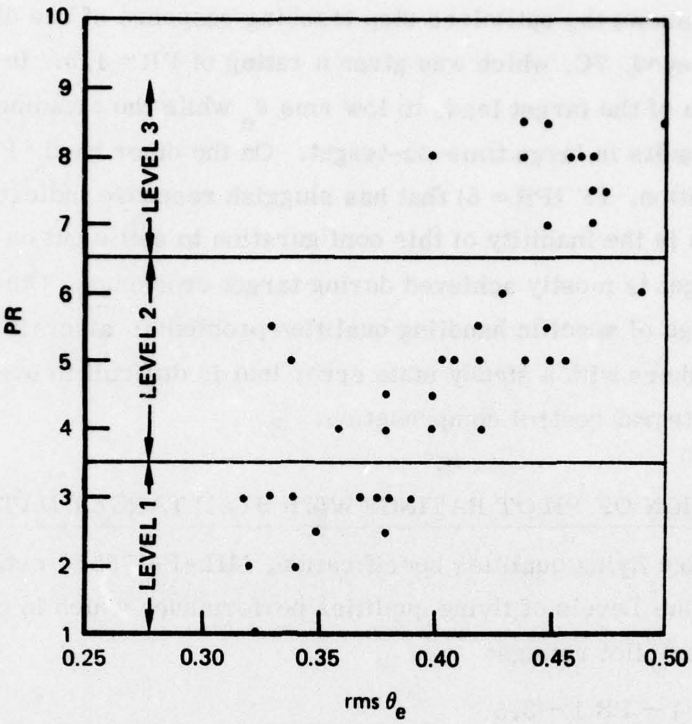

Figure 156. Correlation of rms θ_e with Pilot Ratings

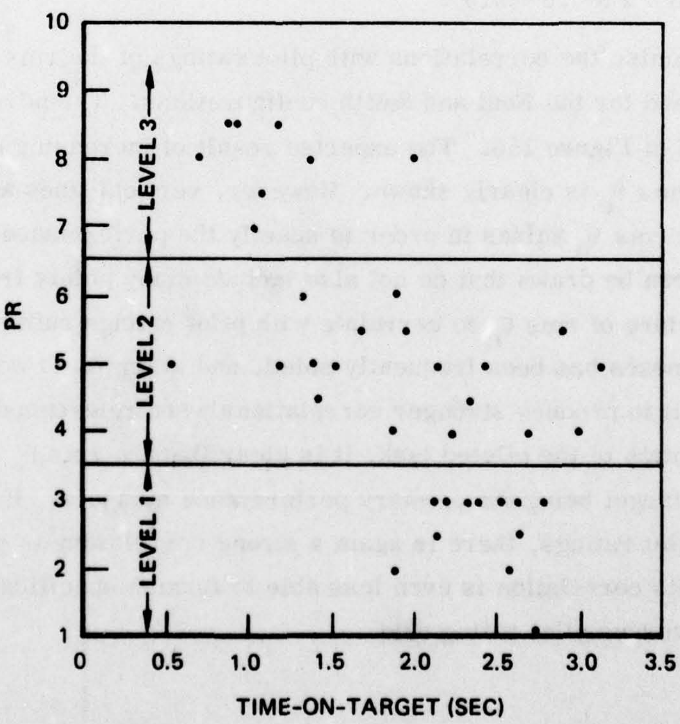

Figure 157. Correlation of Time-On-Target with Pilot Ratings

From the above it is clear that the single performance parameters rms θ_e or time-on-target are not sufficient to specify acceptable performance of the Neal and Smith configurations. If one considers that the pilot might trade rms θ_e and time-on-target against one another in generating his pilot rating, these statistics become more useful. To see how this trade-off may take place, normalized rms θ_e is plotted versus time-on-target with the point indicated by the minimum pilot rating given by a test pilot during the in-flight simulation. This is shown in Figure 158 along with apparent boundaries that neatly separate the regions of Levels 1, 2, and 3. With the exception of seven points out of forty-two, all configurations lie in regions bounded by apparent curves that illustrate the trade-off between the two performance measures. These curves show, for example, that a pilot will tolerate more sluggish response in a given Level if the resulting time-on-target is especially good, and conversely. Since the parameters rms θ_e and time-on-target correlate with pilot ratings obtained during a flight test program that examined various tracking tasks, the representation of target tracking by the step target appears to be justified.

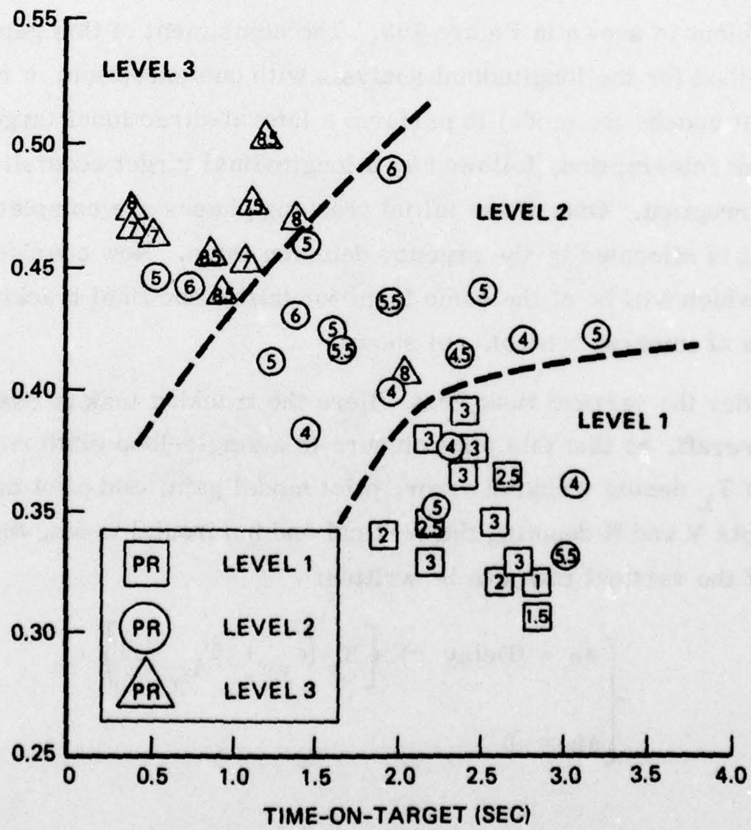

Figure 158. Pilot Ratings as Functions of rms θ_e and Time-On-Target

D. MULTIAXIS STEP TARGET TRACKING

The success of the method of step target tracking applied to longitudinal target tracking evaluation motivates an extension of the method to multiaxis flying qualities. Unfortunately, little published data is available for multiaxis target tracking that could be used to correlate rms error and time-on-target parameters, or other parameters derived from a model for the complete piloted six degree-of-freedom aircraft. Even so, the importance of multiaxis flying qualities cannot be overlooked, and the appropriate multiaxis pilot model will be briefly presented in the expectation of future data comparisons.

The model for multiaxis step target tracking is easy to establish. On each axis, longitudinal and lateral-directional, initial and final compensation strategies are followed as in the longitudinal analysis presented above. All that is needed is the attention allocation algorithm including a rule for the initial target acquisition phases on each axis, which will be referred to as the vertical and horizontal tracking tasks. For this general case, the step target should be established not simply as an attitude error, but as a position relative to the tracking aircraft. A system diagram for this general problem is shown in Figure 159. The adjustment of this general model follows the method for the longitudinal analysis with one exception: a rule must be enforced that causes the model to perform a lateral-directional target acquisition phase without interruption, followed by a longitudinal target acquisition phase also without interruption. Once these initial tracking phases are complete, the attention of the model is allocated by the urgency decision logic. Now consider the pilot compensation, which will be of the same form for initial and final tracking except for the possible use of integral control, not shown.

Consider the vertical task first. Here the tracking task is essentially to point the aircraft, so that this pilot closure is a single-loop pitch tracking task. Now if ϵ, K, and T_L denote tracking error, pilot model gain, and pilot model lead, with the subscripts V and H denoting the vertical and horizontal tasks, the fixed-form compensation of the vertical task can be written:

$$\begin{cases} \delta e = (\text{Delay } \tau) \left\{ K_V \left(\epsilon_V + T_{L_V} \dot{\epsilon}_V \right) \right\} \\ \delta a = 0 \end{cases}$$

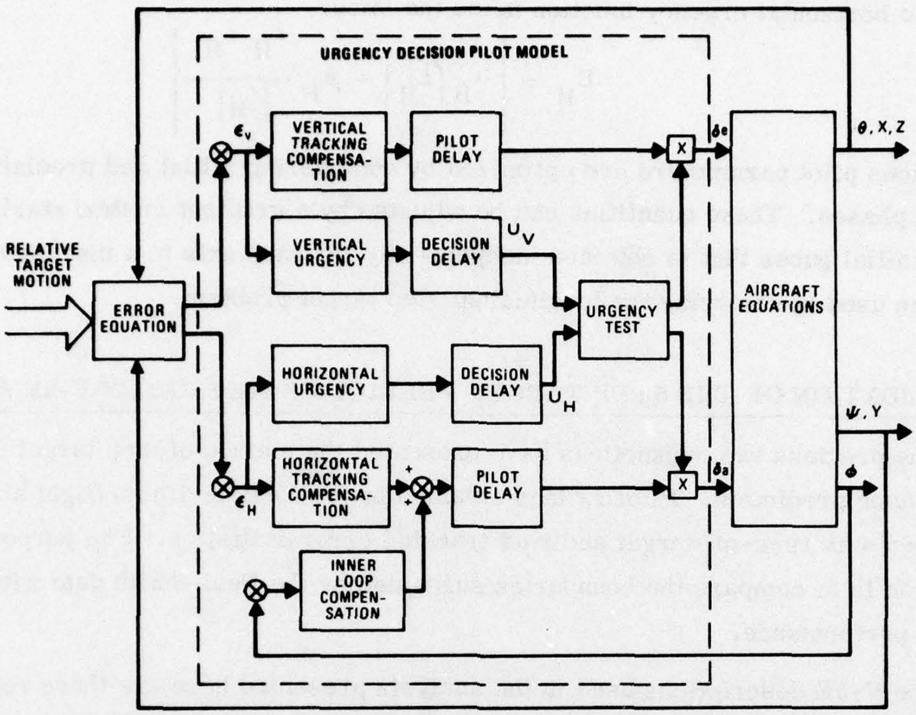

Figure 159. Control Configuration for Step Target Tracking

The associated urgency function of this single-loop component task is then dictated by the general formulation of the Urgency Decision Pilot Model to be of the form:

$$U_V = \left| \alpha_V \left| \epsilon_V \right| + \beta_V \frac{\epsilon_V \dot{\epsilon}_V}{\left| \epsilon_V \right|} \right|$$

When the model is in horizontal control, it is required to track the target through changes in the heading of the tracking aircraft. This multiloop task is modeled by an inner attitude stabilization loop and an outer heading command loop tracking closure. These take the forms:

$$\delta a_1 = (\text{Delay } \tau) \left\{ K_\phi \left(\phi + T_{L_\phi} \dot{\phi} \right) \right\}$$

$$\delta a_2 = (\text{Delay } \tau) \left\{ K_H \left(\epsilon_H + T_{L_H} \dot{\epsilon}_H \right) \right\}$$

$$\begin{cases} \delta a = \delta a_1 + \delta a_2 \\ \delta e = 0 \end{cases}$$

The horizontal urgency function takes the form:

$$U_H = \left| \alpha_H \left| \epsilon_H \right| + \beta_H \frac{\epsilon_H \dot{\epsilon}_H}{\left| \epsilon_H \right|} \right|$$

The various pilot parameters are optimized by considering initial and precision tracking phases. These quantities can be adjusted by a gradient method starting with an initial guess that is obtained independently for each axis in a manner similar to the one used in analyzing the longitudinal step target problem.

E. VALIDATION OF THE STEP TARGET PREDICTION METHOD BY F-5E AIRCRAFT

The previous two Subsections have presented the method of step target tracking performance prediction. Pilot ratings obtained by the Neal-Smith in-flight simulation correlated with time-on-target and rms tracking error statistics. The purpose of this Subsection is to compare the boundaries suggested by the Neal-Smith data with F-5E aircraft performance.

The F-5E descriptions used in the analysis presented here are those reported in Section V. All nine flight conditions shown in Figure 80 have been analyzed with and without augmenter for step target longitudinal tracking response. These were computed using the nonlinear equations of motion presented in Section V. The data for each flight condition and control configuration are given in Figures 160-177.

Comparison of the step tracking responses for each flight condition with and without augmenter shows the importance of proper augmentation for good tracking response. In the augmented cases, the initial response is faster as reflected in the rms tracking error statistic, while the better damped dynamics lead to larger time-on-target values. To demonstrate the validity of the boundaries shown in Figure 158 based on the Neal-Smith data, the F-5E response data is plotted on these boundaries in Figure 178. Since the augmented F-5E has good Level 1 flying qualities, while the unaugmented aircraft may or may not meet Level 1 criteria, the Level 1-Level 2 boundary is consistent with the F-5E data. In this way, not only do the data of Figure 178 show the gradient direction of improving performance which characterized the Neal-Smith data, but the actual suggested boundary position is consistent as well.

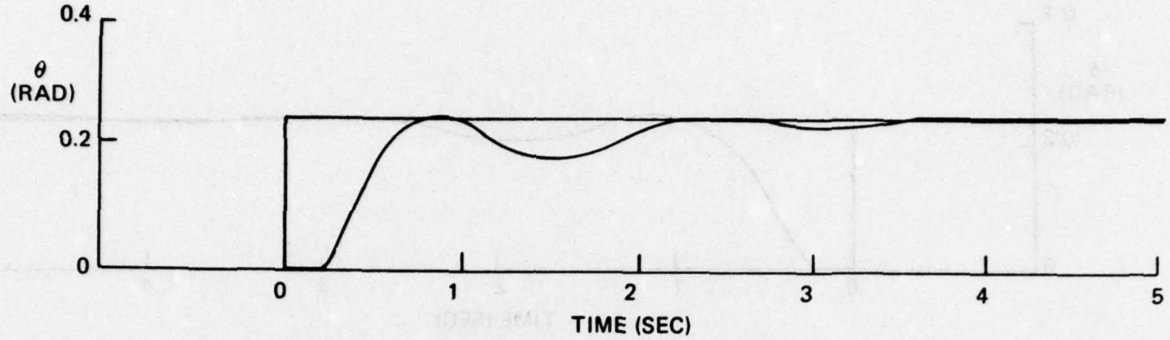

K_{PI}	=	-.54	K_{PF}	=	-.85	TOT	=	2.38
T_{LI}	=	.5	T_{LF}	=	.3	$RMS\theta_e$	=	.31
D	=	.8	K_{IC}	=	.05	AUGMENTER		

Figure 160. F-5E Case 1 Step Target Tracking Response

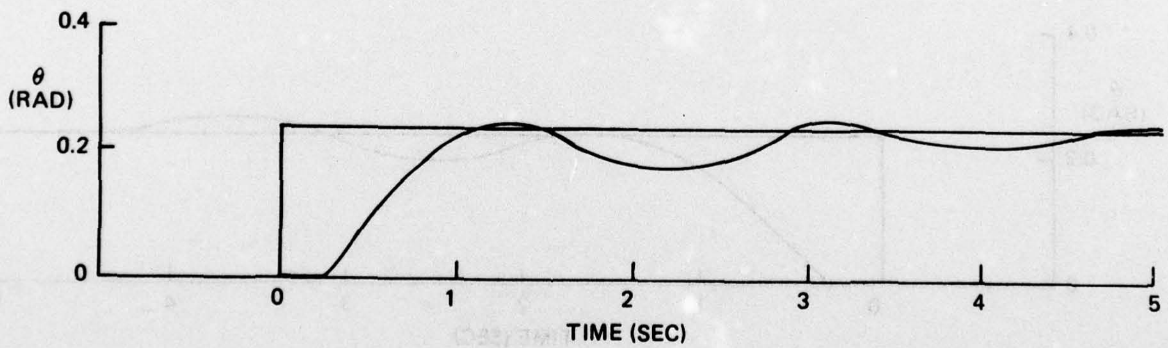

K_{PI}	=	-.28	K_{PF}	=	-.5	TOT	=	1.32
T_{LI}	=	.5	T_{LF}	=	.5	$RMS\theta_e$	=	.34
D	=	1.0	K_{IC}	=	.05	NO AUGMENTER		

Figure 161. F-5E Case 1 Step Target Tracking Response

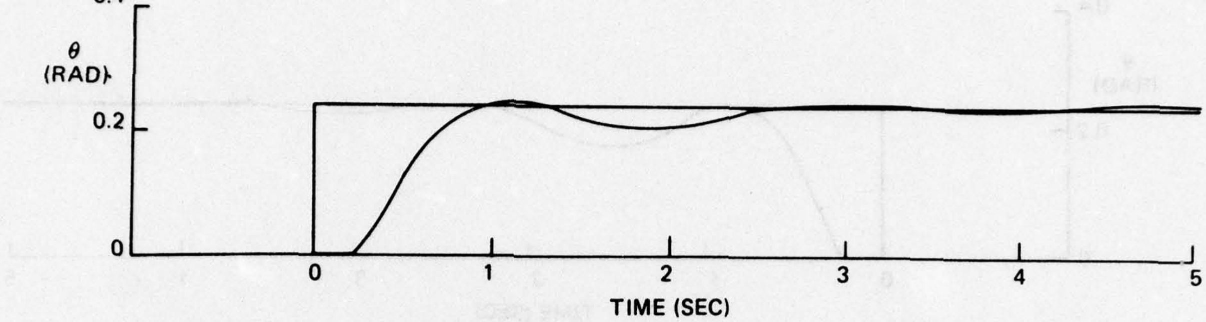

K_{PI}	=	-.57	K_{PF}	=	-1.0	TOT	=	2.68
T_{LI}	=	.5	T_{LF}	=	.3	$RMS\theta_e$	=	.31
D	=	.8	K_{IC}	=	.08	AUGMENTER		

Figure 162. F-5E Case 2 Step Target Tracking Response

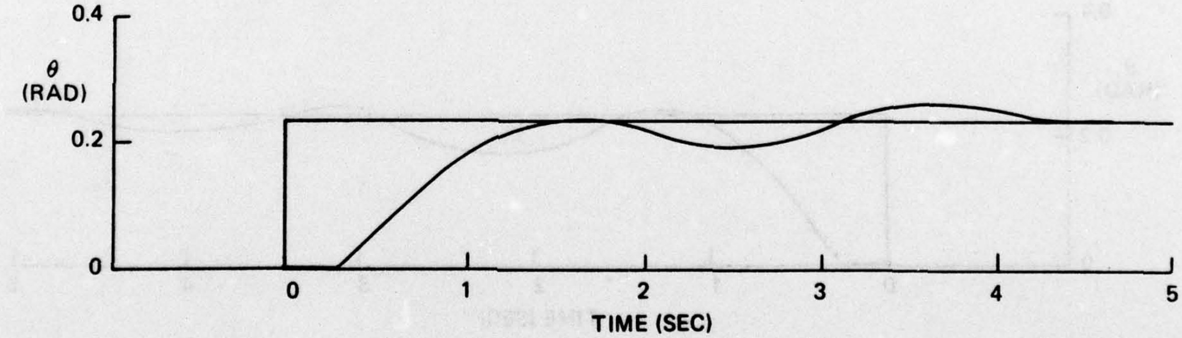

K_{PI}	=	-.27	K_{PF}	=	-.7	TOT	=	1.68
T_{LI}	=	.5	T_{LF}	=	.5	$RMS\theta_e$	=	.36
D	=	1.0	K_{IC}	=	.1	NO AUGMENTER		

Figure 163. F-5E Case 2 Step Target Tracking Response

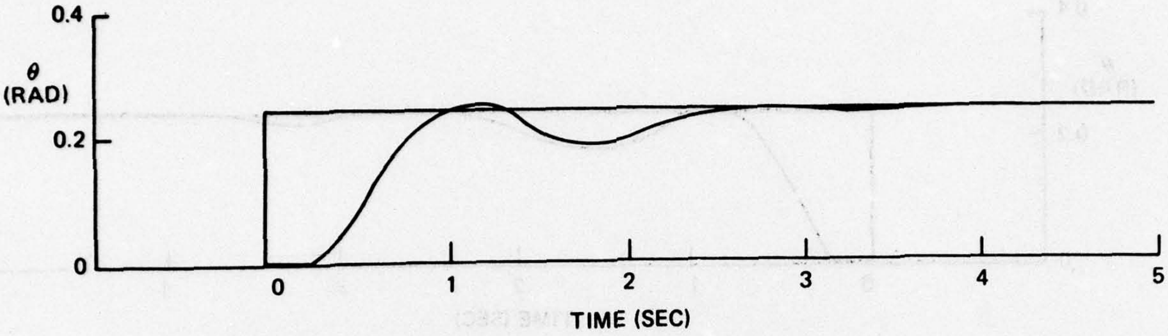

K_{PI}	=	- .355	K_{PF}	=	- .355	TOT	=	2.18
T_{LI}	=	.1	T_{LF}	=	.25	RMSθ_e	=	.34
D	=	1.0	K_{IC}	=	.05	AUGMENTER		

Figure 164. F-5E Case 3 Step Target Tracking Response

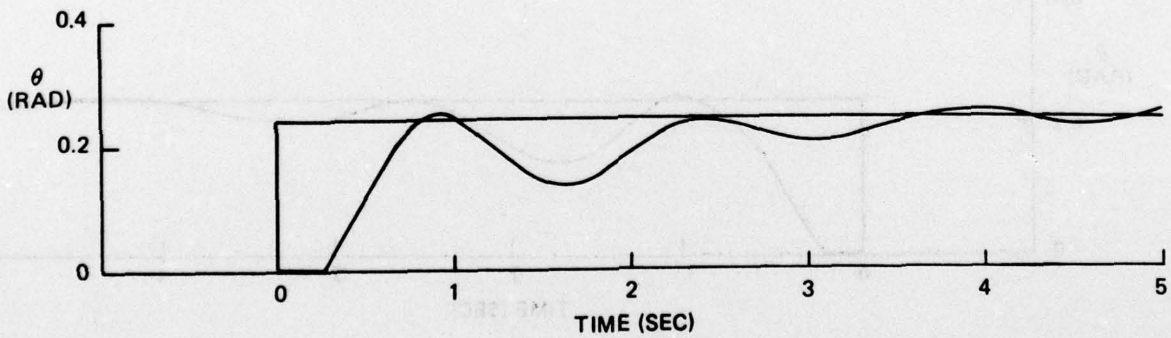

K_{PI}	=	- .2	K_{PF}	=	- .2	TOT	=	1.80
T_{LI}	=	.5	T_{LF}	=	.7	RMSθ_e	=	.34
D	=	.8	K_{IC}	=	.11	NO AUGMENTER		

Figure 165. F-5E Case 3 Step Target Tracking Response

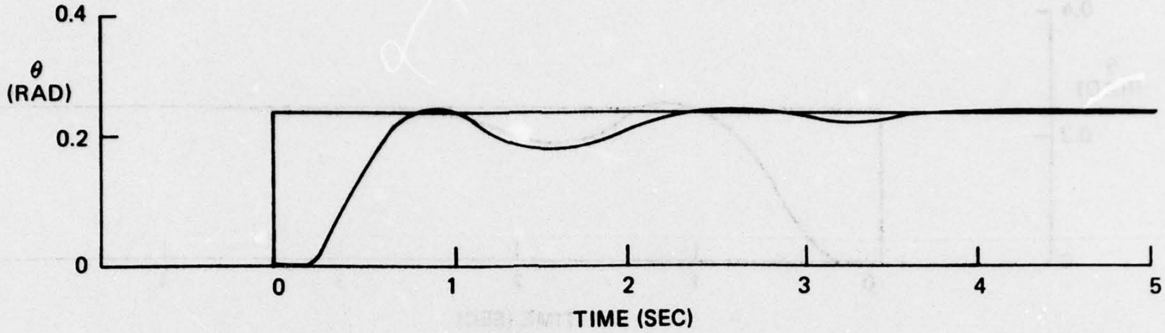

K_{PI}	=	-.49	K_{PF}	=	-.6	TOT	=	2.28
T_{LI}	=	.3	T_{LF}	=	.2	$RMS\theta_e$	=	.31
D	=	.8	K_{IC}	=	.06	AUGMENTER		

Figure 166. F-5E Case 4 Step Target Tracking Response

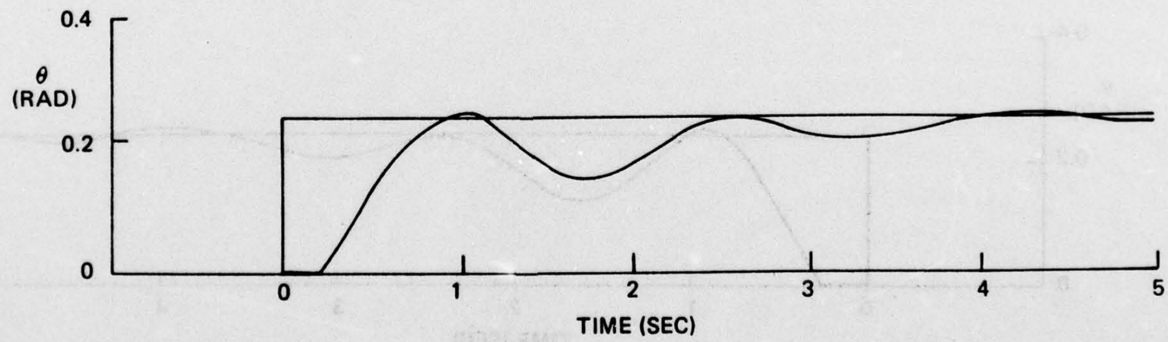

K_{PI}	=	-.23	K_{PF}	=	-.3	TOT	=	1.50
T_{LI}	=	.5	T_{LF}	=	.7	$RMS\theta_e$	=	.34
D	=	.8	K_{IC}	=	.09	NO AUGMENTER		

Figure 167. F-5E Case 4 Step Target Tracking Response

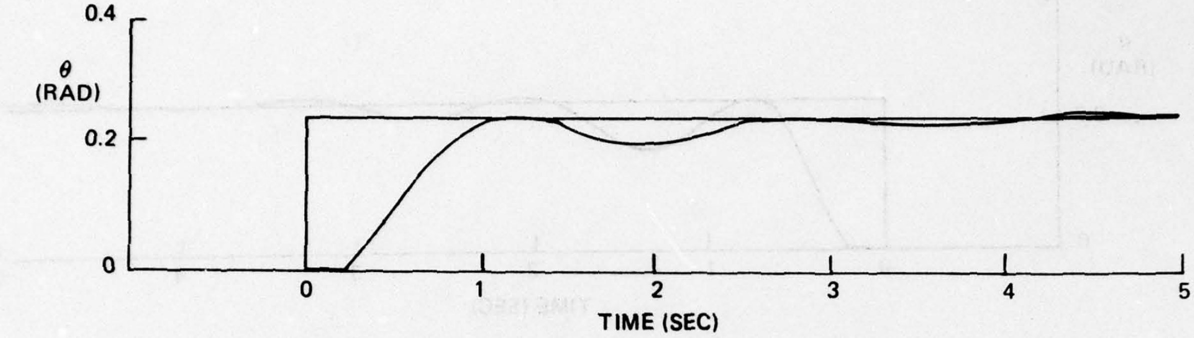

K_{PI}	= -.53		K_{PF}	= -.9		TOT	= 2.20
T_{LI}	= .2		T_{LF}	= .3		$RMS\theta_e$	= .34
D	= 1.0		K_{IC}	= .06		AUGMENTER	

Figure 168. F-5E Case 5 Step Target Tracking Response

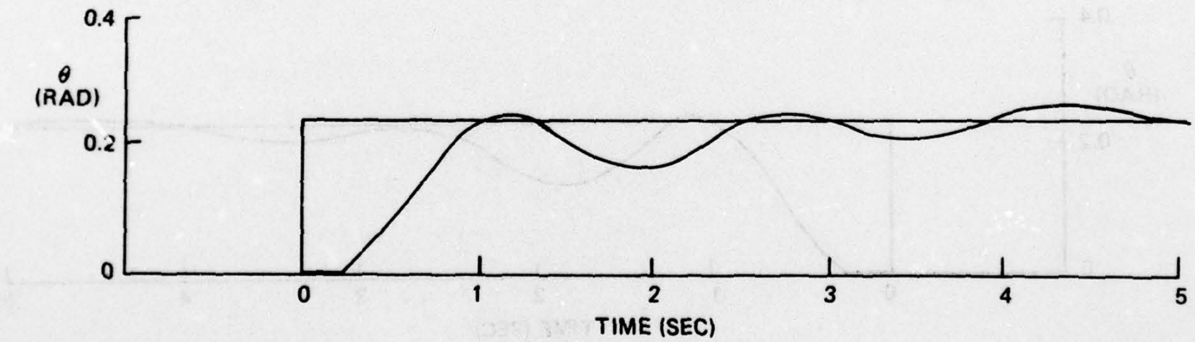

K_{PI}	= -.26		K_{PF}	= -.5		TOT	= 1.40
T_{LI}	= .5		T_{LF}	= .7		$RMS\theta_e$	= .35
D	= .8		K_{IC}	= .1		NO AUGMENTER	

Figure 169. F-5E Case 5 Step Target Tracking Response

AD-A056 983 NORTHROP CORP HAWTHORNE CA AIRCRAFT GROUP F/G 5/8
PREDICTION, EVALUATION, AND SPECIFICATION OF CLOSED LOOP AND MU--ETC(U)
FEB 78 E D ONSTOTT, W H FAULKNER F33615-77-C-3008
UNCLASSIFIED NOR-77-162 AFFDL-TR-78-3 NL

3 OF 3
AD
A056983

END
DATE
FILMED
9-78
DDC

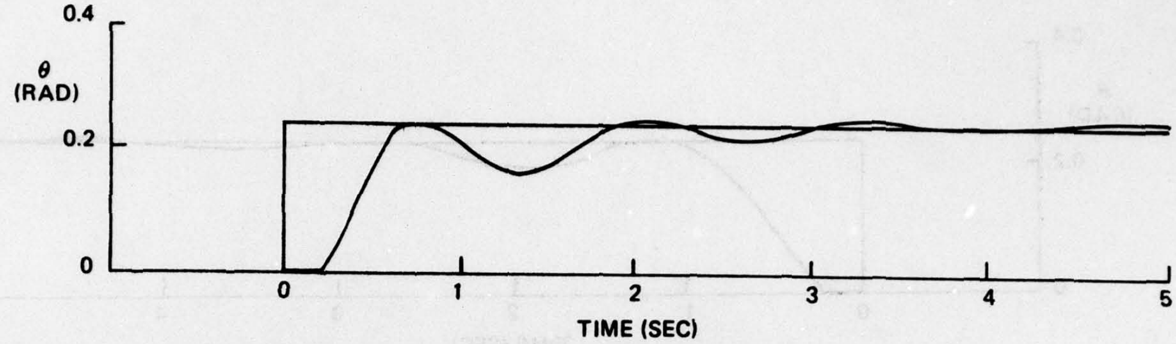

K_{PI} = - .33
T_{LI} = .18
D = 1.0

K_{PF} = - .35
T_{LF} = .15
K_{IC} = .03

TOT = 2.62
RMSθ_e = .31
AUGMENTER

Figure 170. F-5E Case 6 Step Target Tracking Response

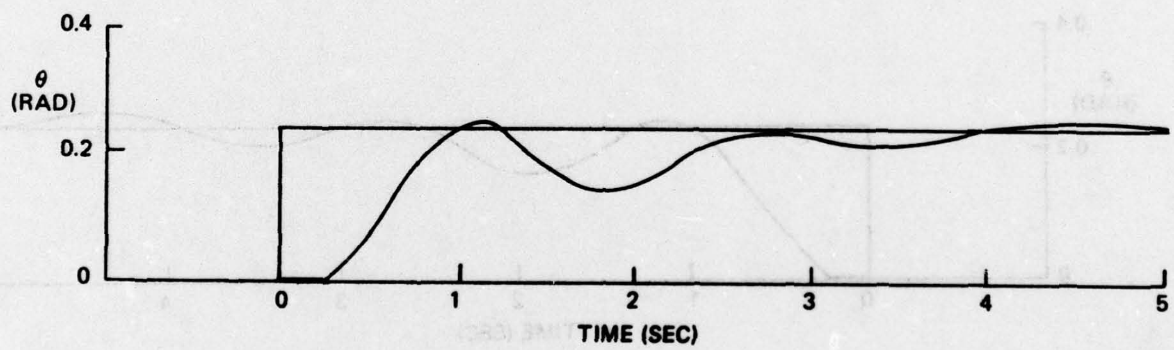

K_{PI} = - .18
T_{LI} = .1
D = .8

K_{PF} = - .1
T_{LF} = .3
K_{IC} = .11

TOT = 1.38
RMSθ_e = .36
NO AUGMENTER

Figure 171. F-5E Case 6 Step Target Tracking Response

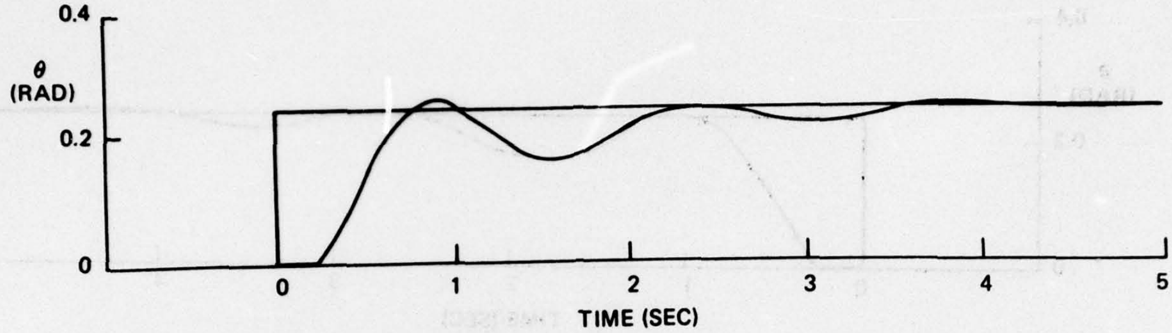

K_{PI}	= - .35	K_{PF}	= - .35	TOT	= 2.12
T_{LI}	= .18	T_{LF}	= .2	$RMS\theta_e$	= .32
D	= 1.0	K_{IC}	= .05	AUGMENTER	

Figure 172. F-5E Case 7 Step Target Tracking Response

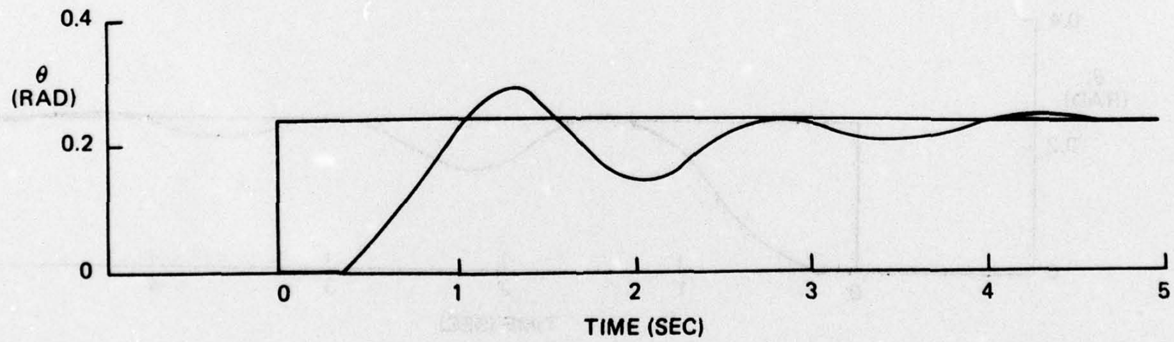

K_{PI}	= - .2	K_{PF}	= - .1	TOT	= 1.32
T_{LI}	= 0	T_{LF}	= 1.0	$RMS\theta_e$	= .39
D	= 1.0	K_{IC}	= .22	NO AUGMENTER	

Figure 173. F-5E Case 7 Step Target Tracking Response

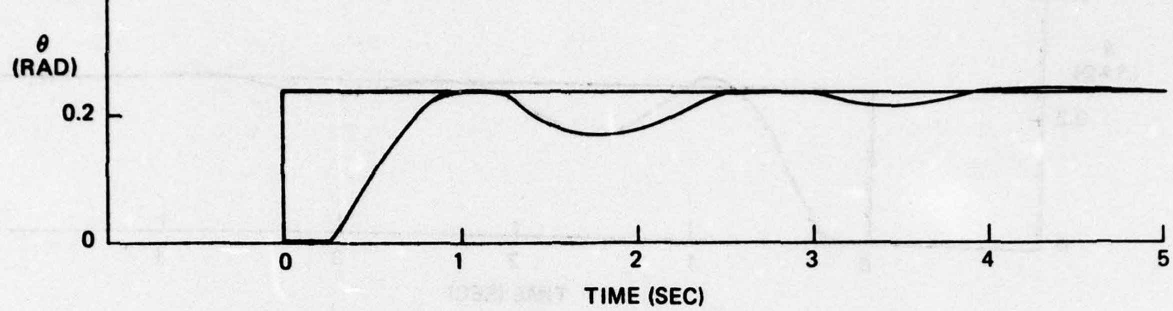

K_{PI}	= - .4	K_{PF}	= - .5	TOT	= 1.90
T_{LI}	= .18	T_{LF}	= .2	$RMS\theta_e$	= .33
D	= 1.0	K_{IC}	= .05	AUGMENTER	

Figure 174. F-5E Case 8 Step Target Tracking Response

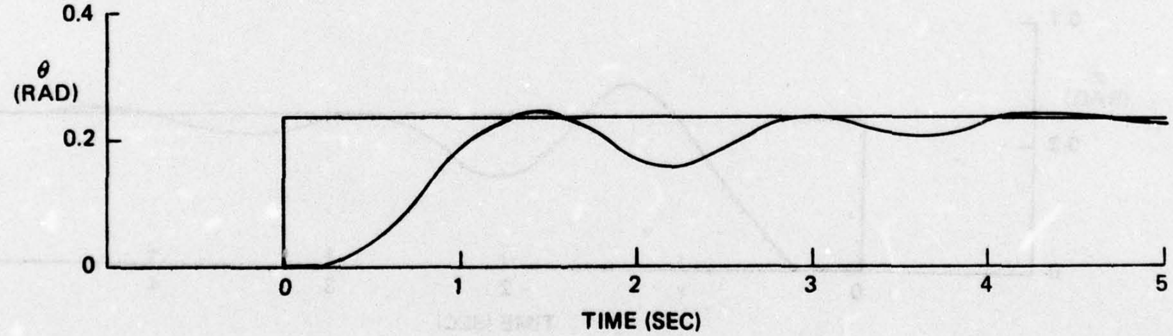

K_{PI}	= - .2	K_{PF}	= .24	TOT	= 1.18
T_{LI}	= .1	T_{LF}	= .8	$RMS\theta_e$	= .39
D	= 1.25	K_{IC}	= .1	NO AUGMENTER	

Figure 175. F-5E Case 8 Step Target Tracking Response

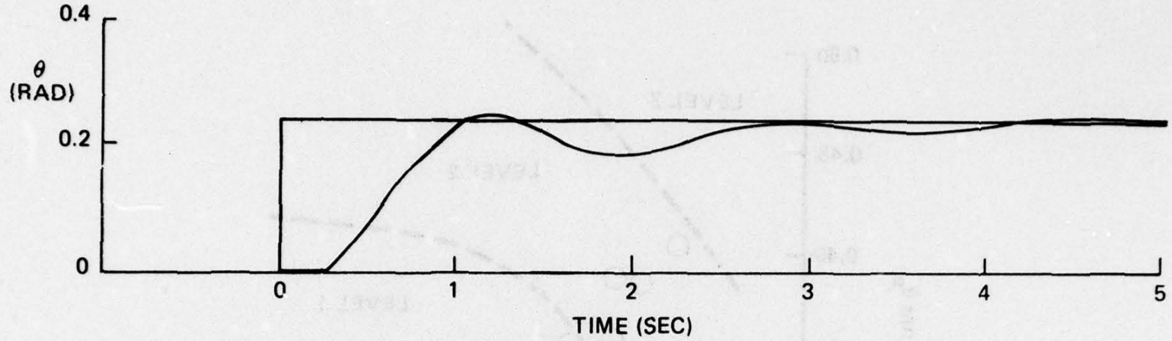

K_{PI} = -.52	K_{PF} = -.75	TOT = 2.15
T_{LI} = .18	T_{LF} = .3	RMS θ_e = .33
D = .9	K_{IC} = .1	AUGMENTER

Figure 176. F-5E Case 9 Step Target Tracking Response

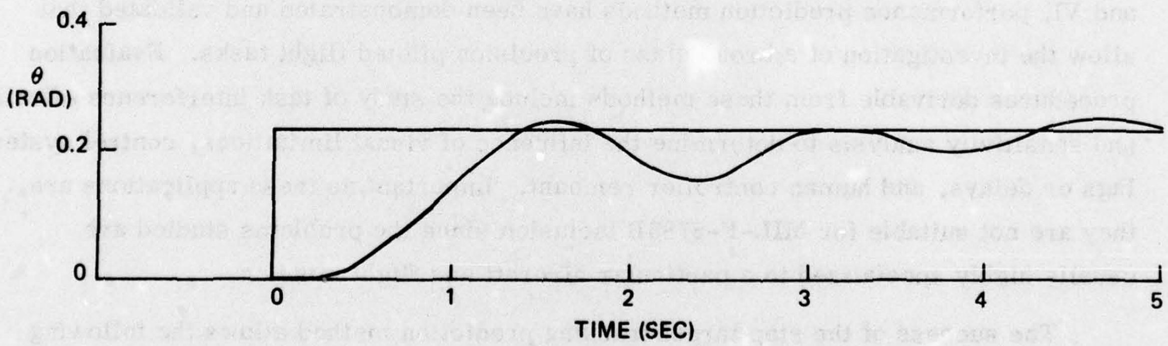

K_{PI} = -.22	K_{PF} = -.4	TOT = .90
T_{LI} = .1	T_{LF} = .8	RMS θ_e = .41
D = 1.25	K_{IC} = .1	NO AUGMENTER

Figure 177. F-5E Case 9 Step Target Tracking Response

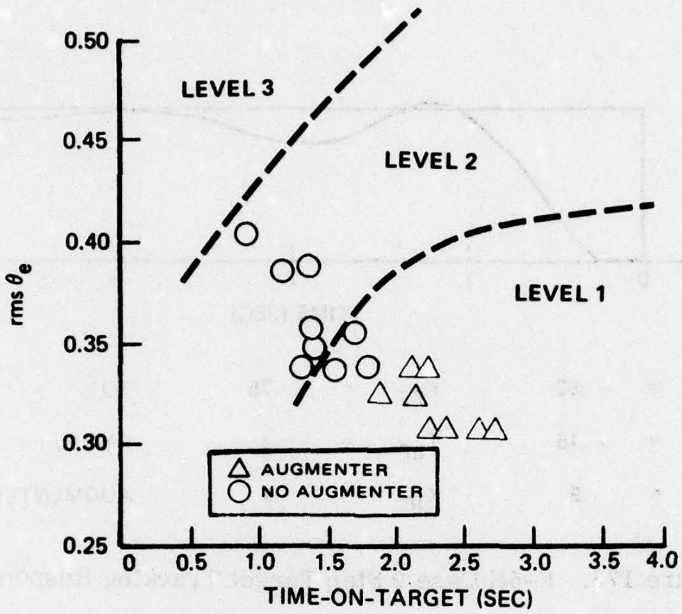

Figure 178. F-5E Validation of Step Target Prediction Method

F. SPECIFICATION OF AIR-TO-AIR TRACKING PERFORMANCE

The main objective of this report is to present methods for the prediction, evaluation and specification of closed loop multiaxis flying qualities. In Sections IV, V, and VI, performance prediction methods have been demonstrated and validated that allow the investigation of a broad class of precision piloted flight tasks. Evaluation procedures derivable from these methods include the study of task interference effects and sensitivity analysis to determine the influence of visual limitations, control system lags or delays, and human controller remnant. Important as these applications are, they are not suitable for MIL-F-8785B inclusion since the problems studied are usually highly specialized to a particular aircraft and flight mission.

The success of the step target tracking prediction method allows the following suggestions for tracking performance specification. For a specification to be a useful, discriminating, and fair criterion for tactical aircraft procurement, the following items must be satisfied:

1) The specification item must be numerical.
2) The specification item must correlate with pilot comments and pilot ratings.
3) The specification item must be easily measured in flight test or flight simulation.

4) The specification item must be reliably predictable by analytical means for use in early design and development evaluation.

5) The method that predicts the specification item must be applicable in a completely standardized form that evaluates the most general models of the candidate aircraft available.

6) The specification item must be valid for all current acceptable aircraft, and must exclude poor or unacceptable aircraft.

Unfortunately, these six requirements for military specification criteria have not all been met by any steady-state approach to the precision tracking problem. However, the transient method of step target tracking potentially satisfies these items. In particular, the step target method has the following characteristics that correspond to the requirements listed above:

1) The step target method is based on the numerical measures of rms tracking error and time-on-target as shown in Figure 158.

2) The two measures correspond with pilot comments in the following way:

rms tracking error	-	quickness of response and overshoot characteristics
time-on-target	-	steadiness on target and precision tracking characteristics

In addition, these two measures strongly correlate with pilot ratings obtained by Neal and Smith.

3) The use of step target tracking is already an established flight test procedure. It is completely standardized and easily tested.

4) The step target response is easily predicted for longitudinal step target tracking, and the extension to multiaxis target tracking is straightforward.

5) The method can be used with all representations of candidate aircraft from linear to full nonlinear equations.

6) The method clearly establishes performance boundaries for the Neal-Smith and F-5E aircraft. The only remaining requirement for MIL-F-8785B inclusion is further validation by current advanced tactical aircraft.

SECTION VII

PREDICTION OF PILOT RESERVE ATTENTION CAPACITY

Section VI demonstrated that pilot ratings and pilot comments obtained during an in-flight simulation of longitudinal flying qualities could be acccunted for by means of two performance statistics that are easily predicted using the time-varying capabilities of the Urgency Decision Pilot Model. Since pilot ratings are thought to reflect pilot workload as well as performance, this correlation of pilot ratings with rms tracking error and time-on-target raises two questions:

1) Do multi-dimensional performance measures inherently contain measures of pilot workload?

2) What is pilot workload, and can it be directly predicted using the Urgency Decision Pilot Model?

A conjecture concerning the first question will be presented at the end of this Section. An analysis presented there will show that the term "pilot workload" covers a number of separate aspects of flying qualities that may or may not be related to one another. One of these interpretations of pilot workload, reserve attention capacity, is an important and much neglected area of flying qualities analysis. A general method for predicting this reserve attention workload measure, and a demonstration of how it is employed for the F-5E aircraft dynamics, are the main subjects for this Section.

A. SIDE TASKS AND PILOT RESERVE ATTENTION

The term "side task" has already been introduced in Section III D where it was defined to be "a component task whose performance is not measured or optimized by an EVALUATION requirement." A side task consistent with this definition was analyzed in the target tracking problem presented in Section IV F in which the simulation pilot was given a task of tapping an electrode strapped to his leg whenever he felt he had the opportunity. The counting rate for this task was intended to measure the extent to which the pilot was necessarily occupied with the main target tracking tasks. A generalization of this method will be presented next.

Depending on the particular TASK, the pilot may have some capability for dealing with other chores or emergencies that may intrude. These intrusions are almost always eliminated in simulation studies, but represent frequent occurrences in actual flight experience. For this reason, such considerations are important in the evaluation of flying qualities. Ideally, during a critical flight phase such as landing, the pilot would be capable of dealing with tasks other than tracking, such as communications, instrument scans, or even emergency procedures.

By postulating that these additional task intrusions can be modeled or simulated by using specific side tasks such as electrode tapping, the sensitivity of a particular aircraft mission to attention diversion can be assessed. Thus the side task can provide information about the performance capability in the <u>other</u> tasks. These considerations motivate the following definition:

> <u>Pilot Reserve Attention Capacity</u> is defined to be the percentage of time that a pilot can be diverted from a specified TASK by a specified side task and still maintain acceptable performance of the TASK in terms of the EVALUATION.

It is necessary to consider how a given side task can be used to produce quantitative measures of performance in order to develop a standardized approach to using side tasks for measuring or predicting pilot reserve attention capacity. The following Subsections will present these methods along with a classification of side tasks and an analysis of the relationship of pilot reserve attention to pilot workload.

B. PREDICTION OF PILOT RESERVE ATTENTION CAPACITY FOR CONSTANT URGENCY SIDE TASKS

The simplest side task to be considered is represented by attention diversion. In the Urgency Decision Pilot Model this is represented by a constant urgency U_{ST} with a minimum dwell time enforced. It will be shown that such a side task model covers a large number of real flight task instrusions, and is a reasonable approximation to many more. Thus, the following presentation of a prediction method based on this simple side task model has broad applicability to flying qualities analysis.

There are two quantities that must be defined in order to present the data obtained using the side task model. The first is <u>tracking task degradation.</u> This quantity, $\Delta\epsilon$, is defined to be the percentage of tracking error increase over the

optimum tracking error with no side task for a given value of side task urgency U_{ST}. Associated with this degradation is the amount of time the model is diverted to the side task. This percentage represents how much attention is associated with the side task and is called the reserve attention, RA.

These two quantities, tracking degradation $\Delta\epsilon$, and reserve attention RA, are monotonically increasing functions of the single variable U_{ST}, and would qualitatively resemble the examples shown in Figures 179 and 180.

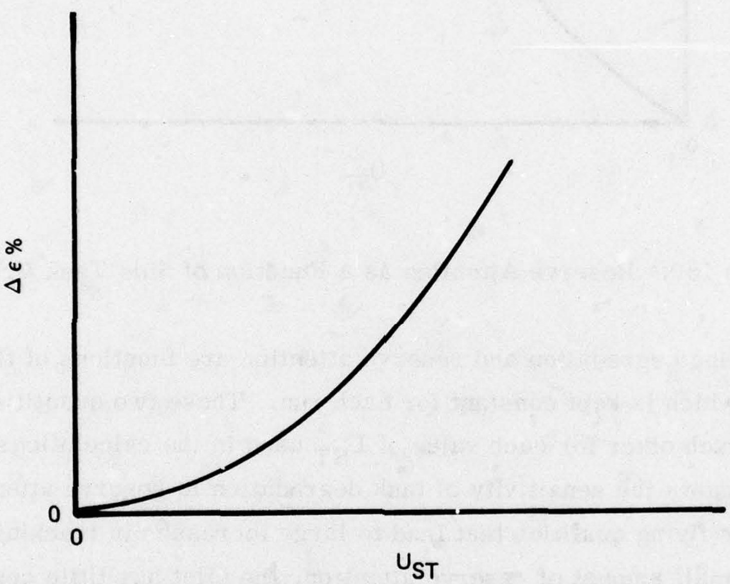

Figure 179. Tracking Degradation as a Function of Side Task Urgency

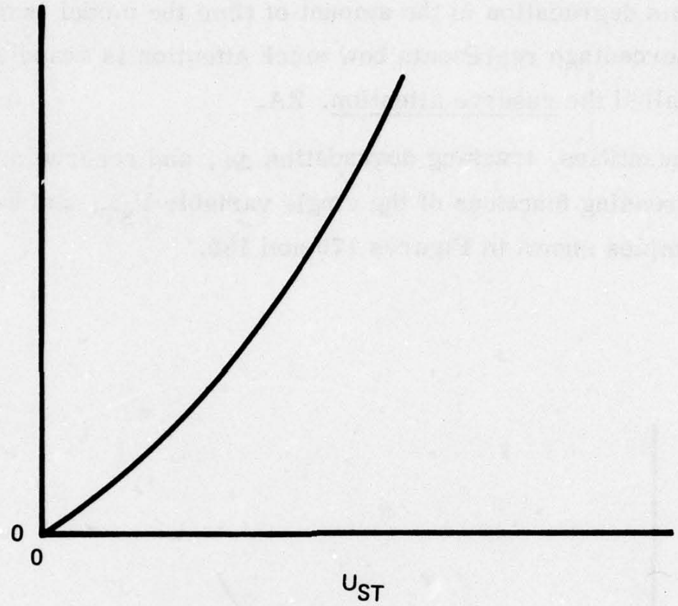

Figure 180. Reserve Attention as a Function of Side Task Urgency

Both tracking degradation and reserve attention are functions of the side task urgency, U_{ST}, which is kept constant for each run. These two quantities can be plotted against each other for each value of U_{ST} used in the calculations. This results in a graph that shows the sensitivity of task degradation to reserve attention capacity. If an aircraft has flying qualities that lead to large increases in tracking task degradation for only a small amount of reserve attention, the pilot has little opportunity to deal with additional task intrusions beyond the main TASK. This means that his workload for the given TASK is high. On the other hand, if a large amount of reserve attention is available with small tracking degradation, the workload level is low. It should be carefully noted that this interpretation is in fact a definition of pilot workload, and that this definition may or may not correlate with other commonly used workload interpretations. This will be discussed later in Subsection E.

The regions of high and low workload are thus predictable in terms of the tracking degradation and reserve attention as shown in Figure 181. In practice, suitable values of U_{ST} can be easily found that give sufficient resolution in $\Delta\epsilon$ and RA.

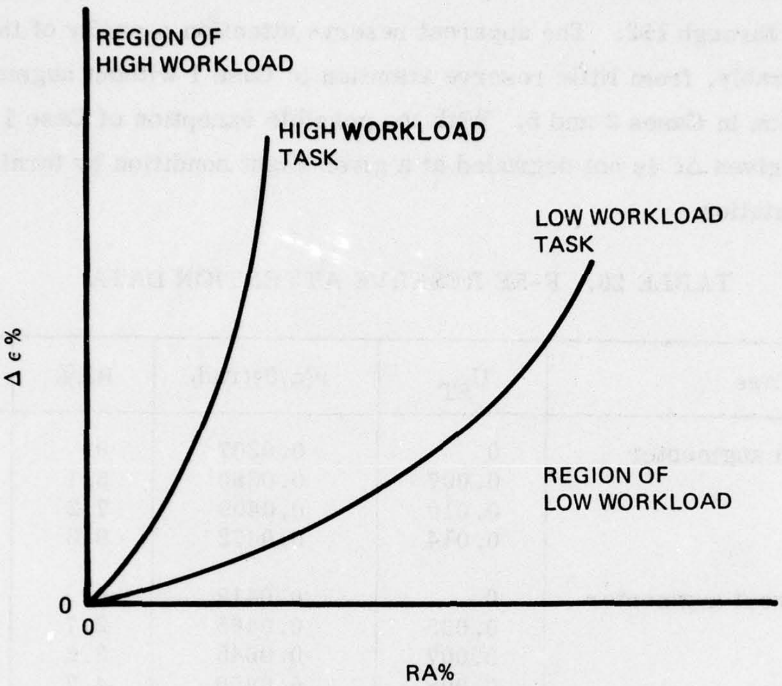

Figure 181. *High and Low Pilot Workload as Functions of Tracking Degradation and Reserve Attention*

C. RESERVE ATTENTION CAPACITY DURING ATTITUDE STABILIZATION IN TURBULENCE

The method of using a constant urgency side task to determine reserve attention capacity will now be demonstrated by evaluating the pilot workload of the F-5E aircraft during the attitude stabilization in turbulence task that was reported in Section V B. In contrast to the target tracking problem presented in Section IV F, the attitude stabilization TASK involves tracking errors of a high frequency nature. For such high frequency TASKS, there is little reserve attention, and the problem is one of studying the sensitivity of tracking degradation for small percentages of reserve attention. For this reason, the coefficients of the optimum model can be used without re-optimizing for each value of the constant side task urgency U_{ST}. A minimum side task dwell time of 0.3 second was enforced. The model "performs" the side task only when the component task urgencies are less than U_{ST}. The side task is incorporated into the pilot model as shown in Figure 9.

The reserve attention and radial tracking error data for the eleven usable F-5E cases presented in Section V are given in Table 26. Model data was obtained from

five-minute runs. The corresponding reserve attention sensitivity graphs are shown in Figures 182 through 192. The apparent reserve attention capacity of these cases varies considerably, from little reserve attention in Case 1 without augmenter to much reserve attention in Cases 2 and 5. With the possible exception of Case 1, the reserve attention for a given $\Delta\epsilon$ is not degraded at a given flight condition by turning off the control augmentation.

TABLE 26. F-5E RESERVE ATTENTION DATA

Case		U_{ST}	$r(\phi,\theta)$(rad)	RA%	$\Delta r(\phi,\theta)$%
1	With augmenter	0	0.0307	0	0
		0.007	0.0380	5.1	23.8
		0.010	0.0409	7.2	33.6
		0.014	0.0472	9.3	53.8
1	Without augmenter	0	0.0419	0	0
		0.005	0.0465	2.7	10.9
		0.007	0.0645	3.2	53.9
		0.008	0.0659	4.7	57.3
2	With augmenter	0	0.0384	0	0
		0.01	0.0403	8.4	4.9
		0.014	0.0422	11.5	9.9
		0.02	0.0461	16.1	20.0
		0.03	0.0662	23.1	72.4
2	Without augmenter	0	0.0454	0	0
		0.01	0.0489	7.7	7.7
		0.014	0.0509	9.9	12.1
		0.02	0.0526	13.4	15.6
		0.03	0.0616	19.5	35.9
3	With augmenter	0	0.0255	0	0
		0.007	0.0280	5.1	9.4
		0.01	0.0330	8.1	32.4
		0.014	0.0498	8.7	95.3
4	With augmenter	0	0.0290	0	0
		0.007	0.0309	5.1	6.6
		0.01	0.0319	8.2	10.0
		0.014	0.0422	11.3	45.5
5	With augmenter	0	0.0329	0	0
		0.006	0.0349	5.9	5.8
		0.01	0.0373	10.3	13.4
		0.014	0.0385	12.6	17.0
		0.02	0.0415	15.9	26.1

TABLE 26. F-5E RESERVE ATTENTION DATA (CONCLUDED)

Case		U_{ST}	$r(\phi,\theta)$(rad)	RA%	$\Delta r(\phi,\theta)$%
5	Without augmenter	0	0.0447	0	0
		0.007	0.0468	3.4	4.7
		0.014	0.0488	8.4	9.2
		0.02	0.0553	13.5	23.7
8	With augmenter	0	0.0273	0	0
		0.01	0.0358	7.40	3.1
		0.016	0.0432	11.9	58.2
9	With augmenter	0	0.0311	0	0
		0.007	0.0348	5.5	11.9
		0.01	0.0385	9.0	23.8
		0.012	0.0402	9.9	29.3
9	Without augmenter	0	0.0466	0	0
		0.01	0.0510	6.1	9.4
		0.02	0.0569	14.3	22.1
		0.03	0.0766	18.1	64.4

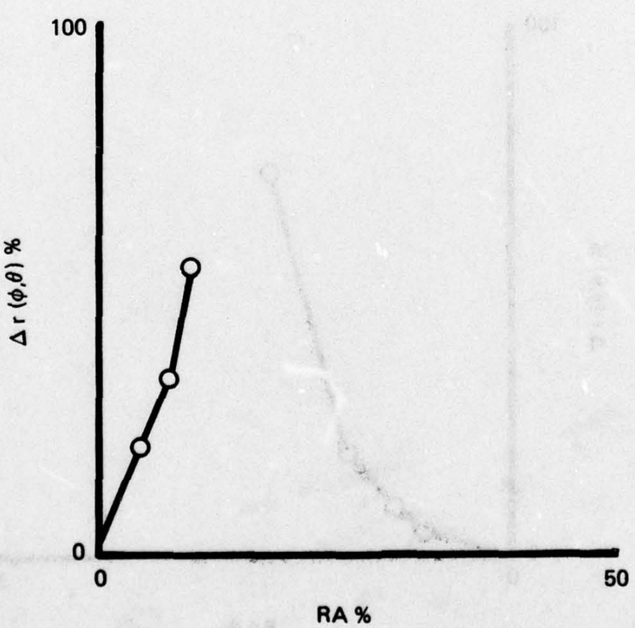

Figure 182. Reserve Attention for F-5E Case 1 with Augmenter

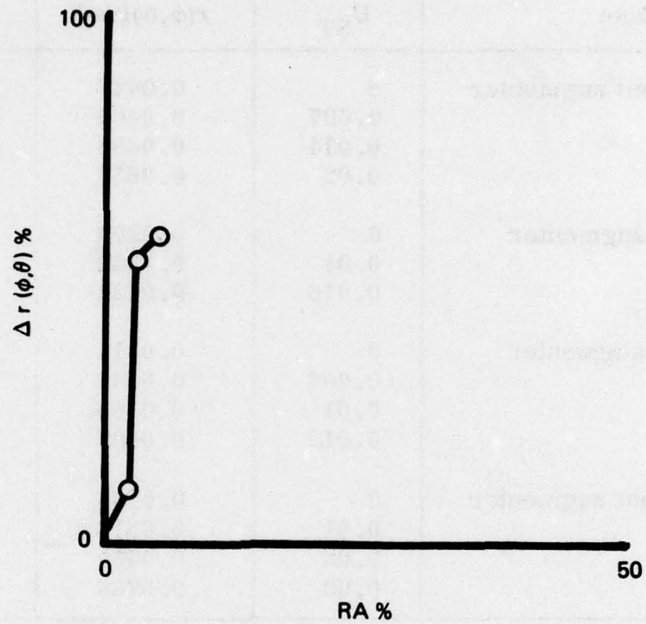

Figure 183. Reserve Attention for F-5E Case 1 Without Augmenter

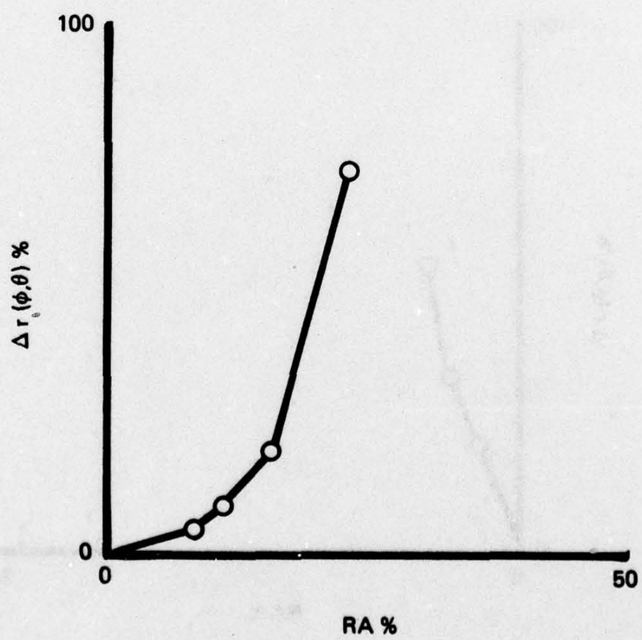

Figure 184. Reserve Attention for F-5E Case 2 With Augmenter

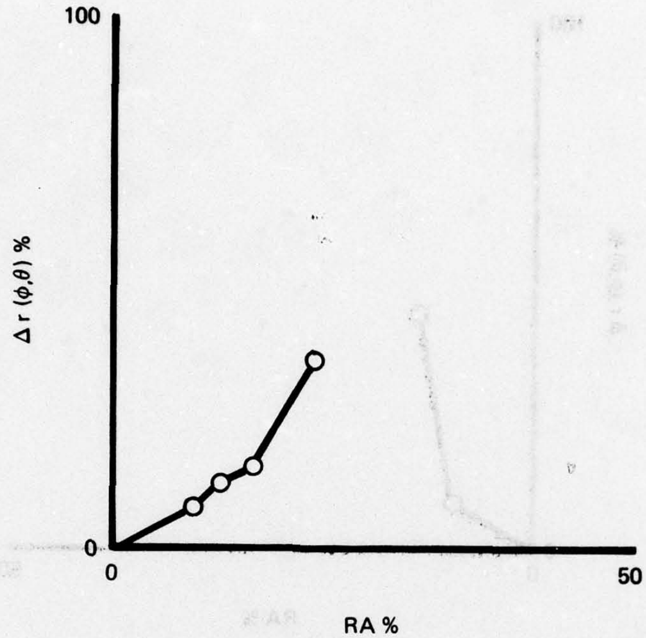

Figure 185. Reserve Attention for F-5E Case 2 Without Augmenter

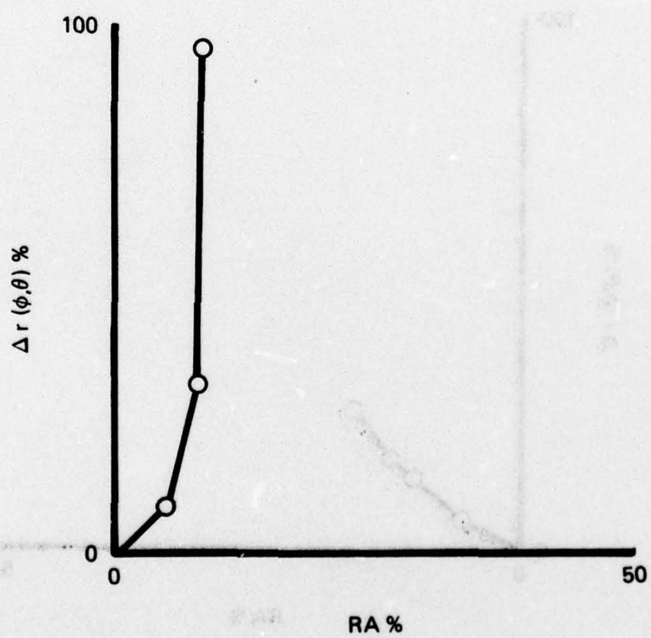

Figure 186. Reserve Attention for F-5E Case 3 With Augmenter

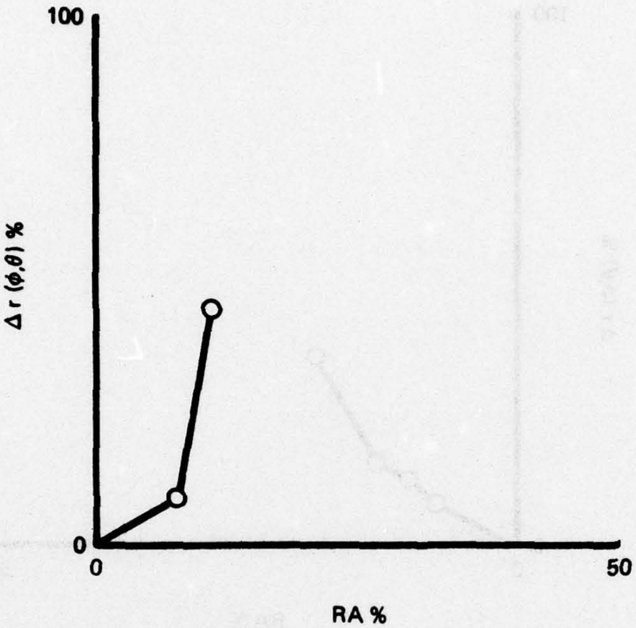

Figure 187. Reserve Attention for F-5E Case 4 With Augmenter

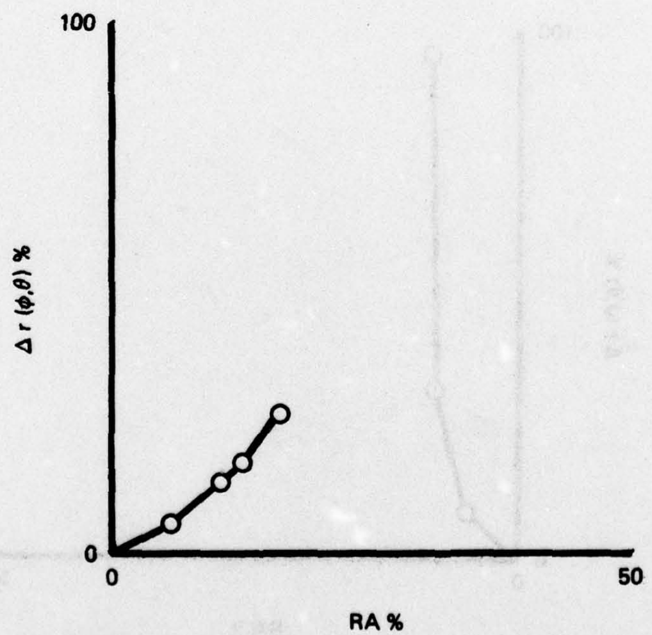

Figure 188. Reserve Attention for F-5E Case 5 With Augmenter

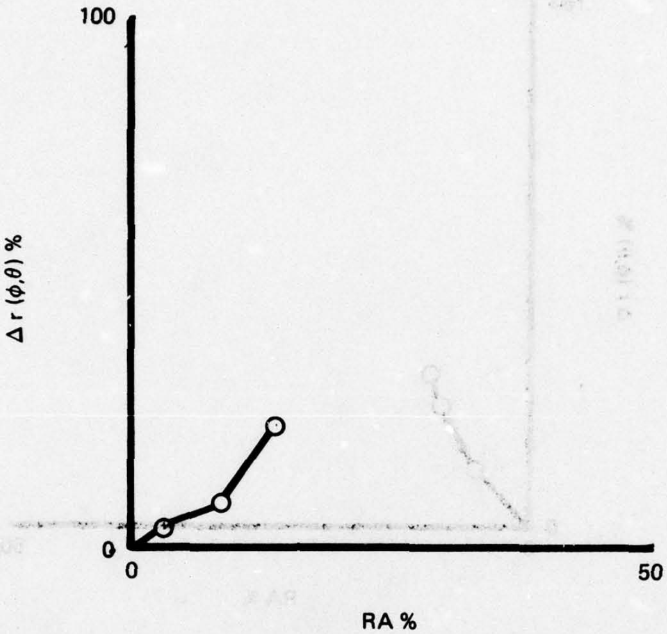

Figure 189. Reserve Attention for F-5E Case 5 Without Augmenter

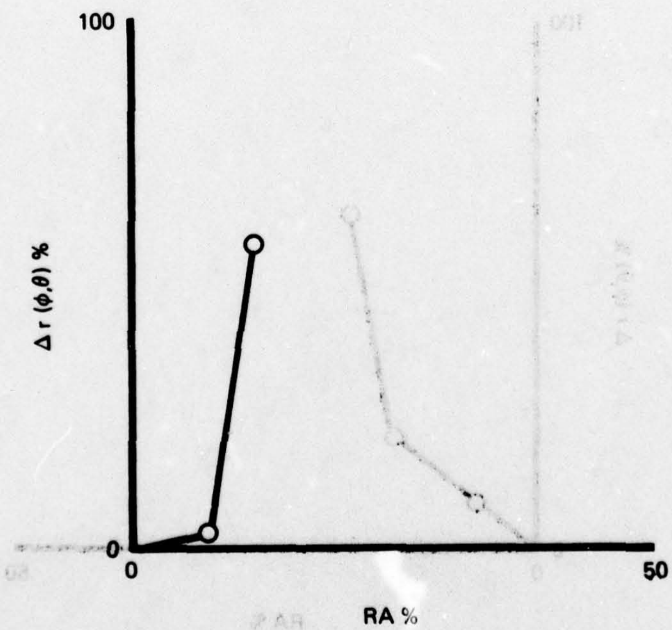

Figure 190. Reserve Attention for F-5E Case 8 With Augmenter

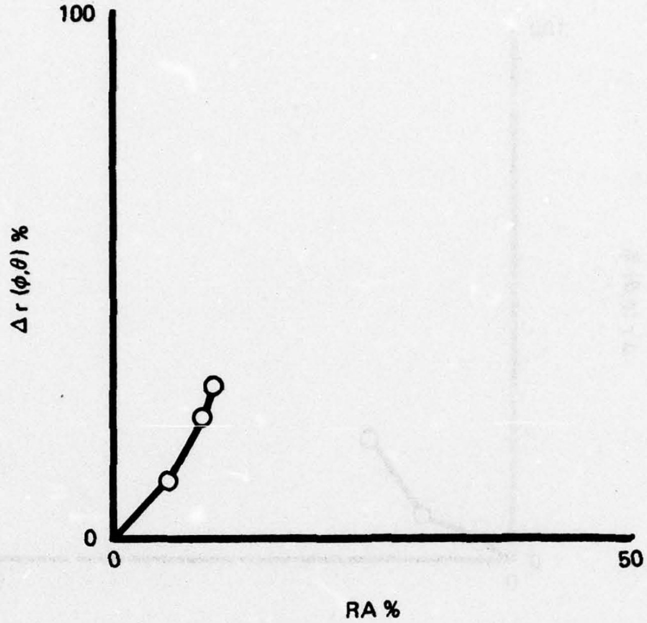

Figure 191. Reserve Attention for F-5E Case 9 With Augmenter

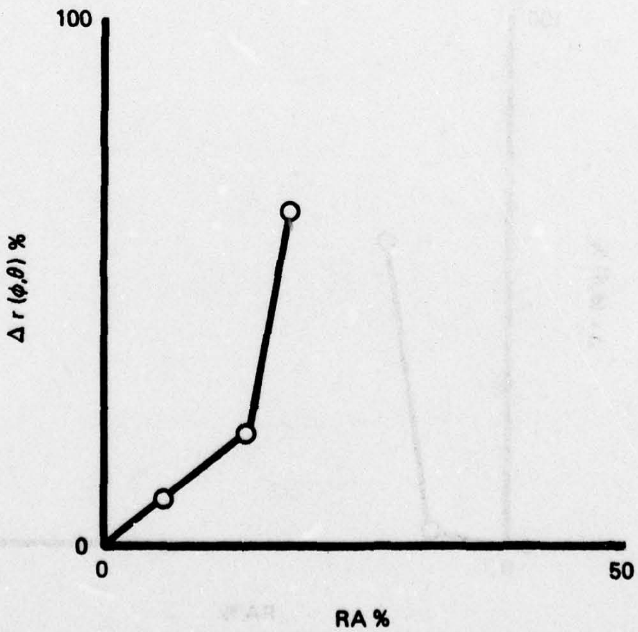

Figure 192. Reserve Attention for F-5E Case 9 Without Augmenter

It is important to keep in mind that the reserve attention capacity represented in Figures 182-192 evaluates a TASK that consists of:

1) Lateral attitude stabilization
2) Longitudinal attitude stabilization

so that the side task used in the EVALUATION plays no part in the TASK description. In other words, the use of the side task in the model analysis is an artifice to evaluate the capacity of the pilot to assume greater task loading <u>should it occur</u>. The exclusive attention allocation of the two-axis TASK implies that the dwell fraction of at least one component task is greater than or equal to one-half. The side task increases the total attention diversion from each task so that the values of RA shown in Figures 182-192 represent total diversions of greater than 50 percent on at least one of the component tasks in every case. It is tempting to evaluate this total attention diversion capacity of each component task by applying the constant urgency side task method to single-axis tasks. This is unrealistic for the following reasons:

1) In an actual flight situation, component tasks are allocated attention according to the urgency demands of all component tasks in the TASK.
2) Task interference effects are of importance in the evaluation of pilot reserve attention capacity.
3) Diversion of the attention from one component task to the side task influences the relative urgency state of the other component task.

In spite of these objections to evaluating the pilot reserve attention capacity in single-axis tasks, an attempt was made to do just this using the data of References 17 and 18 which report pilot ratings for attitude stabilization in turbulence. All configurations in these reports were examined, and little correlation was found between the pilot ratings and the reserve attention capacity. Since the intent of these references was to obtain pilot ratings that reflected workload, the results of these calculations appeared paradoxical. Further investigation revealed that the pilot ratings of References 17 and 18 are strongly correlated with performance normalized by the apparent lateral ride qualities. This demonstrates influence of ride qualities on pilot ratings; an analysis of this data has been included in Appendix A.

The above discussion has depended upon using side tasks that can be modeled as attention diversions based on constant urgency. An analysis of possible side tasks will be presented next to show how this assumption relates to other side tasks.

D. <u>SELECTION OF CANDIDATE SIDE TASKS FOR RESERVE ATTENTION PREDICTION</u>

The last Subsection presented a method for predicting the reserve attention capacity of a pilot for a given TASK by using a fictive constant urgency side task in the Urgency Decision Pilot Model. This side task had the following features:

1) The main task components were interrupted only when all of their associated urgencies were least, i.e. when they could best afford interruption.

2) Other than the enforced minimum dwell time of 0.3 second, no descriptive information of the side task was required.

3) The side task did not depend in any way on the TASK.

4) The side task did not alter the TASK description, or the adjustment procedures for the model.

5) The side task urgency function constants U_{ST} were not used in the analysis other than as a means of obtaining task degradation as a function of reserve attention.

6) The side task was completely unbiased toward any aircraft or TASK.

For any method of assessing flying qualities that depends on the use of urgency-based analytical or experimental test side tasks, the above six conditions must be met. The objective now is to determine whether other side tasks also may qualify, and if so, what advantages they may have.

As explained above, the constant urgency side task led to task interruptions that occurred at the best times in terms of the component task urgencies. Such tasks that divert attention according to an urgency measure that competes with the other urgency functions are called <u>housekeeping side tasks</u> since they are performed whenever it is most convenient to do so. On the other hand, tasks that instantly interrupt on the basis of probabilistic or other models are called <u>emergency side tasks</u>. All side tasks can be thought of as falling into one of these two categories, and depending on the TASK, one or the other may be more appropriate: navigation and communication intrusions into a landing TASK may be best studied as housekeeping side tasks in contrast to emergency side tasks that represent procedures resulting from crowded airspace or equipment failure.

If U_{MT} represents the greatest of the main component task urgencies at any given time, the logic associated with the two categories of side tasks can be represented as shown in Figure 193. A fixed minimum side task dwell time should be imposed in conjunction with these tests. Side task urgency U_{ST} is constant in both cases.

ATTENTION SHIFT TEST	EMERGENCY SIDE TASK	HOUSEKEEPING SIDE TASK
TO SIDE TASK	PROBABILITY CONDITION MET	$U_{ST} \geqslant U_{MT}$
TO MAIN TASK	FIXED DWELL TIME ON SIDE TASK OR PROBABILITY CONDITION MET	$U_{ST} < U_{MT}$

Figure 193. Attention Allocation Logic for Side Tasks

Emergency Side Task Models

The emergency side task interrupts the main tasks on the basis of conditions that do not involve task urgencies, and any desired statistical distribution of side task events can be arranged easily. The simplest of these is by use of a uniformly distributed random number sequence. The side task is initiated when this random number generated every iteration during the model computation is greater than some assigned value. The side task activity can then either be maintained for a fixed dwell time, or terminated by another probability model based on another random number.

A limited number of calculations using the fixed-dwell emergency model were made for the artificial problem of single-axis bank angle stabilization in turbulence. Comparison showed that for a given reserve attention capacity, the task degradation was lower for the emergency side task than for the constant urgency housekeeping side task. This appears to be opposite to the result the reader may anticipate, but the high frequency nature of the problem appears to allow error rates to build during the mean dwell times of the housekeeping side task which exceed the fixed dwell time of the emergency side task. No data has been computed for the full two-axis TASK.

Housekeeping Side Task Models

As stated above, housekeeping side tasks are modeled by the use of urgency functions to determine the initiation of side task activity. Section VII B has shown how pilot reserve attention capacity can be evaluated by plotting task degradation versus reserve attention. Although this discussion was restricted to constant urgency side tasks, the same method can be employed for housekeeping side tasks that are modeled by other urgency functions. A partial classification of housekeeping side tasks is given in Figure 194, along with postulated structures for the urgency functions.

TASK INTRUSION	HOUSEKEEPING SIDE TASK MODEL URGENCY FUNCTION STRUCTURE
I TRACKING 1. COMMAND 2. "CRITICAL TASK"	U = U (TRACKING ERROR AND ERROR RATE)
II MONITORING 1. INSTRUMENT SCAN 2. EXTERNAL SURVEILLANCE	U = U (TIME SINCE LAST OBSERVATION)
III DISCRETE-RESPONSE 1. SELF-INITIATED 2. AUDITORY RESPONSE 3. MANUAL RESPONSE	U = U (PRESENCE OF STIMULUS)

Figure 194. Classification of Housekeeping Side Tasks

A tracking housekeeping side task was employed in the study of Wanamaker and Sower that was discussed in Section IV E. This side task consisted of maintaining control of unstable dynamics. An ingenious method developed by H.R. Jex, References 19 and 20, employs unstable "critical tasks" in the following way: the instability of the side task is increased to the point at which the pilot cannot maintain control over both the side task and the main dynamics being evaluated. The side task instability parameter at that point is the measure of main task difficulty. This technique has been mainly an experimental method, but the Urgency Decision Pilot Model easily predicts the performance of the critical task. This is presented in Appendix B.

No data exists on the use of the urgency approach to instrument monitoring and surveillance tasks; however, the use of urgency functions that reflect the time since last observation appear to be possible candidates. If this is so, much data that has been obtained experimentally by the use of oculometers should lead to the necessary calibrations of these functions.

Discrete-response self-initiated side tasks have been presented in Section IV F, where the electrode tapping task was not initiated by a cue to the pilot. The data presented in that Section indicates that the assumed model of constant urgency is appropriate for this task, and by extension to similar self-initiated tasks. This is the basis of the proposed method of evaluating pilot reserve attention presented in Section VII B. Much data has been obtained for auditory and manual response initiated by auditory and visual stimuli. This data would also be suitable for the validation and calibration of the postulated urgency function.

Since many non-emergency situations can be performed with considerable discretion by the pilot, they can be thought of as self-initiated discrete-response housekeeping side tasks. This is the reason why the constant urgency side task has been postulated as a useful measure of pilot reserve attention capacity. The possible relation of reserve attention capacity to pilot workload will be discussed next.

E. INTERPRETATIONS OF PILOT WORKLOAD

Although the concept of pilot workload has been explicitly mentioned only in this Section, questions concerning it have been latent in many earlier discussion in this report. It is the objective here to present an interpretation of the workload concept that is consistent with the results presented above.

Since pilot ratings are intended to reflect both performance and workload, a comparison of different pilot rating scales reveals much about the role of workload in pilot ratings. This is analyzed in Reference 20, and will not be discussed here.

The aspect of pilot workload to be discussed is not comparative, but definitional. It is clear that reserve attention capacity measured by using one side task *may not correspond* with the reserve attention capacity measured by means of another. This illustrates that workload postulated as reserve attention depends on the defining side task.

It is a contention of the authors that this definitional aspect of pilot workload should be made clear with respect to all instances of the workload concept, and that the failure for established workload measures to be adopted derives from inadequate workload definitions. In particular, workload is frequently postulated to be, or be measured by, the following items shown in Figure 195.

1) Cooper - Harper pilot rating "demands on the pilot"
2) The extent of assumed pilot lead compensation, "Paper Pilot"
3) Pilot gain and phase margins
4) Aircraft total angular rate
5) Critical Task "lambda" constant, Appendix B
6) Pilot compensation sensitivities
7) Reserve attention capacity measures

Figure 195. Interpretations of Pilot Workload

Available data indicates that all of these approaches to pilot workload measurement have demonstrated success in particular analyses. For this reason, each must be regarded as having importance to certain areas of flying qualities analysis and specification. The difficulty appears to come about when attempts are made to correlate the workload measured by one approach with workload measured by another. For example, it was stated earlier that the pilot reserve attention capacity predicted from the attitude stabilization in turbulence data of References 17 and 18 did not correlate with the pilot ratings in those reports, and Appendix A showed that those ratings were based on performance in terms of tracking error and ride qualities. This correlation of the turbulence pilot ratings with tracking error and ride qualities does not mean that the turbulence pilot ratings are not workload; it means that the workload that the pilots reported is measured by tracking error and ride acceleration. Similarly, the correlation of the Neal - Smith pilot ratings presented in Section VI with a two-dimensional performance index indicates that the workload levels identified by the pilots in deciding upon a given rating is already inherent in these two performance ratings.

On the basis of these observations, the following suggestions for future application of workload measurement are offered:

1) The Cooper - Harper pilot opinion rating must be the primary flying qualities evaluation parameter.

2) Items 2) through 7) of Figure 195 are relevant to the Cooper - Harper rating only if the evaluation task tests these aspects of pilot ratings.

3) When testing or flying qualities analysis involves specific workload concepts, they should be precisely defined in a manner that is both measurable and predictable.

4) Correlations among the items of Figure 195 should not be assumed unless demonstrated for the particular problem.

F. CORRELATION OF PILOT WORKLOAD AND PILOT RATINGS WITH PERFORMANCE

In view of the success of correlating the Neal - Smith pilot rating data with the two performance measures, rms tracking error and time-on-target, in Section VI, the following conjecture is offered for the prediction of pilot ratings for precision flying qualities. Also see Appendix B.

Conjecture:

I Pilot workload can be correlated with performance measures, hence

II Pilot ratings for precision flight TASKS can always be correlated with regions in a multi-dimensional space parameterized by measurable and predictable performance measures.

G. SPECIFICATION OF PILOT RESERVE ATTENTION

As shown above, reserve attention capacity is important for the pilot during critical tasks where flight safety is a main issue, such as landing and in-flight refueling. The analysis presented in Section VII D indicates that a large number of pilot task intrusions can be represented by a constant urgency housekeeping side task.

The method of predicting pilot reserve attention with respect to constant urgency side tasks is generally applicable to any precision TASK, without modification. With the exception of items 4 and 6 the method satisfies all of the characteristics that are necessary for a MIL-F-8785B specification item. In particular:

1) The specification item would specify the percent TASK degradation for a given reserve attention capacity.
2) The item would be specifically simulated or flight tested to obtain pilot ratings and comments that reflect pilot reserve attention capacity.
3) The reserve attention capacity can be measured by the use of artificial side tasks as well as by use of actual or simulated typical task intrusions.
4) The prediction method for pilot reserve attention capacity must be validated, using the methods indicated in 2) and 3).
5) The method is generally applicable to all aircraft models and flight TASKS.
6) Data for a large number of current acceptable and unacceptable aircraft must be obtained and correlated with data predicted by the reserve attention capacity prediction method.

SECTION VIII

SUMMARY AND RECOMMENDATIONS

The study documented in this report has demonstrated a new and comprehensive approach to the prediction, evaluation, and specification of closed loop multiaxis flying qualities. The methods set forth allow the study of fully general aircraft models in the analysis of continuous and discrete multiaxis piloted maneuvers. Many demonstrations of these methods have been presented, and new areas of promising research and applications have been suggested. Briefly, these are as follows:

Classification of Precision Piloted Tasks

In order to present a comprehensive approach to closed loop multiaxis flying qualities, it is necessary to develop a classification of all such piloted activities. This is accomplished in Section II where precision piloted tasks are classified in terms of

- TASK - what the pilot is told to do,
- CONTROL - how the pilot does it, and
- EVALUATION - the criteria by which the results are judged.

A generic classification of possible TASK, CONTROL, and EVALUATION items is presented in Figure 2, and a survey of examples covered in this report is presented in Figure 3.

The Urgency Decision Pilot Model

A comprehensive approach to the analysis of flying qualities problems classified in the above manner requires a very general representation of the aircraft, the pilot, and the piloted tasks. This is achieved by using the Urgency Decision Pilot Model developed by Northrop in 1966, Reference 10. This model is exercised in the time domain by time-history simulation, and pilot attention allocation is assigned on the basis of "urgency functions" which determine where attention is needed most.

This time-domain urgency decision pilot - aircraft model presented in Section III enjoys the following features:

- The model is extremely easy to program and append to existing simulations.
- All nonlinearities and time-varying quantities can be modeled directly without resort to equivalent linear models.
- The Urgency Decision Pilot Model will assign a specific CONTROL model for any combination of TASK and EVALUATION items classified in Figure 2.
- The model is validated for a large number of TASK and EVALUATION generic descriptions as shown in Figure 3.

This report contains a complete guide that will allow the reader to apply the model to a large number of flying qualities problems.

Prediction of Piloted Aircraft Performance

Section IV presents a number of validations of the model that Northrop reported over the last five years, in order to provide a clear picture of the comprehensive manner in which the Urgency Decision Pilot Model applies to the classified precision flight tasks. These demonstrations include the following items:

- F-5 and YF-17 attitude stabilization in turbulence.
- VTOL hover.
- Two-axis command tracking.
- Two-axis air-to-air target tracking with visual delays and side task.

Each of these studies considered numerous flying qualities aspects, and complete flight simulation validation data is presented.

Comparison of Gaussian and Non-Gaussian Turbulence Model Effects

Further applications were developed, analyzed, and validated using F-5E aircraft configurations at seven flight conditions. Nonlinear aircraft equations were used for these studies. Since the Urgency Decision Pilot Model accpets all system nonlinearities, it is completely suited to analyzing both nonlinear aircraft descriptions and non-Gaussian processes.

Non-Gaussian turbulence models are coming into wide use. Section V presents a validation of the model for the nonlinear F-5E aircraft description for attitude stabilization with the Reeves non-Gaussian turbulence model.

Effects of Control System Lags on Tracking Performance

Section V also contains an analysis of the performance degradation produced by hypothetical control system lags introduced into the F-5E validation aircraft models. This study demonstrates the usefulness of evaluating control system effects by means of the Urgency Decision Pilot Model. Since the model is validated for problems of this kind, this method may be used for the design and evaluation of flight control systems and flight simulations.

Specification of Flying Qualities by Means of Step Target Tracking

An important feature of the Urgency Decision Pilot Model is the ability to incorporate time-varying and discrete maneuvers. This is illustrated in Section VI where an analysis of tracking a step target is presented.

In tracking a longitudinal step target the pilot has to acquire the target by initiating a pull-up, followed by precision tracking for the allowed tracking time. The model performs these two maneuvers by changing its compensation during the five seconds of allotted tracking time. Tracking error, rms θ_e, and time-on-target statistics are then used to evaluate the flying qualities as follows:

- rms θ_e - evaluates initial response and overshoot characteristics
- time-on-target - evaluates steadiness on target

Predictions of these statistics for 42 Neal - Smith NT-33 aircraft configurations showed that pilot ratings correlate with regions of an rms θ_e versus time-on-target plot. This is shown in Figure 158. Figure 178 presents similar data for the F-5E.

The universal and unbiased nature of this method is discussed in Section VI F where it is shown that the boundaries presented in Figure 158 are reasonable candidates for inclusion in MIL-F-8785B. The following must be accomplished to validate such an item:

- The method must be validated by correlating model predictions with current aircraft experience.
- The method must be validated by correlating flight test and flight simulation data with the boundaries suggested by the Neal-Smith data, Figure 158.
- The method must be extended and validated for lateral-directional step target tracking.

An analysis presented at the end of Section VII indicates that flying qualities boundaries may always be derived by correlating multi-dimensional performance measures with pilot ratings.

Prediction and Specification of Pilot Reserve Attention Capacity

In addition to predicting performance, the Urgency Decision Pilot Model can also be used to predict the pilot reserve attention capacity of a pilot for any given flight task. The method uses a hypothetical side task of constant attention demand to determine the sensitivity of the main task performance to attention diversion. This method is presented in Section VII along with a definition and classification of evaluation side tasks and pilot workload measures. Calculations for the F-5E configurations used for validation are presented. It is also shown that this important aspect of flying qualities can be specified in a manner that meets the requirements for inclusion in military flying qualities specifications, as set forth in Section VI F.

Computer Program and User Guide

The methods presented in this report are only useful to the reader if they can be easily learned and adapted to specific problems. To assist in this, a computer program is available to qualified requesters from AFFDL/FGC, Wright-Patterson AFB, Ohio 45433. A complete user guide is presented in Appendix C. There are three uses for the computer program:

- To serve as an example of one possible implementation of the TASK-CONTROL-EVALUATION approach to piloted aircraft precision task analysis.
- To assist those who may wish to modify the existing program for some particular problem analysis.
- To serve as a guide for those who may wish to use the program for immediate problem application or to gain some experience in the analysis methods presented in this report.

REFERENCES

1. Onstott, E.D., Multi-Axis Pilot-Vehicle Dynamics, Proceedings of the Tenth Annual Conference on Manual Control, Wright-Patterson Air Force Base, Ohio, April 1974.

2. Onstott, E.D., Validation of the Northrop Multi-Axis Pilot Model, NOR 74-61, Northrop Corporation, Hawthorne, California, March 1975.

3. Onstott, E.D., Task Interference in Multi-Axis Aircraft Stabilization, Proceedings of the Twelfth Annual Conference on Manual Control, University of Illinois, May 1976.

4. McRuer, D.T., and Krendel, E.S., Mathematical Models of Human Pilot Behavior, AGARDograph No. 188, Advisory Group for Aerospace Research and Development, January 1974.

5. Kleinman, D.L., and Baron, S., Manned Vehicle Systems Analysis by Means of Modern Control Theory, NASA CR-1753, National Aeronautics and Space Administration, Washington, D.C., June 1971.

6. Smith, R.H., A Theory for Handling Qualities with Applications to MIL-F-8785B, AFFDL-TR-75-119, Air Force Flight Dynamics Laboratory, Wright-Patterson Air Force Base, Ohio, October 1976.

7. Young, L.R., Research on Biophysical Evaluation of the Human Vestibular System, NASA CR-140063, National Aeronautics and Space Administration, Washington, D.C., August 1974.

8. Wanamaker, J.E., and Sower, W.A., Extension of Pilot Describing Functions to Multiple Compensatory Tracking Tasks, Air Force Institute of Technology Thesis GE/EE/69-18, Dayton, Ohio, 1969.

9. Rankine, R.R., The Effects of Aircraft Dynamics and Pilot Performance on Tactical Weapon Delivery Accuracy, UCLA-ENG-7085, University of California at Los Angeles, November 1970.

10. Onstott, E.D., and Sinacori, J.B., Sampled Data Pilot Behavior During VTOL Hover Simulation, NOR 67-13, Northrop Corporation, Hawthorne, California, January 1967.

11. Queijo, M.J., and Riley, D.R., Fixed-Base Simulator Study of the Effect of Time Delays in Visual Cues on Pilot Tracking Performance, NASA TN D-8001, National Aeronautics and Space Administration, Washington, D.C., October 1975.

12. Chalk, C.R., Woodcock, R.J., et al, Background and User Guide for MIL-F-8785B (ASG), Military Specification -- Flying Qualities of Piloted Airplanes, AFFDL-TR-69-72, Air Force Flight Dynamics Laboratory, Wright-Patterson Air Force Base, Ohio, August 1969.

13. Reeves, P.M., et al, Development and Application of a Non-Gaussian Atmospheric Turbulence Model for Use in Flight Simulators, NASA CR-2451, National Aeronautics and Space Administration, Washington, D.C., September 1974.

14. Anonymous, Military Specification, Flying Qualities of Piloted Airplanes, MIL-F-8785B, August 1969.

15. Anderson, R.O., A New Approach to the Specification and Evaluation of Flying Qualities, AFFDL-TR-69-120, Air Force Flight Dynamics Laboratory, Wright-Patterson Air Force Base, Ohio, May 1970.

16. Neal, T.P., and Smith, R.E., An In-Flight Investigation to Develop Control System Design Criteria for Fighter Airplanes, Volumes I and II, AFFDL-TR-70-74, Air Force Flight Dynamics Laboratory, Wright-Patterson Air Force Base, Ohio, December 1970.

17. Onstott, E.D., and Salmon, E.P., Airplane Flying Qualities in Turbulence, AFFDL-TR-70-143, Air Force Flight Dynamics Laboratory, Wright Patterson Air Force Base, Ohio, February 1971.

18. Onstott, E.D., Salmon, E.P., and McCormick, R.L., Prediction and Evaluation of Flying Qualities in Turbulence, AFFDL-TR-71-162, Air Force Flight Dynamics Laboratory, Wright-Patterson Air Force Base, Ohio, February 1972.

19. Jex, H.R., McDonnell, J.D., and Phatak, A.V., A "Critical" Tracking Task for Man-Machine Research Related to the Operator's Effective Delay Time, Part I: Theory and Experiments with a First-Order Divergent Element, NASA CR-616, National Aeronautics and Space Administration, Washington, D.C., November 1966.

20. McDonnell, J.D., Pilot Rating Techniques for the Estimation and Evaluation of Handling Qualities, AFFDL-TR-68-76, Air Force Flight Dynamics Laboratory, Wright-Patterson Air Force Base, Ohio, December 1968.

21. Baxter, D.C., The Digital Simulation of Transfer Functions, Report MK-13, National Research Laboratories, Ottawa, Canada, April 1964.

APPENDIX A

INFLUENCE OF MOTION CUES ON PILOT RATINGS IN TURBULENCE

As indicated in Section VII C, the pilot rating data of References 17 and 18 are natural candidates for correlation with the method of pilot reserve attention. These ratings were obtained during an extensive moving-base flight simulation of F-5, A-7, and NT-33 aircraft configurations in simulated turbulence. The study was performed using either lateral-directional or longitudinal tasks independently. The pilots were instructed to hold trim attitude for varying levels of turbulence using an instrument display. Pilot ratings evaluated the simulator flight just completed in terms of how difficult the assigned control task was to carry out.

Recognizing that the pilots can only sense the attitude and acceleration response of the aircraft, the authors of References 17 and 18 reasoned that since the pilot does not directly know the turbulence intensity, he cannot estimate the normalized tracking performance. Thus his rating does not reflect performance, but workload: as the turbulence levels increase, the pilot ratings become worse, ranging from a 2 or 3 at low levels to an 8 or higher at severe gust intensity. Since these ratings were intended to reflect only pilot workload, and the data seemed consistent with this intention, the authors of this report attempted to correlate the reserve attention curves for these turbulence simulation data with the reported pilot ratings.

It turned out that good correlation is not possible. In the first place, the pilot workload reflected in the turbulence pilot ratings is of a different sort than attention loading. This is discussed in Section VII C. Secondly, the pilot ratings obtained in the simulations of attitude stabilization in turbulence turn out to be performance measures after all.

The frequent and wide use of the pilot rating data in References 17 and 18 has sometimes led to inconclusive or anomalous results. This appears to be the result of the performance nature of the pilot ratings. To help avoid further difficulties in using these data in the future, an analysis of the pilot rating data will be given here to demonstrate how motion cues or ride quality effects can influence pilot ratings.

First of all, notice that there are no obvious correlations between pilot ratings and performance in the reported data. Figure 196 reproduced from Reference 18 (Figure 31 in that report) shows a wide range of optimum pilot tracking errors for almost all of the pilot ratings. However, examination of the data for each configuration shows a steadily increasing pilot rating with turbulence level. By plotting pilot rating versus gust level, linear correlations can be seen, so that a linear relation between these two quantities can be postulated. All that is necessary to compare these linear relationships for various configurations is the slope of each line. These are just the average pilot ratings normalized for a nominal turbulence level of 10 ft/sec rms.

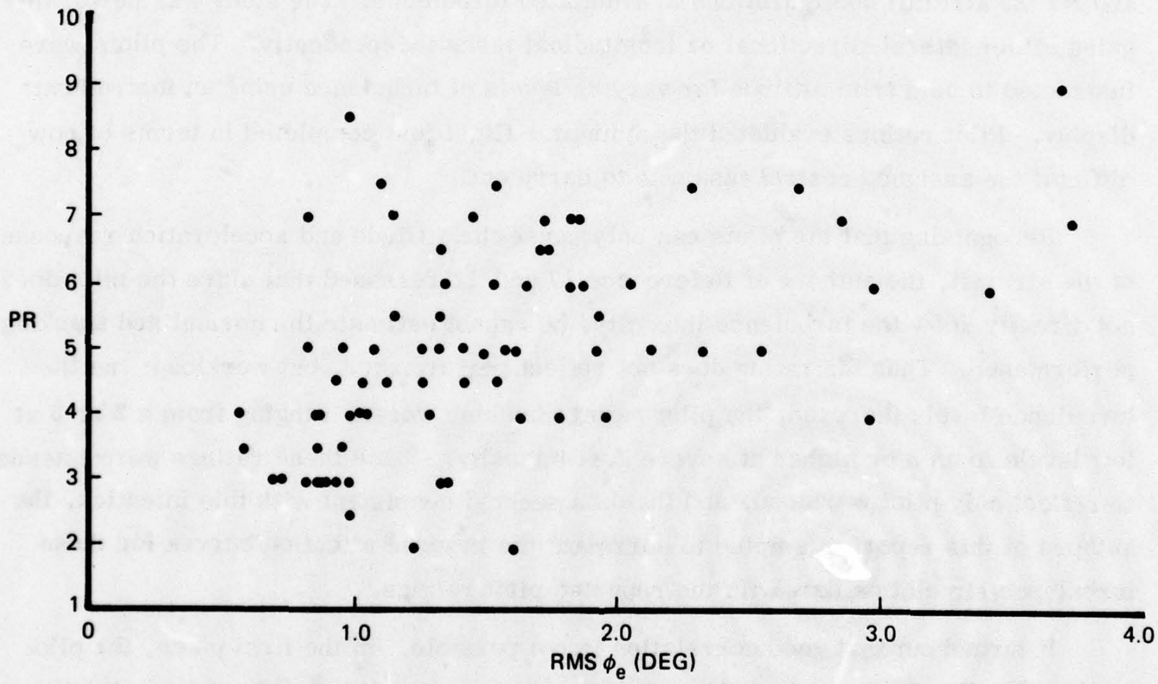

Figure 196. Bank Angle Errors Versus Pilot Rating for Normal Mode F-5 and A-7 Airplanes for all Gust Levels (Reference 18)

Consider the variable stability NT-33 data of Reference 17 first. Figure 197 shows the individual simulator flight data for the BB 2.3 configuration at light, moderate, and heavy turbulence levels. The line drawn through the data represents the average of the pilot ratings normalized to 10 ft/sec rms intensity using the equations shown in the figure. This strong linear relation is to be seen in all cases and any reader who intends to employ the pilot rating data in References 17 and 18 should complete the data analysis by the means described here.

In this way, an average pilot rating $\overline{PR}$ is obtained for each of the NT-33 configurations studied in Reference 17. These average pilot ratings, $\overline{PR}$, can then be plotted versus the average normalized tracking errors $\bar{\phi}_\epsilon$ obtained from the flight simulation. This is shown in Figure 198. It is clear that for the NT-33 configurations the average pilot ratings correlate strongly with the average tracking performance, so that these pilot ratings reflect performance with little possibility of further functional dependence on other quantities such as parameters correlating with workload.

Now consider the F-5 data reported in Reference 18. Figure 199 shows a typical flight condition, Case 1 without augmenter. Again, each F-5 configuration is assigned an average pilot rating $\overline{PR}$ normalized to the nominal turbulence level. If these are plotted versus the normalized tracking errors, the result is poor correlation as shown in Figure 200. Thus the F-5 data tends to dispute the correlation of Figure 198 obtained for the NT-33 data.

This conflict can be resolved as follows. Assume that the pilots not only observe the tracking errors, but also take into account the lateral accelerations that were provided with good fidelity by the motion system of the large amplitude simulator. If the pilots used this ride qualities cue to determine how much tracking error per level of shaking of the simulator cab that they experienced, they would have a means of rating the aircraft configurations against one another in terms of performance. To test this assumption, the average normalized pilot ratings $\overline{PR}$ can be divided by the lateral side force per side wind velocity stability derivative, Y_v, for each aircraft configuration as an estimate of the amount of acceleration the pilot would experience for a given amount of turbulence intensity.

When this normalization over Y_v is carried out for the NT-33 average pilot ratings $\overline{PR}$, the result is still a strong linear correlation, since the Y_v derivatives vary little among the NT-33 configurations tested. This is shown in Figure 201.

On the other hand, the F-5 configurations have a varying Y_v associated with them. Normalizing over Y_v then transforms the data of Figure 200 into the strong linear correlation shown in Figure 202, justifying the above assumption.

The success in producing linear correlations of pilot rating averages with tracking errors when the ride qualities accelerations are taken into account demonstrates that the pilot rating data in References 17 and 18 reflect primarily performance and not workload, a result consistent with the hypothesis presented in Section VII E.

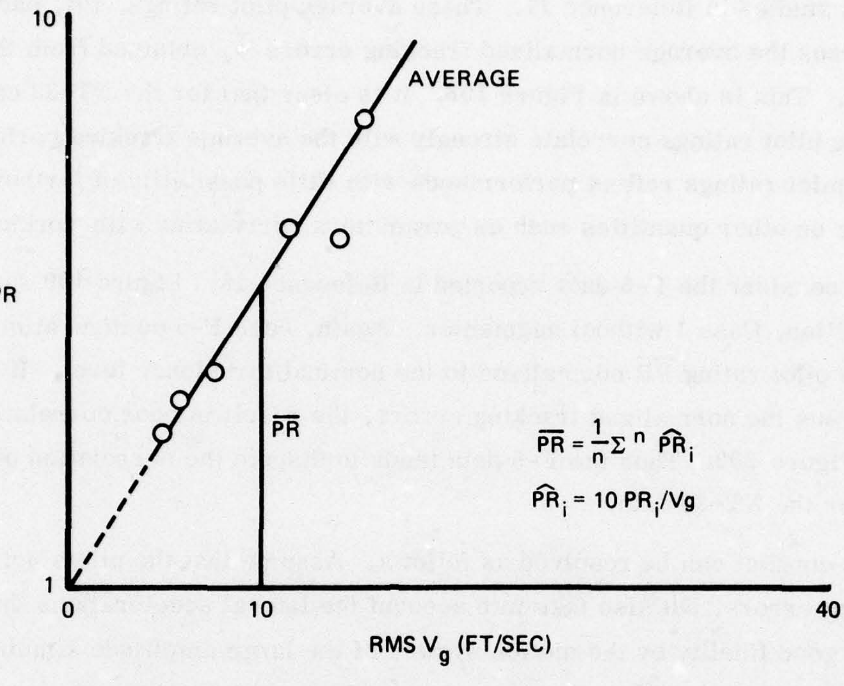

Figure 197. NT-33 BB2.3 Average Pilot Rating

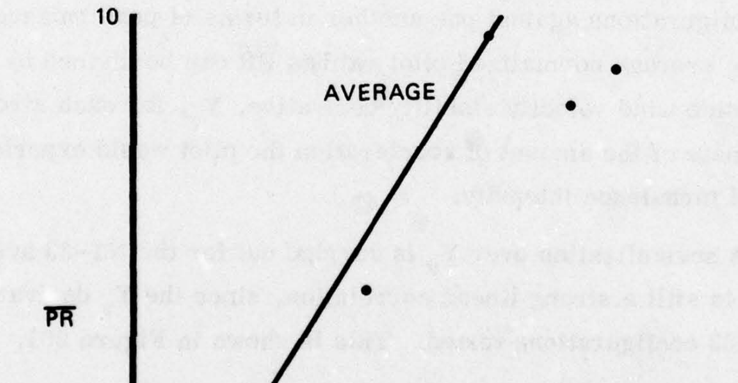

Figure 198. Average NT-33 Pilot Ratings as Functions of Tracking Error

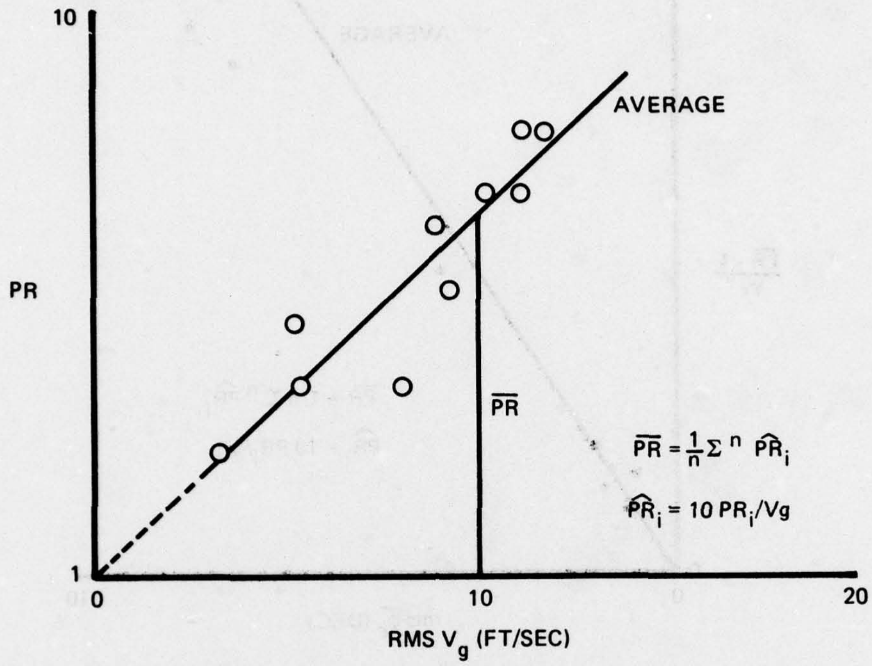

Figure 199. F-5 Case 1 Without Augmenter Average Pilot Rating

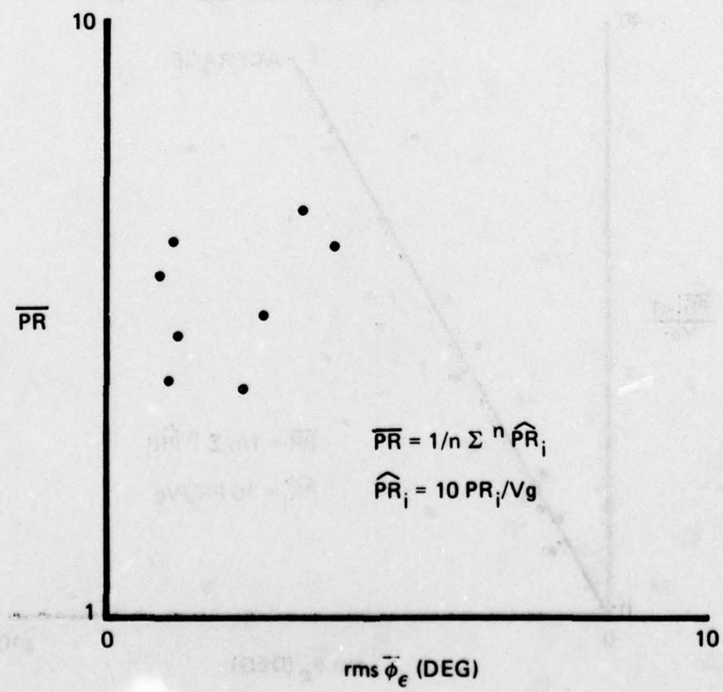

Figure 200. F-5 Turbulence Data Showing Poor Correlation of Average Pilot Rating With Tracking Error

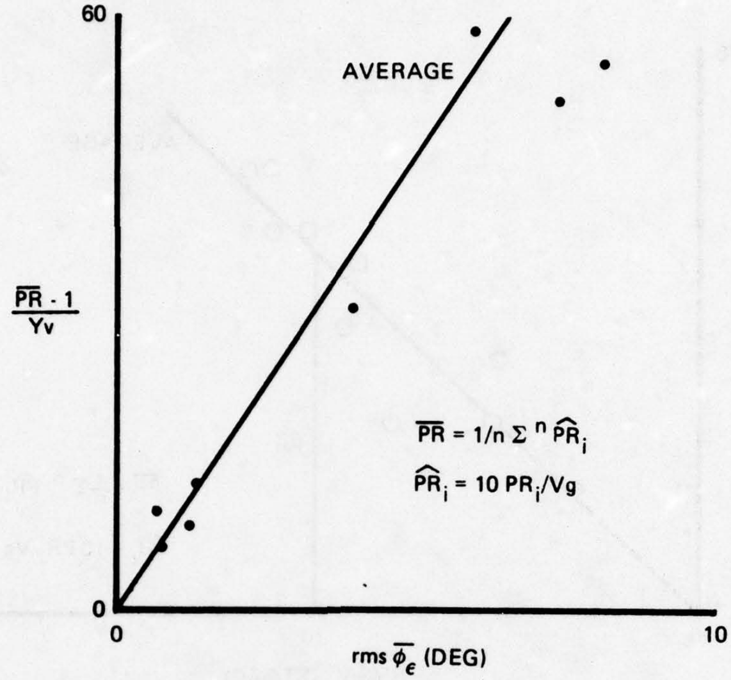

Figure 201. NT-33 Turbulence Data Showing Influence of Motion Cues on Pilot Ratings

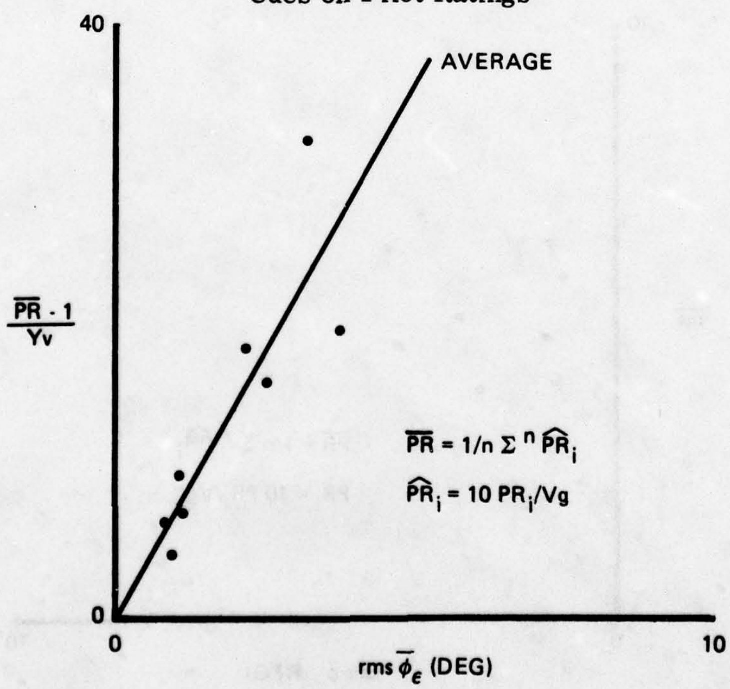

Figure 202. F-5 Turbulence Data Showing Influence of Motion Cues on Pilot Ratings

APPENDIX B

PREDICTION OF CRITICAL TASK PERFORMANCE

Section VII D presented a classification of side tasks for use in predicting pilot reserve attention capacity. This classification included the "critical task" method developed by H. R. Jex, References 19 and 20. This method has become a standard experimental procedure, and the objective of this Appendix is to demonstrate that the Urgency Decision Pilot Model predicts performance of the critical task that is consistent with data reported by McDonnell, Reference 20.

Suppose a longitudinal aircraft configuration is to be evaluated using the critical task approach. A flight simulation is arranged in which the pilot has a compensatory display of pitch angle θ. To evaluate how much reserve attention capacity is available to the pilot, the display also includes the tracking error of a secondary task, call it roll angle ϕ. The roll angle is not driven by a random command as is done with θ, but is the result of drift induced by the unstable dynamics chosen for the side task. The test is then performed by increasing the instability of the roll task until the pilot is no longer able to maintain acceptable performance on the pitch task while keeping the roll task from diverging. Figure 203 shows a block diagram of the simulation task including the automatic adjustment of the instability parameter, where the side task dynamics are represented by

$$\frac{\phi}{\delta a} = \frac{\lambda}{(s-\lambda)}$$

The flight simulation then results in a value of λ_c that represents the difficulty or workload of the task evaluated. Figure 204, re-drawn from Reference 20, shows the values of λ_c determined by McDonnell for four types of plant dynamics. The correlation between λ_c and pilot ratings is clearly shown, and provides additional support for the conjecture presented at the end of Section VII.

To use the Urgency Decision Pilot Model to predict the critical task λ_c, all that is necessary is to replace the two human pilot blocks of Figure 203 by optimized gain - lead - delay pilot compensation dynamics and the urgency function test.

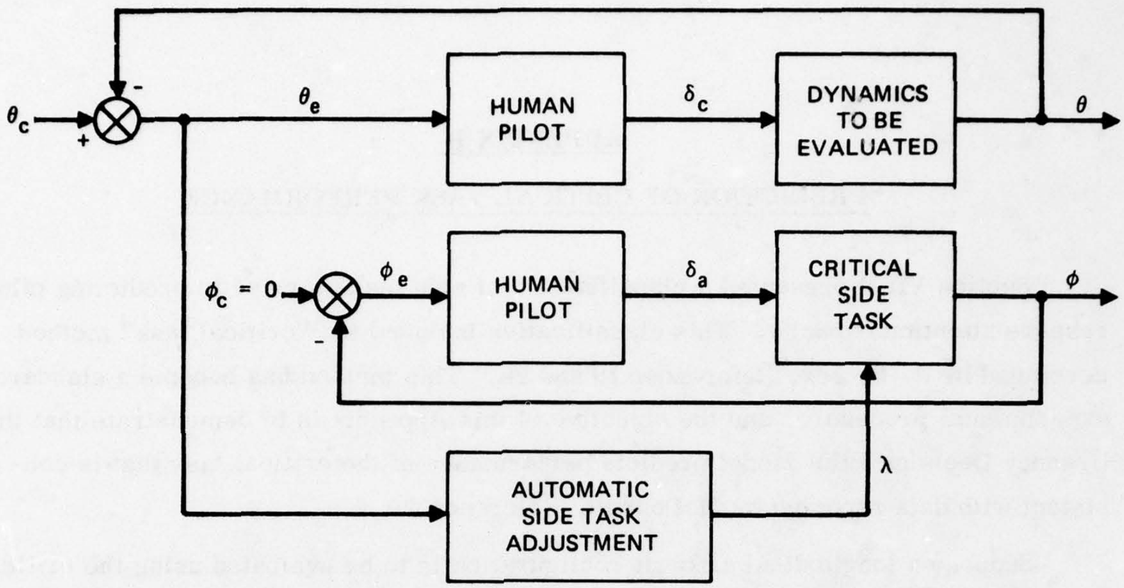

Figure 203. Flight Simulation to Determine Critical Side Task

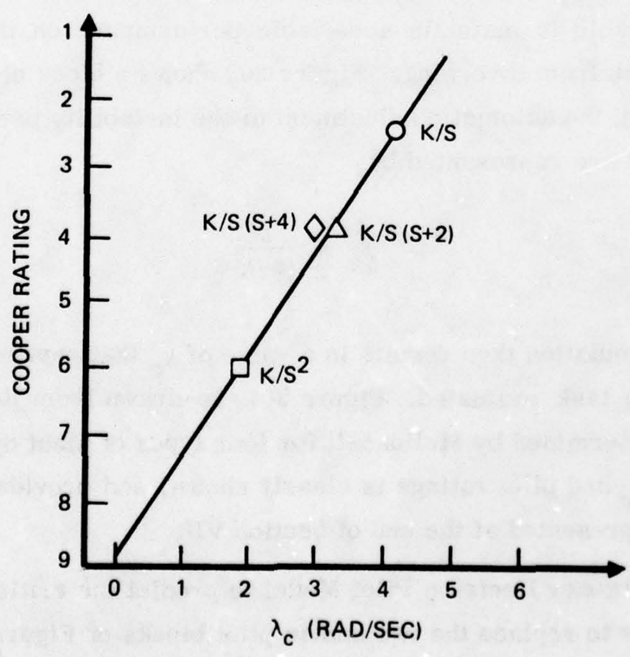

Figure 204. Pilot Rating as a Function of Critical Task λ_c

For this problem, the urgency functions are assumed to be simply the absolute values of the tracking errors with unity coefficients. Four statistics, RA and rms θ_c, ϕ, $\dot{\phi}$, were kept for each of the four plants shown in Figure 204. The automatic adjustment of λ was not used in these calculations; the value of λ was varied to show sensitivity of the statistics to side task loading. These sensitivity graphs are shown with the values of λ_c determined by McDonnell indicated. Figure 205 shows the sensitivity of pitch angle tracking errors to side task λ, and Figures 206-208 present similar data for the other statistics.

In the case of K/s and K/s^2 plant dynamics, the McDonnell values of λ_c occur where sharply increased sensitivity to λ is predicted by the Urgency Decision Pilot Model. In the other cases, there is no clear evidence of the critical value of λ. Since the McDonnel data does not discriminate between the $K/s(s+2)$ and the $K/s(s+4)$ plants, the model predictions are apparently consistent with the reported critical values of λ for these plants.

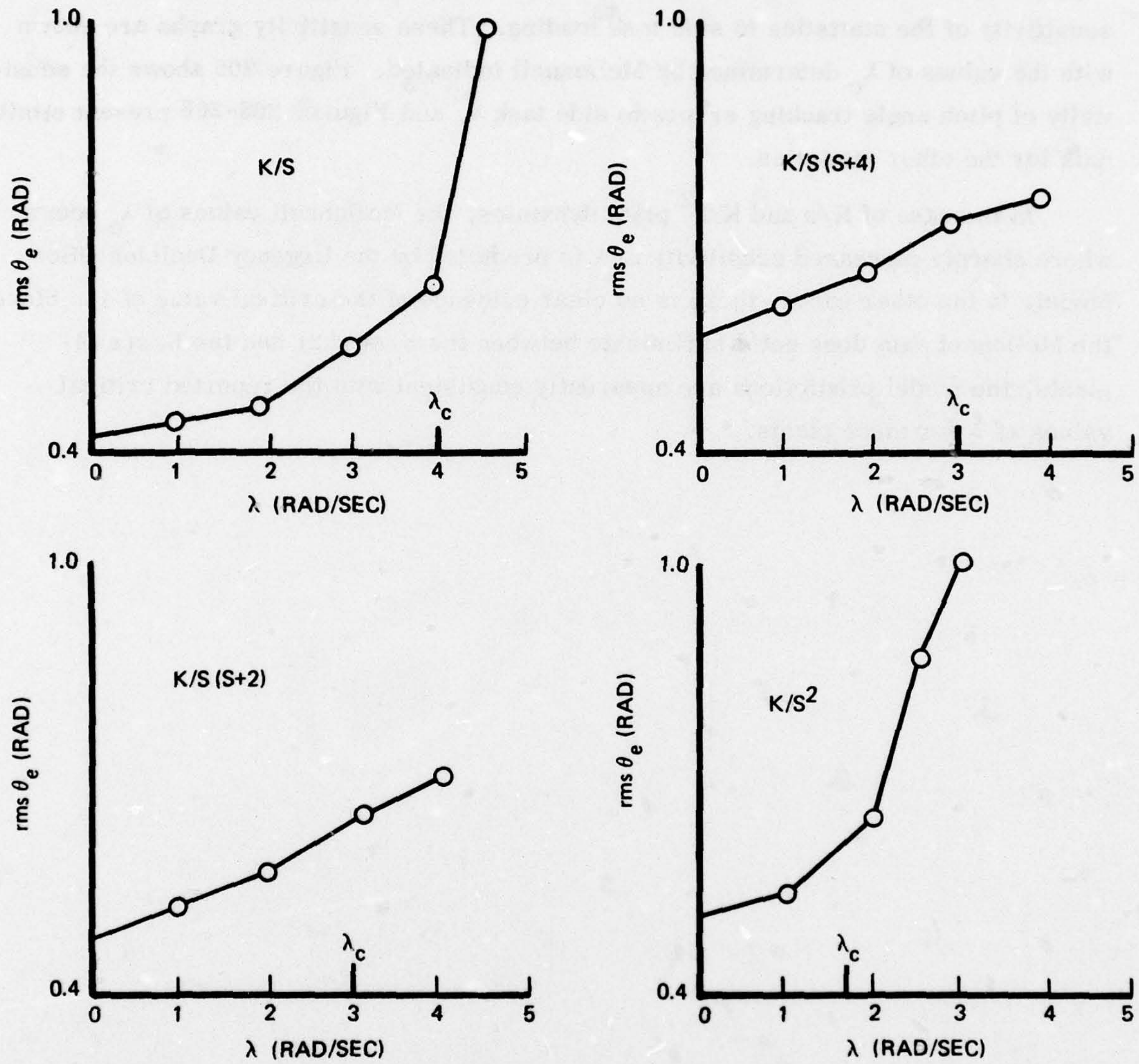

Figure 205. Pitch Angle Tracking Errors as Functions of Side Task

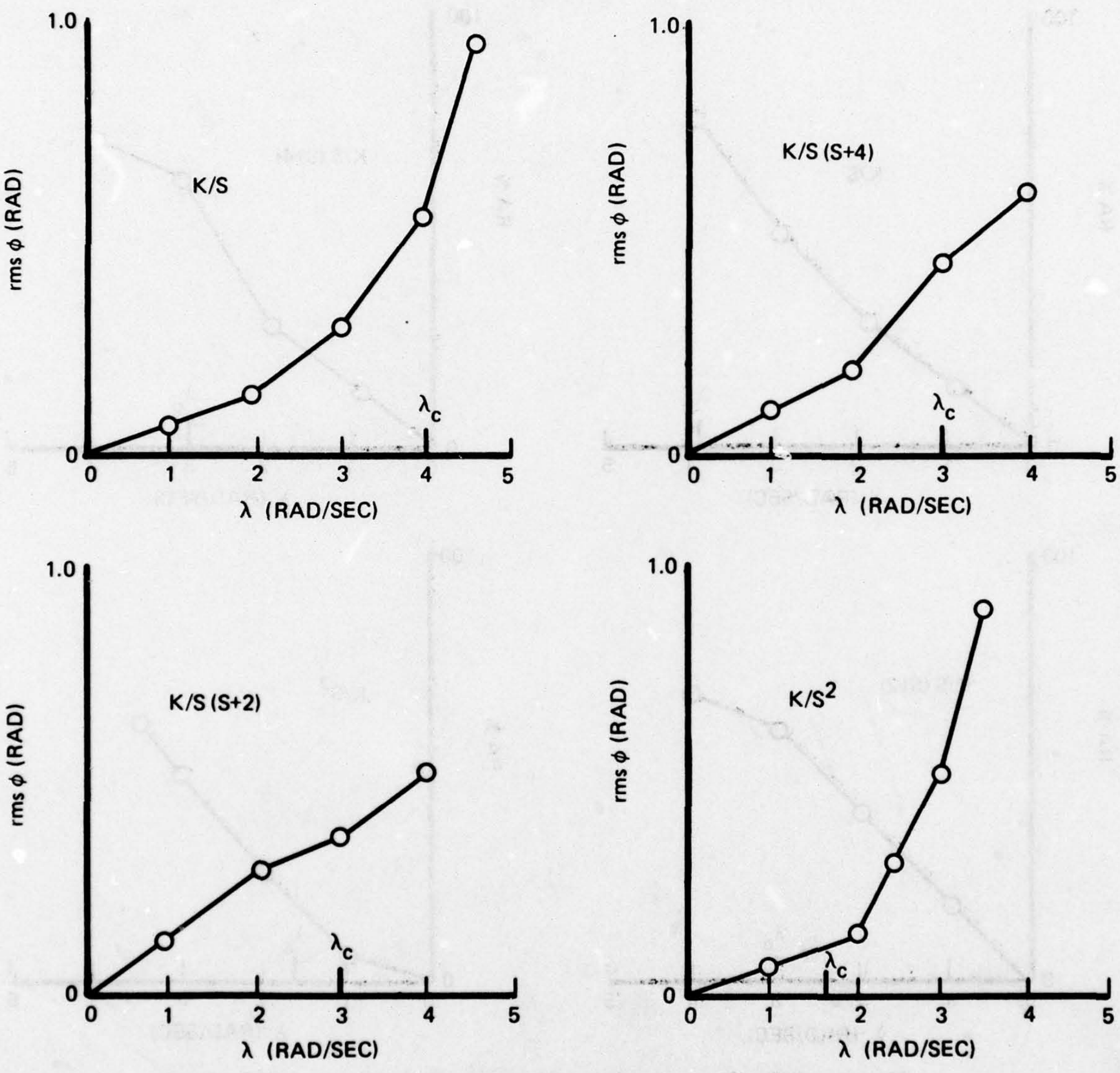

Figure 206. Bank Angle Tracking Errors as Functions of Side Task

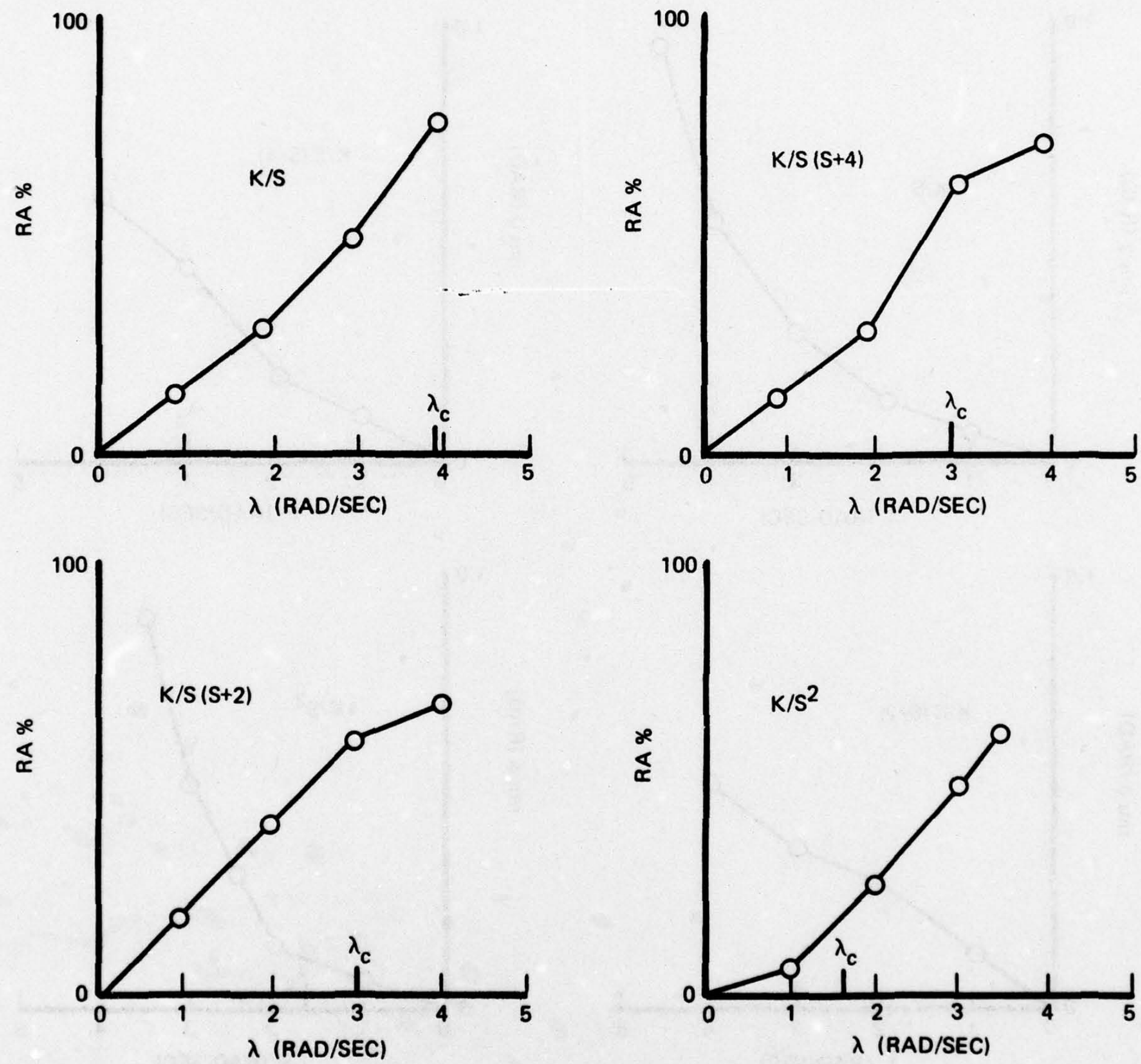

Figure 207. Reserve Attentions as Functions of Side Task

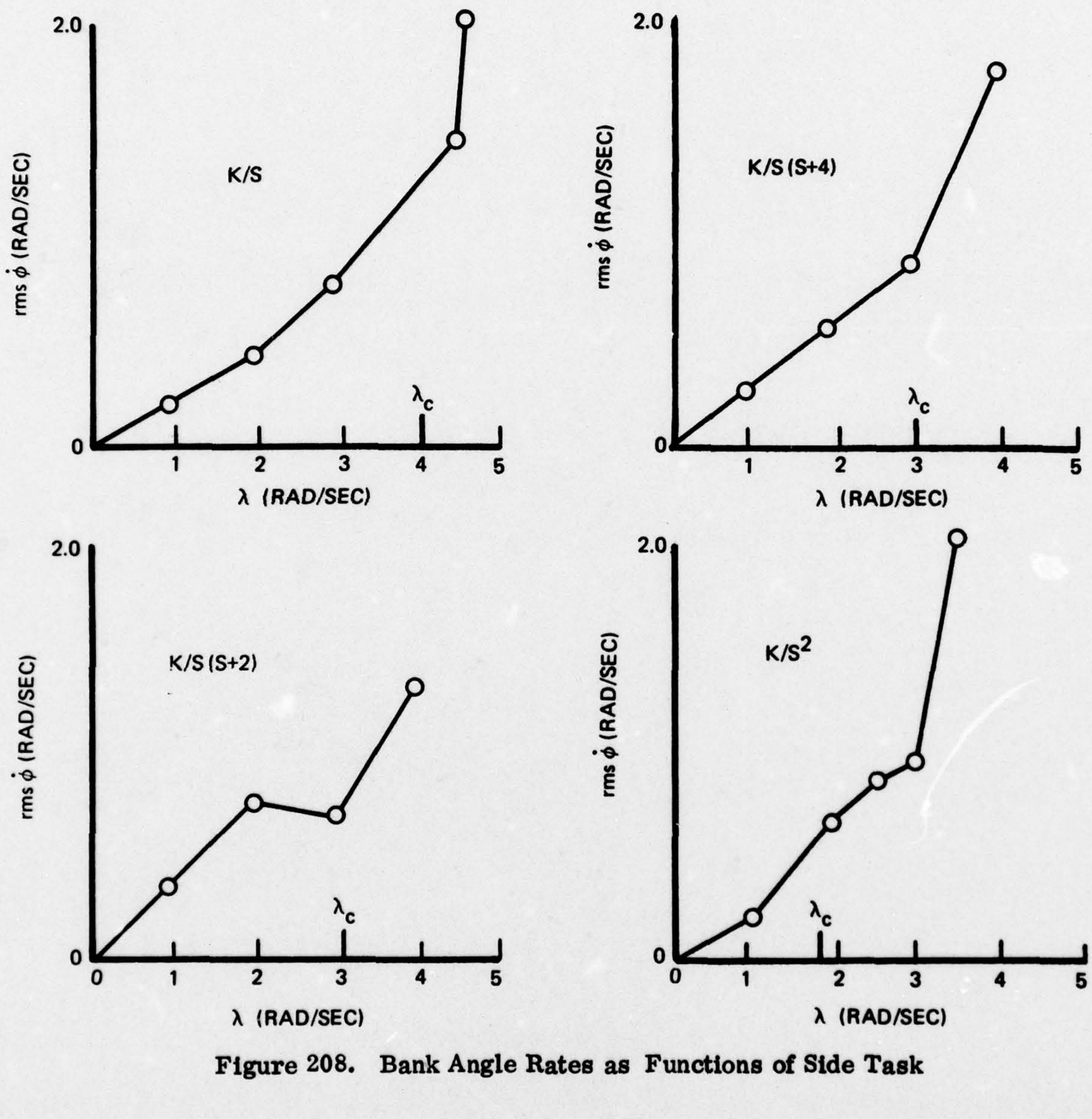

Figure 208. Bank Angle Rates as Functions of Side Task

APPENDIX C

COMPUTER PROGRAM USER GUIDE

Much of the fixed-base flight simulation and pilot model analysis work discussed in this report was performed using a digital program written primarily in FORTRAN IV and running on a Harris Slash 4 computer system. The program could be operated in a batch mode for pilot model analysis, or could be operated in real-time, accepting stick input commands from either a human pilot or the pilot model.

This Appendix describes a version of the program that was converted for batch operation on the Control Data Corporation 6600 computer and which is available to qualified requesters from the Air Force Flight Dynamics Laboratory (FGC), Wright-Patterson AFB, Ohio 45433. The purpose of the program description is threefold:

1) To serve as an example of one possible implementation of the TASK-CONTROL-EVALUATION approach to piloted aircraft precision task analysis.
2) To assist those who may wish to modify the existing program for some particular problem analysis.
3) To serve as a guide for those who may wish to use the program for immediate problem application or to gain some experience in the analysis methods presented in this report.

It is hoped that this discussion will demonstrate the simple, straightforward manner in which the Urgency Decision Pilot Model can be programmed and applied to the analysis of a variety of precision piloted tasks.

PROGRAM ORGANIZATION

The program performs time-domain calculations and produces time histories of aircraft and pilot model variables, from which various statistical measures are computed. In overall structure, the program follows the TASK-CONTROL-EVALUATION approach to flying qualities analysis. A discussion of the program organization in this context will be presented next.

TASK The precision task simulated is two-axis command tracking. There are three options:

1) $\phi - \theta$ compensatory command tracking, with or without turbulence. This is the default case.

2) $\Psi - \theta$ compensatory command tracking, with or without turbulence.

3) $\Psi - \theta$ pursuit command tracking, with or without turbulence.

Attitude stabilization in turbulence is a special case of 1) or 2) with the tracking commands identically zero. Either Dryden Gaussian or Reeves non-Gaussian turbulence models can be generated.

The coupled six degree-of-freedom body axis equations presented in Section V, Figure 81, are used.

CONTROL There are gain-lead-lag-delay pilot compensation models for the lateral and longitudinal axes, producing aileron and elevator commands. On the lateral axis, there is provision for both inner loop and outer loop compensation. In addition, an augmenter produces elevator and rudder commands, and there are lags for the lateral and longitudinal control commands. Finally, remnant can be injected into the pilot model's control inputs.

There are three control switching options:

1) Two-axis task with urgency function test and switching logic.

2) Two-axis task and constant urgency side task with urgency function test and switching logic.

3) Two-axis task with regular sampling and specified dwell times on each axis; there is no urgency function test.

In all cases, it is possible to impose a minimum dwell time that the model must spend on a task before being allowed to switch to another.

EVALUATION Statistics on dwell fractions and mean dwell times for lateral, longitudinal, and side tasks are always kept and printed out. In addition, statistics on up to 24 other aircraft and pilot model variables can be kept; the output for each of these will include the mean, standard deviation, rms, skewness, and peakedness.

Figure 209 illustrates the overall organization and computational flow of the program.

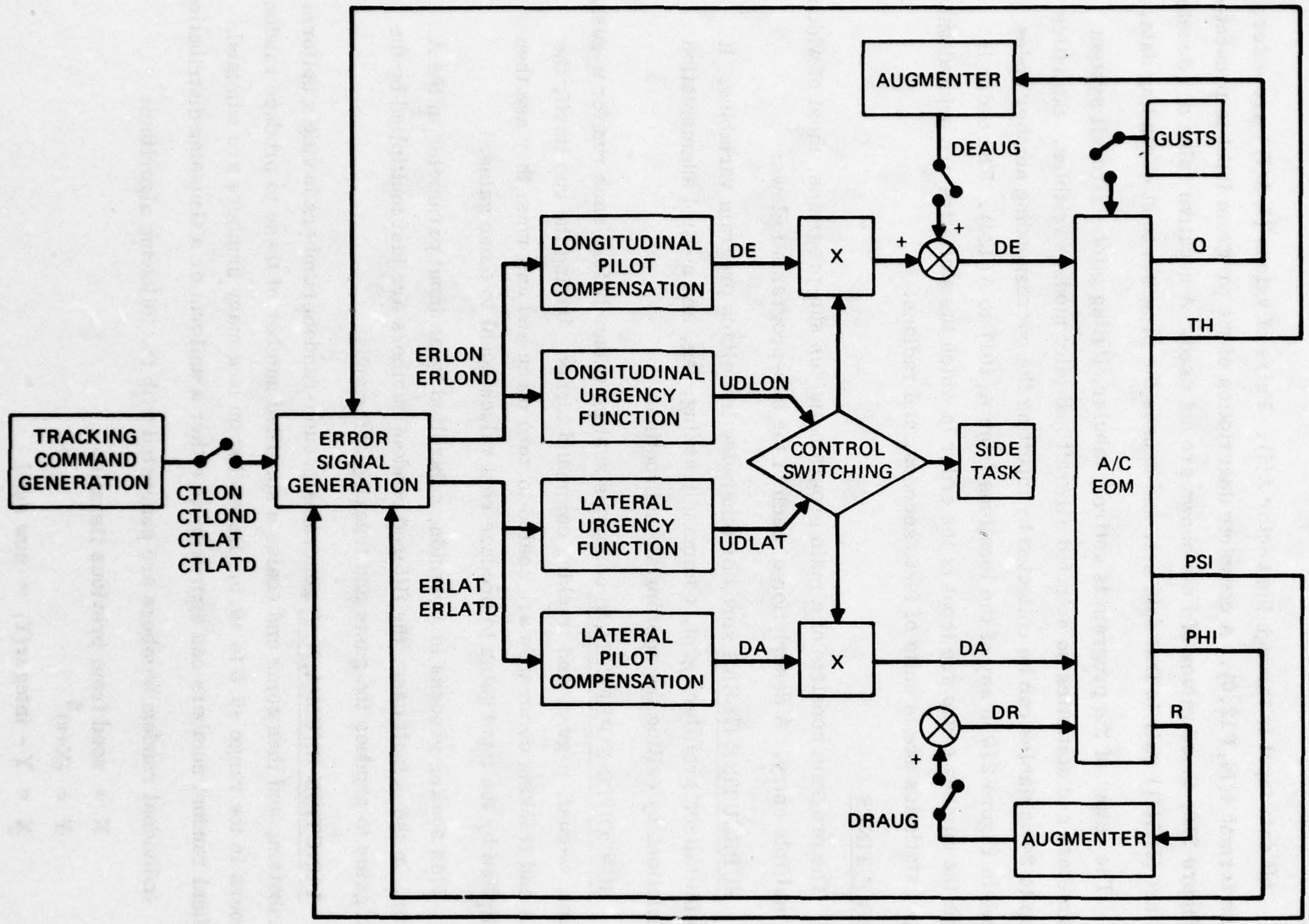

Figure 209. Organization of Major Program Elements

INPUT/OUTPUT

All data input is through the vector A(I). Pairs of values (I, A(I)) are entered in the format 4(I4, F12.0). A complete description of the program input is presented in Figure 210; those values of I not shown are not used. A negative value of I denotes the last (I, A(I)) pair in that data set, and causes the program to stop reading data.

The output of the program is entirely tabular, listing pilot - aircraft system parameters and statistics on selected aircraft and pilot model variables. Statistics on up to 24 variables can be collected by inputting the corresponding number codes shown in Figure 210 in any of the locations from A(101) to A(124). The order in which the number codes are input is the order in which the statistics are printed out. Output statistics are in units of feet, seconds, and radians.

SUBROUTINES

The program consists of a main program and ten sub-programs, most of which are multiple entry. A description of each of the sub-programs follows:

SUBROUTINE CLEAR zeros or otherwise initializes program variables. It also initializes prefilter, gust, command tracking, lag, and control augmentation calculations by calling the appropriate subroutines.

SUBROUTINE PRECOM(A) computes scaling values before each run for u-gust, v-gust, w-gust, p-gust, and tracking command terms. During the run itself, the gusts and tracking commands are scaled to zero mean and unit rms; they are then multiplied by the input gains to produce rms values equal to those gains.

This scaling process is an option, controlled by an input parameter in the A vector. In the default case, the filtered random numbers are just multiplied by the input gains to produce the gusts and tracking commands.

FUNCTION RNUM(A, K, J) generates pseudo-random numbers having a uniform distribution, and then sums and scales a specified number of these to produce random numbers in the range -0.5 to +0.5. Depending on how many numbers are summed, the final random numbers can approximate either a uniform or a Gaussian distribution.

Individual random numbers are generated with the following algorithm:

X = seed from previous iteration

$Y = (X+\pi)^5$

$X = Y - \text{integer}(Y)$ = new seed

random number $= X - 0.5$

I	A(I)
1	Integration frame time (sec)
2	Number of iterations computed each run
3	Number of uniformly distributed random numbers summed in random number algorithm
4	< 0 : precompute and scale gusts and tracking commands to zero mean and unit rms
5	$= -1$: $\psi - \theta$ compensatory command tracking task $= -2$: $\psi - \theta$ pursuit command tracking task
6	< 0 : generate Reeves turbulence
9	Random number seed increment
10	Number of runs computed
12	d, coefficient of prefilter
13	< 0 : prefilter gusts
14	< 0 : prefilter tracking commands
15	< 0 : prefilter remnant
17	Pilot gain, lateral
18	Pilot gain, longitudinal
19	Pilot gain, heading
21	Pilot lead, lateral (sec)
22	Pilot lead, longitudinal (sec)
23	Pilot lead, heading (sec)
25	Pilot neuromuscular lag, lateral (sec)
26	Pilot neuromuscular lag, longitudinal (sec)
27	Minimum dwell time (sec)
29	Pilot delay, lateral (sec)
30	Pilot delay, longitudinal (sec)
31	Urgency delay, lateral (sec)
32	Urgency delay, longitudinal (sec)
33	a, lateral
34	β, lateral
35	a, longitudinal
36	β, longitudinal
37	u-gust gain
38	v-gust gain
39	w-gust gain
40	p-gust gain
41	Turbulence scale length (ft)
42	Aircraft wingspan (ft)
43	< 0 : generate q-gust
44	< 0 : generate r-gust
45	Y_v (1/sec)
46	Y_p (ft/sec)
47	Y_r (ft/sec)
48	$Y_{\delta a}$ (ft/sec^2)
49	$Y_{\delta r}$ (ft/sec^2)

Figure 210. Program Input Format

I	A(I)
50	L_v (1/ft-sec)
51	L_p (1/sec)
52	L_r (1/sec)
53	$L_{\delta a}$ (1/sec^2)
54	$L_{\delta r}$ (1/sec^2)
55	N_v (1/ft-sec)
56	N_p (1/sec)
57	N_r (1/sec)
58	$N_{\delta a}$ (1/sec^2)
59	$N_{\delta r}$ (1/sec^2)
60	X_u (1/sec)
61	X_w (1/sec)
62	$X_{\dot{w}}$
63	X_q (ft/sec)
64	$X_{\delta e}$ (ft/sec^2)
65	Z_u (1/sec)
66	Z_w (1/sec)
67	$Z_{\dot{w}}$
68	Z_q (ft/sec)
69	$Z_{\delta e}$ (ft/sec^2)
70	M_u (1/ft-sec)
71	M_w (1/ft-sec)
72	$M_{\dot{w}}$ (1/ft)
73	M_q (1/sec)
74	$M_{\delta e}$ (1/sec^2)
75	u_o (ft/sec)
76	w_o (ft/sec)
77	I_{xx} (ft-lb-sec^2)
78	I_{yy} (ft-lb-sec^2)
79	I_{zz} (ft-lb-sec^2)
80	θ_o (deg)
81	Random number seed for Gaussian u-gust
82	Random number seed for Gaussian v-gust
83	Random number seed for Gaussian w-gust
84	Random number seed for Gaussian p-gust
85	Random number seed for lateral tracking commands
86	Random number seed for longitudinal tracking commands
87	Random number seed for lateral remnant
88	Random number seed for longitudinal remnant

Figure 210. Program Input Format (Continued)

I	A(I)
91, 92, 93	Random number seeds for Reeves u-gust
94, 95, 96	Random number seeds for Reeves v-gust
97, 98, 99	Random number seeds for Reeves w-gust
101-124	Variables for which statistics are to be kept

1. u (ft/sec)
2. v (ft/sec)
3. w (ft/sec)
4. p (rad/sec)
5. q (rad/sec)
6. r (rad/sec)
7. ϕ (rad)
8. θ (rad)
9. ψ (rad)
10. α (rad)
11. β (rad)
12. u-gust (ft/sec)
13. v-gust (ft/sec)
14. w-gust (ft/sec)
15. p-gust (rad/sec)
16. q-gust (rad/sec)
17. r-gust (rad/sec)
18. lateral tracking commands (rad)
19. longitudinal tracking commands (rad)
20. lateral error (rad)
21. longitudinal error (rad)
22. radial error (rad)
23. δa (rad)
24. δe (rad)
25. δr (rad)

I	A(I)
125	Lateral tracking command gain
126, 127, 128	a, e, b — coefficients of lateral command tracking filter
129	Longitudinal tracking command gain
130, 131, 132	a, e, b — coefficients of longitudinal command tracking filter
133	Control system lag, lateral (sec)
134	Control system lag, longitudinal (sec)
137	Remnant gain, lateral
138	Remnant gain, longitudinal
141	Lateral dwell time, regular sampling (sec)

Figure 210. Program Input Format (Continued)

I	A(I)
142	Longitudinal dwell time, regular sampling (sec)
143	Side task urgency
193	< 0 : augmenter on
194	K_A } augmenter gains
195	K_V } augmenter gains
196	K_Y } augmenter gains

Figure 210. Program Input Format (Concluded)

A separate random number stream is generated for each of the program variables that uses random numbers.

The function argument K specifies how many numbers are to be summed to produce the final random numbers; J specifies the location in the A vector in which the current seed for the particular stream in question is stored.

SUBROUTINE PREFIL(A, K) prefilters the random numbers produced by RNUM to remove low frequency drift. The prefilter transfer function is of the form:

$$\frac{s^2}{(s+d)^2}$$

where d is specified in the input data vector A.

The subroutine argument K identifies the random number stream being prefiltered:

K = 1: u-gust
2: v-gust
3: w-gust
4: p-gust
5: lateral tracking command
6: longitudinal tracking command
7: lateral remnant
8: longitudinal remnant

Prefiltering of the random numbers is an option, controlled by input parameters in the A vector. In the default case, the random numbers are not prefiltered.

Other entry point: PRE.

SUBROUTINE GUST(A) generates Gaussian turbulence components by filtering white noise. Uncorrelated u-, v-, w-, and p-gusts can be generated, as well as correlated q- and r-gusts. The Dryden continuous turbulence model is used, as discussed in Reference 12.

Other entry points: GUSTU, GUSTV, GUSTW, GUSTP, GUSTQ, GUSTR.

SUBROUTINE COMTRK(A, L) generates lateral and longitudinal tracking commands by filtering white noise. The transfer function of the command tracking filters is of the form:

$$\frac{as+e}{(bs+1)^2}$$

where a, e, and b for each of the two filters, lateral and longitudinal, are specified in the input vector A.

The subroutine argument L identifies the tracking command being calculated:

L = 1: lateral
2: longitudinal

Other entry point: CTRACK.

SUBROUTINE LAG(A, K) lags four variables by amounts specified in the input vector A. The standard transfer function for a first order lag is programmed:

$$\frac{1}{\tau s+1}$$

The subroutine argument K identifies which lag is to be computed:

K = 1: lateral pilot neuromuscular lag
2: longitudinal pilot neuromuscular lag
3: lateral control system lag
4: longitudinal control system lag

Lag calculations are optional and are not performed in the default case, where a particular τ is zero.

Other entry point: LAGOUT.

SUBROUTINE AUGMNT(A, Q, R) models the F-5E augmentation system, shown in Figure 211, and generates elevator and rudder commands based on pitch and yaw rate, Q and R.

Control augmenter calculations are performed only if the corresponding parameter in the A vector is set to the proper value.

Other entry point: AUG.

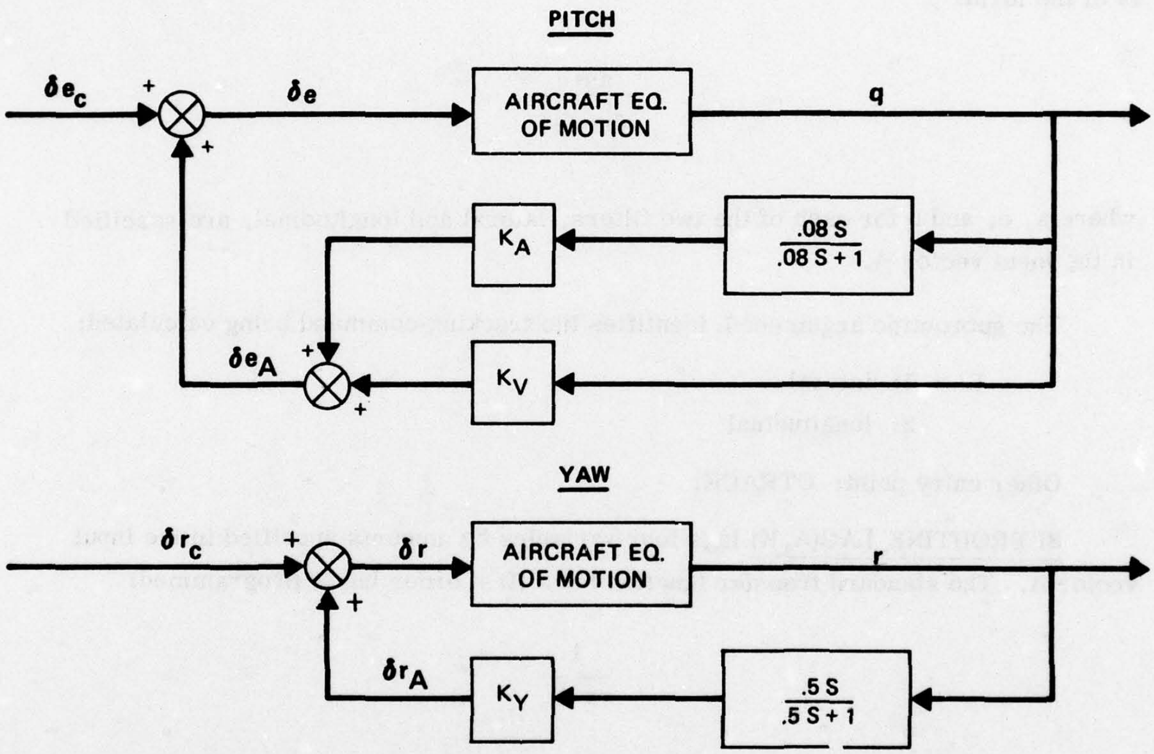

Figure 211. F-5E Stability Augmentation System

SUBROUTINE REEVES(A) generates uncorrelated u-, v-, and w-gusts using a reduced form of the total Reeves model discussed in Reference 13.

Precomputing and scaling of the gusts to zero mean and unit rms is automatic; it is not an option as it is with Gaussian turbulence. Moreover, there is no provision for prefiltering the random numbers used.

Reeves turbulence is generated only if a parameter in the input vector A is set to the proper value. In the default case, Gaussian turbulence is generated.

Other entry points: GUSTUR, GUSTVR, GUSTWR.

SUBROUTINE INOUT(I) performs all input/output operations in the program. The argument I identifies what particular read or write operation is to be executed.

VARIABLES

A description of the major program variables, arranged by COMMON blocks, is presented in Figure 212.

PROGRAM OPERATION

This section will describe the operation of the program through discussion of an example data set. The program's sequence of calculations and major branching is shown in the flow chart in Figure 213.

The sample data set is presented in Figure 214. The TASK being simulated is two-axis attitude stablization in Gaussian turbulence; this is the default case, since A(5) = A(6) = A(125) = A(129) = 0 and A(37) - A(39) are non-zero. The aircraft configuration used is F-5E Case 2; the appropriate parameters are specified in A(45) - A(80) and A(194) - A(196).

Random number seeds for the calculation of Gaussian u-, v-, and w- gusts are specified in A(81) - A(83). In addition, random number seeds for the calculation of Reeves u-, v-, and w- gusts are specified in A(91) - A(99); making A(6) negative would cause the program to generate Reeves turbulence rather than Gaussian.

The parameters A(101) - A(109) will cause statistics to be kept and printed out for u-, v-, and w-gusts; lateral, longitudinal, and radial errors; and aileron, elevator, and rudder commands.

The data set will cause three successive jobs to be run, with the input data set updated after the first and second jobs.

COMMON/SYSCOM/

A(I)	input data vector – see Figure 210
DFLAT	dwell fraction, lateral task
DFLON	dwell fraction, longitudinal task
DFSIDE	dwell fraction, side task
FMSTR	mean dwell time, lateral task
FMSTP	mean dwell time, longitudinal task
FMSTS	mean dwell time, side task
AVGI STDI RMSI SKWI PKDI N1	temporary storage locations for output statistics
ICOUNT	current iteration number

COMMON/EOM/

U(I), UD(I)	$u, \dot{u}$
V(I), VD(I)	$v, \dot{v}$
W(I), WD(I)	$w, \dot{w}$
P(I), PD(I)	$p, \dot{p}$
Q(I), QD(I)	$q, \dot{q}$
R(I), RD(I)	$r, \dot{r}$
PHI(I), PHID(I)	$\phi, \dot{\phi}$
TH(I), THD(I)	$\theta, \dot{\theta}$
PSI(I), PSID(I)	$\psi, \dot{\psi}$
I = 1 :	current value
2 :	first past value

COMMON/RANDOM/

RI(I, J)	random numbers from the generator
RF(I, J)	random numbers used in calculations
I = 1 :	u-gust
2 :	v-gust
3 :	w-gust
4 :	p-gust
5 :	lateral tracking command
6 :	longitudinal tracking command
7 :	lateral remnant
8 :	longitudinal remnant
J = 1 :	current value
2 :	first past value
3 :	second past value

Figure 212. Program COMMON Blocks

COMMON/GUSTS/

UGUST	u-gust
VGUST	v-gust
WGUST	w-gust
PGUST	p-gust
QGUST	q-gust
RGUST	r-gust

COMMON/TRACK/

CT(I, J)	tracking commands, unscaled
I = 1 :	lateral
2 :	longitudinal
J = 1 :	current value
2 :	first past value
3 :	second past value
CTLAT	lateral tracking command
CTLON	longitudinal tracking command
CTLATD	lateral tracking command rate
CTLOND	longitudinal tracking command rate

COMMON/STATS/

VAR(I) SUM1(I) SUM2(I) SUM3(I) SUM4(I)	storage vectors for the collection of statistical data on specified program variables — see A(101)-A(124) in Figure 210

COMMON/DELAYS/

DELAY (I, 50)	delay table, fifty locations
I = 1 :	lateral pilot
2 :	longitudinal pilot
3 :	lateral urgency
4 :	longitudinal urgency

COMMON/DWELL/

N	task control parameter = 0 : model controlling longitudinal task = 1 : model controlling lateral task
NR	number of iterations in current lateral control episode
NP	number of iterations in current longitudinal control episode
NS	number of iterations in current side task episode
NREP	number of lateral control episodes
NPEP	number of longitudinal control episodes
NSEP	number of side task episodes
NRTOT	total number of iterations on lateral control

Figure 212. Program COMMON Blocks (Continued)

NPTOT	total number of iterations on longitudinal control
NSTOT	total number of iterations on side task
ISIDE	side task parameter = 0 : model not in side task = 1 : model in side task
MINDT	minimum dwell time, iterations
MSTR	iterations in each lateral control episode, regular sampling
MSTP	iterations in each longitudinal control episode, regular sampling

COMMON/LAGS/

DLAG(I, J)	inputs to lags
GLAG(I, J)	outputs from lags
I = 1 :	lateral pilot
2 :	longitudinal pilot
3 :	lateral control
4 :	longitudinal control
J = 1 :	current value
2 :	first past value

COMMON/SCALE/

AV(I)	scale factors for mean
SD(I)	scale factors for standard deviation
I = 1 :	u-gust
2 :	v-gust
3 :	w-gust
4 :	p-gust
5 :	lateral tracking command
6 :	longitudinal tracking command

COMMON/STICK/

DA	aileron command
DE	elevator command
DR	rudder command
DEAUG	augmenter elevator command
DRAUG	augmenter rudder command

COMMON/INIT/

AH(I)	temporary storage vector for random number seeds
SINPHI	$\sin \phi$
COSPHI	$\cos \phi$
SINTH	$\sin \theta$
COSTH	$\cos \theta$
SINPSI	$\sin \psi$
COSPSI	$\cos \psi$
SINTH0	$\sin \theta_o$
COSTH0	$\cos \theta_o$

Figure 212. Program COMMON Blocks (Continued)

FI1	I_1
FI2	I_2
FI3	I_3
DH	one-half of integration frame time
NITER	number of iterations to be computed
ISUM	number of random numbers to be summed in generator

Figure 212. Program COMMON Blocks (Concluded)

In the first job, ten thirty-second flights will be simulated. The flights will be identical except for different gust sequences caused by different random number seeds. Since the pilot model gains are zero, the flights will be open loop.

After the first job is completed, the data set will be updated; the pilot model optimum gains and leads will be read in. Thus, the second job will be identical to the first, except that now the pilot model will close the loop and minimize the tracking errors.

After the second job is completed, the data set will be updated once more, and the third job will be run. The third job will be like the second except that now one 300-second flight will be simulated, and a constant urgency side task has been added.

NOTES AND CAUTIONS

For calculations in the program, all differential equations and transfer functions were converted to difference equations using the trapezoidal corrector integration formula, discussed in Reference 21.

This particular integration formula is simple to implement, and worked well in the simulations discussed in this report. The authors used a frame time of 0.025 sec; for other simulations, a shorter or longer frame time may be appropriate.

It has been the authors' experience that for proper operation of the numerical integrations and in particular the random number generator, a precision of at least ten decimal digits must be maintained. This presents no problem for large word size computers such as the CDC 6600. But when operating on computers having 24- or 32-bit words, double precision calculations are advisable.

The printout statistics mean, standard deviation, rms, etc., apply to the time histories generated by the program. The user must compute means and standard deviations of the rms statistics of individual runs to compare with the tabulated data in this report.

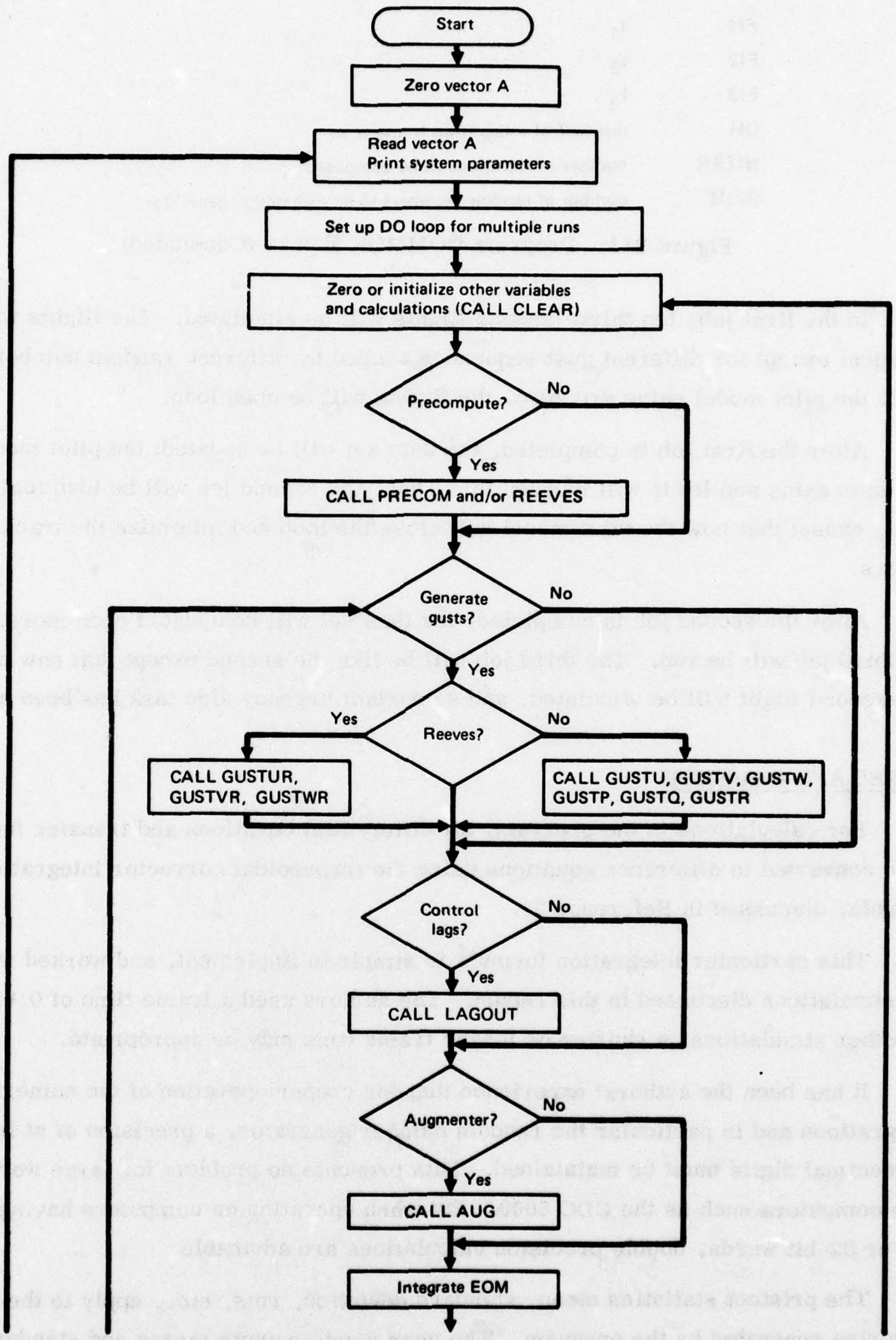

Figure 213. Program Flow Chart

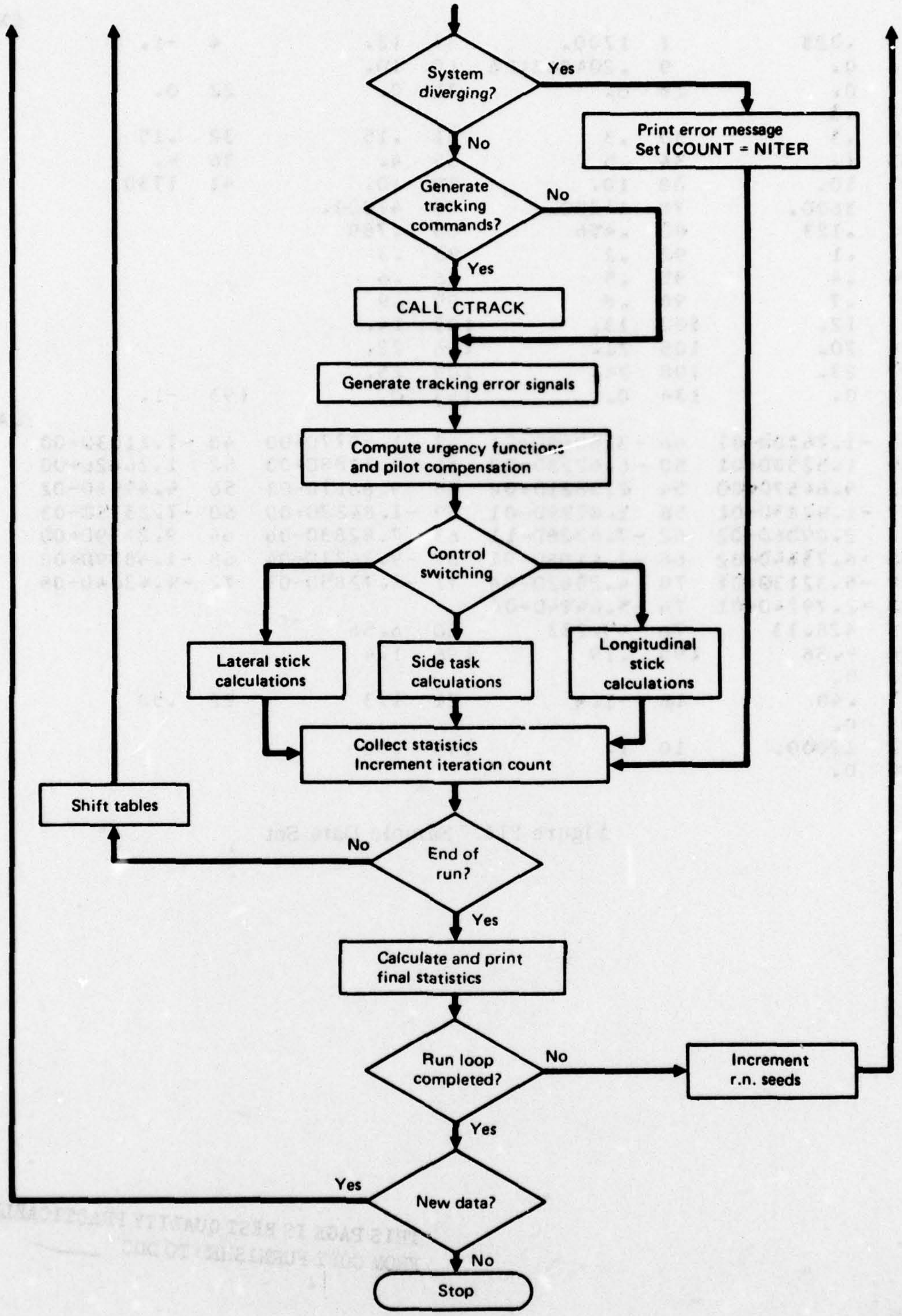

Figure 213. Program Flow Chart (Concluded)

1	.025	2	1200.	3	12.	4	-1.	EXAMPLE
6	0.	9	.204863128	10	10.			
17	0.	18	0.	21	0.	22	0.	
27	.3							
29	.3	30	.3	31	.15	32	.15	
33	1.	34	.5	35	4.	36	4.	
37	10.	38	10.	39	10.	41	1750.	
77	3600.	78	44200.	79	47000.			
81	.123	82	.456	83	.789			
91	.1	92	.2	93	.3			
94	.4	95	.5	96	.6			
97	.7	98	.8	99	.9			
101	12.	102	13.	103	14.			
104	20.	105	21.	106	22.			
107	23.	108	24.	109	25.			
133	0.	134	0.	143	0.	193	-1.	
								CASE 2
45	-1.7620D-01	46	-3.8068D-01	47	1.5977D+00	48	-1.1103D+00	
49	1.5250D+01	50	-6.4223D-02	51	-2.3288D+00	52	1.2662D+00	
53	9.6457D+00	54	2.5821D+00	55	9.8817D-03	56	4.4958D-02	
57	-1.9285D-01	58	1.0709D-01	59	-1.8427D+00	60	-7.2375D-03	
61	2.0906D-02	62	-7.6328D-11	63	7.8283D-06	64	9.2139D+00	
65	-6.7564D-02	66	-7.1198D-01	67	-9.2421D-04	68	-1.4839D+00	
69	-5.3213D+01	70	4.2882D-04	71	-3.7285D-03	72	-9.4304D-05	
73	-2.7924D-01	74	-5.6494D+00					
75	428.13	76	49.233	80	6.56			
194	-.36	195	.19	196	1.4			
-200	0.							
17	.40	18	-1.4	21	1.3	22	.50	
-200	0.							
2	12000.	10	1.	143	.02			
-200	0.							

Figure 214. Sample Data Set

PROGRAM LISTING

```
C*********************************************************************
C
C       TWO-AXIS COMMAND TRACKING IN TURBULENCE SIMULATION PROGRAM
C
C                    BATCH VERSION FOR CDC COMPUTERS
C
C*********************************************************************
*DECK TACTIT
      PROGRAM TACTIT(INPUT,OUTPUT,TAPE7=INPUT,TAPE2=OUTPUT)
      DIMENSION BOUND(9)
      COMMON/SYSCOM/A(200).DFLAT.DFLON.DFSIDE.FMSTR,FMSTP,FMSTS,
     1              AVGI,STDI,RMSI,SKWI,PKDI,N1,ICOUNT
      COMMON/EOM/UD(2),U(2),VD(2),V(2),WD(2),W(2),PD(2),P(2),QD(2),Q(2).
     1           RD(2),R(2),PHID(2),PHI(2),THD(2),TH(2),PSID(2),PSI(2)
      COMMON/RANDOM/RI(8,3),RF(8,3)
      COMMON/GUSTS/UGUST.VGUST.WGUST.PGUST.QGUST.RGUST
      COMMON/TRACK/CT(2,3),CTLAT,CTLON,CTLATD,CTLOND
      COMMON/STATS/VAR(25),SUM1(24),SUM2(24),SUM3(24),SUM4(24)
      COMMON/DELAYS/DELAY(4,50)
      COMMON/DWELL/N,NR,NP,NS,NREP,NPEP,NSEP,NRTOT,NPTOT,NSTOT,
     1             ISIDE.MINDT.MSTR.MSTP
      COMMON/LAGS/DLAG(4,2),GLAG(4,2)
      COMMON/SCALE/AV(6),SD(6)
      COMMON/STICK/DA,DE,DR,DEAUG,DRAUG
      COMMON/INIT/AH(20),SINPHI,COSPHI,SINTH,COSTH,SINPSI,COSPSI,
     1             SINTHO.COSTHO.FI1.FI2.FI3.DH.NITER.ISUM
      DATA BOUND/1000.,500.,500.,10.,10.,10.,3.,2.,5./
C*********************************************************************
C        INITIALIZATION
C*********************************************************************
      DO 10 I=1,200
   10 A(I)=0.
C
   20 CALL INOUT(12)
      CALL INOUT(1)
      CALL INOUT(2)
C
      NGAM=A(10)+.1
      IF (A(10).LE.1.) NGAM=1
      DO 500 JGAM=1,NGAM
C
      CALL CLEAR
      IF (A(4).LT.0.) CALL PRECOM(A)
      IF (A(6).LT.0.) CALL REEVES(A)
C*********************************************************************
C        GUST GENERATION
C*********************************************************************
  190 IF (A(6).LT.0.) GO TO 206
      IF (A(37).LT.1.E-5) GO TO 201
      RI(1,1)=RNUM(A,ISUM,81)
```

```
      IF (A(13).GE.O.) RF(1,1)=RI(1,1)
      IF (A(13).LT.O.) CALL PRE(A,1)
      CALL GUSTU(A)
      UGUST=A(37)*(UGUST-AV(1))/SD(1)
  201 IF (A(38).LT.1.E-5) GO TO 203
      RI(2,1)=RNUM(A,ISUM,82)
      IF (A(13).GE.O.) RF(2,1)=RI(2,1)
      IF (A(13).LT.O.) CALL PRE(A,2)
      CALL GUSTV(A)
      VGUST=A(38)*(VGUST-AV(2))/SD(2)
      IF (A(44).LT.O.) CALL GUSTR(A)
  203 IF (A(39).LT.1.E-5) GO TO 205
      RI(3,1)=RNUM(A,ISUM,83)
      IF (A(13).GE.O.) RF(3,1)=RI(3,1)
      IF(A(13).LT.O.) CALL PRE(A,3)
      CALL GUSTW(A)
      WGUST=A(39)*(WGUST-AV(3))/SD(3)
      IF (A(43).LT.O.) CALL GUSTQ(A)
  205 IF (A(40).LT.1.E-5) GO TO 210
      RI(4,1)=RNUM(A,ISUM,84)
      IF (A(13).GE.O.) RF(4,1)=RI(4,1)
      IF (A(13).LT.O.) CALL PRE(A,4)
      CALL GUSTP(A)
      PGUST=A(40)*(PGUST-AV(4))/SD(4)
      GO TO 210
  206 IF (A(37).GT.1.E-5) CALL GUSTUR(A)
      IF (A(38).GT.1.E-5) CALL GUSTVR(A)
      IF (A(39).GT.1.E-5) CALL GUSTWR(A)
C***********************************************************************
C             CONTROL LAGS AND AUGMENTERS
C***********************************************************************
  210 IF (A(133).LT.1.E-5) GO TO 211
      DLAG(3,1)=DA
      CALL LAGOUT(A,3)
      DA=GLAG(3,1)
  211 IF (A(134).LT.1.E-5) GO TO 212
      DLAG(4,1)=DE
      CALL LAGOUT(A,4)
      DE=GLAG(4,1)
  212 IF (A(193).GE.O.) GO TO 214
      CALL AUG(A,Q,R)
      DE=DE+DEAUG
      DR=DRAUG
C***********************************************************************
C             INTEGRATION OF EQUATIONS OF MOTION
C***********************************************************************
  214 UD(1)=32.174*(SINTHO*(1.-COSTH*COSPSI)-COSTHO*SINTH)
     1         -Q(1)*(A(76)+W(1))+R(1)*V(1)
     2         +A(60)*(U(1)+UGUST)+A(61)*(W(1)+WGUST)+A(62)*WD(1)
     3         +A(63)*(Q(1)+QGUST)+A(64)*DE
      U(1)=U(2)+DH*(UD(1)+UD(2))
      WD(1)=32.174*(COSTHO*(COSTH*COSPHI-1.)
     1               -SINTHO*(SINTH*COSPHI*COSPSI+SINPHI*SINPSI))
     2         +Q(1)*(A(75)+U(1))-P(1)*V(1)
```

```
3         +A(65)*(U(1)+UGUST)+A(66)*(W(1)+WGUST)
4         +A(68)*(Q(1)+QGUST)+A(69)*DE
      WD(1)=WD(1)/(1.-A(67))
      W(1)=W(2)+DH*(WD(1)+WD(2))
      QD(1)=FI2*P(1)*R(1)+A(70)*(U(1)+UGUST)+A(71)*(W(1)+WGUST)
1         +A(72)*WD(1)+A(73)*(Q(1)+QGUST)+A(74)*DE
      Q(1)=Q(2)+DH*(QD(1)+QD(2))
      RD(1)=FI3*P(1)*Q(1)+A(55)*(V(1)+VGUST)+A(56)*(P(1)+PGUST)
1         +A(57)*(R(1)+RGUST)+A(58)*DA+A(59)*DR
      R(1)=R(2)+DH*(RD(1)+RD(2))
      VD(1)=32.174*(COSTHO*COSTH*SINPHI
1               -SINTHO*(SINTH*SINPHI*COSPSI-COSPHI*SINPSI))
2         -R(1)*(A(75)+U(1))+P(1)*(A(76)+W(1))
3         +A(45)*(V(1)+VGUST)+A(46)*(P(1)+PGUST)+A(47)*(R(1)+RGUST)
4         +A(48)*DA+A(49)*DR
      V(1)=V(2)+DH*(VD(1)+VD(2))
      PD(1)=FI1*Q(1)*R(1)+A(50)*(V(1)+VGUST)+A(51)*(P(1)+PGUST)
1         +A(52)*(R(1)+RGUST)+A(53)*DA+A(54)*DR
      P(1)=P(2)+DH*(PD(1)+PD(2))
C
      THD(1)=Q(1)*COSPHI-R(1)*SINPHI
      TH(1)=TH(2)+DH*(THD(1)+THD(2))
      SINTH=SIN(TH(1))
      COSTH=COS(TH(1))
      PHID(1)=P(1)+(Q(1)*SINPHI+R(1)*COSPHI)*SINTH/COSTH
      PHI(1)=PHI(2)+DH*(PHID(1)+PHID(2))
      SINPHI=SIN(PHI(1))
      COSPHI=COS(PHI(1))
      PSID(1)=(R(1)*COSPHI+Q(1)*SINPHI)/COSTH
      PSI(1)=PSI(2)+DH*(PSID(1)+PSID(2))
      SINPSI=SIN(PSI(1))
      COSPSI=COS(PSI(1))
C
      ALPHA=ATAN2(W(1)+A(76),U(1)+A(75))
      BETA=ATAN2(V(1),U(1)+A(75))
C
      FL1=COSPSI*COSTH
      FL2=SINPSI*COSTH
      FL3=-SINTH
      FM1=COSPSI*SINTH*SINPHI-SINPSI*COSPHI
      FM2=SINPSI*SINTH*SINPHI+COSPSI*COSPHI
      FM3=COSTH*SINPHI
      FN1=COSPSI*SINTH*COSPHI+SINPSI*SINPHI
      FN2=SINPSI*SINTH*COSPHI-COSPSI*SINPHI
      FN3=COSTH*COSPHI
C
      VX=FL1*U(1)+FM1*V(1)+FN1*W(1)
      VY=FL2*U(1)+FM2*V(1)+FN2*W(1)
      VZ=FL3*U(1)+FM3*V(1)+FN3*W(1)
C*************************************************************************
C         TEST FOR DIVERGENCE
C*************************************************************************
      VAR(1)=U(1)
      VAR(2)=V(1)
```

```
      VAR(3)=W(1)
      VAR(4)=P(1)
      VAR(5)=Q(1)
      VAR(6)=R(1)
      VAR(7)=PHI(1)
      VAR(8)=TH(1)
      VAR(9)=PSI(1)
C
      DO 216 I=1,9
      IF(ABS(VAR(I)).LT.BOUND(I))GO TO 216
      CALL INOUT(3)
      NITER=ICOUNT
      GO TO 325
  216 CONTINUE
C***********************************************************************
C          COMMAND TRACKING SIGNAL GENERATION
C***********************************************************************
  218 IF (A(125).LT.1.E-5) GO TO 217
      RI(5,1)=RNUM(A,ISUM,85)
      IF (A(14).GE.0.) RF(5,1)=RI(5,1)
      IF (A(14).LT.0.) CALL PRE(A,5)
      CALL CTRACK(A,1)
      CTLAT=A(125)*(CT(1,1)-AV(5))/SD(5)
      CTLATD=(A(125)/SD(5))*(CT(1,1)-CT(1,2))/A(1)
  217 IF (A(129).LT.1.E-5) GO TO 220
      RI(6,1)=RNUM(A,ISUM,86)
      IF (A(14).GE.0.) RF(6,1)=RI(6,1)
      IF (A(14).LT.0.) CALL PRE(A,6)
      CALL CTRACK(A,2)
      CTLON=A(129)*(CT(2,1)-AV(6))/SD(6)
      CTLOND=(A(129)/SD(6))*(CT(2,1)-CT(2,2))/A(1)
C***********************************************************************
C          ERROR SIGNAL GENERATION
C***********************************************************************
  220 PHIE=CTLAT-PHI(1)
      PSIE=CTLAT-PSI(1)
      THE=CTLON-TH(1)
      PHIED=CTLATD-PHID(1)
      PSIED=CTLATD-PSID(1)
      THED=CTLOND-THD(1)
      ITR=A(5)-.1
      IF (ITR.LT.0) GO TO 213
      ERLAT=PHIE
      ERLATD=PHIED
      ERLON=THE
      ERLOND=THED
      GO TO 219
  213 IF (ITR.EQ.-2) GO TO 215
      ERLAT=PSIE
      ERLATD=PSIED
      ERLON=THE
      ERLOND=THED
      GO TO 219
  215 ERLAT=PSIE*COSPHI-THE*SINPHI
```

```
      ERLATD=(PSIED-PHID(1)*THE)*COSPHI-
     1        (THED+PHID(1)*PSIE)*SINPHI
      ERLON=PSIE*SINPHI+THE*COSPHI
      ERLOND=(PSIED-PHID(1)*THE)*SINPHI+
     1        (THED+PHID(1)*PSIE)*COSPHI
C****************************************************************************
C           URGENCY FUNCTION AND PILOT COMPENSATION CALCULATIONS
C****************************************************************************
 219  DELAY(1,1)=A(17)*(ERLAT+A(21)*ERLATD)
      IF (ITR.LT.0) DELAY(1,1)=A(19)*(ERLAT+A(23)*ERLATD)+
     1                             A(17)*(PHI(1)+A(21)*PHID(1))
      DELAY(2,1)=A(18)*(ERLON+A(22)*ERLOND)
      IF (ERLAT.EQ.0.) DELAY(3,1)=ABS(A(34)*ERLATD)
      IF (ERLAT.NE.0.) DELAY(3,1)=ABS(A(33)*ABS(ERLAT)+
     1                                  A(34)*ERLAT*ERLATD/ABS(ERLAT))
      IF (ERLON.EQ.0.) DELAY(4,1)=ABS(A(36)*ERLOND)
      IF (ERLON.NE.0.) DELAY(4,1)=ABS(A(35)*ABS(ERLON)+
     1                                  A(36)*ERLON*ERLOND/ABS(ERLON))
C
      UDLAT=DELAY(3,1)
      IF (A(31).LT.1.E-5) GO TO 240
      FIA=A(31)/A(1)+0.1-1.
      IA=1 + INT(FIA)
      FRAC=FIA -  FLOAT(IA-1)-0.1
      IF(IA.LE.49)GO TO 235
      CALL INOUT(4)
      GO TO 343
 235  UDLAT=DELAY(3,IA)+FRAC*(DELAY(3,IA+1)-DELAY(3,IA))
 240  UDLON=DELAY(4.1)
      IF (A(32).LT.1.E-5) GO TO 246
      FIA=A(32)/A(1)+0.1-1.
      IA=1 + INT(FIA)
      FRAC=FIA -  FLOAT(IA-1)-0.1
      IF(IA.LE.49)GO TO 245
      CALL INOUT(5)
      GO TO 343
 245  UDLON=DELAY(4.IA)+FRAC*(DELAY(4.IA+1)-DELAY(4,IA))
C****************************************************************************
C           CONTROL SWITCHING
C****************************************************************************
 246  IF (MSTP.EQ.0.AND.MSTR.EQ.0) GO TO 249
      IF (N.EQ.1) GO TO 247
      IF (NP.LT.MSTP) GO TO 320
      GO TO 285
 247  IF (NR.LT.MSTR) GO TO 320
      GO TO 250
 249  IF (ISIDE.EQ.1.AND.NS.LT.MINDT) GO TO 316
      IF (ISIDE.EQ.0.AND.NP.LT.MINDT.AND.NR.LT.MINDT) GO TO 320
      IF (UDLAT.LT.A(143).AND.UDLON.LT.A(143)) GO TO 316
      IF (UDLAT.EQ.UDLON) GO TO 320
      IF (UDLAT.GT.UDLON) GO TO 285
      GO TO 250
C
 320  NR=NR + N
```

```
      NP=NP - N + 1
      IF(N.EQ.1)GO TO 291
      IF(N.EQ.0)GO TO 256
      CALL INOUT(8)
      STOP
C***********************************************************************
C          LONGITUDINAL STICK CALCULATIONS
C***********************************************************************
 250  IF (ISIDE.EQ.1) GO TO 253
      IF(NR.EQ.0)GO TO 255
      NRTOT=NRTOT + NR
      NREP=NREP+1
      DO 251 I=1,2
      DLAG(1,I)=0.
 251  GLAG(1,I)=0.
      GO TO 255
 253  NSTOT=NSTOT+NS
      NSEP=NSEP+1
 255  N=0
      NP=NP+1
      NR=0
      NS=0
      ISIDE=0
 256  PCLON=DELAY(2,1)
      IF (A(30).LT.1.E-5) GO TO 265
      FIA=A(30)/A(1)+0.1-1.
      IA=1 + INT(FIA)
      FRAC=FIA -  FLOAT(IA-1)-0.1
      IF(IA.LE.49)GO TO 260
      CALL INOUT(6)
      GO TO 343
 260  PCLON=DELAY(2,IA)+FRAC*(DELAY(2,IA+1)-DELAY(2,IA))
 265  DLAG(2,1)=PCLON
      DA =0.
      IF (A(26).GT.1.E-5) CALL LAGOUT(A,2)
      IF (A(26).LE.1.E-5) GLAG(2.1)=DLAG(2.1)
      DE =GLAG(2,1)
      IF (A(138).LT.1.E-5) GO TO 325
      RI(8,1)=RNUM(A,ISUM,88)
      IF (A(15).GE.0.) RF(8,1)=RI(8,1)
      IF (A(15).LT.0.) CALL PRE(A,8)
      DE =DE +A(138)*RF(8,1)
      GO TO 325
C***********************************************************************
C          LATERAL STICK CALCULATIONS
C***********************************************************************
 285  IF (ISIDE.EQ.1) GO TO 288
      IF(NP.EQ.0)GO TO 290
      NPTOT=NPTOT + NP
      NPEP=NPEP+1
      DO 286 I=1,2
      DLAG(2.I)=0.
 286  GLAG(2,I)=0.
      GO TO 290
```

```
 288   NSTOT=NSTOT+NS
       NSEP=NSEP+1
 290   N=1
       NR=NR + 1
       NP=0
       NS=0
       ISIDE=0
 291   PCLAT=DELAY(1,1)
       IF (A(29).LT.1.E-5) GO TO 300
       FIA=A(29)/A(1)+0.1-1.
       IA=1 + INT(FIA)
       FRAC=FIA -  FLOAT(IA-1)-0.1
       IF(IA.LE.49)GO TO 295
       CALL INOUT(7)
       GO TO 343
 295   PCLAT=DELAY(1,IA)+FRAC*(DELAY(1,IA+1)-DELAY(1,IA))
 300   DLAG(1,1)=PCLAT
       DE =0.
       IF (A(25).GT.1.E-5) CALL LAGOUT(A,1)
       IF (A(25).LE.1.E-5) GLAG(1.1)=DLAG(1.1)
       DA =GLAG(1,1)
       IF (A(137).LT.1.E-5) GO TO 325
       RI(7.1)=RNUM(A.ISUM.87)
       IF (A(15).GE.0.) RF(7,1)=RI(7,1)
       IF (A(15).LT.0.) CALL PRE(A,7)
       DA =DA +A(137)*RF(7,1)
       GO TO 325
C*************************************************************************
C          SIDE TASK CALCULATIONS
C*************************************************************************
 316   IF (ISIDE.EQ.1) GO TO 318
       DO 317 I=1,2
       DO 317 J=1,2
       DLAG(I,J)=0.
 317   GLAG(I,J)=0.
       NRTOT=NRTOT+NR
       NPTOT=NPTOT+NP
       NREP=NREP+N
       NPEP=NPEP-N+1
 318   ISIDE=1
       NS=NS+1
       NR=0
       NP=0
       DA=0.
       DE=0.
C*************************************************************************
C          COLLECTION OF STATISTICS
C*************************************************************************
 325   VAR(10)=ALPHA
       VAR(11)=BETA
       VAR(12)=UGUST
       VAR(13)=VGUST
       VAR(14)=WGUST
       VAR(15)=PGUST
```

```
      VAR(16)=QGUST
      VAR(17)=RGUST
      VAR(18)=CTLAT
      VAR(19)=CTLON
      VAR(20)=ERLAT
      VAR(21)=ERLON
      VAR(22)=SQRT((A(33)*ERLAT)**2+(A(35)*ERLON)**2)
      VAR(23)=DA
      VAR(24)=DE
      VAR(25)=DR
C
      ICOUNT=ICOUNT + 1
      COUNT= FLOAT(ICOUNT)
C
      DO 326 I=1,24
      N1=A(100+I)+.1
      IF (N1.EQ.0) GO TO 326
      SUM1(I)=SUM1(I)+VAR(N1)
      SUM2(I)=SUM2(I)+VAR(N1)**2
      SUM3(I)=SUM3(I)+VAR(N1)**3
      SUM4(I)=SUM4(I)+VAR(N1)**4
 326  CONTINUE
      IF(NITER.LE.ICOUNT)GO TO 334
C*****************************************************************************
C          TABLE SHIFTING
C*****************************************************************************
      UD(2)=UD(1)
      U(2)=U(1)
      VD(2)=VD(1)
      V(2)=V(1)
      WD(2)=WD(1)
      W(2)=W(1)
      PD(2)=PD(1)
      P(2)=P(1)
      QD(2)=QD(1)
      Q(2)=Q(1)
      RD(2)=RD(1)
      R(2)=R(1)
      PHID(2)=PHID(1)
      PHI(2)=PHI(1)
      THD(2)=THD(1)
      TH(2)=TH(1)
      PSID(2)=PSID(1)
      PSI(2)=PSI(1)
C
      DO 336 K=1,4
      DO 336 I=1,49
      J=51 - I
 336  DELAY(K,J)=DELAY(K,J-1)
      DO 337 I=1,4
      DLAG(I,2)=DLAG(I,1)
 337  GLAG(I,2)=GLAG(I,1)
      DO 338 I=1,8
      RI(I,3)=RI(I,2)
```

```
      RI(I,2)=RI(I,1)
      RF(I,3)=RF(I,2)
  338 RF(I,2)=RF(I,1)
      DO 339 I=1,2
      CT(I,3)=CT(I,2)
  339 CT(I,2)=CT(I,1)
C
      GO TO 190
C***********************************************************************
C          CALCULATION OF OUTPUT QUANTITIES
C***********************************************************************
  334 DFLAT= FLOAT(NR+NRTOT)/COUNT
      DFLON= FLOAT(NP+NPTOT)/COUNT
      DFSIDE=FLOAT(NS+NSTOT)/COUNT
      IF (NPEP.NE.0) FMSTP=A(1)*FLOAT(NPTOT)/FLOAT(NPEP)
      IF (NREP.NE.0) FMSTR=A(1)*FLOAT(NRTOT)/FLOAT(NREP)
      IF (NSEP.NE.0) FMSTS=A(1)*FLOAT(NSTOT)/FLOAT(NSEP)
      CALL INOUT(9)
C
      JTITLE=0
      DO 341 I=1,24
      NI=A(100+I)+.1
      IF (NI.EQ.0) GO TO 341
      AVGI=0.
      RMSI=0.
      STDI=0.
      SKWI=0.
      PKDI=0.
      AVGI=SUM1(I)/COUNT
      RMSI=SQRT(SUM2(I)/COUNT)
      STDI=SQRT(SUM2(I)/COUNT-AVGI**2)
      IF (STDI.EQ.0.) GO TO 342
      SKWI=(SUM3(I)-3.*AVGI*SUM2(I)+2.*SUM1(I)*AVGI**2)/
     1     (COUNT*STDI**3)
      PKDI=(SUM4(I)-4.*AVGI*SUM3(I)+6.*SUM2(I)*AVGI**2-
     1     3.*SUM1(I)*AVGI**3)/(COUNT*STDI**4)
  342 IF (JTITLE.NE.0) GO TO 340
      JTITLE=1
      CALL INOUT(10)
  340 CONTINUE
      CALL INOUT(11)
  341 CONTINUE
      CALL INOUT(2)
C
  343 DO 345 I=1,20
  345 A(80+I)=AH(I)+A(9)
C
  500 CONTINUE
      CALL INOUT(2)
      GO TO 20
      END
*DECK CLEAR
C***********************************************************************
      SUBROUTINE CLEAR
```

```
C***************************************************************************
      COMMON/SYSCOM/A(200),DFLAT,DFLON,DFSIDE,FMSTR,FMSTP,FMSTS,
     1              AVGI,STDI,RMSI,SKWI,PKDI,N1,ICOUNT
      COMMON/EOM/UD(2),U(2),VD(2),V(2),WD(2),W(2),PD(2),P(2),QD(2),Q(2),
     1           RD(2),R(2),PHID(2),PHI(2),THD(2),TH(2),PSID(2),PSI(2)
      COMMON/RANDOM/RI(8,3),RF(8,3)
      COMMON/GUSTS/UGUST,VGUST,WGUST,PGUST,QGUST,RGUST
      COMMON/TRACK/CT(2,3),CTLAT,CTLON,CTLATD,CTLOND
      COMMON/STATS/VAR(25),SUM1(24),SUM2(24),SUM3(24),SUM4(24)
      COMMON/DELAYS/DELAY(4,50)
      COMMON/DWELL/N,NR,NP,NS,NREP,NPEP,NSEP,NRTOT,NPTOT,NSTOT,
     1             ISIDE,MINDT,MSTR,MSTP
      COMMON/LAGS/DLAG(4,2),GLAG(4,2)
      COMMON/SCALE/AV(6),SD(6)
      COMMON/STICK/DA,DE,DR,DEAUG,DRAUG
      COMMON/INIT/AH(20),SINPHI,COSPHI,SINTH,COSTH,SINPSI,COSPSI,
     1             SINTHO,COSTHO,FI1,FI2,FI3,DH,NITER,ISUM
C
      DA=0.
      DE=0.
      DR=0.
      DEAUG=0.
      DRAUG=0.
      FMSTP = 0.
      FMSTR = 0.
      FMSTS = 0.
      N=0
      IF (A(35).LT.1.E-5.AND.A(36).LT.1.E-5) N=1
      IF (A(141).LT.0.) N=1
      NR=0
      NP=0
      NS=0
      NPEP=0
      NREP=0
      NSEP=0
      NRTOT=0
      NPTOT=0
      NSTOT=0
      ISIDE=0
      ICOUNT=0
      DO 1 I=1,4
      DO 1 J=1,50
    1 DELAY(I,J)=0.
      DO 2 I=1,25
    2 VAR(I)=0.
      DO 3 I=1,2
      UD(I)=0.
      U(I)=0.
      VD(I)=0.
      V(I)=0.
      WD(I)=0.
      W(I)=0.
      PD(I)=0.
      P(I)=0.
```

THIS PAGE IS BEST QUALITY PRACTICABLE
FROM COPY FURNISHED TO DDC

```
      QD(I)=0.
      Q(I)=0.
      RD(I)=0.
      R(I)=0.
      PHID(I)=0.
      PHI(I)=0.
      THD(I)=0.
      TH(I)=0.
      PSID(I)=0.
    3 PSI(I)=0.
      DO 4 I=1,24
      SUM1(I)=0.
      SUM2(I)=0.
      SUM3(I)=0.
    4 SUM4(I)=0.
      DO 5 I=1,6
      AV(I)=0.
    5 SD(I)=1.
      DO 6 I=1,20
    6 AH(I)=A(80+I)
      MINDT=A(27)/A(1)+.1
      MSTP=A(142)/A(1)+.1
      MSTR=ABS(A(141))/A(1)+.1
      NITER=A(2)+.1
      DH=A(1)/2.
      ISUM=A(3)+.1
      SINPHI=0.
      COSPHI=1.
      SINTH=0.
      COSTH=1.
      SINPSI=0.
      COSPSI=1.
      SINTHO=SIN(A(80)/57.295779513)
      COSTHO=COS(A(80)/57.295779513)
      FI1=(A(78)-A(79))/A(77)
      FI2=(A(79)-A(77))/A(78)
      FI3=(A(77)-A(78))/A(79)
      CALL PREFIL(A,0)
      CALL GUST(A)
      CALL COMTRK(A,0)
      CALL LAG(A,0)
      IF (A(193).LT.0.) CALL AUGMNT(A,Q,R)
      RETURN
      END
*DECK PRECOM
C***********************************************************************
      SUBROUTINE PRECOM(A)
C***********************************************************************
      DIMENSION A(200),ASAVE(20)
      COMMON/RANDOM/RI(8,3),RF(8,3)
      COMMON/GUSTS/UGUST,VGUST,WGUST,PGUST,QGUST,RGUST
      COMMON/TRACK/CT(2,3),CTLAT,CTLON,CTLATD,CTLOND
      COMMON/SCALE/AV(6),SD(6)
C
```

```
      ISUM=A(3)+.1
      NITER=A(2)+.1
      DO 5 I=1,20
    5 ASAVE(I)=A(80+I)
      IF (A(6).LT.O.) GO TO 22
      DO 20 I=1,4
      IF (A(36+I).LT.1.E-5) GO TO 20
      SUM1=0.
      SUM2=0.
      IGAM=80+I
      DO 18 J=1,NITER
      RI(I,1)=RNUM(A,ISUM,IGAM)
      IF (A(13).GE.0.) RF(I,1)=RI(I,1)
      IF (A(13).LT.0.) CALL PRE(A,I)
      GO TO (11,12,13,14), I
   11 CALL GUSTU(A)
      G=UGUST
      GO TO 15
   12 CALL GUSTV(A)
      G=VGUST
      GO TO 15
   13 CALL GUSTW(A)
      G=WGUST
      GO TO 15
   14 CALL GUSTP(A)
      G=PGUST
   15 SUM1=SUM1+G
      SUM2=SUM2+G*G
      DO 18 II=1,8
      RI(II,3)=RI(II,2)
      RI(II,2)=RI(II,1)
      RF(II,3)=RF(II,2)
   18 RF(II,2)=RF(II,1)
      AV(I)=SUM1/FLOAT(NITER)
      SD(I)=SQRT(SUM2/FLOAT(NITER)-AV(I)**2)
   20 CONTINUE
   22 DO 30 I=1,2
      IF (A(121+4*I).LT.1.E-5) GO TO 30
      SUM1=0.
      SUM2=0.
      J=I+4
      IGAM=80+J
      DO 25 K=1,NITER
      RI(J,1)=RNUM(A,ISUM,IGAM)
      IF (A(14).GE.0.) RF(J,1)=RI(J,1)
      IF (A(14).LT.0.) CALL PRE(A,J)
      CALL CTRACK(A,I)
      SUM1=SUM1+CT(I,1)
      SUM2=SUM2+CT(I,1)**2
      DO 24 II=1,8
      RI(II,3)=RI(II,2)
      RI(II,2)=RI(II,1)
      RF(II,3)=RF(II,2)
   24 RF(II,2)=RF(II,1)
```

```
      DO 25 II=1,2
      CT(II,3)=CT(II,2)
   25 CT(II,2)=CT(II,1)
      AV(J)=SUM1/FLOAT(NITER)
      SD(J)=SQRT(SUM2/FLOAT(NITER)-AV(J)**2)
   30 CONTINUE
      DO 40 I=1,10
   40 A(80+I)=ASAVE(I)
      CALL PREFIL(A,0)
      CALL GUST(A)
      CALL COMTRK(A,0)
      RETURN
      END
*DECK RNUM
C***********************************************************************
      FUNCTION RNUM(A,K,J)
C***********************************************************************
      DIMENSION A(200)
C
      PI=3.14159265359
      RNUM=0.
      DO 1 I=1,K
      ATOM=(A(J)+PI)**5
      Z=ATOM-INT(ATOM)
      A(J)=Z
    1 RNUM=RNUM+Z
      RNUM=RNUM/FLOAT(K)-0.5
      RETURN
      END
*DECK PREFIL
C***********************************************************************
      SUBROUTINE PREFIL(A,K)
C***********************************************************************
      DIMENSION A(200)
      COMMON/RANDOM/RI(8,3),RF(8,3)
C
      DT=A(12)*A(1)
      DELT=4.+4.*DT+DT*DT
      A0=4./DELT
      B1=(8.-2.*DT*DT)/DELT
      B2=(-4.+4.*DT-DT*DT)/DELT
      DO 1 I=1,8
      DO 1 J=1,3
      RI(I,J)=0.
    1 RF(I,J)=0.
      RETURN
C
      ENTRY PRE
      RF(K,1)=A0*(RI(K,1)-2.*RI(K,2)+RI(K,3))+B1*RF(K,2)+B2*RF(K,3)
      RETURN
      END
*DECK GUST
C***********************************************************************
      SUBROUTINE GUST(A)
```

```
C*********************************************************************************
      DIMENSION A(200)
      COMMON/RANDOM/RI(8,3),RF(8,3)
      COMMON/GUSTS/UGUST,VGUST,WGUST,PGUST,QGUST,RGUST
C
      T=A(1)
      T2=T*T
      VO=SQRT(A(75)**2+A(76)**2)
      FLV=A(41)/VO
      FLV2=FLV**2
      BPV=A(42)/(VO*3.14159265359)
      R32=3.464101615
      DELT=2.*FLV+T
      AU=T/DELT
      BU=(2.*FLV-T)/DELT
      DELT=8.*BPV+T
      AP=T/DELT
      BP=(8.*BPV-T)/DELT
      AQ=(2./VO)/DELT
      BQ=BP
      DELT=6.*BPV+T
      AR=(-2./VO)/DELT
      BR=(6.*BPV-T)/DELT
      DELT=4.*FLV2+4.*FLV*T+T2
      A0=(R32*FLV*T+T2)/DELT
      A1=2.*T2/DELT
      A2=(-R32*FLV*T+T2)/DELT
      B1=(8.*FLV2-2.*T2)/DELT
      B2=(-4.*FLV2+4.*FLV*T-T2)/DELT
      UGUST=0.
      VGUST=0.
      WGUST=0.
      PGUST=0.
      QGUST=0.
      RGUST=0.
      UGO=0.
      VGO=0.
      VG1=0.
      WGO=0.
      WG1=0.
      PGO=0.
      QGO=0.
      WQO=0.
      RGO=0.
      VRO=0.
      RETURN
C
      ENTRY GUSTU
      UG1=UGO
      RNO=RF(1,1)
      RN1=RF(1,2)
      UGO=AU*(RNO+RN1)+BU*UG1
      UGUST=UGO
      RETURN
```

```
C
      ENTRY GUSTV
      VG2=VG1
      VG1=VG0
      RN0=RF(2,1)
      RN1=RF(2,2)
      RN2=RF(2,3)
      VG0=A0*RN0+A1*RN1+A2*RN2+B1*VG1+B2*VG2
      VGUST=VG0
      RETURN
C
      ENTRY GUSTW
      WG2=WG1
      WG1=WG0
      RN0=RF(3,1)
      RN1=RF(3,2)
      RN2=RF(3,3)
      WG0=A0*RN0+A1*RN1+A2*RN2+B1*WG1+B2*WG2
      WGUST=WG0
      RETURN
C
      ENTRY GUSTP
      PG1=PG0
      RN0=RF(4,1)
      RN1=RF(4,2)
      PG0=AP*(RN0+RN1)+BP*PG1
      PGUST=PG0
      RETURN
C
      ENTRY GUSTQ
      QG1=QG0
      WQ1=WQ0
      WQ0=WGUST
      QG0=AQ*(WQ0-WQ1)+BQ*QG1
      QGUST=QG0
      RETURN
C
      ENTRY GUSTR
      RG1=RG0
      VR1=VR0
      VR0=VGUST
      RG0=AR*(VR0-VR1)+BR*RG1
      RGUST=RG0
      RETURN
      END
*DECK COMTRK
C***********************************************************************
      SUBROUTINE COMTRK(A,L)
C***********************************************************************
      DIMENSION A(200),A0(2),A1(2),A2(2),B1(2),B2(2)
      COMMON/RANDOM/RI(8,3),RF(8,3)
      COMMON/TRACK/CT(2,3),CTLAT,CTLON,CTLATD,CTLOND
C
      T=A(1)
```

```
      DO 5 I=1,2
      J=126+4*(I-1)
      AA=A(J)
      EE=A(J+1)
      BB=A(J+2)
      DELT=4.*BB*BB+4.*BB*T+T*T
      A0(I)=(2.*AA*T+EE*T*T)/DELT
      A1(I)=(2.*EE*T*T)/DELT
      A2(I)=(-2.*AA*T+EE*T*T)/DELT
      B1(I)=(8.*BB*BB-2.*T*T)/DELT
      B2(I)=(-4.*BB*BB+4.*BB*T-T*T)/DELT
      DO 5 K=1,3
    5 CT(I,K)=0.
      CTLAT=0.
      CTLON=0.
      CTLATD=0.
      CTLOND=0.
      RETURN
C
      ENTRY CTRACK
      J=L+4
      CT(L,1)=A0(L)*RF(J,1)+A1(L)*RF(J,2)+A2(L)*RF(J,3)
     1                      +B1(L)*CT(L,2)+B2(L)*CT(L,3)
      RETURN
      END
*DECK LAG
C*************************************************************************
      SUBROUTINE LAG(A,K)
C*************************************************************************
      DIMENSION A(200),A0(4),B1(4)
      COMMON/LAGS/DLAG(4,2),GLAG(4,2)
C
      T=A(1)
      DO 5 I=1,4
      TAU=A(24+I)
      IF (I.GT.2) TAU=A(130+I)
      DELT=2.*TAU+T
      A0(I)=T/DELT
      B1(I)=(2.*TAU-T)/DELT
      DO 5 J=1,2
      DLAG(I,J)=0.
    5 GLAG(I,J)=0.
      RETURN
C
      ENTRY LAGOUT
      GLAG(K,1)=A0(K)*(DLAG(K,1)+DLAG(K,2))+B1(K)*GLAG(K,2)
      RETURN
      END
*DECK AUGMNT
C*************************************************************************
      SUBROUTINE AUGMNT(A,Q,R)
C*************************************************************************
      DIMENSION A(200),Q(2),R(2)
      COMMON/STICK/DA,DE,DR,DEAUG,DRAUG
```

```
C
      DELT=1.+A(1)
      RA=1./DELT
      RB=(1.-A(1))/DELT
      DELT=.16+A(1)
      EA=.16/DELT
      EB=(.16-A(1))/DELT
      R2=0.
      DR2=0.
      Q2=0.
      DE2=0.
      RETURN
C
      ENTRY AUG
      R1=R(1)
      DR1=RA*(R1-R2)+RB*DR2
      DRAUG=DR1*A(196)
      DR2=DR1
      R2=R1
C
      Q1=Q(1)
      DE1=EA*(Q1-Q2)+EB*DE2
      DEAUG=DE1*A(194)+Q1*A(195)
      DE2=DE1
      Q2=Q1
      RETURN
      END
*DECK REEVES
C*************************************************************************
      SUBROUTINE REEVES(A)
C*************************************************************************
      DIMENSION A(200),AV(6),SD(6),ASAVE(9),RN(9,3),GC(9,3),
     1          S1X(3),S2X(3),S1YZ(3),S2YZ(3),SXYZ(3)
      COMMON/GUSTS/UGUST,VGUST,WGUST,PGUST,QGUST,RGUST
C
      FILT1(RO,R1,G1)=A10*(RO+R1)+B11*G1
      FILT2(RO,R1,G1)=A20*(RO+R1)+B21*G1
      FILT3(RO,R1,G1,G2)=A30*(RO-R1)+B31*G1+B32*G2
      FILT4(RO,R1,R2,G1,G2)=A40*RO+A41*R1+A42*R2+B41*G1+B42*G2
C
      T=A(1)
      ISUM=A(3)+.1
      NITER=A(2)+.1
      FL=A(41)/SQRT(A(75)**2+A(76)**2)
      FL3=FL*SQRT(3.)
      DELT=2.*FL+T
      A10=T/DELT
      B11=(2.*FL-T)/DELT
      DELT=4.*FL+T
      A20=T/DELT
      B21=(4.*FL-T)/DELT
      DELT=16.*FL*FL+8.*FL*T+T*T
      A30=2.*T/DELT
      B31=(32.*FL*FL-2.*T*T)/DELT
```

```
      B32=(-16.*FL*FL+8.*FL*T-T*T)/DELT
      DELT=4.*FL*FL+4.*FL*T+T*T
      A40=(2.*T*FL3+T*T)/DELT
      A41=2.*T*T/DELT
      A42=(-2.*T*FL3+T*T)/DELT
      B41=(8.*FL*FL-2.*T*T)/DELT
      B42=(-4.*FL*FL+4.*FL*T-T*T)/DELT
C
      DO 1 I=1,9
      ASAVE(I)=A(90+I)
      DO 1 J=1,3
      RN(I,J)=0.
    1 GC(I,J)=0.
      DO 3 I=1,3
      S1X(I)=0.
      S2X(I)=0.
      S1YZ(I)=0.
      S2YZ(I)=0.
    3 SXYZ(I)=0.
      DO 4 I=1,6
      AV(I)=0.
    4 SD(I)=1.
C
      DO 20 IT=1,NITER
      DO 10 I=1,9
   10 RN(I,1)=RNUM(A,ISUM,90+I)
      GC(1,1)=FILT1(RN(1,1),RN(1,2),GC(1,2))
      GC(2,1)=FILT2(RN(2,1),RN(2,2),GC(2,2))
      GC(3,1)=FILT2(RN(3,1),RN(3,2),GC(3,2))
      GC(4,1)=FILT1(RN(4,1),RN(4,2),GC(4,2))
      GC(5,1)=FILT2(RN(5,1),RN(5,2),GC(5,2))
      GC(6,1)=FILT2(RN(6,1),RN(6,2),GC(6,2))
      GC(7,1)=FILT4(RN(7,1),RN(7,2),RN(7,3),GC(7,2),GC(7,3))
      GC(8,1)=FILT2(RN(8,1),RN(8,2),GC(8,2))
      GC(9,1)=FILT3(RN(9,1),RN(9,3),GC(9,2),GC(9,3))
      DO 15 I=1,3
      J=3*I-2
      S1X(I)=S1X(I)+GC(J,1)
      S2X(I)=S2X(I)+GC(J,1)**2
      S1YZ(I)=S1YZ(I)+GC(J+1,1)*GC(J+2,1)
      S2YZ(I)=S2YZ(I)+(GC(J+1,1)*GC(J+2,1))**2
   15 SXYZ(I)=SXYZ(I)+GC(J,1)*GC(J+1,1)*GC(J+2,1)
      DO 20 I=1,9
      RN(I,3)=RN(I,2)
      RN(I,2)=RN(I,1)
      GC(I,3)=GC(I,2)
   20 GC(I,2)=GC(I,1)
      COUNT=FLOAT(NITER)
      J=0
      DO 30 I=1,5,2
      J=J+1
      AV(I)=S1X(J)/COUNT
   30 SD(I)=SQRT(S2X(J)/COUNT-AV(I)**2)
      J=0
```

```
      DO 35 I=2,6,2
      J=J+1
      AV(I)=S1YZ(J)/COUNT
   35 SD(I)=SQRT(S2YZ(J)/COUNT-AV(I)**2)
      DO 40 I=1,9
      A(90+I)=ASAVE(I)
      DO 40 J=1,3
      RN(I,J)=0.
   40 GC(I,J)=0.
      RETURN
C
      ENTRY GUSTUR
      DO 70 I=1,3
   70 RN(I,1)=RNUM(A,ISUM,90+I)
      GC(1,1)=FILT1(RN(1,1),RN(1,2),GC(1,2))
      GC(2,1)=FILT2(RN(2,1),RN(2,2),GC(2,2))
      GC(3,1)=FILT2(RN(3,1),RN(3,2),GC(3,2))
      UGUST=(GC(1,1)-AV(1))/SD(1)+(GC(2,1)*GC(3,1)-AV(2))/SD(2)
      SCL=SQRT(2.+2.*(SXYZ(1)/COUNT-AV(1)*AV(2))/(SD(1)*SD(2)))
      UGUST=UGUST*A(37)/SCL
      DO 75 I=1,3
      RN(I,3)=RN(I,2)
      RN(I,2)=RN(I,1)
      GC(I,3)=GC(I,2)
   75 GC(I,2)=GC(I,1)
      RETURN
C
      ENTRY GUSTVR
      DO 80 I=4,6
   80 RN(I,1)=RNUM(A,ISUM,90+I)
      GC(4,1)=FILT1(RN(4,1),RN(4,2),GC(4,2))
      GC(5,1)=FILT2(RN(5,1),RN(5,2),GC(5,2))
      GC(6,1)=FILT2(RN(6,1),RN(6,2),GC(6,2))
      VGUST=(GC(4,1)-AV(3))/SD(3)+(GC(5,1)*GC(6,1)-AV(4))/SD(4)
      SCL=SQRT(2.+2.*(SXYZ(2)/COUNT-AV(3)*AV(4))/(SD(3)*SD(4)))
      VGUST=VGUST*A(38)/SCL
      DO 85 I=4,6
      RN(I,3)=RN(I,2)
      RN(I,2)=RN(I,1)
      GC(I,3)=GC(I,2)
   85 GC(I,2)=GC(I,1)
      RETURN
C
      ENTRY GUSTWR
      DO 90 I=7,9
   90 RN(I,1)=RNUM(A,ISUM,90+I)
      GC(7,1)=FILT4(RN(7,1),RN(7,2),RN(7,3),GC(7,2),GC(7,3))
      GC(8,1)=FILT2(RN(8,1),RN(8,2),GC(8,2))
      GC(9,1)=FILT3(RN(9,1),RN(9,3),GC(9,2),GC(9,3))
      WGUST=(GC(7,1)-AV(5))/SD(5)+(GC(8,1)*GC(9,1)-AV(6))/SD(6)
      SCL=SQRT(2.+2.*(SXYZ(3)/COUNT-AV(5)*AV(6))/(SD(5)*SD(6)))
      WGUST=WGUST*A(39)/SCL
      DO 95 I=7,9
      RN(I,3)=RN(I,2)
```

```
      RN(I,2)=RN(I,1)
      GC(I,3)=GC(I,2)
   95 GC(I,2)=GC(I,1)
      RETURN
      END
*DECK INOUT
C*****************************************************************************
      SUBROUTINE INOUT(I)
C*****************************************************************************
      DIMENSION L(4),T(4),VARNAM(50),YN(2)
      COMMON/SYSCOM/A(200),DFLAT,DFLON,DFSIDE,FMSTR,FMSTP,FMSTS,
     1               AVGI,STDI,RMSI,SKWI,PKDI,N1,ICOUNT
      DATA VARNAM/4H   U,4H    ,4H   V,4H    ,4H   W,4H    ,
     1            4H   P,4H    ,4H   Q,4H    ,4H   R,4H    ,
     2            4H   P,4HHI  ,4H  TH,4HETA ,4H   P,4HSI  ,
     3            4H  AL,4HPHA ,4H  BE,4HTA  ,4H U G,4HUST ,
     4            4H V G,4HUST ,4H W G,4HUST ,4H P G,4HUST ,
     5            4H Q G,4HUST ,4H R G,4HUST ,4H LAT,4H CT ,
     6            4H LON,4H CT ,4H LAT,4H ERR,4H LON,4H ERR,
     7            4H RAD,4H ERR,4H   D,4HA   ,4H   D,4HE   ,
     8            4H   D,4HR    /
      DATA YN/4H YES,4H NO /
C
      GO TO (1,2,3,4,5,6,7,8,9,10,11,12),I
    1 CONTINUE
      WRITE(2,201)
  201 FORMAT(1H1)
      IF (A(125).LT.1.E-5.AND.A(129).LT.1.E-5) WRITE(2,2001)
 2001 FORMAT(20X,*++++  PHI-THETA ATTITUDE STABILIZATION  ++++*/)
      ITR=A(5)-.1
      IF ((A(125).GT.1.E-5.OR.A(129).GT.1.E-5).AND.ITR.EQ.0)
     1         WRITE(2,2101)
 2101 FORMAT(15X,*++++  PHI-THETA COMMAND TRACKING (COMPENSATORY)  ++++*/)
      IF (ITR.EQ.-1) WRITE(2,2201)
 2201 FORMAT(15X,*++++  PSI-THETA COMMAND TRACKING (COMPENSATORY)  ++++*/)
      IF (ITR.EQ.-2) WRITE(2,2301)
 2301 FORMAT(18X,*++++  PSI-THETA COMMAND TRACKING (PURSUIT)  ++++*/)
      NUMIT=A(2)+.2
      JSUM=A(3)+.1
      WRITE(2,101) A(1),NUMIT,JSUM
  101 FORMAT(* FRAME TIME =*,F5.3,5X,*ITERATIONS =*,I5,5X,
     1       *RANDOM NUMBERS SUMMED =*,I3/)
      WRITE(2,301)
  301 FORMAT(18X,*++++  LONGITUDINAL STABILITY DERIVATIVES  ++++*)
      WRITE(2,401) (A(K),K=60,74)
  401 FORMAT(* XU=*,1PD10.3,*   XW=*,D10.3,*   XWD=*,D10.3,*   XQ=*,
     1       D10.3,*  XDE=*,D10.3/* ZU=*,D10.3,*   ZW=*,D10.3,*   ZWD=*
     2       ,D10.3,*   ZQ=*,D10.3,*   ZDE=*,D10.3/* MU=*,D10.3,*   MW=*
     3       ,D10.3,*   MWD=*,D10.3,*   MQ=*,D10.3,*   MDE=*,D10.3/)
      WRITE(2,501)
  501 FORMAT(21X,*++++  LATERAL STABILITY DERIVATIVES  ++++*)
      WRITE(2,601) (A(K),K=45,55)
  601 FORMAT(* YV=*,1PD10.3,*   YP=*,D10.3,*   YR=*,D10.3,*   YDA=*,
     1       D10.3,*  YDR=*,D10.3/* LV=*,D10.3,*   LP=*,D10.3,*   LR=*,
```

```
2        D10.3,*   LDA=*,D10.3,*   LDR=*,D10.3/* NV=*,D10.3,*   NP=*
3        ,D10.3,*   NR=*,D10.3,*    NDA=*,D10.3,*   NDR=*,D10.3/)
     WRITE(2,701) A(80),A(75),A(76)
701  FORMAT(* THETA0=*,F5.2,* DEG*,5X,*U0=*,F6.1,* FT/SEC*,5X,*W0=*,
1        F6.1,* FT/SEC*/)
     WRITE(2,801) A(77),A(78),A(79)
801  FORMAT(* IXX =*,1PD10.3,4X,*IYY =*,D10.3,4X,*IZZ =*,D10.3,4X,
1        14H(FT-LB-SEC**2)/)
     IF (A(125).GT.1.E-5.OR.A(129).GT.1.E-5) WRITE(2,901)
1                                           (A(K),K=125,132)
901  FORMAT(* COMMAND TRACKING FILTERS*,7X,*K*,11X,*A*,11X,*E*,11X,
1        *B*/12X,*LATERAL*,6X,4(3X,1PD9.2)/12X,*LONGITUDINAL *,
2        4(3X,1PD9.2)/)
     IF (A(14).LT.0.) WRITE(2,1001) A(12)
1001 FORMAT(* COMMAND TRACKING PREFILTER   +++  D =*,F4.2/)
     IF (A(37).LT.1.E-5.AND.A(38).LT.1.E-5.AND.A(39).LT.1.E-5.AND.
1       A(40).LT.1.E-5) GO TO 9901
     IF (A(6).GE.0.) WRITE(2,1101) (A(K),K=37,40)
1101 FORMAT(* DRYDEN GUST GAINS  ++  U=*,1PD9.2,3X,*V=*,D9.2,3X,
1        *W=*,D9.2,3X,*P=*,D9.2/)
     IF (A(6).LT.0.) WRITE(2,1501) A(37),A(38),A(39)
1501 FORMAT(* REEVES GUST GAINS  ++  U=*,1PD9.2,3X,*V=*,D9.2,3X,
1        *W=*,D9.2/)
     VQG=YN(2)
     IF (A(43).LT.0.) VQG=YN(1)
     VRG=YN(2)
     IF (A(44).LT.0.) VRG=YN(1)
     IF (VQG.EQ.YN(1).OR.VRG.EQ.YN(1).OR.A(40).GT.1.E-5)
1        WRITE(2,1201) VQG,VRG,A(42)
1201 FORMAT(* QGUST? *,A4,4X,*RGUST? *,A4,6X,*WINGSPAN =*,F6.1,* FT*/)
     WRITE(2,1301) A(41)
1301 FORMAT(* SCALE LENGTH =*,F7.1,* FT*/)
     IF (A(13).LT.0.) WRITE(2,1401) A(12)
1401 FORMAT(* GUST PREFILTER   +++  D =*,F4.2/)
9901 CONTINUE
     WRITE(2,1601) A(17),A(18),A(19),A(21),A(22),A(23),A(25),A(26),
1                  A(29),A(30),A(31),A(32),A(33),A(35),A(34),A(36),
2                  A(137),A(138)
1601 FORMAT(* PILOT MODEL PARAMETERS*,5X,*LATERAL*,4X,*LONGITUDINAL*,
1        3X,*HEADING*/3X,*PILOT GAIN*,10X,3(4X,1PD9.2)/3X,
2        *PILOT LEAD*,10X,3(4X,D9.2)/3X,*PILOT LAG*,11X,2(4X,D9.2)/
3        3X,*PILOT DELAY*,9X,2(4X,D9.2)/3X,*URGENCY DELAY*,7X,
4        2(4X,D9.2)/3X,*ALPHA*,15X,2(4X,D9.2)/3X,*BETA*,16X,
5        2(4X,D9.2)/3X,*REMNANT GAIN*,8X,2(4X,D9.2)/)
     IF (A(198).GE.0..AND.A(15).LT.0.) WRITE(2,1701) A(12)
1701 FORMAT(* REMNANT PREFILTER   +++  D =*,F4.2/)
     IF (A(143).GT.1.E-5) WRITE(2,2401) A(143)
2401 FORMAT(* SIDE TASK URGENCY = *,F7.4/)
     IF (A(193).LT.0.) WRITE(2,1801) A(194),A(195),A(196)
1801 FORMAT(* AUGMENTER GAINS   ++++*,4X,*KA =*,F7.3,4X,*KV =*,F7.3,4X,
1        *KY =*,F7.3/)
     IF (A(133).GT.1.E-5.OR.A(134).GT.1.E-5) WRITE(2,1901) A(133),
1                                                         A(134)
1901 FORMAT(* CONTROL SYSTEM LAGS  +++     LATERAL =*,F6.3,5X,
```

```
 1        *LONGITUDINAL =*,F6.3/)
      GO TO 999
 2    CONTINUE
      WRITE(2,102)
102   FORMAT(1X,80(*+*)/)
      GO TO 999
 3    CONTINUE
      WRITE(2,103) ICOUNT
103   FORMAT(/18X,*+++ SYSTEM DIVERGED AFTER*,I6,* ITERATIONS ++++*//)
      GO TO 999
 4    CONTINUE
      WRITE(2,104)
104   FORMAT(//30H LATERAL URGENCY DELAY TOO BIG//)
      GO TO 999
 5    CONTINUE
      WRITE(2,105)
105   FORMAT(//35H LONGITUDINAL URGENCY DELAY TOO BIG//)
      GO TO 999
 6    CONTINUE
      WRITE(2,106)
106   FORMAT(//33H LONGITUDINAL PILOT DELAY TOO BIG//)
      GO TO 999
 7    CONTINUE
      WRITE(2,107)
107   FORMAT(//28H LATERAL PILOT DELAY TOO BIG//)
      GO TO 999
 8    CONTINUE
      WRITE(2,108)
108   FORMAT(//25H LOGIC ERROR IN SWITCHING//)
      GO TO 999
 9    CONTINUE
      WRITE(2,1109) DFLAT,DFLON,DFSIDE,FMSTR,FMSTP,FMSTS,A(27)
1109  FORMAT(6X,*DWELL FRACTIONS*,14X,*MEAN DWELL TIMES*,9X,
  1        *MINIMUM DWELL TIME*/3X,*LAT*,5X,*LONG*,5X,*SIDE*,8X,
  2        *LAT*,6X,*LONG*,6X,*SIDE*/1X,F6.4,3X,F6.4,3X,F6.4,4X,F7.4,
  3        3X,F7.4,3X,F7.4,10X,F5.3/)
      GO TO 999
 10   CONTINUE
      WRITE(2,110)
110   FORMAT(* VARIABLE*,6X,*MEAN*,8X,*STD. DEV.*,8X,*RMS*,8X,
  1        *SKEWNESS*,5X,*PEAKEDNESS*/)
      GO TO 999
 11   CONTINUE
      NAME=2*N1-1
      WRITE(2,111) VARNAM(NAME),VARNAM(NAME+1),AVGI,STDI,RMSI,SKWI,PKDI
111   FORMAT(1X,2A4,3X,1PD10.3,4(4X,D10.3)/)
      GO TO 999
 12   CONTINUE
      ISTOP=0
112   READ(7,212) (L(K),T(K),K=1,4)
212   FORMAT(4(I4,F12.0))
      IF (EOF(7)) 998,412
412   DO 312 M=1,4
      IF(L(M).EQ.0)GO TO 312
```

```
      IF(L(M).LT.0)ISTOP=1
      LOC=IABS(L(M))
      A(LOC)=T(M)
      IF(ISTOP.EQ.1)GO TO 999
312   CONTINUE
      GO TO 112
998   STOP
999   RETURN
      END
```

THIS PAGE IS BEST QUALITY PRACTICABLE
FROM COPY FURNISHED TO DDC

☆U.S.Government Printing Office: 1978 — 757-080/716